



HAL
open science

Study of the Mechanisms Underlying Neurostimulation Induced by Low- Energy Pulsed Ultrasound : Towards Approaches for the Management of Cancer-Related Chronic Pain

Jérémy Vion

► **To cite this version:**

Jérémy Vion. Study of the Mechanisms Underlying Neurostimulation Induced by Low- Energy Pulsed Ultrasound : Towards Approaches for the Management of Cancer-Related Chronic Pain. Bioengineering. Université de Lyon, 2019. English. NNT : 2019LYSE1045 . tel-02522907

HAL Id: tel-02522907

<https://theses.hal.science/tel-02522907>

Submitted on 28 Mar 2020

HAL is a multi-disciplinary open access archive for the deposit and dissemination of scientific research documents, whether they are published or not. The documents may come from teaching and research institutions in France or abroad, or from public or private research centers.

L'archive ouverte pluridisciplinaire **HAL**, est destinée au dépôt et à la diffusion de documents scientifiques de niveau recherche, publiés ou non, émanant des établissements d'enseignement et de recherche français ou étrangers, des laboratoires publics ou privés.

N°d'ordre NNT : xxx



THESE de DOCTORAT DE L'UNIVERSITE DE LYON
opérée au sein de

l'Université Claude Bernard Lyon 1

Ecole Doctorale Interdisciplinaire Sciences-Santé (EDISS, n°205)

Spécialité de doctorat : Ingénierie Biomédicale

Soutenue publiquement le 27 mars 2019

par

Jérémy VION-BAILLY

Study of the Mechanisms Underlying Neurostimulation Induced by Low-Energy Pulsed Ultrasound: Towards Approaches for the Management of Cancer-Related Chronic Pain

-

Etude des Mécanismes de Neurostimulation par Ultrasons Pulsés de Faible Energie et Applications à la Gestion des Douleurs Chroniques d'Origine Tumorale

Directeur de thèse : M. CHAPELON Jean-Yves
Co-directeur de thèse : M. N'DJIN William Apoutou

Devant le jury composé de :

Mme. FRANCESCHINI Emilie	Chargée de Recherche CNRS, <i>Rapporteur</i>
M. AUBRY Jean-François	Directeur de Recherche CNRS, <i>Rapporteur</i>
Mme. TER HAAR Gail	Professeur, <i>Rapporteur</i>
Mme. DEHAY Colette	Directrice de recherche CNRS, <i>Examinatrice</i>
M. LIEBGOTT Hervé	Professeur des Universités, <i>Examinateur</i>
M. CARPENTIER Alexandre	Professeur des Universités – Praticien Hospitalier, <i>Examinateur</i>
M. CHAPELON Jean-Yves	Directeur de Recherche INSERM, <i>Directeur de thèse</i>
M. N'DJIN William Apoutou	Chargé de Recherche INSERM, <i>Co-directeur de thèse, Membre invité</i>

RESUME en français

Les ultrasons (US) focalisés sont considérés comme une base prometteuse pour le développement d'une nouvelle modalité de neurostimulation thérapeutique. Un modèle nerveux invertébré *in vivo* (système de fibres géantes du ver de terre commun, *Lumbricus terrestris*) a été proposé pour étudier les mécanismes biophysiques sous-jacents au phénomène de neurostimulation US. Après avoir prouvé la faisabilité, les réponses respectives du modèle nerveux à différentes modalités de stimulation (mécanique, électrique, US) ont été caractérisées et comparées. Par un raisonnement causal, il a été déduit que les nerfs afférents sont les structures interagissant avec le stimulus US (pulsé, 1.1 MHz, 2% DT, 2.5 kW/cm²). Les influences respectives des paramètres acoustiques sur le taux de succès de neurostimulation ont été évaluées. Les résultats suggèrent une sensibilité des nerfs afférents à la « force de radiation moyenne » transportée par le stimulus US, pouvant être obtenue par différentes combinaisons de paramètres. Le rôle joué par la cavitation dans le phénomène de neurostimulation US a été étudié, en s'appuyant sur le suivi d'indices de cavitation et l'imagerie ultra-rapide. Il a été conclu que la réponse du modèle nerveux à un stimulus US ne nécessite pas l'occurrence d'un événement de cavitation stable, ni de niveaux particulièrement élevés de cavitation inertielle. Il a été entrepris de répliquer la méthodologie d'étude employée sur ce modèle invertébré à un modèle nerveux plus complexe. La faisabilité d'enregistrer via Microelectrode Arrays (MEA) les réponses nerveuses de tranches de cortex murin induites par US focalisés a été démontrée, et d'autres essais sont à venir.

MOTS-CLES en français

Neurostimulation, neuromodulation, ultrasons focalisés, ver de terre, *Lumbricus terrestris*, axones géants, potentiel d'action.

TITRE en anglais

Study of the Mechanisms Underlying Neurostimulation Induced by Low-Energy Pulsed Ultrasound: Towards Approaches for the Management of Cancer-Related Chronic Pain

RESUME en anglais

Focused ultrasound (US) are considered as a promising tool to develop a new modality of therapeutic neurostimulation. An *in vivo* invertebrate nervous model (system of giant fibers of the common earthworm, *Lumbricus terrestris*) has been proposed to study the biophysical mechanisms underlying the phenomenon of US neurostimulation. After proving the feasibility, the nervous responses associated with different stimulation modalities (mechanical, electrical, US) were characterized and compared together. Following a causal approach of interpretation, the afferent nerves were deduced to be the locus of interaction between the nervous system and the US stimulus (pulsed, 1.1 MHz, 2% DT, 2.5 kW/cm²). The respective influences of each acoustic parameter on the neurostimulation success rate were evaluated. Results suggest afferent nerves are sensitive to the value of the 'mean radiation force' carried by the US stimulus, whatever combination of parameters leading to it. Complementarily, the role played by cavitation in the phenomenon of US neurostimulation was investigated, using both the monitoring of cavitation indexes and ultra-fast imaging. It was concluded that neither the occurrence of stable cavitation nor particularly high levels of inertial cavitation were necessary conditions for the occurrence of US-induced nervous responses. A new experimental campaign was launched, aiming to apply the methodology developed for the invertebrate nervous model to a nervous model of higher complexity. The feasibility of using Microelectrode Arrays (MEA) to record US-induced nervous responses from mouse cortical slices was demonstrated, and further trials are currently undertaken.

MOTS-CLES en anglais

Neurostimulation, neuromodulation, focus ultrasound, earthworm, *Lumbricus terrestris*, giant axons, Medial Giant Fiber, MGF, Lateral Giant Fiber, LGF, action potential.

INTITULE ET ADRESSE DU LABORATOIRE

Laboratoire de Thérapies et Applications Ultrasonores (LabTAU INSERM U1032)
151 Cours Albert Thomas
69424 Lyon Cedex 03

Résumé substantiel en français

Les techniques de neurostimulation telles que la Stimulation Corticale Profonde ou la Stimulation Magnétique Transcrânienne ont été appliquées avec succès au traitement de divers affections neurologiques, allant des troubles moteurs et sensoriels à l'épilepsie, en passant par les douleurs chroniques et certains troubles affectifs. Toutefois ces techniques ne sont pas encore optimales, chacune d'entre elles présentant ses limitations propres, que ce soit en termes d'invasivité, de résolution spatial ou d'accès aux tissus profonds. Il existe donc un intérêt croissant pour le développement de nouvelles modalités de neurostimulation. En particulier, il existe de nombreuses preuves, obtenues principalement sur des modèles mammifères, de la capacité des ultrasons à déclencher ou moduler une activité neuronale de manière non-invasive. La neurostimulation ultrasonore représente donc un terrain de recherche très prometteur, auquel il fait pourtant défaut un modèle valide décrivant les biomécanismes sous-jacents. Or, la compréhension de ces interactions biophysique est essentielle afin d'atteindre un niveau de compréhension et de contrôle du phénomène qui permettra d'aboutir à des applications cliniques. Dans ce contexte, il apparait comme nécessaire de reporter les efforts d'investigation de ce domaine vers des modèles nerveux plus simples que ceux qui ont fourni les preuves de faisabilité actuelles, afin de mener des études mécanistiques approfondies, valider des modèles, et les confronter à des modèles nerveux de complexité progressivement croissante.

Ainsi, le premier objectif de ce travail de thèse était de proposer un modèle nerveux relativement simple et propice à une étude mécanistique du phénomène de neurostimulation ultrasonore. L'objectif suivant était de prouver l'intérêt d'exploiter ce modèle pour recueillir des informations concernant les interactions biophysiques ayant lieu entre les ultrasons focalisés et le système nerveux. La majorité des études réalisées a porté sur le système nerveux du ver de terre commun, *Lumbricus terrestris*. Le nerf ventral de *Lumbricus terrestris* présente notamment trois axones géants (une fibre médiale, MGF, et deux fibres latérales, LGF) dont il est possible d'enregistrer l'activité nerveuse dans des conditions *in vivo*. Ces fibres géantes sont impliquées dans le réflexe de fuite de l'animal, et à ce titre elles sont associées en amont avec les voies afférentes. Les premières études réalisées ont consisté d'une part à comparer entre

elles les caractéristiques temporelles des réponses nerveuses associées à différentes modalités de stimulation (mécanique, électrique et ultrasonore), et d'autre part à évaluer l'influence de chacun des paramètres acoustiques du stimulus ultrasonore sur le taux de succès de neurostimulation (NSR). Dans les deux cas, la méthodologie suivie reposait sur l'administration de différents stimuli aléatoirement alternés.

Il a été prouvé que des séquences d'ultrasons pulsés étaient en mesure de déclencher des réponses nerveuses chez le ver de terre avec un niveau de succès relativement élevé (>90%). Ces réponses nerveuses se présentaient sous la forme de potentiels d'actions enregistrés dans les fibres géantes conséquemment à l'exposition aux ultrasons. Les aires sensorielles et la dynamique de réponses associées aux trois modalités de stimulation ont été caractérisées. En tirant partie d'une propriété particulière de la connexion synaptique entre les nerfs afférents et les fibres géantes (deux gradients de force synaptique existent le long de MGF et LGF, dans des directions opposées) il a été possible de situer le locus d'interaction entre le faisceau ultrasonore et le système nerveux au niveau des voies afférentes, en amont de la connexion synaptique. Ainsi, en se basant sur une mesure électrophysiologique indirecte, le modèle nerveux proposé permet d'étudier la réponse d'une structure nerveuse qui n'aurait autrement pu être détectée dans des conditions *in vivo*.

Les résultats des études paramétriques ont indiqué que le NSR augmente avec l'intensité acoustique, la durée de pulse et la fréquence de répétition des pulses. Sur la base de ces tendances, il a été proposé que la structure nerveuse activée par le stimulus ultrasonore est sensible à la « force de radiation moyenne » transportée par ce stimulus, indépendamment de la combinaison de paramètres ayant mené à sa valeur.

Complémentairement, l'hypothèse de la cavitation comme mécanisme sous-jacent à la neurostimulation ultrasonore, proposée dans la littérature, a été étudiée. Ces études ont consisté d'une part à imager le nuage de cavitation pouvant être généré dans le milieu sous l'effet d'un burst ultrasonore, et d'autre part à rechercher une possible corrélation entre les indices de cavitation et la réponse du nerveux à un stimulus ultrasonore. La mise en évidence de nombreux contre-exemples a abouti à la conclusion selon laquelle ni la survenue de cavitation stable ni la survenue de particulièrement hauts niveaux de cavitation inertielle n'étaient des conditions nécessaires au déclenchement de réponses nerveuses par le biais d'ultrasons focalisés.

Ainsi, en s'appuyant sur les différentes conclusions mentionnées ci-avant, l'hypothèse a été faite que, dans le modèle nerveux employé, la principale interaction avec le système nerveux implique la force de radiation acoustique, ce qui n'exclut pas la contribution d'autres biomécanismes concomitants. Capitalisant sur ce premier volet d'études, une nouvelle campagne expérimentale a été initiée sur un modèle nerveux invertébré *ex vivo*. Les essais préliminaires ont permis de démontrer la faisabilité d'utiliser ce modèle pour étudier le phénomène de neurostimulation ultrasonore.

Table des matières

Résumé substantiel en français	3
Table des matières	6
Chapter 1: New therapeutic approaches for the management of cancer pain	14
I. Cancer pain: identification and management.....	14
I.A. Pain: generalities.....	14
I.A.1. Pain function	14
I.A.2. Pain pathway.....	14
I.A.3. Pain classification	15
<i>I.A.3.i. Acute vs. Chronic pain</i>	<i>15</i>
<i>I.A.3.ii. Nociceptive vs. neuropathic pain</i>	<i>15</i>
<i>I.A.3.iii. Somatic vs. visceral pain.....</i>	<i>15</i>
I.B. Pain directly associated with cancer and related disorders.....	16
I.B.1. Acute pain directly related to cancer.....	16
I.B.2. Acute pain related to infections.....	16
I.B.3. Acute pain related to thrombotic events.....	17
<i>I.B.3.i. Deep vein thrombosis</i>	<i>17</i>
<i>I.B.3.ii. Superior vena cava obstruction</i>	<i>17</i>
I.B.4. Nociceptive somatic pain syndromes related to the tumor	17
<i>I.B.4.i. Bone metastases</i>	<i>17</i>
<i>I.B.4.ii. Soft tissues.....</i>	<i>18</i>
I.B.5. Nociceptive visceral pain syndromes related to cancer	18
I.B.6. Neuropathic pain syndromes directly related to cancer	19
<i>I.B.6.i. Malignant Spinal Cord Compression.....</i>	<i>19</i>
<i>I.B.6.ii. Malignant plexopathy</i>	<i>20</i>
I.C. Pain associated with therapeutic and diagnostic modalities	21
I.C.1. Acute pain associated with diagnostic procedures.....	21
I.C.2. Acute pain associated with operative and analgesic procedures.....	21
I.C.3. Chronic pain associated with surgery	22
<i>I.C.3.i. General issues related to surgery-induced pain</i>	<i>22</i>
<i>I.C.3.ii. Post-mastectomy pain syndrome.....</i>	<i>22</i>
<i>I.C.3.iii. Post-thoracotomy pain.....</i>	<i>23</i>
<i>I.C.3.iv. Post-neck dissection pain</i>	<i>23</i>

I.C.3.v. <i>Post-amputation pain</i>	24
I.C.4. Pain associated with chemotherapy	24
I.C.4.i. <i>Acute pain due to infusion technics</i>	24
I.C.4.ii. <i>Mucositis</i>	24
I.C.4.iii. <i>Painful peripheral neuropathy</i>	25
I.C.4.iv. <i>Headaches</i>	25
I.C.4.v. <i>Other pain syndromes</i>	25
I.C.5. Pain associated with radiotherapy	26
I.C.5.i. <i>Radiation-induced peripheral neuropathy</i>	26
I.C.5.ii. <i>Pain flare</i>	26
I.C.5.iii. <i>Pain related to injury of the digestive system</i>	27
I.C.5.iv. <i>Radiation-induced malignancies</i>	27
I.D. Conclusion on the pain management of cancer-related pain	28
II. Neurostimulation: an alternative to the pharmacological approach for chronic pain management	29
II.A. The nervous system	29
II.A.1. Functional architecture	29
II.A.2. Nerve cell: the system's unit.....	31
II.A.3. Action potential: the information support.....	31
II.A.4. Parameters influencing the axon conduction velocity.....	33
II.A.5. Modelling the propagation of an action potential.....	34
II.A.5.i. <i>Hodgkin-Huxley model</i>	34
II.A.5.ii. <i>Non-electrical aspects of the AP propagation</i>	35
II.A.5.iii. <i>Alternative models</i>	36
II.A.6. Mechanotransduction	37
II.B. Interacting with the nervous system	38
II.B.1. History of the field of electrical stimulation.....	38
II.B.1.i. <i>Early intuitions and foundational discoveries</i>	38
II.B.1.ii. <i>Applications to functional neurosurgery</i>	42
II.B.1.iii. <i>First attempts of therapeutic applications</i>	42
II.B.1.iv. <i>Birth of the field of neuromodulation</i>	43
II.B.1.v. <i>The path towards Deep Brain Stimulation</i>	43
II.B.2. Modern Deep Brain Stimulation.....	44
II.B.2.i. <i>Components</i>	44
II.B.2.ii. <i>Therapeutic applications of DBS to movement disorders</i>	45

II.B.2.iii. Therapeutic applications of DBS to non-movement disorders	49
II.B.2.iv. Chronic pain	51
II.B.2.v. DBS-related complications	52
II.B.3. Non-invasive neurostimulation technics	52
II.B.3.i. Transcranial magnetic stimulation	52
II.B.3.ii. Transcranial Direct Current Stimulation	53
III. Focused ultrasound: a new modality of neurostimulation	54
III.A. Ultrasound: a mechanical wave	54
III.A.1. Terminology	54
III.A.2. Physical definition of a sound wave	55
III.A.3. How to produce ultrasound ?	58
III.A.3.i. The piezoelectric transducer	58
III.A.3.ii. Next generations of US transducers	59
III.A.3.iii. The different geometries of US transducers	60
III.B. Interactions of US with biological tissues and related therapeutic applications	61
III.B.1. Attenuation and thermal effects	62
III.B.2. Cavitation and mechanical effects	64
III.B.3. Main developments of therapeutic US using thermal mechanisms: thermal ablation of localized cancer	66
III.B.3.i. Presentation of HIFU	66
III.B.3.ii. Application of HIFU to cancer treatment	67
III.B.4. Main development of therapeutic US using mechanical effects	68
III.B.4.i. Kidney stones	68
III.B.4.ii. Treatment of kidney stones	68
III.C. Interactions of US with nervous structures	69
III.C.1. Early proofs of feasibility	69
III.C.2. Recent results	70
III.C.3. Possible mechanisms	71
III.C.3.i. Postulated general mechanisms	71
III.C.3.ii. The “continuum mechanics” hypothesis	71
III.C.3.iii. The NICE model	72
Conclusion	76
Chapter 2: Feasibility and demonstration of interest of using a simple invertebrate <i>in vivo</i> nervous model to study ultrasound neurostimulation	78
Introduction	78

I. Presentation of the nervous model : the earthworm’s system of giant fibers	79
I.A. Giant fibers and their role in the animal kingdom	79
I.A.1. About startle, rapid escape, and giant fiber-mediated responses	79
I.A.2. Giant fibers distribution in the animal kingdom and their diversity of function ..	81
I.B. Introduction to earthworms, their role in nature and science.....	84
I.B.1. Interaction of earthworms with their natural environment	84
I.B.2. Earthworms in sciences: “The subject may appear an insignificant one ...” (Darwin).....	86
I.C. General anatomical and functional organization of the earthworm.....	88
I.C.1. Longitudinal and radial anatomical organizations of the earthworm.....	88
<i>I.C.1.i. Longitudinal body segmentation.....</i>	88
<i>I.C.1.ii. The body wall.....</i>	90
<i>I.C.1.iii. The coelom.....</i>	91
<i>I.C.1.i. The digestive track.....</i>	91
I.C.2. Physiological characteristics of <i>Lumbricus terrestris</i>	93
<i>I.C.2.i. Respiration.....</i>	93
<i>I.C.2.ii. Coelomic secretion.....</i>	93
<i>I.C.2.iii. Vascular organization.....</i>	94
<i>I.C.2.i. Sexual differentiation</i>	95
I.D. Earthworm nervous architecture and its system of giant fibers.....	95
I.D.1. Ganglia and segmental nerves distribution	96
I.D.2. Nerve plexuses	98
I.D.3. Anatomical organization of giant fibers in <i>Lumbricus terrestris</i>	99
<i>I.D.3.i. The ventral nerve cord.....</i>	99
<i>I.D.3.ii. The medial giant fiber.....</i>	102
<i>I.D.3.iii. The Lateral Giant Fibers.....</i>	103
I.D.4. Conduction properties of giant fibers in <i>Lumbricus terrestris</i>	105
<i>I.D.4.i. Typical values of conduction velocities in MGF and LGF</i>	105
<i>I.D.4.ii. Large diameter.....</i>	105
<i>I.D.4.iii. Insulating sheath</i>	106
<i>I.D.4.iv. Formation of syncytia</i>	106
<i>I.D.4.v. Facilitation of conduction velocity.....</i>	106
I.D.5. Afferent pathway in <i>Lumbricus terrestris</i>	107
<i>I.D.5.i. Sensory fields of MGF and LGF.....</i>	107
<i>I.D.5.ii. Characterization of mechanosensory neurons</i>	107

I.D.5.iii. <i>Synaptic inputs to MGF and LGF</i>	108
I.D.6. Efferent pathway	109
I.D.7. Rapid escape movement	110
I.D.7.i. <i>Anterior stimulation</i>	110
I.D.7.ii. <i>Posterior stimulation</i>	111
II. Characterization of the ultrasound transducer	112
II.A. Methods	112
II.A.1. Acoustic pressure field	112
II.A.2. Radiation force	113
II.A.3. Definition and calculation of the “pulse intensity”	116
II.B. Results.....	117
II.B.1. Acoustic pressure field.....	117
II.B.2. Radiation force and pulse intensity.....	121
II.C. Discussion.....	122
III. Application of the proposed nervous model to a comparative study between different modalities of stimulation.....	123
III.A. Methods.....	123
III.A.1. General approach of the comparative study.....	123
III.A.2. Animal preparation.....	124
III.A.3. Experimental set-up	125
III.A.4. Electrophysiological recording	127
III.A.5. Mechanical stimulation (MStim)	130
III.A.6. Electrical stimulation (EStim).....	131
III.A.7. Terminology relative to US stimuli	131
III.A.8. Ultrasound stimulation (UStim).....	132
III.A.9. Definition and calculation of particular times.....	133
III.A.10. Methodology followed in the comparative trials	133
III.A.11. Assessment of the results.....	134
III.B. Results	134
III.B.1. Criteria of inclusion in the studies.....	134
III.B.2. Preliminary evaluation of the electrical activation threshold.....	135
III.B.3. Nervous response to electrical stimulation (EStim).....	136
III.B.4. Stability of the conduction velocity over time	136
III.B.5. Nervous response to mechanical stimulation (MStim)	136
III.B.6. Feasibility of response to US stimulation.....	137

III.B.7. Qualitative characterization of nervous response to ultrasound stimulation (UStim).....	139
III.B.8. Quantitative comparison between respective nervous responses to mechanical and ultrasound stimulation.....	141
III.C. Discussion	142
III.C.1. Dynamics of the nervous response to electrical stimulation: an instantaneous depolarization of the membrane of the giant axons	142
III.C.2. Dynamics of the nervous response to mechanical stimulation: an excitation of giant axons mediated by the afferent pathway	143
III.C.3. Deductions on the interaction between ultrasound and the earthworm nervous system.....	146
Conclusion.....	148
Chapter 3: Investigation of the acoustic bio-effects involved during <i>in-vivo</i> ultrasound neurostimulation in a simple invertebrate system of giant fibers	149
Introduction	149
I. Parametric study of the influence of acoustic parameters on the success rate of neurostimulation	150
I.A. Methods	150
I.A.1. General approach of the parametric studies.....	150
<i>I.A.1.i. Terminology relative to US stimuli.....</i>	<i>150</i>
<i>I.A.1.ii. Motivations for the randomization.....</i>	<i>151</i>
<i>I.A.1.iii. Burst of reference.....</i>	<i>152</i>
<i>I.A.1.iv. Definition of the Neurostimulation Success Rate (NSR).....</i>	<i>152</i>
I.A.2. Influence of US pulse intensity and duration on the NSR.....	153
I.A.3. Influence of US PRF on the NSR	153
I.A.4. Influence of the number of US pulses per burst on the NSR.....	154
I.A.5. Investigation of the influence of higher US frequency on the NSR	154
I.A.6. Assessment of the results	155
I.B. Results.....	155
I.B.1. Influence of pulse intensity on the NSR	155
I.B.2. Influence of pulse duration on the NSR.....	157
I.B.3. Combined influence of I_{sapa} and PD on the NSR	159
I.B.4. Influence of pulse repetition frequency on the NSR.....	161
I.B.5. Influence of the number of pulses per burst on the NSR	163
I.B.6. Influence of a higher US frequency on the NSR	167
I.C. Discussion	168

I.C.1. Cross-analysis of the influence of three US parameters on the NSR: I_{sapa} , PD and PRF.....	168
I.C.2. Influence of the number of US pulses per burst.....	170
I.C.3. Feasibility of using a higher US frequency.....	171
II. Study of the cavitation as a possible mechanism underlying US neurostimulation.....	172
II.A. Methods.....	172
II.A.1. Imaging of the cavitation cloud.....	172
II.A.2. Monitoring of the cavitation indexes.....	172
II.B. Results.....	175
II.B.1. Characteristics of the cavitation cloud.....	175
II.B.2. Correlation between cavitation events and stimulating events.....	176
II.B.2.i. MOD-1: distribution of each cavitation index over a single trial.....	177
II.B.2.ii. MOD-2 : distribution of combination of cavitation index over the whole set of trials.....	179
II.B.2.iii. MOD-3 : display of the regional NSR in the IC-ESC space.....	181
II.C. Discussion.....	181
Conclusion.....	183
Chapter 4: Feasibility of using a vertebrate ex vivo nervous model to study ultrasound stimulation.....	184
Introduction.....	184
I. Feasibility of generating and recording US-induced nervous responses from a mouse cortical slice, using an MEA device.....	185
I.A. Methods.....	185
I.A.1. Ethical statement.....	185
I.A.2. Slice preparation.....	185
I.A.3. Experimental set-up.....	186
I.A.4. Electrophysiological recording.....	187
I.A.5. Electrical stimulation.....	188
I.A.6. Ultrasound stimulation.....	188
I.A.7. Control experiments.....	189
I.B. Results.....	189
I.B.1. Comparison of the neural model's response to electrical and ultrasound stimulation.....	189
I.B.2. Spatial distribution of the US-induced neural responses.....	190
I.B.3. US-induced MEA-recorded signal evolution as a function of pulse duration....	191
I.B.4. Influence of the introduction of a channel-blocker in the medium on the waveform	

characteristic of the signal.....	193
I.C. Discussion	195
II. Refinement of the experimental protocol and further investigations	195
II.A. Methods	195
II.A.1. Improvement of the quality of the MEA-recorded signal	196
II.A.2. Acoustic parameters.....	196
II.B. Results.....	197
II.B.1. Waveforms characteristics of the US-pulse-induced signal with the refined recording protocol	197
II.B.2. Nervous response to a train of US pulses	198
II.C. Discussion.....	201
Conclusion.....	203
General conclusion	205
Références	208
Annexes	223
Annexe I – Reproductive system of <i>Lumbricus terrestris</i>	223

Chapter 1: New therapeutic approaches for the management of cancer pain

I. Cancer pain: identification and management

I.A. Pain: generalities

I.A.1. Pain function

Pain is a conceptual, subjective notion, involving physical, psychological and social factors, and for these reasons it is challenging to give a simple definition of it. However, the physiological function of pain has been clearly identified since the Renaissance, and can be simply define as alerting the body of an immediate threat to its integrity. Hence, feeling pain brings a considerable advantage to an animal in terms of survival, for it causes it to withdraw from the pain source, protect the painful body area during healing, and will leave a conscious or unconscious label of “danger” associated with the situation in which pain was experienced, encouraging the animal to avoid those in the future – *once burned, twice shy* (Holden and Winlow, 1984).

I.A.2. Pain pathway

The detection of stimuli which could be associated with a threat for the body integrity is supported by specialized nervous receptors called nociceptors. The nature of these stimuli can be either thermal, mechanical or chemical. The pain pathway, initiated when nociceptors detect such stimuli, works in 4 times. Firstly, the nociceptors convert the energy provided by the stimulus in electrical pulses (transduction). This electrical signal is then transmitted along the nerves to the central nervous system (transmission). Once the signal reaches the thalamus, the individual starts being aware of the pain, its location and intensity (perception). Based on this information, the brain reacts and sends appropriate commands (ex: removing a limb from a heat source) and inhibitory agent to provide analgesic relief (Potter and Perry, 2004).

I.A.3. Pain classification

I.A.3.i. Acute vs. Chronic pain

According to its duration, pain will be considered as acute or chronic. Although there is no quantitative threshold universally agreed on to distinguish these two class of pain, qualitative identifications exist (Turk and Okifuji, 2001). **Acute pain** is pain experienced immediately after the noxious event and during the following weeks or months, and will resorb after healing. **Chronic pain** is a long-lasting pain, which remains months or years after the healing process, or which appears with no identifiable reasons (idiopathic pain).

I.A.3.ii. Nociceptive vs. neuropathic pain

According to the origin where the nerve impulse was triggered along the pain pathway, pain is classified as nociceptive or neuropathic. **Nociceptive pain** is pain triggered by nociceptors themselves, when detecting noxious stimuli. It is provoked by « real » damages, which are clearly identified, in terms of location and nature, by the brain. Nociceptive pain can be acute (e.g. pain following a trauma or a burn), or can be chronic (e.g. rheumatism and some forms of cancer pain). **Neuropathic pain** is induced by damage or irritation of one of the constitutive elements, central or peripheral, of the pain pathway. This form of pain involves abnormal feeling coming from body regions where there is no apparent tissue damage, and is almost always chronic.

I.A.3.iii. Somatic vs. visceral pain

Among nociceptive pains, two subgroups can be distinguished, according to the situation of the nociceptors in the body: somatic pain and visceral pain. **Somatic pain** comes from nociceptors connected to skin, muscles and articulations. It can be superficial, when the involved nociceptors are situated in the superficial layer of the skin and mucous membranes, or profound, when the involved nociceptors are situated in the deep layers of the skins, muscles

and articulations. Profound somatic pain is burning, diffuse, often chronic, and involves tissue damage. **Visceral pain** comes from nociceptors situated in the organs of the thoracic and abdominal cavity. It can either be a dull, burning or stabbing pain, triggered by extreme tissue stretching, ischemia, irritating chemicals or muscle spasms.

I.B. Pain directly associated with cancer and related disorders

I.B.1. Acute pain directly related to cancer

Amongst the multiple types of acute cancer pain, very few are directly related to cancer itself. One example is the spontaneous rupture of hepatocellular carcinoma, which induces severe right upper quadrant pain, may be life-threatening and must be treated in emergency (Recordare et al., 2002). Bones metastases can lead to pathological fractures of the spine, leading to paralysis if a decompression operation is not performed within 48 hours, or pathological fractures of the extremities, usually in the femur and humerus (Tateishi et al., 1997). Obstruction of the biliary tract or urethra because of intra-abdominal cancer can also lead to acute severe pain, which can be managed by relieving the obstruction through surgery or stenting, when possible (Rotariu 2004).

I.B.2. Acute pain related to infections

Cancer has been reported to be an important risk factor in the development of herpes zoster, an infection provoked by the varicella zoster virus. Patients who have undergone radiotherapy (Dunst 2000), or who are immunocompromised (Rusthoven 1988, in Cancer), are most likely to contract the disease. The non-specific symptoms include headache, fever and malaise. The specific symptoms are sensations of burning pain, itching, hyperesthesia and paresthesia (Stankus 2007) and the dermatomal location of the infection is often associated with the site of malignancy (Rustoven 1988, in Arch Inter Med).

I.B.3. Acute pain related to thrombotic events

I.B.3.i. Deep vein thrombosis

Venous thrombosis is the formation of a blood clot, or thrombus, in a vein. The triad of Virchow describes the main risk factors contributing to venous thrombosis (Bagot and Arya, 2008), which are hypercoagulability, venous stasis (reduction of the venous blood flow) and any structural or functional change in the vascular wall (Martinelli et al., 2010). Cancer promotes two of these risk factors. On one hand, the presence of a tumor growth pressuring or infiltrating a deep vein will lead to stasis. On the other hand, tumor cells may promote the release from affected organs or release themselves tissue factors, which play a key role in the clotting process. Hence, cancer is an important cause of venous thrombosis, with 15 to 25% of deep vein thrombosis (DVT) attributable to cancer (White, 2003). The cancers which are more likely to induce DVT are advanced pelvic tumors, pancreatic cancer, gastric cancer, advanced breast cancer and brain tumors (Bruera and Portenoy, 2009). DVT most commonly occurs in low-extremities, and will be associated with variable degrees of pain, especially induced by stretching.

I.B.3.ii. Superior vena cava obstruction

Superior vena cava syndrome can be caused by a compression exerted by a tumor growth, generally lung cancer. Although not systematic, intense pain can occur in the form of headache and vascular congestion of the head and neck. Other symptoms include dyspnea, swelling of the face and neck, and dilated veins.

I.B.4. Nociceptive somatic pain syndromes related to the tumor

I.B.4.i. Bone metastases

Bone metastases are considered to be the most common cause for cancer pain (Reale et al., 2001). The pain induced by bone metastases can be multifocal, radiating, local or referred,

exacerbated by particular movements (neck flexion, walking...) or postures (sitting, ...), and is often associated with neurological deficits. Spine is the most common area of involvement, with a majority of vertebral metastases located in the thoracic spine. Vertebral metastases can induce a wide range of local and referred pain, and neurological deficits in one or several extremities. Tumors located near the end of the spinal cord can cause *cauda equina* syndrome, which symptoms are severe low back pain, sciatica, saddle or genital sensory disturbance, bladder, bowel and sexual dysfunction (Gardner et al., 2011). Metastases to the pelvis can result in a large region of deep aching continuous pain, with severe movement-associated breakthrough pain. Base-of-skull metastases can cause pain in different areas of the skull, neck and shoulders, as well as headache associated with neurological deficits such as blurred vision, diplopia, facial numbness, paresthesia, dysphagia, atrophy of the tongue and dysarthria (Bruera and Portenoy, 2009).

I.B.4.ii. Soft tissues

Tumor infiltrations of soft tissues were reported to account for more than 28 % of the major pain syndromes, according to a former classification (Caraceni and Portenoy, 1999). The tissues affected by the tumor infiltration include muscles, organs, skin and different body membranes, which can cause pain by either directly stimulating the nociceptors or destroying mobile structures. The symptoms and degree of pain associated with these tumors will depend on the organ where it develops. For example, soft tissue sarcomas developing in the abdomen may cause abdominal pain, vomiting and painful constipation, but sarcomas developing in other regions have been reported to be associated in particular with highly painful cramps, and pleural pain. (Mindell, 2001).

I.B.5. Nociceptive visceral pain syndromes related to cancer

Visceral pain can be encountered in patients with primary cancer or metastases having infiltrated visceral organs such as the pancreas, liver, lung and gastrointestinal tract. This type of pain is diffuse, poorly localized, often referred to distant and superficial somatic structures such as skin, and may be accompanied by autonomic reflexes (nausea, vomiting). Visceral

structures do not respond to painful triggers such as burning or cutting which would normally evoke pain in cutaneous tissues, but they are highly sensitive to luminal distension, ischemia and inflammation. This is why visceral tumors are often painless at the beginning of their growth, until they reach a size inducing an intraluminal pressure above the pain threshold. In some cases, visceral tumors may release pain-relieving chemicals which will activate nociceptors and may lower the thresholds of activation of the pain pathway (Urch et al., 2008).

I.B.6. Neuropathic pain syndromes directly related to cancer

I.B.6.i. Malignant Spinal Cord Compression

Malignant Spinal Cord Compression (MSCC) is the second most common cancer-related neurological complication after brain metastasis (Spinazzé et al., 2005). MSCC can be caused either by spinal metastasis growing in different locations, within and peripherally to the spine (**Figure 1**), or by bone fragments displaced in the epidural space after the collapse of the vertebral body. MSCC can induce motor weakness and autonomic dysfunction, but the main symptom is pain, which is experienced by 88-96% of patients with MSCC (Rajer and Kovač, 2008). Pain is located at the level of compression, is amplified by certain movements, and can be similar to the pain related to degenerative disease of the spine. However, unlike this latter form of pain, MSCC-related pain cannot be relieved by rest, and even get worse when the patient lays down. Because it is highly debilitating, MSCC should be treated as soon as possible when diagnosed, studies having shown that to delay the treatment of only a few hours can cause permanent neurological impairment (Higdon and Higdon, 2006).

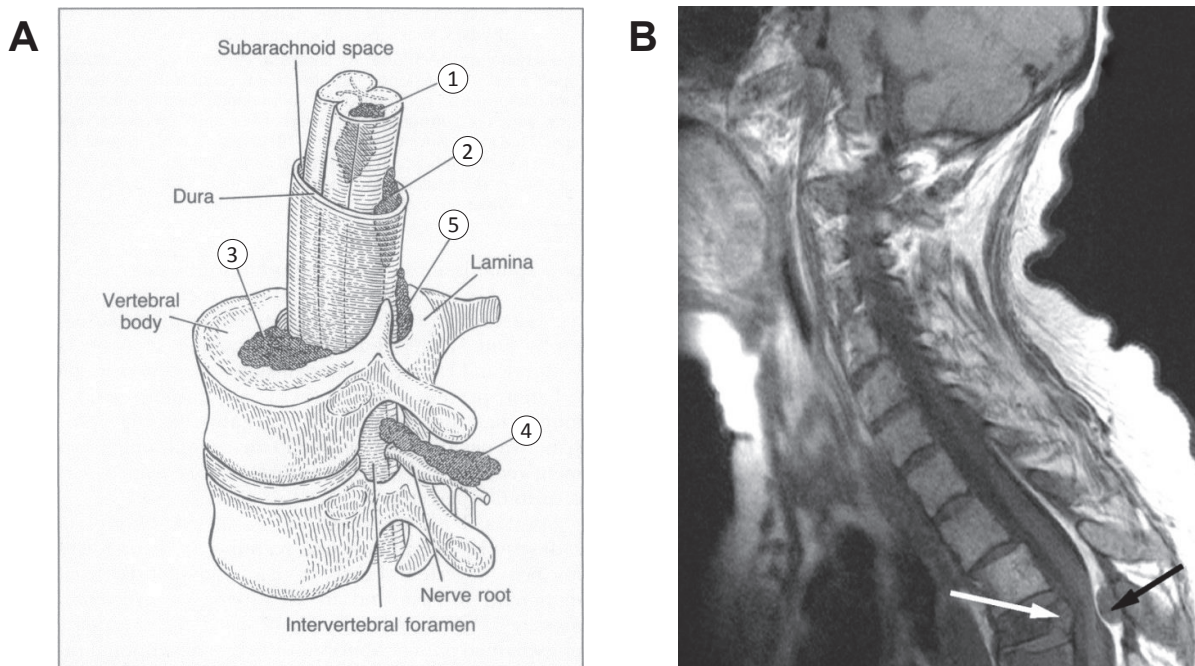


Figure 1 – Locations of spinal metastases responsible for Malignant Spinal Cord Compression (MSCC). (A) Schematic representation of the locations of metastases to the spine: (1) within the spinal cord, (2) in the subarachnoid space, (3) in the adjacent vertebral space, (4) in the paravertebral space through and (5) in the epidural space (from Byrne, 1992). (B) MR image of an extradural compression caused by anterior and posterior masses showed by arrows (Prasad and Schiff, 2005).

I.B.6.ii. Malignant plexopathy

Primary head and neck malignancies, or neoplasms extending from cervical lymph nodes, may lead to the invasion or compression of the cervical plexus. **Cervical plexopathy** is associated with an aching and burning pain in the neck, referred pain in the face, head or shoulder, and may worsen by neck movement or swallowing.

In cases of apical lung neoplasm, or when a primary breast or lung cancer has spread to axillary lymph nodes, invasion of the brachial plexus may occur. The primary symptom of **malignant brachial plexopathy** is a deep, aching pain in the shoulder with radiation to the medial arm and hand. If the tumor extends into the epidural space, there is the risk for the patient developing MSSC.

Lastly, **malignant lumbrosacral plexopathy** may occur in cases of colorectal, cervical, or breast tumors, sarcoma and lymphoma. Similarly, to brachial plexopathy, the initial symptom is pain, which may be followed by various neurological deficits occurring weeks to months later. Pain associated with lumbrosacral plexopathy present both focal and referred components. Depending on the site of tumor invasion (lower or upper lumbrosacral, sacral), pain may be experienced in buttocks, perineum, thigh, knee or legs, and its severity increases when sitting.

I.C. Pain associated with therapeutic and diagnostic modalities

I.C.1. Acute pain associated with diagnostic procedures

Most diagnostic procedures such as lumbar puncture, blood sampling and biopsy can induce immediate or post-procedural acute pain. In particular, lumbar puncture, which consists in extracting cerebrospinal fluid from the subarachnoid cavity with a needle inserted between two lumbar vertebrae, may lead to severe headache, known as post-dural-puncture headache (PDPH). PDPH is the result of the reduction of cerebrospinal fluid levels in the brain and spinal cord due to leakage through the epidural space. In the majority of cases, headaches will stop after a few days or weeks, but in some cases, they will last for months or years, and hence will be classified as chronic pain (Turnbull and Shepherd, 2003). Although its effectiveness has been questioned (Khan et al., 1993), epidural blood patch is currently the gold standard to prevent PDPH, and surgical closure of the dural perforation is a last resort intervention.

I.C.2. Acute pain associated with operative and analgesic procedures

Numerous therapeutic interventions can cause severe acute pain to cancer patients, such as surgery, cryosurgery, tumor embolization, percutaneous biliary drainage, suprapubic catheter insertions or percutaneous nephrostomy tube insertions. Local anesthesia can be necessary to relieve postoperative pain, or to prevent pain, and can be associated with morphine premedication. Regrettably, analgesic interventions themselves can participate in the apparition of pain syndromes. Patients following a chronic opioid therapy may experience escalating pain

as opioid doses are increased, known as opioid-induced hyperalgesia (Yi and Pryzbylkowski, 2015). The intradermal, subcutaneous and especially intramuscular injection of analgesic agents can cause a transient burning pain before the analgesia takes effects. A solution to avoid this injection-associated immediate pain can be the addition of corticosteroid to the injectate. Finally, epidural drug delivery may cause compression and irritation of nerve roots, which leads to back, pelvis, or leg pain (Bruera and Portenoy, 2009).

I.C.3. Chronic pain associated with surgery

I.C.3.i. General issues related to surgery-induced pain

Several surgical interventions, including cancer surgical ablation, have been associated with chronic pain syndromes. Residual pain can most likely be explained by the invasion of soft tissues, muscles and vasculatures during the surgical procedure, and the different damage brought directly or indirectly to the nerves. Although the mechanisms are not entirely understood, it has been suggested that these tissues damages are at the basis of an inflammatory chain reaction leading to the permanent sensitization of neurons, which would be responsible for chronic neuralgia (Carr and Goudas, 1999). Strong evidences suggest that there is a correlation between the intensity of the postoperative pain experienced by a patient and the likelihood of his keeping severe chronic pain (Kehlet et al., 2006). It has been shown that peroperative and postoperative pain control can lower the incidence and severity of surgery-associated chronic pain syndromes.

I.C.3.ii. Post-mastectomy pain syndrome

Post-mastectomy pain syndrome (PMPS) is **one of the most commonly seen postoperative pain syndromes**. According to a retrospective cohort study, PMPS is experienced by 43% having undergone mastectomy (Smith et al., 1999, p. 199). Injury to the intercostobrachial nerve during the surgery is thought to be the main cause of PMPS. PMPS is a neuropathic pain syndrome which can resolve over several months or become chronic and

worsen. It is characterized by burning, shooting, and electric shock-like sensations in the skin around the surgical sites, but also pain in the chest wall and armpit, and secondary myofascial pain in some cases (Bruera and Portenoy, 2009). These symptoms are quite debilitating and can interfere with occupational and domestic activities, leading to a poorer health-related quality of life (QOL) amongst cancer breast survivors experiencing chronic PMPS (Macdonald et al., 2005). Regarding PMPS treatment, **interdisciplinary approaches** have been so far associated with the best outcomes, as with most chronic pain conditions. Interdisciplinary pain care programs may include **medical management** (anti-seizure medications, antidepressants, opioids, topical medications), **interventional therapy**, active **physical therapy** (thought to help preventing functional limitations in the affected arm and the “frozen shoulder” symptoms) as well as **cognitive-behavioral therapy** (to help patient learn to live with their chronic syndromes).

I.C.3.iii. Post-thoracotomy pain

It is common for patients having undergone thoracotomy to experience chronic pain syndrome, characterized by severe local pain along the scar and less systematically by myofascial pain and pain from a “frozen” shoulder. Pain is most likely due to damage of a coastal nerve during the procedure, and can be prevented or attenuated by choosing a less invasive surgical approach (using video guidance), administering epidural analgesia before and during the procedure, and implementing an aggressive multimodal therapy to treat postoperative pain.

I.C.3.iv. Post-neck dissection pain

Treatment of head and neck carcinomas might involve neck dissection, which goes with a risk of damaging local muscle, bone or nerve. The pain associated with this procedure can last up to 3 months (Chua et al., 1999), and presents both neuropathic and nociceptive components, as well as reduced shoulder abduction, shoulder and neck pain, which are major factors in the reduction of the QOL. Unfortunately, none of the pain management strategies

mentioned earlier has brought effective results in the treatment of post-neck dissection syndrome.

I.C.3.v. Post-amputation pain

Post-amputation pain presents two components: residual-limb pain and phantom pain. **Residual-limb pain** (or **stump pain**) is pain felt in the area adjacent to the amputated body part, and **phantom pain** regroups all forms of pain or feelings which are reported to be felt in the amputated body part. Residual-limb pain can be caused by a long scarring process, the development of a neuroma (nervous tissue growth) or by a poorly fitted prosthetic. The pathophysiology behind phantom pain is more complex, and involves both central and peripheral factors (Flor, 2002).

I.C.4. Pain associated with chemotherapy

I.C.4.i. Acute pain due to infusion technics

Chemotherapy can induce severe acute pain, either related to the infusion technics or the toxicity of the treatment itself. Depending on the chemotherapeutic agents, intravenous infusion may lead to painful skin reactions (irritation, erythema, desquamation, ulceration), venous reactions (spasms, phlebitis) and extreme pain along the vessels. It may be prevented or attenuated by slowing the rate of infusion, applying a warm compress or ketoprofen gel in the site of infusion. Hepatic artery infusion and intraperitoneal chemotherapy can cause severe abdominal pain. Intravesical chemotherapy can also cause abdominal pain, along with bladder inflammation (cystitis) and bladder erosion.

I.C.4.ii. Mucositis

The most common cause of pain related to chemotherapy toxicity is mucositis, which is the inflammation and denudation of the mucous membranes of the digestive tract. Patients

suffering from mucositis cannot eat or drink comfortably, and in the most severe cases, are afflicted with intense pain, deep ulcers and superinfections. Mucositis-related pain management includes opioid therapy, oral coating therapy, cryotherapy and growth factor-based therapy.

I.C.4.iii. Painful peripheral neuropathy

Many chemotherapeutic agents affect peripheral nerves, either by damaging axons, destroying myelin or increasing nerve excitability. This damage can lead to painful peripheral neuropathies, namely characterized by burning pain in the distribution of the injured nerves. The severity of this pain syndrome is dose-dependent, and in some cases the symptoms will disappear after reducing the dose or the end of the treatment. However, many patients keep long-term neurological deficits and chronic neuropathic pain.

I.C.4.iv. Headaches

Severe headaches are a common side-effect of many chemotherapeutic agents, and can be associated with fever, nuchal rigidity, vomiting, pseudotumor cerebri (idiopathic intracranial hypertension) and focal neurological deficits.

I.C.4.v. Other pain syndromes

Hand-foot syndrome has been associated with continuous low-infusion of specific chemotherapeutic agents such as liposomal doxorubicin. It manifests as painful rash on the palms and soles, which may progress in bulla formation and desquamation. Other drugs can induce Raynaud syndrome or transient ischemia of the extremities, but also cardiac ischemia (angina pectoris), perineal burning and diffuse bone pain.

I.C.5. Pain associated with radiotherapy

I.C.5.i. Radiation-induced peripheral neuropathy

Radiation received during radiotherapy can cause direct or indirect injury to peripheral nerves, leading to chronic neuropathy in cancer survivors. Radiation-induced peripheral neuropathy is a condition particularly frightening for the patients, for it appears usually several years following radiotherapy, is progressive and mostly irreversible. Its occurrence is rare but increasing with improved long-term cancer survival (Delanian et al., 2012).

Brachial plexopathy and lumbosacral plexopathy are well-known forms of radiation-induced peripheral neuropathy. Brachial plexopathy occurs most frequently following treatment of breast cancer and is associated with pain in the arm and shoulder. Lumbosacral plexopathy occurs most frequently following treatment of pelvic and abdominal malignancies, and is associated with pain in the thigh, buttocks and leg area (Shimazaki and Nakano, 2008).

The pathophysiology behind radiation-induced neuropathy is not yet fully understood. It is presumed that the compression of the nerve root by the radiation-induced fibrous tissues plays a major role. Direct injuries to the nerves (axonal damage and demyelination) and injuries to the nerve vasculature (injury to microvasculature, blood vessels obstruction and ischemia) are also likely involved in the neuropathic pain causes (Shimazaki and Nakano, 2008; Delanian et al., 2012).

I.C.5.ii. Pain flare

Radiotherapy is an effective option to treat pain syndromes associated with bone metastases, with an overall pain response rates approaching 80% (Berk, 1995). However, acute pain flare has been reported to have an incidence up to 68% in stereotactic body radiation therapy and up to 44% for external beam radiation therapy (Chiang et al., 2013).

Pain flare can be qualitatively defined as “a temporary worsening of bone pain in the irradiated metastatic site” (Hird et al., 2009). Quantitatively, a first way to define pain flare is as a 2-point increase in worst pain score (on a scale of 10) when compared to baseline, with no decrease in analgesic intake. A second way is to define it as a 25% increase in analgesic intake,

with no decrease in worst pain score. In both cases, pain score and analgesic intake must return to baseline after the flare, to distinguish it from a progression of pain.

Pain flare has been reported to be associated with a poor health-related QOL, patients describing interference with daily activities and general functioning, as well as anxiety and worry regarding the success of the treatment (Hird et al., 2009; McDonald et al., 2014).

I.C.5.iii. Pain related to injury of the digestive system

Following treatment of head and neck cancers, irradiation can cause the muscles and mucosal lining of the mouth, throat and esophagus to become stiff and deformed. Consequently, patients will experience difficulty to swallow and move food and liquids from mouth to throat (oropharyngeal dysphagia), or from throat to throat to esophagus (esophageal dysphagia) because the esophagus has narrowed and been scarred (stricture). Corollary forms of pain include frequent heartburn and stomach acid backing up into the throat (Cook and Kahrilas, 1999; Lind, 2003).

Acute radiation-induced esophagitis is another disorder affecting the digestive system, which occurs within 3 months after completion of radiotherapy (“Radiation Induced Dysphagia,” 2017). Symptoms are similar to an esophageal stricture, but reversible.

I.C.5.iv. Radiation-induced malignancies

Mutagenesis is one of the most significant effects of radiation therapy on normal tissues, which is the basis for radiation-induced malignancies. Radiation-induced malignancies are late complications arising after radiotherapy, and their frequency increases among cancer survivors. Hence, all forms of pain directly related to tumors, presented in section I.B., can be considered as collateral pain caused by radiotherapy.

I.D. Conclusion on the pain management of cancer-related pain

In this part, the various forms of cancer-related pain have been described. Pain can be directly related to the tumor, the consequence of a cascade of biological events, or induced by diagnostic, therapeutic and even analgesic procedures. Several modalities of pain management, adapted to each form of cancer-related pain, are currently employed with variable success.

The management of cancer-related chronic pain is particularly challenging, as illustrated by the case of surgery-induced pain. If most acute forms of surgery-induced pain can be prevented or alleviated by the use of anesthetic and analgesic agents before and during the procedure, chronic forms of surgery-induced pain such as post-mastectomy or post-thoracotomy pain syndromes require aggressive multimodal therapies. These interdisciplinary approaches, which include medical management, physical therapy and psychotherapy, can be experienced as a burden by the patients, even though they are designed to manage their pain. These interdisciplinary approaches, which include medical management, physical therapy and psychotherapy can be experienced as a burden by the patients, even more when they are ineffective (*e.g.* post-neck dissection syndrome).

Painful peripheral neuropathies, regardless they are the consequence of chemotherapy or radiotherapy, are another important challenge in terms of pain management, as they involve irreversible damages of the nerves themselves, and do not respond to classical painkillers.

Neurostimulation has emerged as an alternative therapeutic approach to medication, in the case of drug-resistant chronic pain. The next part introduces the foundation and history of this approach, different techniques and applications.

II. Neurostimulation: an alternative to the pharmacological approach for chronic pain management

II.A. The nervous system

II.A.1. Functional architecture

Just as the cardiovascular system is in charge of conveying the blood to the different organs of the body, the nervous system is in charge of conveying « information » across the animal body. It is responsible for the processing of perception, and the coordination of action. In vertebrates, the nervous system is compound of two main structures: the **central nervous system** (CNS) and the **peripheral nervous system** (PNS).

The CNS is compound of the encephalon (brain, cerebellum and brainstem) and the spinal cord. As these organs are critically vital for the survival of the animal, they are protected by the crane and the spine, respectively. The main functions of the CNS are:

- Gathering information coming from the different regions of the body
- Processing sensorial inputs
- Designing appropriate motor response

The PNS is compound of the cranial and spinal nerves, which acts as communication channels between the different regions of the CNS and the numerous systems of the animal organism. Hence, two pathways can be distinguished: the **sensory pathway** (or **afferent pathway**), in charge of conducting to the CNS the nervous signals coming from the different receptors of the body, and the **motor pathway** (or **efferent pathway**), in charge of conducting nervous signals coming from the CNS to the muscles and certain, some glands.

The motor division of the PNS can be further divided in autonomic and somatic nervous system. The **somatic nervous system** conducts nervous signals to the skeletal muscles, and hence is in charge of voluntary movement. The **autonomic nervous system** conducts impulses from the CNS to cardiac muscles, smooth muscles and glands the is in charge of involuntary movement of the organisms, or visceral motricity.

THE NERVOUS SYSTEM	
CENTRAL NERVOUS SYSTEM Body's coordinator & decision maker	BRAIN Directs & coordinates more complex innate reflexes and learned reflexive responses.
	SPINAL CORD Directs & coordinates less complex innate reflexes.
PERIPHERAL NERVOUS SYSTEM Network of peripheral nerves connecting the Central Nervous System to the body.	SOMATIC NERVOUS SYSTEM Manages somatic reflexive responses: <ul style="list-style-type: none"> • Triggered thru skeletal muscles • Innate, involuntary & non-directed • Learned, voluntary & directed
	AUTONOMIC NERVOUS SYSTEM Manages autonomic reflexive responses: <ul style="list-style-type: none"> • Triggered thru smooth muscles of the organs, glands & blood vessels • Innate, involuntary & non-directed • Can be learned and directed thru conditional association
	PARASYMPATHETIC NERVOUS SYSTEM Engages & moderates non-alarm state reflexes, maintaining vital functions, fostering calm, & optimizing growth through: <ul style="list-style-type: none"> • <i>Restoration</i> • <i>Social Engagement</i>
	SYMPATHETIC NERVOUS SYSTEM Engages & moderates mobilization state reflexes, readying the body for action through: <ul style="list-style-type: none"> • <i>Focus & Advance, or Fight & Flight</i>
	NON-MYELINATED VAGUS NERVE Engages & moderates immobilization state reflexes, stilling the body's vital functions to a minimum to ensure preservation through: <ul style="list-style-type: none"> • <i>Pause, or Freeze</i>
	ENTERIC NERVOUS SYSTEM Manages the gastrointestinal system

Figure 2 – Basic structure of the human nervous system.

II.A.2. Nerve cell: the system's unit

Neurons, or nerve's cells, are ones of the constitutive element of the nervous system. They are specialized in communication, that is: **processing** and **spatially propagating information**. As any eukaryotes cells, the present a soma, or cellular body, which contains the genetic information enclosed within the nucleus and different organelles necessary to cell functioning. Two kinds of extensions, or **neurites**, expand from the soma. One to several **dendrites**, are responsible for receiving incoming data from others neurons. The axon is the process along which the information will propagate and at the end of which it will be communicated to another nerve cell, or another type of excitable cell (**Figure 3**).

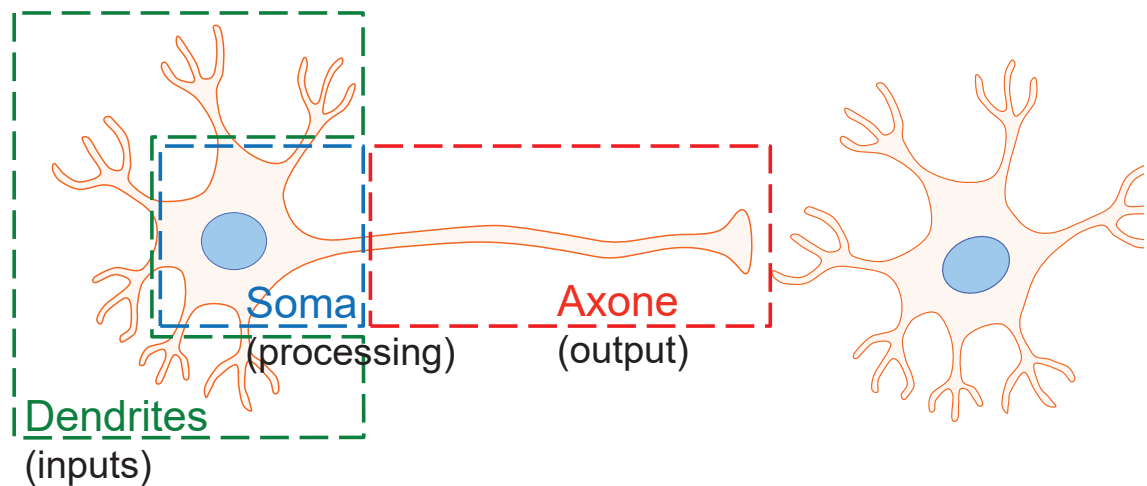


Figure 3 – Schematic representation of the main structures of a neuron. Basically, one to several dendrites receive incoming data from others neurons. Those data are processed into a new message which will be spatially carried along the axon and deliver to another neuron.

II.A.3. Action potential: the information support

The information mediated by neurons is encoded in the form of a succession of Action Potentials (APs). An AP is millisecond-scale electrochemical impulse, propagating along axon through the successive opening and closing of membrane ion channels. The speed of propagation of an AP is a property of the axon, referred to as its conduction velocity. It ranges

from 1 m/s to 100 m/s, depending on axon's characteristics such as its diameter, the presence of an insulation sheath (typically, myelin) and the type of ions channels it is constituted of.

To describe the kinetics of the passage of an AP at a given point, it is common to consider the consequences of this event in terms of membrane potential. Membrane potential is the difference between the intra- and extra-membrane electric potentials, locally measured. In its baseline state, the membrane potential of a neuron is relatively stable, and is called the resting potential. The resting potential of a neuron is negative (typically around -70 mV), due to a higher concentration in cations outside the membrane than inside the membrane. This concentration imbalance is caused and maintained by a mechanism involving cation pumps. When an event such as the arrival of the passage of an AP causes the membrane potential to increase (*ie* becoming less negative) and reach a certain threshold called the activation threshold, voltage-depend ion channels open. In this open state, ions channels allow the membrane crossing of specific ions: calcium ions can only cross calcic channels, sodium channels can only cross sodic channels, etc. Hence, immediately after activation threshold is reached, an inward flux of cations is set into motion across the membrane in response to the concentration gradient, exactly at is would happen with a semi-porous membrane. This cationic flux induces a rapid rise of the membrane potential, referred to as depolarization phase (**Figure 4**). Ion channels stay open only transiently. As they close, other types of ions channels will open, inducing an outward anionic flux leading to a phase of repolarization where the membrane potential will decrease. Eventually, the membrane potential will reach a value slightly inferior to its resting potential (hyperpolarization) before going back to its baseline value. These successive opening and closing of ions channels and associated flows are continuously repeated along the axon, leading to the propagation of a “wave”, which is the AP.

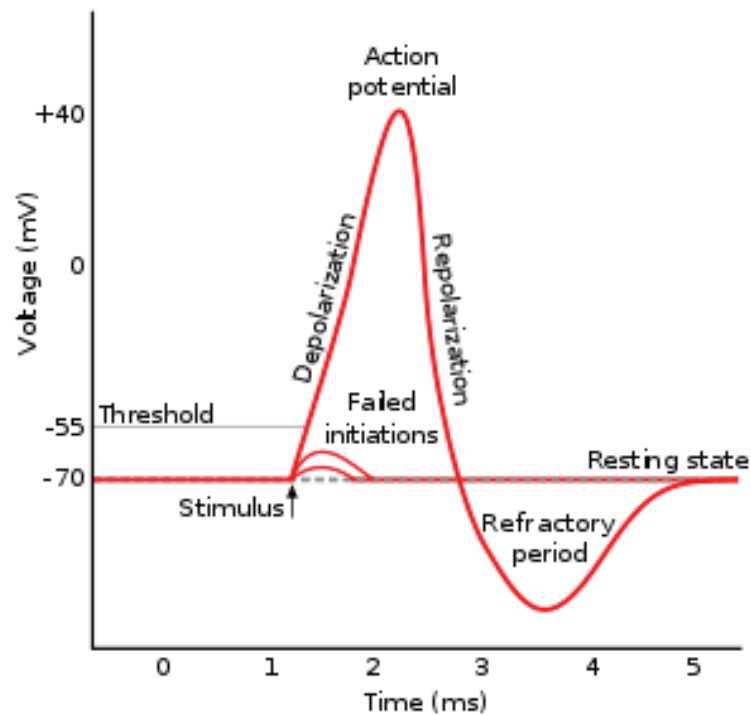


Figure 4 – Typical waveform characteristics of an action potential (AP). The electrochemical signal associated with an AP is characterized by three phases: depolarization, repolarization and hyperpolarization.

II.A.4. Parameters influencing the axon conduction velocity

Over the course of evolution, as animals were pressed to invade riskier environments and developed more sophisticated behaviors, the ability of their nervous system to rapidly conduct nerve impulses must have become a critical advantage. For instance, rapid conduction velocity enhances the timeliness of escape responses and the efficiency of predatory-capture capabilities. Hence, nerve-fiber parameters influencing the conduction velocity have been and still are under evolutionary pressure, amongst which two are particularly critical: the longitudinal resistance of the fiber to electrical current, and the transverse capacitance of the membrane. Two main strategies have been developed in the animal kingdom to modulate these parameters: **axonal gigantism** and **myelin insulation (Figure 5)** (Hartline and Colman, 2007).

One solution to decrease the longitudinal resistance is increasing the interior diameter of the nerve fiber. Among invertebrates, this strategy has been used by cephalopod to adapt nerve

conduction to their larger body size. However, due to the physical constraint imposed by the skull and spine, vertebrates had to find an alternative solution. This was achieved by introducing the myelin sheath (Zalc, 2006). Myelin is lipid-rich substance produced by glial cells: Schwann cells in the vertebrate PNS and oligodendrocytes in the vertebrate CNS. Some invertebrate axons are also unsheathed by glial cells, but those do not produce a multilamellar compact sheath, which is a necessary property to effectively insulate the axon, thus decreasing its transverse capacitance (Hartline and Colman, 2007).

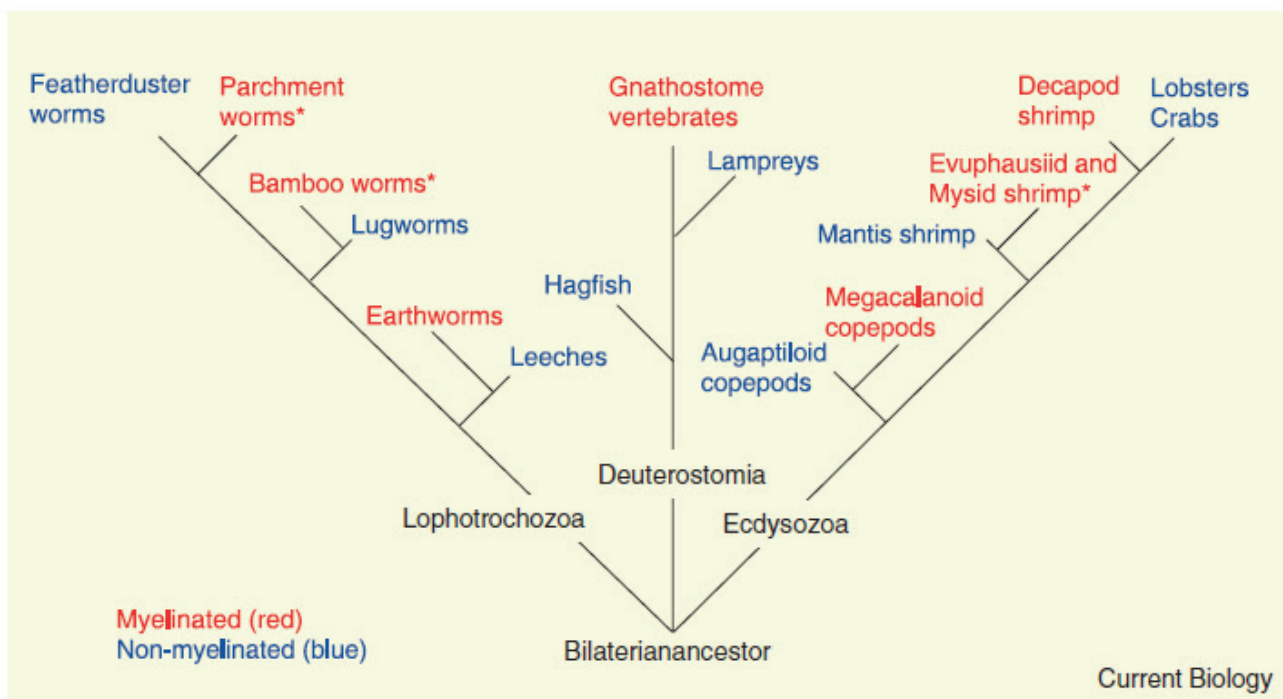


Figure 5 – Phylogenetic tree of the strategies used in the animal kingdom to increase conduction velocity (Hartline and Colman, 2007).

II.A.5. Modelling the propagation of an action potential

II.A.5.i. Hodgkin-Huxley model

In 1963, Alan Hodgkin and Andrew Huxley received the Nobel Prize in Physiology or Medicine for their work on the modelling of the initiation and propagation of actions potentials.

They provided a mathematical model, known as the Hodgkin-Huxley model, describing the ionic mechanisms responsible for these phenomena, based on experimental findings obtained from the squid giant axons. Since its introduction, this model has been widely used by electrophysiologists.

The core idea of the Hodgkin-Huxley model is an analogy with an electrical circuit, compound of resistors, capacitors, and batteries. Current is carried through the circuit either as ions passing through the membrane or by charging the membrane. The membrane is modeled as a capacitor, ion channels are modeled as voltage-dependent and time-dependent resistors, and leak channels are modeled as linear resistors. Current sources represent the ion pumps, and voltage sources represent the transmembrane electrochemical gradient.

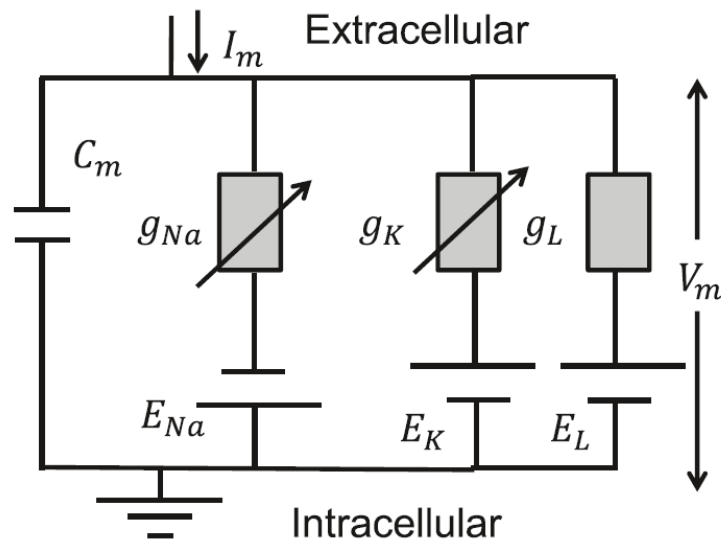


Figure 6 – Equivalent circuit for the Hodgkin-Huxley model (Sassaroli and Vykhodtseva, 2016).

II.A.5.ii. Non-electrical aspects of the AP propagation

Several experimental findings have highlighted thermodynamic phenomenon associated with the AP propagation, which are not explain by the HH model. Using highly accurate metric technics (optical coherence tomography, atomic force microscopy), several teams showed that the AP propagation is accompanied by a transient swelling of the membrane of order of 1nm,

which peak is coinciding with the peak of the action potential (Iwasa et al., 1980; Tasaki, 1988; Tasaki et al., 1989). Simultaneously with this displacement, a longitudinal shortening of the nerve was observed (Sassaroli and Vykhodtseva, 2016). Particularly striking is also the finding of reversible heat changes in the membrane during the AP. A number of authors have shown that, within experimental errors, heat released during the initial phase of AP is reabsorbed in the final phase of AP.

II.A.5.iii. Alternative models

It has been proposed that the AP is an electromechanical phenomenon rather than a strictly electrical phenomenon (Heimburg and D Jackson, 2005). In their “soliton model”, Heimburg and Jackson consider the AP as a “propagating density pulse”, or soliton. A soliton is a localized pulse propagating without attenuation or change of shape. Two conditions on the pulse speed are necessary for the existence of solitons: it should be frequency-dependent and a non-linear function of the pulse amplitude. The thermodynamics and phase behavior of lipid bilayers brings those two conditions. In the currently accepted model for biological membranes, lipids layers may undergo phase transition between liquid and gel, which can be induced in particular by temperature. Thus the soliton model is compatible with the thermodynamics findings previously exposed regarding the AP propagation. However, this model cannot explain the role of the voltage-gated ion channels in the generation and propagation of AP.

Another model is based on the concept of flexoelectricity, which is close to that of piezoelectricity. In flexoelectricity, the membrane electrical charging is induced by its bending. Just as in the case of piezoelectricity, it is possible to define a direct flexoelectric effect and a reverse flexoelectric effect. In the direct effect, a change in the membrane curvature induces a proportional change in the membrane potential, and in the reverse effect, symmetrically, a change in the membrane potential induces a proportional change in the membrane curvature. Relying on this two effects, Petrov (Petrov, 1975) has hypothesized that the AP can be considered as a flexoelectric wave: a strong enough local membrane depolarization leads to the local bending of the membrane (revers flexoelectric effect), which induce mechanical constraints in the adjacent area which in turn induces changes in the voltage of this adjacent

area (direct flexoelectric effect) and so on. This model could provide an explanation for the nerve shortening and local increase in membrane thickness observed during AP propagation (Sassaroli and Vykhodtseva, 2016). However, to this date, no mathematical model has been proposed to describe the propagation of such a flexoelectric wave along a cell membrane.

II.A.6. Mechanotransduction

In multicellular organisms, mechanoreceptors can be either neurons or peripheral afferent cells with synapses, which allow the cells to stimulate other neurons (Krey and Gillespie, 2012). When the tissues in which the mechanoreceptors lie are deformed or stimulated, ion channels of the mechanoreceptors open, neurotransmitters are released, eventually leading to the generation of APs. Ion channel gating can be elicited by voltage, ligand binding or force, but in all cases, it involves relative movement of internal domains. Several models have been generated from the study of bacteria and other cell types to explain how a force can influence domain movements within ion channels. These models have been used to compare and classify the multiple types of mechanoreceptors found within the animal kingdom. A first type of mechanoreceptor is sensitive to membrane tension: ion channels are forced to open in order to reduce tension and preserve the membrane integrity (Sukharev and Corey, 2004). In this model, the force is felt in the plane of the membrane. In another type of mechanoreceptor, ion channels are tethered on both sides of the membrane, and an external force causes a net displacement of the two anchors, transmitting force to the channel and triggering a net domain movement that opens the channel (Gillespie and Walker, 2001). In this model, the force vector is perpendicular to the membrane. A third model, intermediate between the two previous ones, is called the “elevator model” (Kung, 2005). In this model, the ion channels of the mechanoreceptor are attached to a single extracellular tether. The application of an external force leads to a net displacement of the channel with respect to the membrane, altering the exposure of side chains to the membrane lipids, which would lead to a modified conformation of the gates of the channel.

II.B. Interacting with the nervous system

II.B.1. History of the field of electrical stimulation

II.B.1.i. Early intuitions and foundational discoveries

The first reported case of electrical stimulation is two millennia old, and was provided by Scribonius Largus, a court physician to the Roman emperor Claudius. Antero, a freedman of Nero, was cured of the pains of gout by accidentally stepping on a torpedo fish (**Figure 7**) and receiving an electrical discharge from it. Subsequently, Scribonius recommended electroichthiotherapy for the treatment of a number of affections (Stillings, 1975).

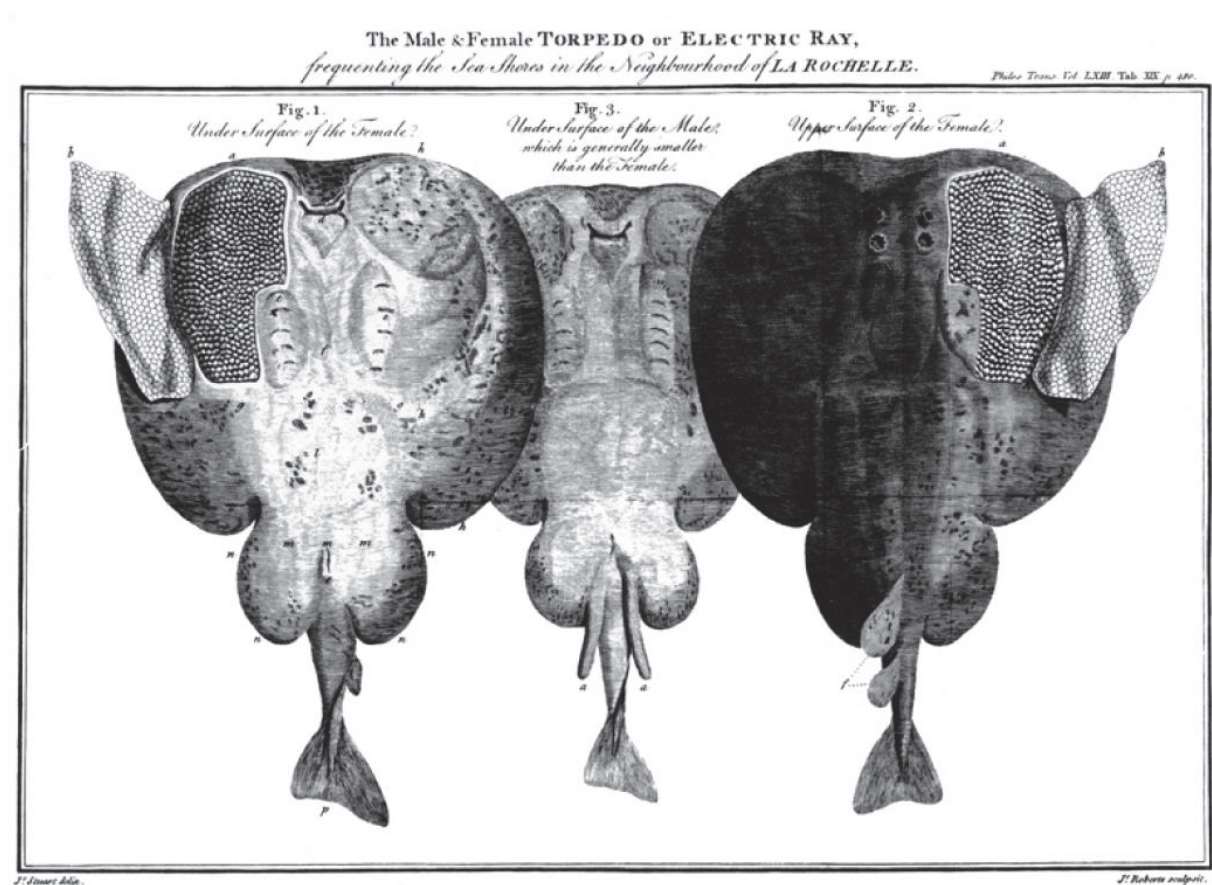


Figure 7 - Male and female Torpedo. From John Walsh, "Of the Electric Property of the Torpedo," *Philosophical Transactions* 63 (1773): 480.

In 1774, Benjamin Franklin noted muscle contraction on exposure to static electricity (Isaacson, 2003). In 1786, Luigi Galvani discovered that, if a piece of copper and a piece of zinc are put in contact with the nerves and the muscles of a frog's leg, respectively, their joining will lead to violent convulsions of the leg (**Figure 8**) (Galvani and Aldini, 1792). Galvani thought he had proved the existence of “animal electricity”, but was found to be wrong by Alessandro Volta, who, in his effort to demonstrate the actual biophysical phenomenon involved in Galvani's experiment, ended up inventing the first electrical battery. The biological galvanism - the contraction of a muscle under the effect of an electric stimulation - was at the basis of modern electrophysiology.

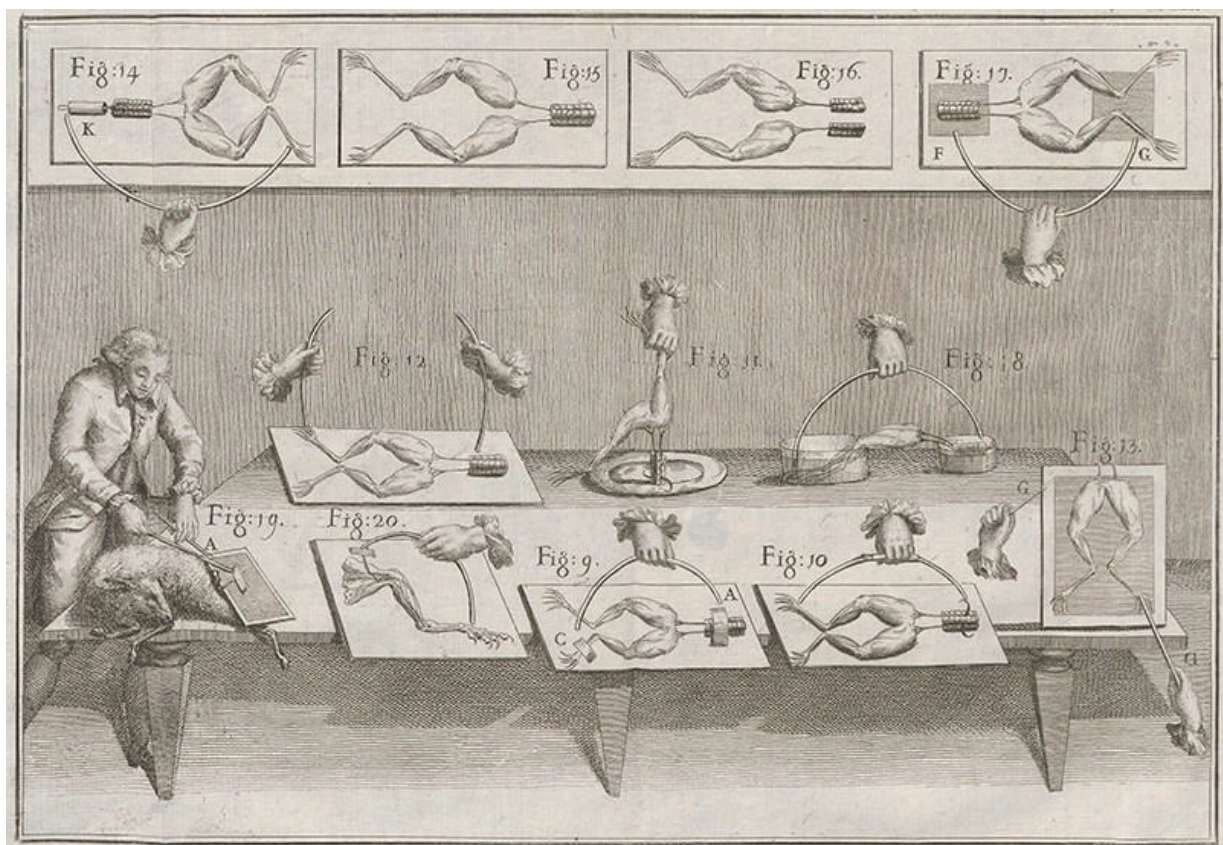


Figure 8 - Illustration of Italian physician Luigi Galvani's experiments, in which he applied electricity to frogs legs; from his book *De Viribus Electricitatis in Motu Musculari* (1792).

In 1803, while demonstrations of galvanism had become fashionable, Galvani's own nephew, Aldini, went so far as briefly 'reanimating' the dead body of a recently executed criminal by applying electrical shocks to it (**Figure 9**). This macabre experimentation was both polemic and inspirational, for some years later, in the introduction to her novel *Frankenstein*, Mary Shelley speculated on the therapeutic use of galvanism: 'Perhaps a corpse would be re-animated; galvanism had given token of such things: perhaps the component parts of a creature might be manufactured, brought together, and endued with vital warmth.' (Introduction to *Frankenstein; or, the modern Prometheus*, Mary Shelley, 1818).

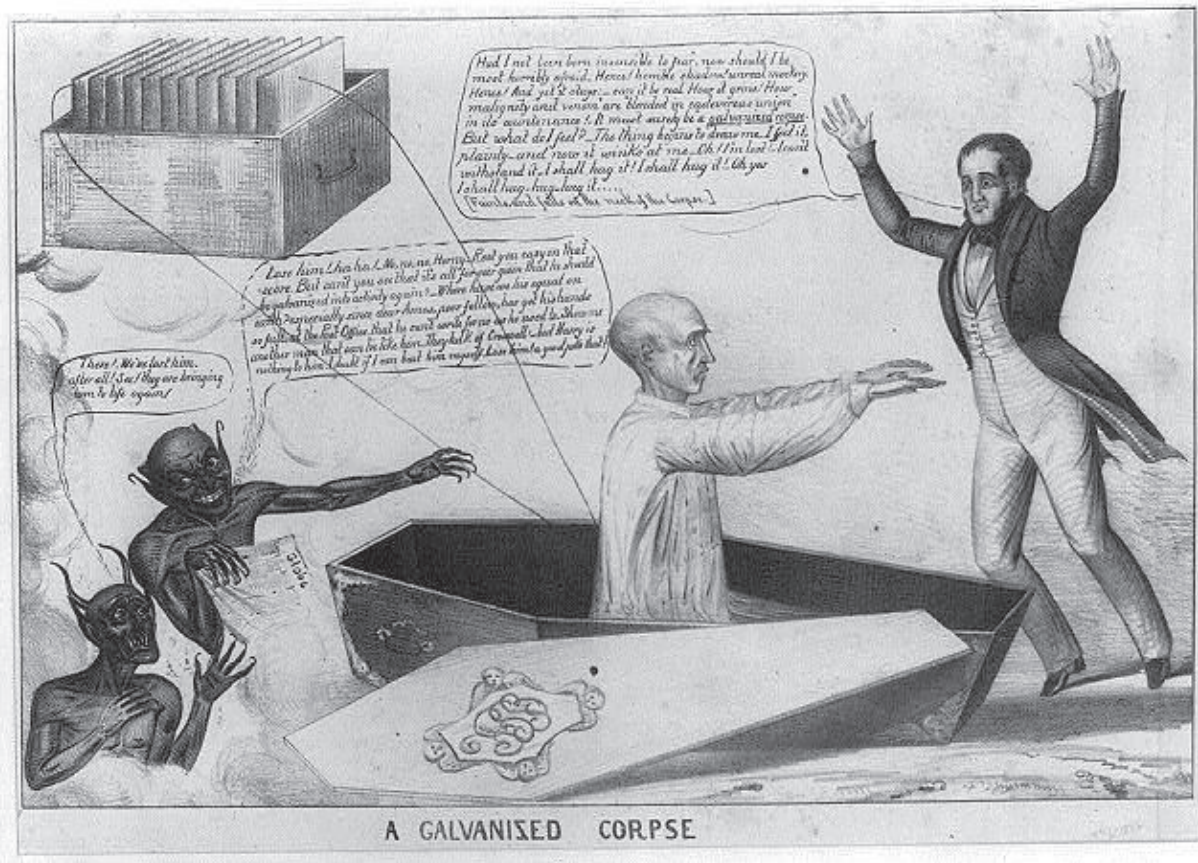


Figure 9 - A Galvanized corpse. Published in 1836, this cartoon depicts Galvani's nephew electrifying a criminal's corpse (*A galvanized corpse*, Printed and published by Henry R. Robinson in 1836, Library of Congress, Washington, D.C.)

Early in the 19th century, the investigation of the effects of electricity on animal bodies took a new turn, with the apparition of the first devices for the generation of faradic current. In

1824, Flourens was able to trigger motor response by electrically stimulating the brain stem of vertebrates, after motor cortex ablation (Flourens, 1842). He erroneously concluded that that cortex was not excitable, and that the brain stem was the center for motor control. It was not until 1870 that the excitability and actual role of the motor cortex was proven, when Fritsch and Hitzig demonstrated that limb movement occurred on stimulating the motor cortex of the dog (Fritsch, 1870).

In 1874, a patient was admitted by Dr. Roberts Bartholow in the Good Samaritan Hospital, in Cincinnati. In order to treat the purulent ulcer of the scalp the patient was afflicted with, Bartholow attempted a debridement and, by doing so, exposed the parietal area of the patient's brain. The physician stimulated the exposed cortex mechanically and then using a faradic current delivered by a device of his own making (**Figure 10**). Bartholow noticed muscle contraction in response to electrical stimulation (Bartholow, 1874). This was the first documented attempt of electrical stimulation of the human brain.

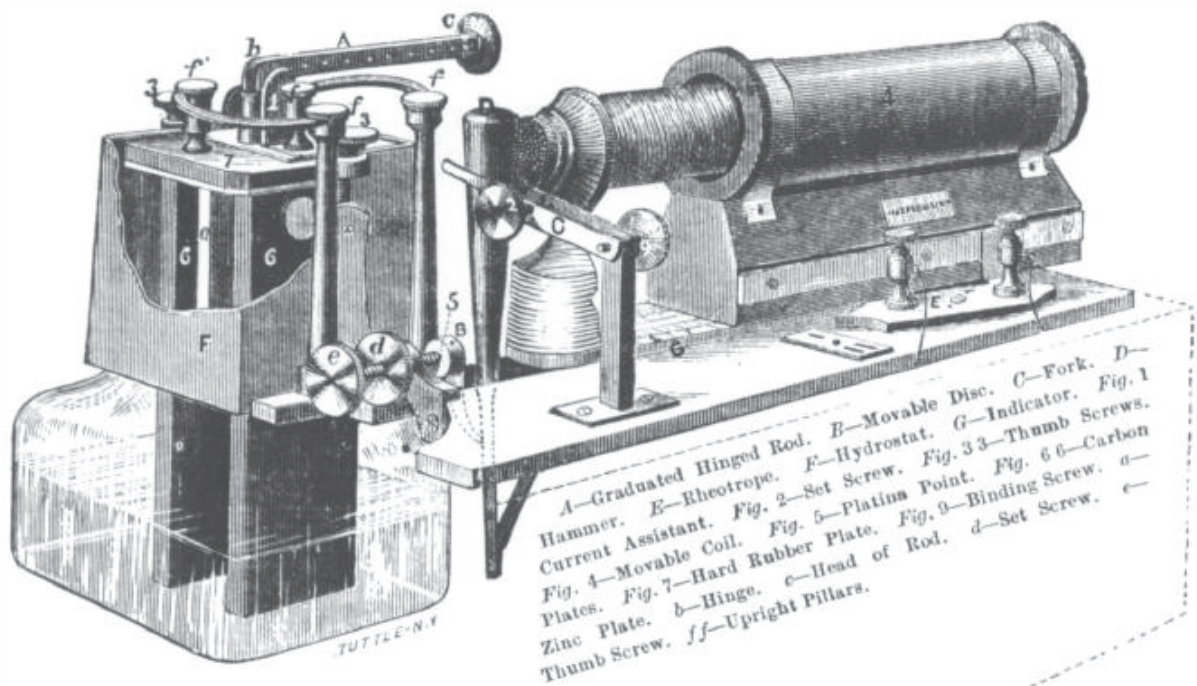


Figure 10 – Woodcut of Bartholow's faradic stimulation device (Morgan, 1982, from Bartholow, 'The electric room of the Good Samaritan Hospital', *The Clinic, Cincinn.*, 1872).

II.B.1.ii. Applications to functional neurosurgery

In 1884, Sir Victor Horsley was one of the first surgeons to rely on the physical response conjugated to an electrical stimulation (eye movements, thumb twitch) to identify specific brain areas prior to performing a resection (Vilensky and Gilman, 2002). The field of functional neurosurgery was born. Horsley refined his technic by developing, together with his colleague Clarke, the first animal stereotactic apparatus, which was described in their 1908 publication (Clarke, 1908). Some decades later, in 1947, Spiegel and colleagues described the first human stereotactic apparatus and a number of indications for their technique (Spiegel et al., 1947). As stereotactic surgery progressed, electrical stimulation started to be routinely used for intraoperative localization of the therapeutic target, but lesions remained the therapeutic modality. However, in the process of using it as a localization tool, some surgeons started to glimpse the therapeutic potential of the electrical stimulation of the brain. In 1960, Hassler et al. reported that electrical stimulation within the ventral intermediate nucleus of the thalamus (Vim) during stereotactic localization could induce cessation of tremor (Hassler et al., 1960). Another example was provided by Albert et al. in 1966, who documented that electrical stimulation in awake patients with Parkinson's disease or other dyskinesia could initiate, augment but also occasionally suppress tremor (Alberts et al., 1966).

II.B.1.iii. First attempts of therapeutic applications

The development of electrical stimulation as a therapeutic modality was limited for a time by the lack of solution to provide stimulation on an on-going basis. However, it did not prevent several clinicians to explore the possible therapeutic applications in fields ranging from psychiatry to pain alleviation, by inserting electrodes that were intermittently connected through the scalp of patients. One of the earliest of these attempts is due to Pool, in 1948, who stimulated frontal tracts as a form of psychosurgery (Pool, 1956). Shortly after, Olds and Milner demonstrated stimulation-seeking behavior in rats implanted with septal electrodes (Olds and Milner, 1954). The same year, building on this preclinical result and assuming that pleasure is the opposite of pain, Heath managed to alleviate the cancer pain of a patient in her remaining 7 months, by performing daily stimulation of the septal region (Heath, 1996). In

1972, Bechtereva and colleagues were the first to report the use of long-term stimulation to treat movement disorders. The therapeutic approach involved outpatient intermittent stimulation of electrodes implanted in the thalamus and globus pallidus (the method was reported in English in Bechtereva et al., 1975).

II.B.1.iv. Birth of the field of neuromodulation

In 1965, Melzack and Walls proposed a new theory to model pain mechanisms (Melzack and Wall, 1965). Their concept was that pain perception concerns a gate that is opened on stimulation of small nerves, associated with pain, and closed on stimulation of large nerves, associated with touch and proprioception. This would explain why we instinctively rub our skin to lessen a painful sensation. According to them, the same analgesic effect could be induced by selectively stimulating large fibers in peripheral nerves, using an appropriate voltage where sensation but no pain is felt (Gildenberg, 2005). This idea was one of the foundations of the field of pain management by neuromodulation and, together with the emergence of implantable stimulators, led to the development of the first spinal cord stimulators in the 70's (Shealy et al., 1967).

II.B.1.v. The path towards Deep Brain Stimulation

As we just mentioned, spinal cord stimulation was initially used for pain management. However, in 1976, Cook (Cook, 1976) and Dooley (Dooley et al., 1976) coincidentally observed, in patients who stimulators implanted for muscle pain, that spinal stimulation could also improve spasticity. The following year, the therapeutic effect was confirmed by Siegfried who treated spasticity in patients without pain (Siegfried, 1977). The natural next steps were to investigate chronic stimulation of the cerebellum and eventually of subcortical structures, which proved to be successful in the treatment of epilepsy (Cooper et al., 1976a), cerebral palsy (Cooper et al., 1976b) and chronic pain (Hosobuchi et al., 1973). **Deep Brain Stimulation (DBS) was born.**

II.B.2. Modern Deep Brain Stimulation

Deep Brain Stimulation (DBS) is a form of electric stimulation therapy involving the implantation of electrodes in the brain, which has shown notable benefits for patients with movement disorders, treatment-resistant affective disorders and chronic pain (Kringelbach et al., 2007).

II.B.2.i. Components

A typical DBS system is composed of one or several leads, a neurostimulator and an extension connecting the latter to the lead(s). The **lead** is an insulated wire with typically 4 electrodes at its tip (quadripolar lead), 1.5 mm wide and spaced 0.5 – 1.5 mm apart. The lead implantation requires a trepanation about 15 mm wide, and is either performed under local (Awake Microelectrode-guided DBS) or general anesthesia (Asleep Interventional-MRI-guided DBS). Under local anesthesia, patient feedback as well as recording of local brain activity with microelectrodes are necessary to identify the optimal position of the lead. Under general anesthesia, the positioning is guided by real-time MR imaging, and does not require a stereotaxic frame. The **neurostimulator** is a battery-powered implanted pulse generator (IPG), implanted subcutaneously below the collarbone or the abdomen. The extension is an insulated wire running subcutaneously behind the ear to the basis of the neck, to the neurostimulator. Both neurostimulator and extension are implanted under general anaesthesia. The lifetime of a non-rechargeable **IPG battery** depends on the manufacturer and the parameters of the therapeutic stimulation program. A 2011 study found that the mean lifetime of the Soletra IPG (Soletra Model 7426, Medtronic Inc., Minneapolis, MN, USA) was slightly over two years (Blahak et al., 2011). In contrast, rechargeable batteries, which use an external device transferring energy by low-intensity induction, are claimed to last up to 15 years by the manufacturer, Medtronic.

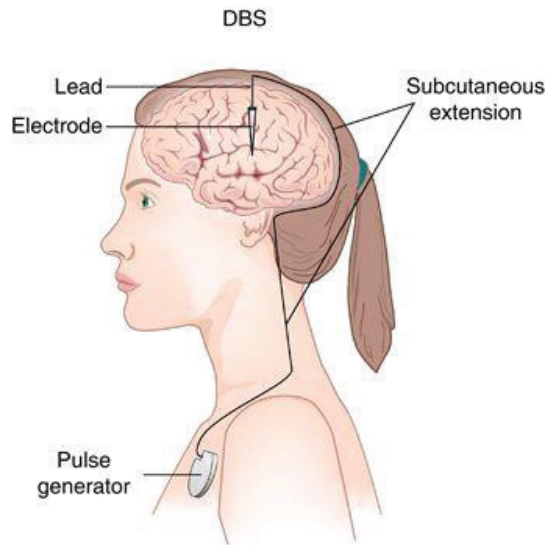


Figure 11 – Constitutive elements of a DBS device (Rosa and Lisanby, 2012).

II.B.2.ii. Therapeutic applications of DBS to movement disorders

DBS has been applied to a variety of movement disorders, but the most common indications for DBS, and FDA-approved, are essential tremor (ET), Parkinson’s disease (PD) and dystonia.

a. Essential tremor

Essential tremor is the most common movement disorder, with a prevalence of 4.0-5.6% in persons over 40 and as high as 9.0% in persons over 60 (Dogu et al., 2003; Louis et al., 1998; Rautakorpi et al., 1982). The tremor involves mainly the upper extremities, but can also affect the head, voice and lower extremities. A distinctive feature between ET and PD is that most patients with ET do not present a resting tremor. The severity of ET is objectively measure using different rating scales, and can be quickly assessed by asking the patient to draw spirales (**Figure 12**). The gold standard to treat ET is a pharmacological approach, involving mainly propranolol and primidone, which provide acceptable tremor control without side effects in only 50-70% of patients (Deuschl et al., 2011).

The historical and only FDA-approved target for DBS in ET is the Vim. Unilateral or bilateral stimulation of the Vim have shown 40-80% reduction of tremor severity in the long term. Bilateral stimulation can induce adverse effects, such as dysarthria, paresthesia and ataxia, in up to 30% of patients (Larson, 2014). Upwards of 15-20% patients show initial improvement before a loss of efficacy within the first year, and 10% do not show tremor reduction at all (Benabid et al., 1991; Favilla et al., 2012; Larson, 2014). Because of those limitations, a new therapeutic target has started to be investigated, the posterior subthalamic area (PSA). Some studies have shown that PSA stimulation provide a level of tremor reduction comparable or even superior to Vim stimulation, without the adverse effects and the loss of efficacy with time.

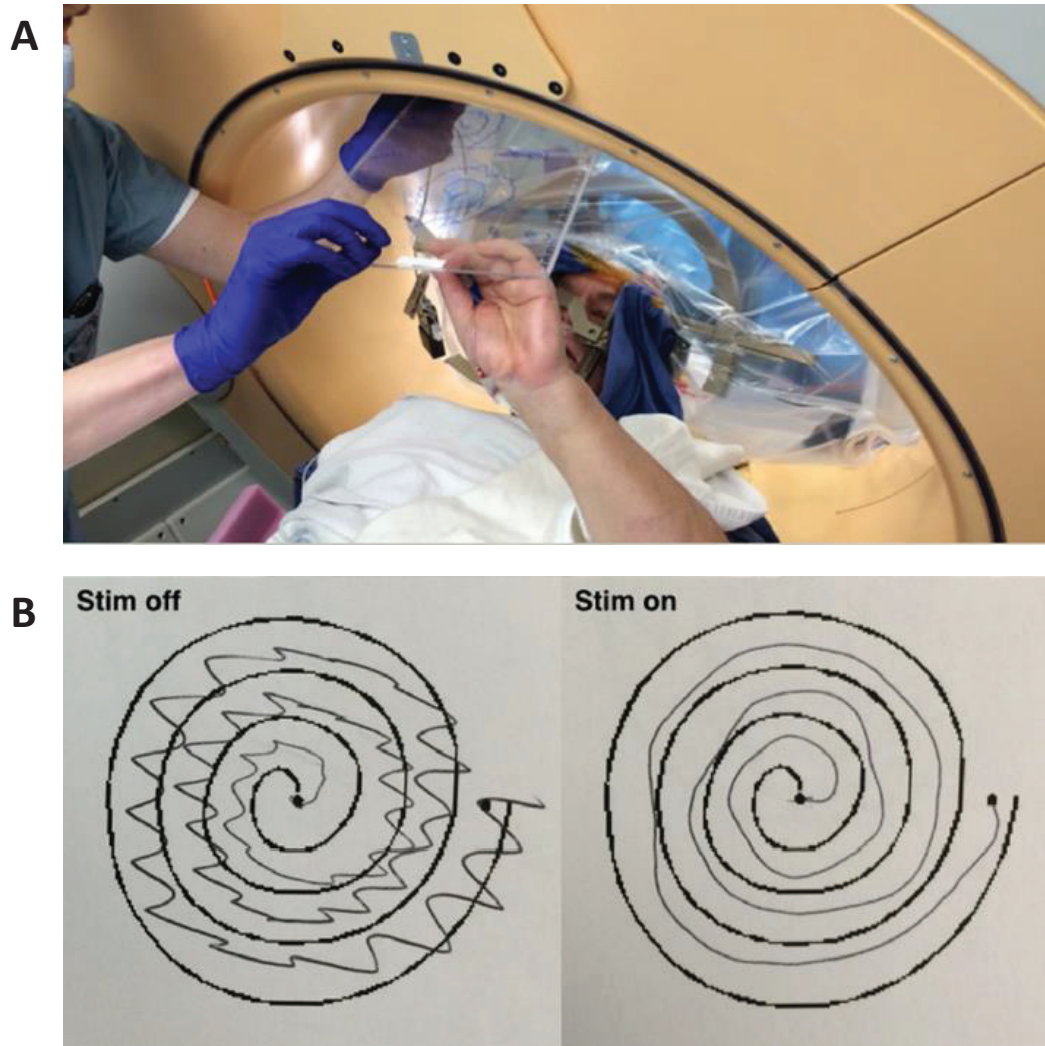


Figure 12 – Application of DBS to the treatment of essential tremor. (A) Stereotactic deep brain stimulation (DBS) implantation in an awake patient with essential tremor. The DBS lead has been placed into the right thalamus, and the patient is being asked to trace a spiral on a clipboard. (B) The ability of the patient to perform this task is compared with stimulation off and stimulation on, and the result is used, in part, to determine intraoperatively if the lead is appropriately placed in the thalamus (Larson, 2014).

b. Parkinson's disease

Parkinson's disease is the second most common degenerative disease, after Alzheimer's (Elbaz et al., 2016). Its prevalence is estimated at 1% in persons above 60, and increases with age (Tysnes and Storstein, 2017). Hence, due to the general aging of the population, the number of PD patients is expected to double by 2030 (Elbaz et al., 2016). The motor symptoms of PD results from a loss of dopaminergic neurons in the brain, and involves varying degree of tremor, rigidity, bradykinesia, akinesia and postural instability (Larson, 2014). The mainstay of treatment is pharmacological, with the primary goal of either elevating the level of dopamine or prolonging the action of the dopamine already present in the brain.

PD is the most common disorder treated with DBS. Most experts recommend DBS when PD patients start to experience complications due to the increasing amounts of medications needed to compensate the progression of the disease, which happens typically after 5-15 years of medical treatment (Larson, 2014). The main targets of DBS for PD are the subthalamic nucleus (STN) and globus pallidus (GPi), which equivalently improve the cardinal motor symptoms of PD (Follett et al., 2010; Larson, 2014). STN stimulation has been shown to be associated with a higher rate of cognitive worsening, but would allow higher medication reduction after surgery (Follett et al., 2010). In very elderly or cognitively borderline patients with tremor-dominant PD, Vim is generally considered a more reasonable therapeutic target, for it does not improve any PD symptoms aside from tremor, but is safer in terms of cognitive adverse effects.

c. Dystonia

Dystonia is a movement disorder characterized by abnormal and sustained muscle contractions, resulting in abnormal postures or repetitive movements. The initial treatment is pharmacological, combined with physical and occupational therapy (Jankovic, 2013). However, medication-induced adverse side effects are common. DBS is considered as an alternative treatment when medication is ineffective or not tolerated, and the degree of disability and disease burden is high enough to warrant surgical intervention (Larson, 2014). The main DBS targets for dystonia are the GPi and the STN, which both present specific

drawbacks. GPi stimulation may induce bradykinesia in previously asymptomatic body parts, and a delay of weeks to years before the stimulation shows its maximal clinical benefit (Berman et al., 2009; Zauber et al., 2009; Volkmann et al., 2012). STN stimulation may not induce bradykinesia, but other issues have been observed in some patients, such as transient dyskinesia and weight gain (Kleiner-Fisman et al., 2007; Ostrem et al., 2011; Pahapill and O'connell, 2010). Primary generalized dystonia, which is characterized by a lack of any identifiable cause, has been the most studied, and bilateral GPi stimulation has resulted in a 60-85% improvement in the Burk–Fahn–Marsden Dystonia Rating Scale, in open-label studies, and 40-50% improvement in prospective, double-blind randomized trials with 6-12 months follow-up (Vercueil et al., 2001; Cif et al., 2003; Coubes et al., 2004; Vidailhet et al., 2005; Kupsch et al., 2006; Valldeoriola et al., 2010).

II.B.2.iii. Therapeutic applications of DBS to non-movement disorders

Although psychotherapy and pharmacotherapy have been successfully applied to the treatment of affective disorders such as depression and obsessive-compulsive disorder, a number of patients with these conditions are still not aided by either intervention. In this area, DBS is still in the experimental stage, but promises to offer many advantages over other physically-invasive procedures as a treatment for these psychiatric disorders. In addition, over the last decades, different forms of DBS-based treatments of chronic pain have been investigated.

a. Obsessive-compulsive disorders

Obsessive-compulsive disorder (OCD) is characterized by the presence of recurrent and persistent thoughts, urges or images, which are experienced as intrusive and unwanted (obsessions) and/or repetitive behaviors or mental acts (compulsions) that an individual feels driven to perform in response to an obsession or according to rules that must be applied rigidly (Association, 2013). According to a nationally representative survey of US adults, OCD has a prevalence of 2.3% (Ruscio et al., 2010). OCD patients suffer from substantial dysfunctions in

social adjustment, employment, marriage, family relationships and socioeconomic status (Murray and Lopez, 1997). The mainstays of OCD treatment are behavioral and pharmacological therapy, but it is estimated that 10% of OCD patients are resistant to these forms of therapy and develop functional impairment (Denys, 2006). DBS has been proposed to this group of extremely disabled OCD patient, as a last-resort option and an alternative to stereotactic lesional neurosurgery. In 2015, Alonso et al provided a meta-analysis of the treatment outcome of DBS for OCD, including 31 studies and more than a hundred subjects (Alonso et al., 2015). That data they analyzed showed a global percentage of score reduction on the Yale-Brown Obsessive Compulsive Scale of 45%, and a global percentage of responders of 60%. According to these results, DBS would appear to have an efficacy comparable with that of ablative techniques, ranging from 56% to 64% (Ballantine et al., 1987; Mindus et al., 1994). At last, it is worth noting that some adverse effects were signaled, such as worsening of anxiety or mood disinhibition, but that, in almost all studies taken into account in the meta-analysis, they were described as mild, transient and reversible after the adjustment of the stimulation parameters.

b. Treatment-resistant depression

Major depressive disorder (MDD) is a widespread, severe disorder, characterized by various symptoms including depressed mood, hopelessness, neurovegetative symptoms, anxiety, apathy and cognitive deficits (Morishita et al., 2014). In some case, it can be life-threatening, when MDD patients present with delusions and suicidal ideation. In 2003, the lifetime prevalence of MDD was reported to be 16.2% (Kessler et al., 2003). Medication is considered to be commonly effective, but 20-30% of MDD patients are refractory to pharmacological therapy (Fava, 2003; Rush et al., 2006). Various surgical ablative therapies have been employed to treat patients who are refractory to noninvasive treatments. Although these surgical therapies have proved to be efficient in a number of cases, the studies lack of modern methodological approaches to objectively estimate their efficacy (Greenberg et al., 2003). The development of neuromodulation therapies such as DBS has enabled controlled studies with sham stimulation and offers potential therapeutic options which are both reversible and adjustable. In 2014, Morshita et al. provided a systemic review of the literature on DBS for

treatment-resistant depression (TRD), including 22 clinical research papers, with various therapeutic approaches and targets (Morishita et al., 2014). The response rate of DBS therapy was defined as the percentage of patients with more than 50% improvement on the Hamilton Depression Rating Scale. According to the review, this response rate was estimated at 40-70%. However, the authors expressed some reserves regarding the design of DBS for TRD studies, related to the low number of patients per trial, heterogeneity of inclusion criteria, and the potential role played by the placebo effect. Indeed, the majority of the studies included in their review were open-label trials, and the nature of mood disorders make the placebo effect all the more likely to influence the outcomes of such studies.

II.B.2.iv. Chronic pain

As presented section in II.B.1, DBS was initially developed to treat chronic pain. Over the last decades, applications of DBS to a variety of forms of chronic pain have been investigated, involving different therapeutic targets.

In 2003, the treatment of drug-resistant cluster headache by posterior thalamic stimulation was proved to safe and effective in a preliminary study involving 5 patients (Franzini et al., 2003). Alleviation of phantom limb pain by DBS targeting of the periventricular grey matter (PVG) and somatosensory thalamus was investigated in 3 patients in 2004 (Bittar et al., 2005), showing 62% pain reduction at follow-up (8-20 months). The same targets were investigated for the alleviation of post-stroke pain in 2005 (Owen et al., 2007), resulting in a 70% response rate and a wide variation of the pain score improvement amongst the 15 patients of the study. In 2006 was reported a retrospective analysis of long-term outcomes of DBS targeting of PVG and/or the ventrocaudalis thalamic nucleus in 21 patients, concluding in the relatively low efficacy of DBS for the treatment of neuropathic pain (Hamani et al., 2006).

Although most of the above mentioned studies are encouraging when taken individually, overall, the clinical data gathered so far are not sufficient to ensure the safety and efficacy of DBS as an alternative treatment for chronic pain. The available studies either suffer from too broad criteria of patient admission, or a too small number of patients when the admission in the study is more restrictive. In addition, the plurality of therapeutic targets investigated diminishes the relevance of meta-analyses. For these reasons, there is still no FDA approval for therapeutic

applications of DBS for chronic pain.

II.B.2.v. DBS-related complications

Some of the risks associated with DBS, specific to each therapeutic application, have already been mentioned. One of the adverse effects of some forms of DBS therapy for PD is the worsening of depression (Lakhan and Callaway, 2010). A case of acute transient depression was even reported in 1999, in a 65-year-old PD patient treated by bilateral subthalamic stimulation (Bejjani et al., 1999). The development of irreversible manic behavior (elation, inflated self-esteem, hyperactivity, logorrhea, sexual indiscretion, and insomnia) following bilateral implantation of electrodes has also been observed in 3 patients of a 15-patients panel treated for PD, which was attributed to a misplacement of the electrodes (Kulisevsky et al., 2002).

In addition to these stimulation-induced adverse effects, there are risks associated with the stereotactic procedure itself. In particular, 2-2.5% of DBS implants leads to intracranial bleeding (Kringelbach et al., 2007). At last, hardware-related complications include dislocation, lead fracture and infection, the latter requesting in some cases to explant the stimulator (Hariz, 2002).

II.B.3. Non-invasive neurostimulation technics

II.B.3.i. Transcranial magnetic stimulation

Transcranial magnetic stimulation (TMS) is a non-invasive neurostimulation procedure based on the action of electric currents in the brain created by electromagnetic induction. A TMS device is compound of a pulse generator and a magnetic field generator, more simply called a coil. Fed by an alternate current, the coil generates an alternate magnetic field, which will create an electric field according to Faraday's law of induction, which will in turn create electric currents in the brain called eddy currents. Eddy currents turn in close loop in a small regions of the brain, but their path is difficult to control, as they are not conducted uniformly in nervous tissues.

As a diagnostic tool, TMS is used to assess the neurological damages after various diseases, particularly linked to sensorimotor dysfunction (Groppa et al., 2012). For example, TMS can be used to stimulate a specific zone of the motor cortex and evaluate the integrity of the motor pathway leading to the activation of the corresponding muscle or group of muscles.

As a therapeutic tool, repetitive transcranial magnetic stimulation (rTMS) has showed promising analgesic effects and antidepressant effects when applied to the treatment of certain forms of neuropathic pain and major depressive disorder, respectively (Lefaucheur et al., 2014).

Adverse effects associated with TMS are rare, although it can be notice that therapeutic applications present a higher risk than diagnostic ones (Rossi et al., 2009).

Classical coil geometries (round-shaped, butterfly-shaped) enable the activation of cortical neurons at a depth of 1.5-3 cm. More recently developed geometries allow the targeting of deeper brain structures, up to 6-cm deep, but are less focal.

II.B.3.ii. Transcranial Direct Current Stimulation

In the recent years, Transcranial Direct Current Stimulation (tDCS) has emerged as a promising technic to modulate cognitive and motor skills (Nitsche and Paulus, 2000), which is becoming more and more popular and well-documented (Thair et al., 2017). This technic consists in emitting a weak electrical current through the brain, using surface electrodes placed on the scalp. Traditionally, only two electrodes are required: the target electrode, placed above the region of interest, and a reference electrode. The reference electrode is either placed on an extracephalic region of the body such as the upper arm (unihemispheric stimulation) or on the other hemisphere of the brain, to perform dual stimulation to two parallel cortices (Benwell et al., 2015). More recent tDCS configurations involve multiple electrodes, such as one anode surrounded by a ring of cathodes, and have been shown to enhance spatial resolution (DaSilva et al., 2015; Villamar et al., 2013). Target(s) electrode(s) can either be anodes or cathodes, depending on the intended functional effect. Indeed, it is generally assumed that a positive anodal current depolarizes the neuron membranes, increasing the probability of action potentials firing, and hence facilitating the function associated with the cortical region situated underneath the target electrode. As an example of this facilitating effect, tDCS has been shown to improve delays of syntax acquisition in autism spectrum disorder (Schneider and Hopp,

2011). Symmetrically, a negative cathodal current will have an inhibiting effect on the function associated with the targeted cortical region. For instance, tDSC has been successfully applied to reduce symptoms of depression (Fregni et al., 2006; Nitsche et al., 2009) and hallucinations in people with schizophrenia (Agarwal et al., 2013). With the use of current amplitude within the safety range ($< 2\text{mA}$), tDSC has been reported to be associated with no serious adverse effects (Arul-Anandam et al., 2009). The main limitation of tDSC is that it only elicits the stimulation of brain cortex and not deeper structures such as the hypothalamus.

III. Focused ultrasound: a new modality of neurostimulation

III.A. Ultrasound: a mechanical wave

III.A.1. Terminology

In mechanics, a **perturbation** is defined as any local variation of a mechanical property (position, speed, pressure, energy) in a material medium.

A **mechanical wave** is the propagation of a perturbation through a material medium without material transport. The points of the medium crossed by a mechanical wave oscillate around an equilibrium position but their net displacement is null. A mechanical wave transports energy, in the same direction as it propagates.

Sound waves, or **acoustic waves**, are an example of mechanical waves, propagating through a medium. Specifically, sound waves are **longitudinal mechanic waves**. A longitudinal wave is a wave in which particles of the medium move in a direction parallel to the direction of wave propagation (unlike transverse waves, in which particles move perpendicularly to the direction of propagation). During the propagation of a sound wave in a fluid medium, because of the longitudinal motion of the particles, there are regions where the particles are compressed together (compression region) and region where the particles are spread apart (rarefaction regions). Hence, since a sound wave is associated with a repeating pattern of high and low pressures, it can be characterized as a **pressure wave**.

Ultrasound waves are sound waves whose frequency is greater than 20 kHz. This

threshold corresponds to the upper audible limit of human hearing (although this value is person- and age-dependent).

III.A.2. Physical definition of a sound wave

The velocity potential of longitudinal mechanical wave is defined by the following equation (Cobbold, 2006):

$$v_L = -grad(\phi(M, t)) \quad (1)$$

Where:

- v_L is the longitudinal velocity of the wave,
- $\phi(M, t)$ is the speed potential at point $M(x, y, z)$ and instant t .

Considering a monochromatic progressive wave, the projection of the speed potential with respect to the axis of wave propagation (z axis), $\phi_n(M, t)$, is defined by the following equation:

$$\phi_n(M, t) = \frac{\partial \phi(M, t)}{\partial n} = V_0 e^{-j(\omega t - kz)} \quad (2)$$

Where:

- n is the normal to the source surface,
- V_0 is the maximal speed amplitude with respect to the z axis (m.s^{-1}),
- ω is the pulsation (rad.s^{-1}),
- k is the wave number (m.s^{-1}).

The wave number k is defined by the ratio between the pulsation ω and wave celerity c (m.s^{-1}):

$$k = \frac{\omega}{c} \quad (3)$$

From there, it is possible to define the speed potential generated by a point $M'(x', y', z')$ of the vibrating source at a point $M(x, y, z)$ of the space:

$$d\phi(M, t) = \phi_n(M', t) \frac{e^{j\frac{\omega}{c}r'}}{r'} K dS \quad (4)$$

Where:

- r' is the distance between points M and M' ,
- K is source-dependent factor.

According the Huygens-Fresnel principle, the sum of the contributions of each punctual source M' of the vibrating source is equal to the speed amplitude generated at point M :

$$\phi(M, t) = \iint_S \phi_n(M', t) \frac{e^{j\frac{\omega}{c}r'}}{r'} K dS \quad (5)$$

When considering the case of disc-shaped plane vibrating source, equation (5) can be written:

$$\phi(M, t) = \frac{1}{2\pi} \iint_S \frac{\partial \phi(M', t)}{\partial n} \frac{e^{j\frac{\omega}{c}r'}}{r'} dS \quad (6)$$

The instant pressure produced by a vibrating source at a point M of the space is defined by the equation:

$$P(M, t) = \rho \frac{\partial \phi(M, t)}{\partial t} \quad (7)$$

Where:

- $P(M, t)$ is the instant pressure amplitude (Pa),
- ρ is the medium volumetric mass density, at the equilibrium ($\text{kg}\cdot\text{m}^{-3}$).

The second Newton law applied to a volume element compressed by the mechanic wave gives a relationship between the pressure and normal speed v_n (m.s⁻¹):

$$\rho \frac{\partial v_n(M, t)}{\partial t} + \frac{\partial P(M, t)}{\partial n} = 0 \quad (8)$$

From equations (7) and (8) can be deduced:

$$v_n(M, t) = - \frac{\partial \phi(M, t)}{\partial n} \quad (9)$$

When substituting equation (9) in equation (6), the resulting equation takes the form known as the Rayleigh integral:

$$\phi(M, t) = \frac{1}{2\pi} \iint_S \frac{v_n(M', t - \frac{r'}{c})}{r'} dS \quad (10)$$

Finally, from the Rayleigh integral, we can deduce the pressure field generated by a vibrating source:

$$P(M, t) = \frac{\rho}{2\pi} \iint_S \frac{1}{r'} \frac{\partial v_n(M', t - \frac{r'}{c})}{\partial t} dS \quad (11)$$

These equations are valid in the case of plane surface sources. However, it has been demonstrated that they could be used as approximations for curve surface sources, when the curvature was low enough and the source diameter high enough relatively to the wavelength (O'Neil, 1949).

III.A.3. How to produce ultrasound ?

In nature, some species can produce ultrasound, such as dolphins and bats, and use them as a way to locate themselves in space as well as potential preys – a process known as echolocation. Humans cannot naturally produce, but came up with different technologies to do so. Whether they are produced by living beings or human-made devices, ultrasound requires a **vibrating source** to be produced. A device converting a given source of energy into ultrasound waves is called an **ultrasound transducer**.

III.A.3.i. The piezoelectric transducer

The most widespread technology to design US transducer relies on the **piezoelectric materials**. When submitted to a mechanical strain, the crystallographic structure of a piezoelectric material is deformed in such a way that it presents a global electrical charge. This effect, named direct piezoelectricity, was first demonstrated by Pierre and Jacques Curie in 1880 (Curie and Curie, 1880). One year later, on the basis of thermodynamics considerations, Gabriel Lippmann predicted the existence of a reciprocal effect (Lippmann, 1881), which was proven by the Curie brothers shortly after (Curie and Curie, 1881). This effect, referred to as inverse piezoelectricity, reflects the fact that if a piezoelectric material is submitted to an electrical strain, its crystallographic structure will be deformed. Since their discoveries, both these effects have been used to design high-precision sensors, timing devices and, acoustic waves sources.

Amongst piezoelectric materials, **natural crystals** such as quartz are characterized by a relatively low ability to convert electrical energy into mechanical energy. For example, the electromechanical coupling coefficient (ECC) of quartz is about 10 %. Thus, **synthetic crystals** have been designed to increase this coefficient. Polymers are associated with a higher ECC than natural crystals (*e.g.* 14 % for the polyvinylidene fluoride, or PVDF). Piezoelectric **ceramics** such as Lead zirconate titanate (PZT) were introduced in 1954, and quickly became the gold standard for transducer fabrication due to their relatively high ECC, ranging from 40 to 70 % (Malhis, 2002). In the 70's, piezoelectric **composite** materials emerged. This type of material, more simply referred to as piezocomposites, combines a piezoelectric ceramic with a

non-piezoelectric polymer. Compared to piezoelectric ceramics, piezocomposites present several advantages. Firstly, the flexibility of the polymer matrix allows for shaping the material into focused transducers. Secondly, because of the division of the piezoelectric material into elementary pieces, parasite vibrations are reduced, leading to a better ECC than a bulk ceramic built from the same material. Finally, piezocomposites have an acoustic impedance closer to that of usual propagating media (gel, water, biological tissues) which reduces the level of refracted energy. However, there is a major drawback associated with piezocomposites: heating. Indeed, when used at high power, this type of transducer will generate more electric and mechanical losses than ceramic-based transducers, which can lead to irreversible damages of the device. Hence, piezocomposite transducing devices need to be used in association with a **cooling system**, and their casing built from heat conducting materials.

III.A.3.ii. Next generations of US transducers

The limitations associated with the standard piezoelectric technologies – limited miniaturization capability, limited working frequency range, large self-heating – impose constraints on the design of ultrasound devices for therapy. Capacitive micromachining US transducers, or **CMUTs**, have been investigated for more than 2 decades (Haller and Khuri-Yakub, 1996; Jin et al., 1999; Oralkan et al., 2002; Degertekin et al., 2006; Sako et al., 2009; Khuri-Yakub and Oralkan, 2011; Zhao et al., 2015), and present several advantages making them competitive with conventional piezoelectric transducing technologies. Firstly, the MEMs-based fabrication process and low fabrication cost at the industrial scale allow for a relatively **easy miniaturization** (micrometer-scale cell size). Secondly, the mechanical impedance of the thin vibrating CMUT cells confer to the CMUT elements a total radiation impedance much smaller than the acoustic impedance of water, giving this technology a potential for **high electroacoustic efficiency**. Thirdly, CMUT have an inherently **broad frequency bandwidth**, higher than several megahertz. Finally, silicon and silicon dioxide used in CMUT structure are level II MRI compatible and create no appreciable artifact, allowing for the design of **MRI-compatible** CMUT-based devices, which could allow real-time MRI-monitoring of US treatments but also the possibility of imaging permanent implants. Because of all the aforementioned characteristics, the CMUT technology could be of great interest for developing

new generations of devices for high-intensity US therapy, as confirmed by several feasibility studies (Wong et al., 2008, 2010; N'Djin et al., 2017).

III.A.3.iii. The different geometries of US transducers

Depending on the targeted application, different geometries of ultrasound transducers are currently available. **Diverging transducers** present the shape of a cylinder, a hemi-cylinder or a sphere, while **plan transducers** are generally rectangular-shaped. As far as therapeutic applications are concerned, these kinds of transducer are mostly used for interstitial (Lafon et al., 1999; Makin et al., 2005; N'Djin et al., 2012) and intraluminal treatments (Prat et al., 1997; Melodelima et al., 2008).

Focused transducers are the most commonly-used form of US transducer. They enable the implementation of the High-Intensity Focused Ultrasound (HIFU) therapy, which will be presented in section. Geometric focalization can be due to the shape of the transducer (spherical, toric or cylindrical), but can also be achieved using acoustic lenses combined with plane transducer, or reflectors combined with cylindrical transducers. It allows for concentrating energy in a relatively small volume element. In the case of a spherical transducer, the focal spot has an elliptic shape whose dimensions can be calculated as follows (Fry and Dunn, 1962) (**Figure 13**):

$$D_x = D_y = k_t \lambda \frac{z_0}{2a} \quad (12)$$

$$D_z = k_a D_y \quad (13)$$

Where:

- D_x , D_y , and D_z are the focal spot dimensions,
- a is the transducer radius,
- z_0 is the distance between the transducer border and the geometrical focal point of the transducer (see **Figure 13**),
- λ is the wavelength of the US wave,
- k_t and k_a are non-dimensional factors depending of the outer aperture 'half-

angle' α ; if $\alpha < 50^\circ$ then $k_t = 1$ and $k_a = 15(1 - 0.001\alpha)$

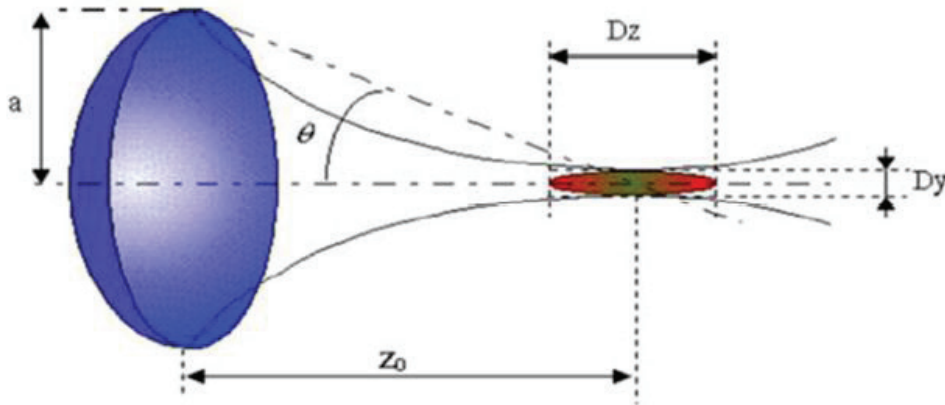


Figure 13 – Geometry of the focal spot generated by a spherical transducer.

One of the advantages of mono-element transducer is their relatively low cost of fabrication, but their main drawback is that they need to be mechanically displaced to treat large volumes. In the context of high temperature ultrasound therapy, this can be a problem, for such mechanical displacements increase the treatment duration and can bring inaccuracies in the targeting (Damianou and Hynynen, 1993). Multi-element transducers are transducer whose active part is divided into multiple elements. Each element can be controlled independently from the other, using an appropriate electronic driving signal. By applying phase differences to the elements, it is possible de electronically focus the ultrasound beam and thus steering the focal spot without movement form the manipulator (Fjield et al., 1996; Wan et al., 1996).

III.B. Interactions of US with biological tissues and related therapeutic applications

Biophysical mechanisms underlying the effects produced by ultrasound on biological tissues are commonly divided in two categories: thermal and non-thermal effect. However, it is often extremely difficult to identify the mechanisms responsible for producing a given biological change, and to isolate thermal from non-thermal contributions (ter Haar, 1999, p. 19).

III.B.1. Attenuation and thermal effects

As it passes through biological tissue, the energy carried by an ultrasound wave is attenuated, due to ultrasound absorption and scattering of the tissue. Ultrasound absorption is due to the viscosity of the medium opposing itself to the oscillating motion of the particles, which creates friction forces. The energy lost because of these elastic frictions is locally converted into heat. Ultrasound scattering is caused by small particles of the medium, reflecting, refracting or diffusing the ultrasound wave. Three types of scattering can occur, depending on the scale ratio between the particle size and the wavelength. If the particle is small relatively to the wavelength, the wave is diffused in every direction. If particle size and wavelength share the same order of magnitude, diffusion is anterograde. And at last, if the particle is large relatively to the wavelength, retro-diffusion occurs. Regardless of the types of diffusion involved, all the ultrasound scattered energy is eventually absorbed and contribute to the temperature rise in the medium. For this reason, when considering the ultrasound propagation in biological media, attenuation is often assimilated to the sole parameter of absorption.

When an ultrasound waves passes through an attenuating medium, its amplitude decreases according to the following equation:

$$P_{att}(M, t) = P(M, t)e^{-\alpha h} \quad (14)$$

Where:

- $P_{att}(M, t)$ is the amplitude of the attenuated pressure wave (Pa),
- $P(M, t)$ is the amplitude of the non-attenuated pressure wave (Pa),
- α is the attenuation coefficient in pressure of the medium (m^{-1}),
- h is the distance travelled by the wave in the medium (m).

The acoustic attenuation can also be expressed in function of the acoustic intensity of the ultrasound beam:

$$I_{att} = I e^{-\mu h} \quad \text{with} \quad I_{att} = \frac{1}{2} \frac{P_{att}^2}{Z} \quad (15)$$

Where:

- I_{att} is the surface intensity of the ultrasound beam (W.m^{-2}),
- I is the surface intensity at the source (W. m^{-2}),
- μ is the attenuation coefficient in intensity of the medium (m^{-1}).

Hence, the attenuation coefficients in pressure and intensity are linked as follows:

$$\mu = 2\alpha \quad (16)$$

In literature, attenuation coefficients are generally expressed under a logarithmic form:

$$\alpha_{dB} = 20\alpha \cdot \log(e) \approx 8.686\alpha \quad (17)$$

$$\mu_{dB} = 20\mu \cdot \log(e) \approx 8.686\mu \quad (18)$$

With α_{dB} and μ_{dB} in dB.m^{-1} . The local heat input brought to the attenuating medium by the ultrasound wave is expressed as follows:

$$Q = \mu I_{att} \quad (19)$$

Where Q is the heat amount per volume unit (W.m^{-3}). In water, the wave attenuation is almost null, but in biological tissues it cannot be neglected. The acoustic attenuation coefficient depends on the nature of the tissue, and varies with the wave frequency according to a non-linear relationship:

$$\alpha(f) = a f^b \quad (20)$$

Where:

- a is the attenuation of the wave at 1 MHz ($\text{m}^{-1}.\text{MHz}$)
- b is the non-linearity coefficient.

For most biological tissues, b is close to 1, and does not depend on the acoustic intensity as long as the propagation regime of the wave is linear. If not, a correcting factor must be applied.

III.B.2. Cavitation and mechanical effects

Acoustic cavitation is defined as the creation or the activity of gas bubbles in a liquid medium when exposed to the variable pressure of an acoustic wave (Fry et al., 1950). As acoustic waves are pressure waves, peak negative pressure can initiate cavitation, depending on the surface tension and vapor pressure of the liquid. Gas bubbles can either be already present in the medium (e.g. contrast agents, gas bubbles trapped in the medium) or created by acoustic pressure itself, given that the peak negative pressure is high enough. Once created, the bubbles exposed to an acoustic field will oscillate around an equilibrium radius. The oscillation amplitude of a bubble is maximal if the bubble is exposed at its resonance frequency, which is dependent of the initial radius of the bubble. According to the oscillating behavior of the bubbles, two cavitation regimens can be distinguished: stable cavitation and inertial cavitation.

When the bubble oscillates over several cycles before collapsing, and their radius do not exceed twice the equilibrium radius, it is described as **stable cavitation** (Flynn, 1964). Stable cavitation occurs when the acoustic intensity is relatively low. In this regimen, bubbles oscillate at a resonance frequency given by the following equation:

$$f_{bulles} = \frac{1}{2\pi R_b} \sqrt{\frac{3\gamma}{\rho} \left(P_0 + 2 \frac{\sigma}{R_b} \right)} \quad (21)$$

Where:

- f_{bulles} is the resonance frequency of the cavitation bubbles (Hz),
- R_b is the bubble radius,
- γ is the ration of the gas specific heats,
- P_0 is the hydrostatic pressure (Pa),
- σ is the surface tension ($\text{N}\cdot\text{m}^{-1}$),
- ρ is the medium volumetric mass density ($\text{kg}\cdot\text{m}^{-3}$).

The phenomenon of cavitation will only affect the bubbles whose radius is associated with a frequency close to the frequency of the acoustic wave. Hence, if the wave frequency is increased, the radius of the bubbles involved in the phenomenon of cavitation will decrease (Wells, 1977).

The oscillation of bubbles in a stable regimen is associated with a variety of physical phenomena such as heat production, micro-streaming of fluid near the bubble, and localized shear stresses. The latter two phenomena have been found to be at the basis of some mechanisms of actions by which ultrasound from transient pores in the cell membrane (sonoporation), as illustrated in **Figure 14.A** and **Figure 14.B** (Wrenn et al., 2012). Bubbles can also interact with each other, coalesce or interact with nearby particles and attract them.

At sufficiently high pressure amplitudes ($>700 \text{ W.cm}^{-2}.\text{MHz}^{-1}$) (Hynynen, 1991), the bubble may expand to a radius higher than twice its initial radius, and then collapse during the compression phase. This regimen is defined as **inertial cavitation**. Several interesting phenomena are associated with the bubble collapse occurring during inertial cavitation. Firstly, if the bubble collapse near a solid surface, this collapse will be asymmetrical and induce liquid microjets which have significant effects on the neighboring surface. This effect is at the basis of certain mechanisms of sonoporation (**Figure 14.C**). Microjets, along with the supersonic shock wave generated during inertial collapse, also play an important role in the fragmentation of kidney stones (lithotripsy) (Chaussy and Schmiedt, 1984). Secondly, during the collapse, temperature within the bubble reaches extremely high values, due to extreme compression of the inner gas (adiabatic heating). Some models predict maximum collapse temperatures exceeding thousands of degrees Kelvin (Flynn, 1964, 1982), which can lead to the creation of plasma within the bubble (sonoluminescence) (Walton and Reynolds, 1984). Finally, collapse temperatures and pressure can cause the formation of free radicals in the medium, which can be employed to generate chemical species or drive chemical reactions (sonochemistry) (Riesz and Kondo, 1992).

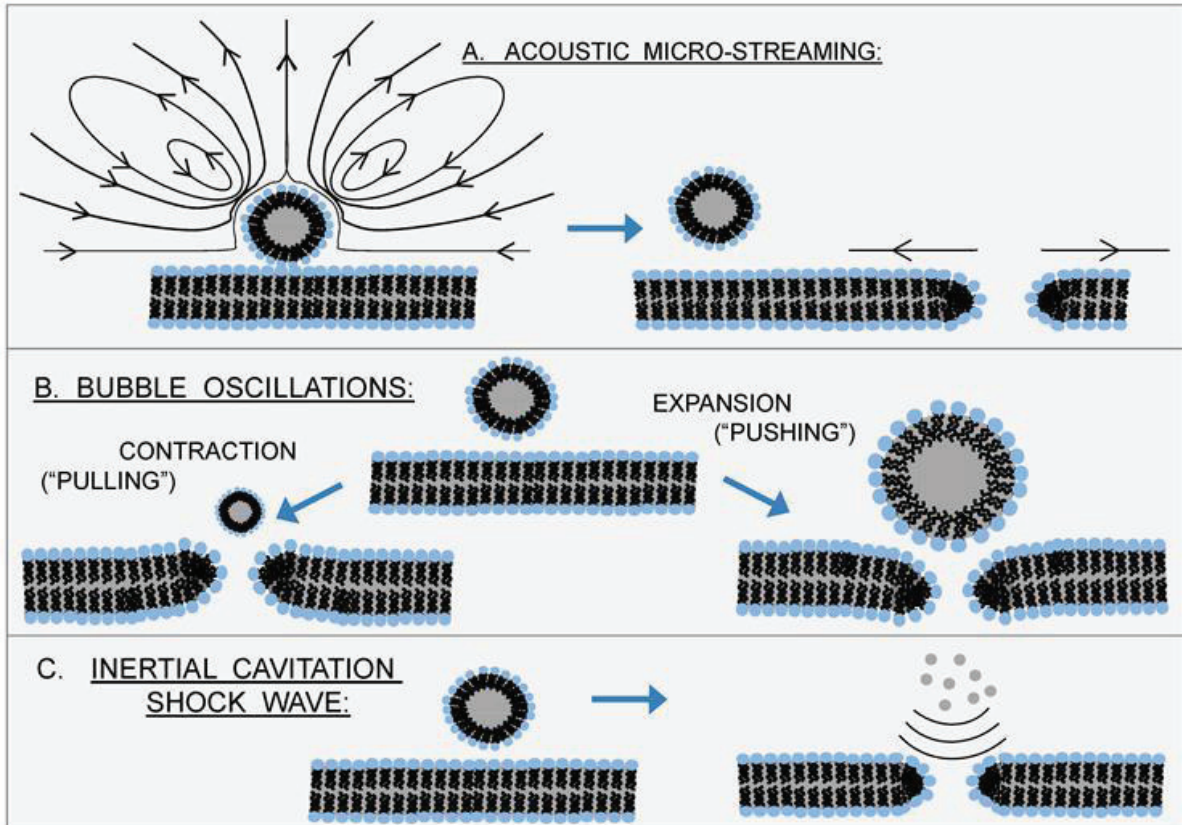


Figure 14 – Sonoporation mechanisms involving microbubbles. Sonoporation usually involves exogenous microbubbles in close proximity to cells, and the mechanism of action is believed to involve various phenomena, including: (A) acoustic streaming associated with stable cavitation; (B) bubble-cell membrane interactions arising from bubble oscillations; (C) shock waves generated by inertial cavitation (Wrenn et al., 2012, from Delalande et al., 2011).

III.B.3. Main developments of therapeutic US using thermal mechanisms: thermal ablation of localized cancer

III.B.3.i. Presentation of HIFU

High Intensity Focused Ultrasound (HIFU), alternatively referenced to as Focused Ultrasound Surgery (FUS), designs a set of therapeutic techniques sharing the same approach: concentrating ultrasound energy, and hence its associated bio-effects, in order to induce irreversible damages in a focal area without affecting the surrounding tissues.

The first description of HIFU was made by Lynn et al. in 1942 (Lynn et al., 1942). However, except for some ophthalmological applications, this therapeutic approach was not clinically investigated until the early 90s. The respective progresses made these last decades in the fields of ultrasound transducer design and medical imaging are the reasons behind this regain of interest. They provided the technological tools to fully express the possibilities offered by HIFU, by allowing pre-treatment planning, precise targeting and real-time treatment monitoring. Today, medical fields where HIFU treatments are used in routine or currently under clinical investigation include oncology, urology, gynecology and neurology.

III.B.3.ii. Application of HIFU to cancer treatment

In its Dictionary of Cancer Terms, the National Cancer Institute (NCI) defines hyperthermia therapy as “a type of treatment in which body tissue is exposed to high temperatures to damage and kill cancer cells or to make cancer cells more sensitive to the effects of radiation and certain anticancer drugs”. Hence, HIFU represent an interesting media to implement high-temperature ($>50^{\circ}\text{C}$) hyperthermia treatment, as they allow delivering acoustic energy, and its associated thermic bio-effects, in a localized area, without affecting the surrounding tissues. Choosing the appropriate acoustic parameters, it is possible to generate a temperature rise high enough to reach coagulation necrosis in tumor tissues. The eligible targets for HIFU hyperthermia treatments are conditioned by ultrasound properties of propagation in biological tissues, and by the tumor configuration and environment. Because the higher the harmonic frequency, the smaller the focal area, and the more attenuated the ultrasound wave, a compromise must be reached between the targeting precision and the depth of penetration. In addition, ultrasound does not propagate well through bones and gas. For these reasons, HIFU were investigated as a priority for the ablation of deep-sited soft tissue tumors, such as those associated with prostate, liver, uterus, kidney and breast. However, emerging strategies and technologies are designed to bypass the acoustic barriers represented by bones (e.g. skull, rib cage), or gas pocket (e.g. lungs, stomach), expanding the range of possible targets for HIFU treatments.

III.B.4. Main development of therapeutic US using mechanical effects

III.B.4.i. Kidney stones

Kidney stones disease, also known as urolithiasis, refers to the presence of hard pieces of material at some level in the urinary tract (kidneys, ureter or bladder). These stones, also referred to as renal calculus or nephrolith, typically form within the kidney, and can be constituted of either calcium, uric acid, struvite or cystine. According to NIH, approximately 11% of men and 6% of women in the United States have kidney stones at least once during their lifetime. Having kidney stones is not a life-threatening condition, but, if they are not treated, they can lead to several complications in the mid-term (?) such as pain, hematuria (blood in the urine), severe pain, kidney infection and loss of kidney function (Litwin et al., 2005).

III.B.4.ii. Treatment of kidney stones

In the past 30 years, urological treatment of kidney stones disease has considerably changed. Various treatment options are available today: ureteroscopic lithotripsy, extracorporeal shock wave lithotripsy, laparoscopic lithotomy, and percutaneous nephrolithotomy.

Historically, the first intracorporeal treatment option was electrohydraulic lithotripsy (EHL) (Smith, 2007). In EHL, stone fragmentation is achieved via an electric discharge in a fluid medium, causing a hydraulic shockwave (Willscher et al., 1988; Denstedt and Clayman, 1990; Cathignol et al., 1991). Other uteroscopic lithotripsy relies on the ultrasonic vibration of the probe (Biri et al., 1999; Kurahashi et al., 2007), the creation of a vapor bubble by photoacoustic or ‘photothermal’ effect (Teichman and Kameron, 2000) or the propelling of a projectile by pneumatic force (Denstedt et al., 1992; Hong and Park, 2009).

Extracorporeal Shock Wave Lithotripsy (ESWL) consists in fragmenting kidney stones by exposing them to short pulses (order of microseconds) of high acoustic pressure (up to 100 MPa) using an extracorporeal ultrasound transducer. Several mechanical mechanisms are involved in this phenomenon, including cavitation (Coleman et al., 1987; Crum, 1988), spallation (Chaussy et al., 1980), shear stress (Gracewski et al., 1993) and squeezing

(Eisenmenger, 2001; Eisenmenger et al., 2002). Cavitation has been found to play the most important part of them all (Church, 1989; Bailey, 1997; Cathignol et al., 1998; Sapozhnikov et al., 2002; Pishchalnikov et al., 2003), and for this reason, the control of this phenomenon has been the focus of numerous studies (Zhong et al., 1997; Bailey et al., 1999; Williams Jr et al., 1999; Cleveland et al., 2000; Xi and Zhong, 2000; Sokolov et al., 2001; Evan et al., 2002; Loske et al., 2002; Zhu et al., 2002).

III.C. Interactions of US with nervous structures

III.C.1. Early proofs of feasibility

In 1958, Fry et al. demonstrated the ability of focused ultrasound, if applied at the appropriate level in the nervous pathway, to temporarily suppress the AP usually evoked in the visual cortex in response to a light stimulus (Fry et al., 1958). These changes were proved to be reversible and were associated with no histologically observable lesions.

In a series of papers published in the 1970s, Gavrilov and fellow researchers provided several proofs of ultrasound-induced activation of the peripheral nervous system (Gavrilov, 1984) (**Figure 15.A**). They targeted different regions of the human hand and forearm, and by varying the parameters of the focused ultrasound sequences (pulse length, pulse intensity), they were able to evoke all the sensations that humans can feel through their skin: tactile, thermic (both warmth and cold) and painful (Gavrilov et al., 1977). Parallel to these investigations on the PNS, the feasibility to stimulate the auditory system was studied. By using ultrasonic waves modulated with audible frequencies, they were able to introduce auditory information in the human brain, with the perceived information corresponding to the modulation frequencies (Gavrilov and Tsirulnikov, 1980) (**Figure 15.B**). They postulated that the stimulated structures were not only the receptors of the internal ear (hair cells) but also auditory nerve cells. Complementary experiences performed on animals whose receptor system of the labyrinth had been destroyed and on deaf human subjects (Gavrilov and Tsirulnikov, 2012), supported this postulation.

At the time of these preliminary successes, focusing US through the human skull was very challenging and required craniotomy. For these reasons, an ultrasound neuro-therapeutic tool

was discarded by most of the scientific and medical communities for decades.

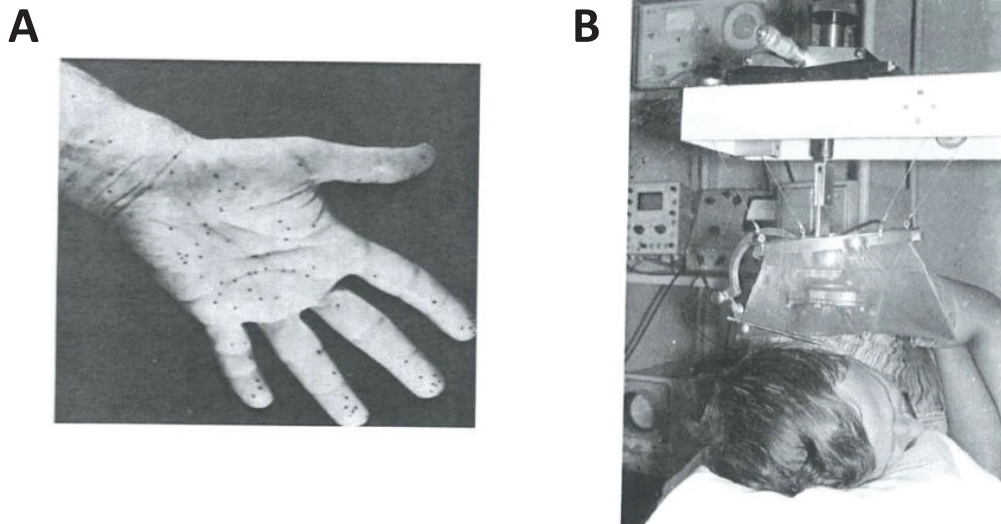


Figure 15 – Pictures from the early research works of Gavrilov and Tsirulnikov intended to demonstrate the feasibility of activating the nervous system. (A) Experiment where various spots of the hand and forearm were targeted by US exposure (Gavrilov et al., 1977). (B) Experiment on US stimulation of nerve structures of the auditory system (Gavrilov and Tsirulnikov, 1980).

III.C.2. Recent results

There has been a recent renewal of interest for the field of ultrasound neurostimulation and neuromodulation, with experimental results related to various nervous structures, at different levels of the nervous activity. Several teams investigated transcranial neurostimulation of the rodent motor cortex (Younan et al., 2013; King et al., 2013). In particular, King and colleagues reported neurostimulation at a frequency of 500 kHz with an increase efficacy by increasing the intensity of the stimulus. Tyler's group also reported, both on the intact brain and on *ex vivo* slices, that low intensity low frequency pulsed ultrasound could induce activity in the cerebral cortex of mice (Tyler et al., 2008; Tufail et al., 2010). Yoo colleagues demonstrated the *in vivo* feasibility of using focused ultrasound to transiently modulate the function of regional brain tissue in rabbits (Yoo et al., 2011). Menz and colleagues used an isolated

salamander retina to show that ultrasound stimuli could evoke stable responses with a temporal precision equal to strong visual responses but with shorter latency (Menz et al., 2013). Regarding cognitive results, Deffieux and colleagues proved that focused ultrasound could significantly modulate the latencies of an anti-saccade task performed by macaques (Deffieux et al., 2013).

III.C.3. Possible mechanisms

III.C.3.i. Postulated general mechanisms

The studies mentioned in the previous section provide evidence of the ability of ultrasound to modulate and stimulate electrical activity of both the PNS and CNS, but they do not focus on investigating the mechanisms underlying this phenomenon.

It has been suggested that US can disrupt the synaptic contact between nerve cells by depleting synaptic vesicle clusters, widening synaptic clefts, and decreasing the sizes of the presynaptic and postsynaptic densities (Borrelli et al., 1981). Another hypothesis relies on the fact that many ions channels possess mechanosensitive properties (Morris and Juranka, 2007; Sukharev and Corey, 2004). Ultrasound could produce mechanical changes in membrane tension, thus altering the ion channels gating properties and the associated ionic flux. Still, these hypotheses are very general and do not address the exact bioeffects involved in such mechanisms.

There have been some attempts to build comprehensive models or formulate hypotheses specifically explaining the biophysical interaction between ultrasound and the nervous system, at the cellular level.

III.C.3.ii. The “continuum mechanics” hypothesis

In 2011, Tyler suggested that continuum mechanics formulations could be employed to study the mechanical interaction between an US wave, the extracellular medium and neuron membrane (Tyler, 2011). Although this hypothesis was justified by an interesting approach regarding the dimensions and known mechanical properties of the structure, it shows several

limitations. Firstly, because the extracellular space of the brain and the dynamics of the cerebrospinal fluid are premises of this hypothesis, it makes it exclusively tailored to explaining the phenomenon of neurostimulation in the human CNS, when a majority of results have been obtained on a variety of different nervous model. Secondly, the eventual statement of this hypothesis does not point to a specific mechanism to explain ultrasound neurostimulation, but to a rather extensive list of mechanisms, including “*a combination of pressure/fluid/membrane actions involving stable cavitation and acoustic streaming (microjet formation, eddying, and turbulence) in addition to acoustic radiation force, shear stress, Bernoulli effects, and other fluid-mechanical consequences*”. This hypothesis therefore makes it difficult to construct a mathematical model that could be tested experimentally.

III.C.3.iii. The NICE model

Krasovitski and colleagues introduced a unifying model, called the bilayer sonophore model (BLS) to explain the underlying mechanisms of multiple bioacoustics interactions (Krasovitski et al., 2011). The BLS model combines the physics of bubble dynamics with cell biomechanics, and predicts that the cellular membrane is intrinsically capable of absorbing mechanical energy from the ultrasound field and transforming it into expansions and contraction of the intramembrane space. During this leaflets oscillation, dissolved gas would accumulate in the hydrophobic zone, creating pockets of gas that expand and contract periodically, eventually leading to various alterations in cells, including the initiation of cellular mechanotransduction process, the induction of membrane pore formation, and permeability changes (**Figure 16**). Using the BLS model, they predicted how the various bioeffects should intensify depending on the acoustic parameters and the environment of the cell. To validate these predictions, they used an *in vivo* model of fish multilayered epithelium exposed to continuous ultrasound, and transmission electron microscopy (TEM) to examine the samples.

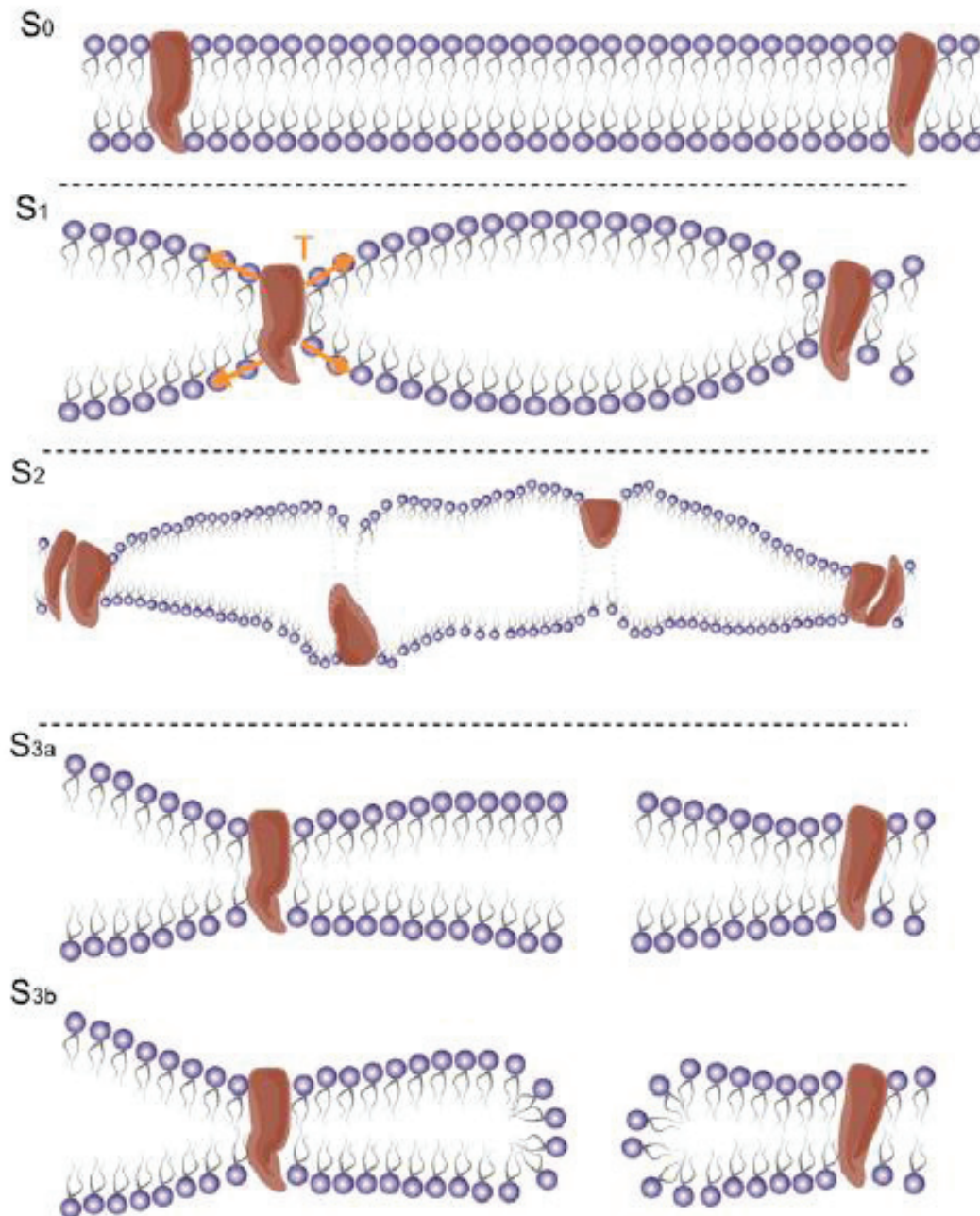


Figure 16 – Different stages in the interaction of a bilayer sonophore (BLS) and an US field can induce different bioeffects on the cell membrane. As tension increases in the leaflets around a pulsating BLS, from the reference stage (S₀), slightly stretched leaflets might activate mechanosensors (S₁). Growing tension in the leaflets might damage membrane proteins (S₂) and then induce pore formation (S_{3a}, S_{3b}) at high levels of stretching (Krasovitski et al., 2011).

Later, Plaksin and colleagues attempted to combine a modified version of the BLS model with the Hodgekin-Huxley model to create a model, referred to as neuronal BLS or NBLS, explaining the mechanisms underlying the interaction between US and excitable tissues (Plaksin et al., 2014). In the NBLS model, the deforming shape of intramembrane cavity is driven by the time-dependent US pressure, leaflet tension and an attraction-repulsion equivalent pressure resulting from phospholipid molecular forces and the electrostatic attraction forces between membrane charges. These dynamics deformations change the average membrane capacitance and induce a capacitive displacement current. The Hodgkin-Huxley equation is modified by taking into account this displacement current, and the time-dependency of the membrane capacitance, which is associated with the geometrical shape of the deformed leaflets. The authors studied the response of NBLS model to continuous ultrasound stimulation, and some results are displayed in **Figure 17**. The NBLS behavior illustrated by **Figure 17.A** is explained as follows by the authors. A continuous US stimulation leads to strong oscillation of the membrane potential between -280 and -60 mV, at the harmonic frequency. The capacitive current oscillation which drive these membrane oscillations are too fast to accumulate and lead only to negligible variation of the membrane potential. These transient periods of higher membrane potential are too short for the ion channels to response. Hence, for a time, all voltage-depend ion channels stay closed, while non-voltage-depend ion channels remain open, allowing current leak to enter and exit the cell, causing a net elevation in the membrane charge. At the end of the stimulus, the membrane capacitance returns to its reference value, while the membrane potential is determined by the accumulated charge. This state leads to the gating of specific ion channels, and the generation of an action potential. The behavior illustrated in **Figure 17.B**, would be explained by a longer stimulus duration allowing membrane potential to rise long enough to reach activation threshold of different ion channels, eventually leading to the generation of several APs.

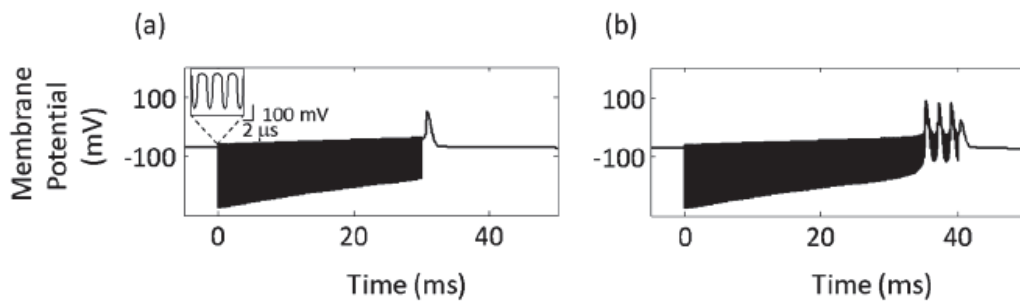


Figure 17 - The effects, predicted by the NBLS, of continuous US stimuli on membrane potential, for stimulus durations of (a) 30 ms and (b) 40 ms (Plaksin et al., 2014).

The NBLS model is one of the most completed attempt to take into account the mechanical and electrical aspects of nervous membrane dynamics, to propose a mechanism explaining the phenomenon of ultrasound neurostimulation. Because it is a mathematical model, it can be tested and confronted to experimental results, as the authors of the model did by comparing the efficiency of ultrasound neurostimulation reported by King (King et al., 2013) in its study on the mouse brain, with the efficiency predicted by the NBLS for the same set of acoustic parameters. However, the main limitation of the NBLS model is the BLS model itself. Indeed, there is no theoretical model or experimental observation supporting the assumption that a nanometer-scale bubble could form and oscillate between two membrane leaflets. The experimental validation of the BLS model relies on *a posteriori* observations of cavities supposedly created by cavitation in a multi-layered cellular structure (Krasovitski et al., 2011). Cavities were mainly observed around the outer membranes and between the cells (**Figure 18**) and in some cases on the perimeter of nuclei, but never in between the membrane leaflets.

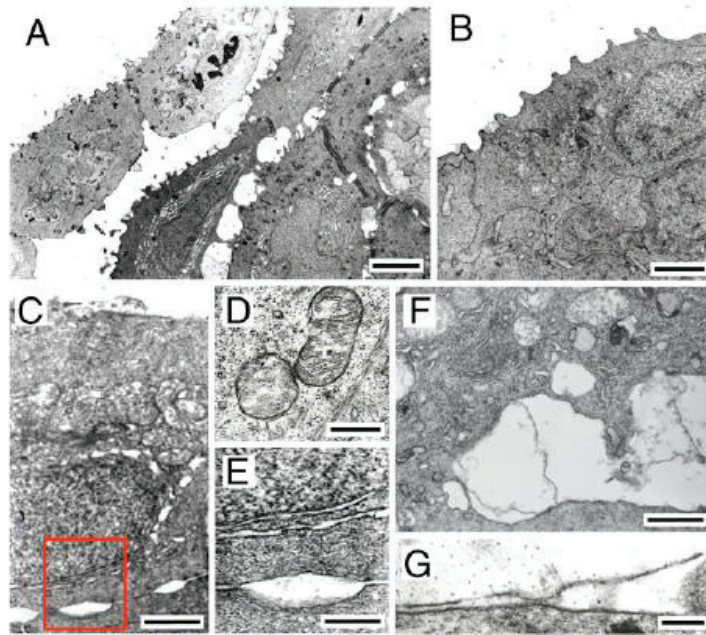


Figure 18 - Membrane-localized cavitation following in vivo ultrasound exposure (Krasovitski et al., 2011).

Conclusion

In this first chapter, we saw that patients with cancer as well as cancer survivors suffer from various forms of pain, acute and chronic, directly or indirectly linked to cancer itself, its diagnosis or treatment. We considered neurostimulation as an approach for pain relief, and especially management of chronic pain. The current neurostimulation techniques (DBS, TMS, tDCS) were presented, along with their limitations (invasiveness, low spatial resolution), which led us to introduce focused ultrasound as a possible new modality of therapeutic neurostimulation, combining the advantages of the different types of techniques, without their respective limitations. We presented some proofs of the ability of ultrasound to induce or modulate nervous activity at the systemic level, and highlighted the lack of validated mechanistic model to explain this phenomenon.

In order to translate the numerous experimental proofs of feasibility into actual therapeutic applications, it is necessary to understand the causality between acoustic parameters

of an ultrasound stimulus and the characteristics of the subsequent nervous response. For this reason, it appears as relevant to re-orientate research efforts towards simple nervous model. In the next chapter, we will introduce an *in vivo* invertebrate nervous model thought to be particularly appropriate for the study of ultrasound neurostimulation, and demonstrate how comparing the nervous response of this model to different modalities of stimulation can bring relevant information regarding the biophysical interaction at play.

Chapter 2: Feasibility and demonstration of interest of using a simple invertebrate *in vivo* nervous model to study ultrasound neurostimulation

Introduction

Understanding the causality between acoustic parameters of an ultrasound stimulus and the characteristics of the subsequent nervous response is a critical step toward the translation of the numerous experimental proofs of feasibility into actual therapeutic applications. Indeed, besides controlling the spatial resolution of the technic, understanding what is happening at the cellular level when ultrasound penetrates the brain and interact with nervous functions will be a key point in developing a safe and treatment-specific technic. In addition, modeling the biomechanisms underlying ultrasound neurostimulation can help guiding the design of ultrasound sequences, to maximize their efficiency or minimize their adverse effects.

Gaining mechanistic knowledge on the basis of trials involving a complex and relatively large nervous structure such as the mouse motor cortex is quite challenging. On the one hand, at megahertz frequencies, the focal area is rather wide relatively to the size of the brain, and is likely to target a large number of neurons. This bring unknown variable to the input of the stimulation procedure. On the other hand, within a complex network such as a mammalian brain, two stimuli administrated at different sites can lead to the same behavioral response. A given motor response such as the lifting of a paw or shivering of a whisker is not specific of a single neuron or small group of neurons, but of a relatively large brain area. In other words, although establishing a correlation between exposure of the mouse brain to ultrasound and motor response is an effective way to prove the feasibility of ultrasound neurostimulation, it allows neither to identify with certainty which precise group of cells was activated nor to locate which part of the cell unit (soma, axon or synapse) was involved in the initiation of the nervous response. Furthermore, in the case of the mouse brain, the cranial barrier induces ultrasound beam aberration and makes it difficult to monitor the mechanisms occurring during ultrasound exposure.

For these reasons, the ventral nerve cord of the common earthworm (*Lumbricus terrestris*)

is particularly appropriate for studying the causality between ultrasound stimulation and nervous response, and investigating the underlying biophysical mechanisms. In this chapter, we will start by presenting the characteristics of this nervous model. We will pursue by detailing the characterization of the ultrasound transducer, before proposing an application of the proposed nervous model to a comparative study between different modalities of stimulation.

I. Presentation of the nervous model : the earthworm's system of giant fibers

I.A. Giant fibers and their role in the animal kingdom

As already briefly discussed in chapter I, axonal gigantism is, in some animals, the neural basis of rapid escape response when confronted to an immediate danger. Before presenting the system of giant axons of *Lumbricus terrestris* and the escape-withdrawal reflex it supports, we shall explore with a bit more details the notions of startle, rapid escape and giant fiber-mediated responses, whose mutual relationship has been discussed by T.H. Bullock in his contribution to the 1984 Edition of *Neural Mechanisms of Startle Behavior* (Bullock, 1984).

I.A.1. About startle, rapid escape, and giant fiber-mediated responses

Rapid escape is a behavioral category difficult to accurately define. It includes quite obviously sudden withdrawal of many burrowing animals from annelids (e.g. *Lumbricus*) to rodents (e.g. prairie dogs), but also other avoidance responses such as jumping, coiling and taking flight. The notion of rapidity must be understood relatively to each species: since the time scale that matters is that of the natural predators, we cannot exclude from the category of rapid escape responses all avoidance movements appearing less than rapid from a human perspective (Bullock, 1984).

Startle is a behavior more prone to be defined and categorized. A startle response is an abrupt motor response to a sudden stimulus that is both unexpected and alarming. The movement may translate the whole body (**Figure 19**) or move only limited parts of the body, such as eye blink (Bullock, 1984).

Now that those two distinct but overlapping notions have been defined, it appears clearer that not all rapid escape responses are startle responses. Indeed, a frog may jump during the slow approach of a threatening stimulus. Conversely, not all startle responses lead to escape. Some of them are too limited in amplitude to achieve translation of the body, or their ultimate goal is simply not special avoidance but another defense mechanism, such as the inflation of pufferfishes.

Furthermore, not all rapid escapes responses, nor all startle responses, are giant fiber-mediated.

Giant nerve fibers and giant fiber systems have been a major subject of study since the discovery of the giant axon in the squid (Young, 1936) and have contributed significantly to our fundamental knowledge of neurobiology (Faber and Korn, 1978; Hodgkin, 1964). The question of their behavioral role was raised long ago, but among many functions proposed, the only one appearing to share some general applicability across diverse taxa is the mediation of startle responses (Bullock, 1948; Bullock, 1953a; Bullock, 1953b). Commonly, giant fibers are not defined as such because of their absolute axonal diameter, but because they are larger than the next largest fibers in the animal (Bullock and Horridge, 1965). We shall insist on the fact that we are not referring to giant cell bodies, which are quite differently distributed and correlate poorly with giant axons.



Figure 19 - The vertical leap of a nine-banded armadillo, *Dasypus novemcinctus*, surprised by the flash of a photographer's lighting system (photograph by Bianca Lavies, © 1982 National Geographic Society).

I.A.2. Giant fibers distribution in the animal kingdom and their diversity of function

System of giant axons are found in a wide variety of taxa, assuming a large diversity of form and function, but are not continuously distributed in terms of phylogeny (**Figure 20**). For example, amongst the phylum *Annelida*, they are general but not universal among the class *Oligochaeta* (earthworms), but absent in the class *Hirudinea* (leeches). Amongst the phylum *Mollusca*, only decapod cephalopods exhibit giant fibers. Giant fibers occur in a number of crustaceans (shrimp, crayfish, lobsters, ...), many arthropods such as scorpions and a few

orders of insects (Bullock, 1984). Giant fibers are common but not universal among the varied taxa of lower vertebrates (fishes and young amphibians) but lack in adult anurans (frogs), reptiles, birds and mammals.

Let us highlight one last time that rapid movements do not necessarily involve giant-fiber-mediation, for many of the fastest animals lack giant systems, such as ghost crabs, humming birds, cheetahs, to name but a few.

In many groups of vertebrates and invertebrates, large caliber axons do not necessarily mediate escape but rather mediate attack. If it is not a startle, prey capture may be startling and can occur in otherwise slow-moving species, as it is the case of an alligator snapping its jaws.

Giant fibers sometimes mediate only an initial phase of the startle response. Even this initial phase may not require but only be quantitatively accelerated by the giant fiber mediation.

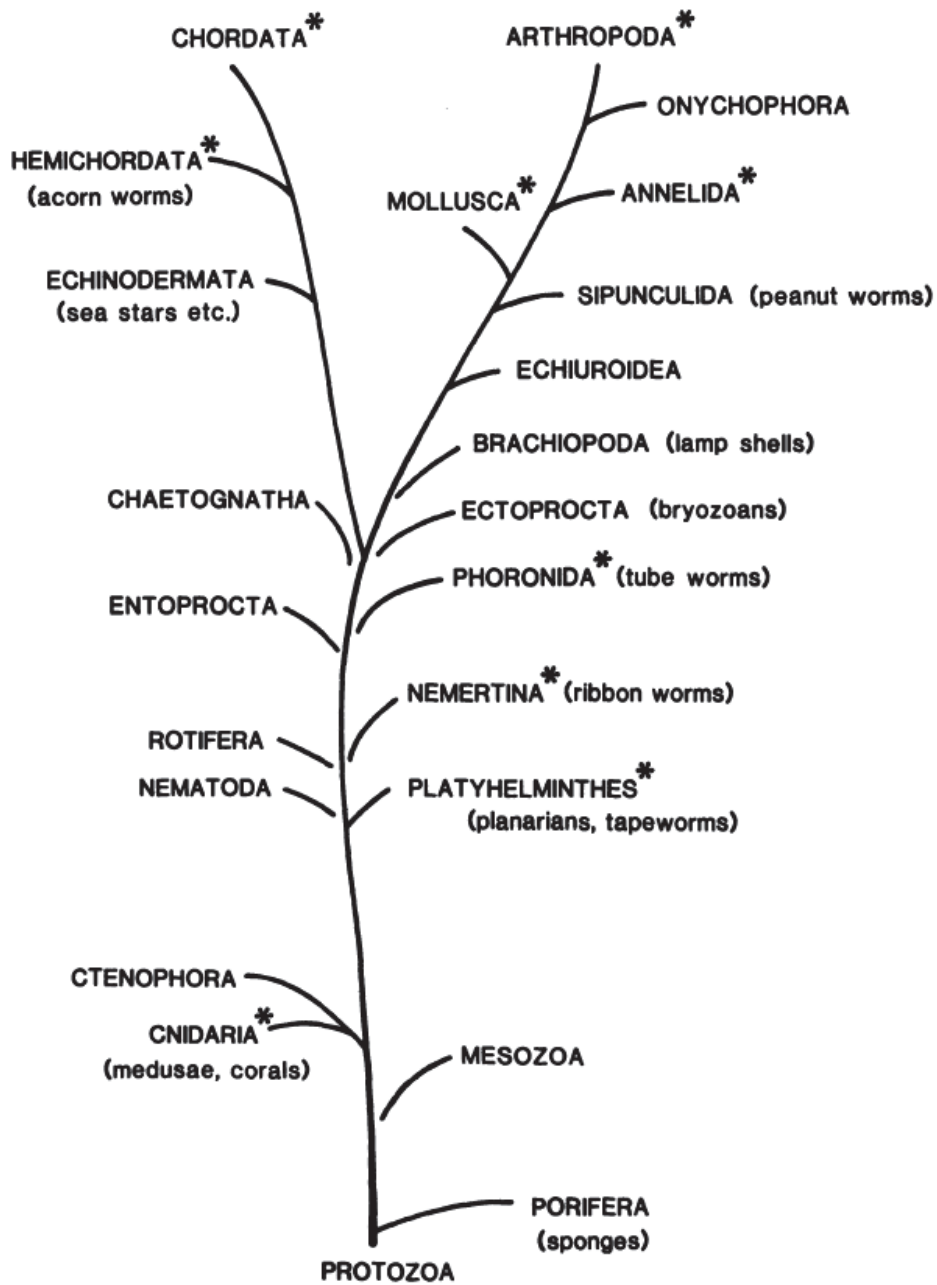


Figure 20 - Evolutionary relationships of major animal groups. Phyla with asterisks have some members, although not necessarily all, with giant fibers (Bullock, 1984).

I.B. Introduction to earthworms, their role in nature and science

I.B.1. Interaction of earthworms with their natural environment

In temperate regions, earthworms are among the most widespread invertebrate animals. They are found mainly in the soil of forests, woodland and grassland, where their population density can reach more than 500 individuals/m² and their biomass more than 80 g/m² (Shakir and Dindal, 1997). Worms are key actors in the enriching of the soil and leveling of the landscape (Darwin, 1892), mainly because of two major interactions with their environment: burrowing through the ground and rejecting **castings** at the surface (**Figure 21**). Firstly, by digging tunnels in the ground, they allow air, water and consequently nutrients to reach the deep layers of the soil. In the process, they loosen and disaggregate the soil, enabling gravity and erosive agents to move the soil more easily from high to low ground, thus leveling the landscape. Secondly, some species of earthworms feed from organic matter from the soil they burrow through and other from organic matter found at the surface (leaves, decaying vegetation or even dead insects), but in both cases they triturate it in smaller particles and rejected it at the ground surface in the form of castings, which contain nutrients that plants can assimilate. Thirdly, these castings, originally spiral in form, are disaggregated by wind and water and spread out to form vegetable mold, the upper-layer of soil.

A

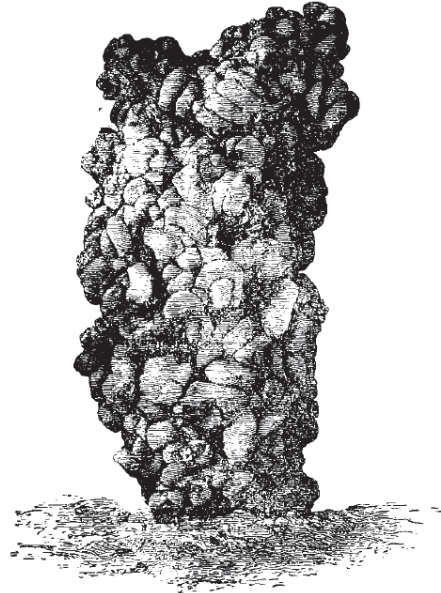


Fig. 2.

Tower-like casting from near Nice, constructed of earth, voided probably by a species of *Perichæta* : of natural size, copied from a photograph.

B



Figure 21 - Earthworms burrow through the ground and reject castings at the surface. (A) Illustration (Darwin, 1892) and (B) photograph of a casting.

*I.B.2. Earthworms in sciences: “The subject may appear an insignificant one ...”
(Darwin)*

The role played by earthworms in the formation of soil was the central theme of Charles Darwin’s last book, originally published 1881, one year prior to its death, and untitled *The Formation of Vegetable Mould, Through the Action of Worms, With Observations on Their Habits*. At the time, Darwin’s choosing to write about earthworms rather than providing a synthesis of his life work and some enlightened pieces of advice for his successors was considered by some as the last eccentricity of a great naturalist in his old age (**Figure 22.A**). Darwin was well aware of the reaction he would trigger, as attested by the preface of his book where he wrote “The subject may appear an insignificant one, but we shall see that it possesses some interest; and the maxim ‘de minimis lex non curat’ [the law is not concerned with trifles] does not apply to science”. Indeed, careful readers have seen since then that Darwin used worms to illustrate the scientific method his mentor Lyell applied to geology and Darwin himself to the study of species: small changes, summed over immense period of times, can lead to great transformations (Gould, 1994). Just as minor genetic variations have shaped present species, the slow and uninterrupted burrowing of worms will one day make the standing stones of Stonehenge disappear in the ground (**Figure 22.B**).

In the history of science, neuroscientists have also show a great interest for this ‘insignificant’ study subject. . As early as 1894, Friedlander published on the central nervous coordination of earthworm movement (Friedlander, 1894). In 1925, Hess acknowledges in the introduction of his article that ‘the nervous system of the earthworm has doubtless received the attention of more morphologists and physiologists than has that of any other invertebrate’ (Hess, 1925). He was proven right along the next decades by the multiplication of investigations led on the central and peripheral structure of the earthworm nervous system (Stephenson, 1930; Coonfield, 1932; Prosser, 1935; Bullock, 1948) and the conduction of action potentials in segmental nerves (Prosser, 1935) and giant fibers (Rushton and Barlow, 1943; Rushton, 1945; Bullock, 1945; Rushton, 1946), even though the electrophysiological recording technics at the time were relatively limited and not necessarily adapted to such a nervous model.

A



B

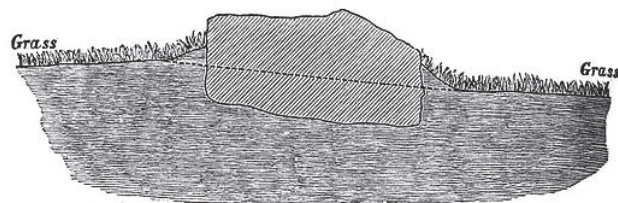


Fig. 7.

Section through one of the fallen Druidical stones at Stonehenge; showing how much it had sunk into the ground. Scale $\frac{1}{2}$ inch to 1 foot.

Figure 22 - Charles Darwin's last book was dedicated to the study of earthworms and their impact on environment. (A) Cover illustration from *Hen's teeth and Horse's toes* by Stephen Jay Gould. (B) Illustration of the sinking of Stonehenge druidical stones under the action of earthworm-mediated soil renewal (Darwin, 1892).

I.C. General anatomical and functional organization of the earthworm

Studying the bioeffects induced by US in an *in vivo* earthworm model calls for knowing the nature and organization of the different tissue layers crossed by the US beam. Thus, the longitudinal and radial organizations of the earthworm anatomy will be described in the following sections. In addition, some physiological characteristics of the animal, which will have an impact on the experimental protocol presented in Part III of this chapter, are also provided.

I.C.1. Longitudinal and radial anatomical organizations of the earthworm

I.C.1.i. Longitudinal body segmentation

The phylum to which belong earthworms, *Annelida*, takes its name from the Latin for “small rings”. Indeed, earthworm’s body is constituted of a **linear series of segments** or “rings”, about 1 mm wide (see **Figure 28** for an illustration this segmentation, at the internal level). The majority of these body segments, called metamerer or somites, are structurally identical. Some of them, however, are specialized to perform special functions, especially in the anterior part of the animal. The **clitellum**, a glandular swelling, is one of the most obvious external discontinuities, and permits to easily identify the anterior part of the animal from its posterior part (**Figure 23.A**). In the cross plan, an earthworm is essentially a ‘tube in a tube’, with the digestive track running along the whole length of the animal, surrounded by the body wall and the coelom in between (**Figure 23.B**).

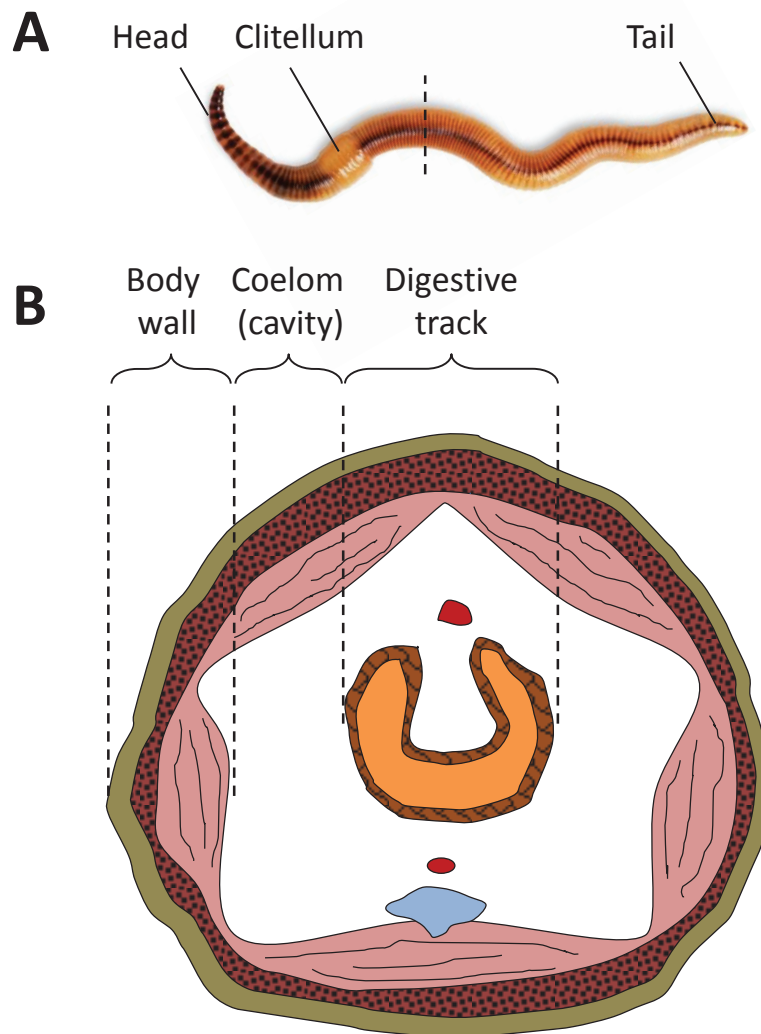


Figure 23 - *Lumbricus terrestris*, as all the members of the phylum *Annelida*, is characterized by a **longitudinal body segmentation** constituted of a majority of structurally identical metameres. (A) A photograph displaying the animal dorsal side up. (B) A scheme of the animal cross section, highlighting how the earthworm's anatomical organization can be viewed as a 'tube in a tube': the digestive track is surrounded by the body wall, and the coelom forms a cavity in between.

I.C.1.ii. The body wall

From the outside to the inside, the different layers constituting the **body wall** are: the cuticle, the epidermis, a layer of nervous tissue, a layer of circular muscle, a layer of longitudinal muscles and finally the peritoneum separating the body wall from the coelom (**Figure 24**).

The **cuticle** is a thin (7- μm thick in *Lumbricus terrestris*), noncellular, transparent layer, composed of both interlacing collagenous fibers and several homogenous non-fibrous layers. It is perforated by small pores, especially where it overlays the epithelial sense organs. In these areas, fine hairs from the sensory cells project through the pores of the cuticle.

The **epidermis** is constituted of a single layer of different kinds of cells (**Figure 24**, dotted line frame). The supporting cells, which are the main structural cells of the epidermis, secrete material to form the cuticle. The mucous cells secrete mucus over the surface of the cuticle, to prevent desiccation and to facilitate movement through soil. Sense organs responding to tactile stimuli are formed by large numbers of sensory cells grouped together, scattered throughout the epidermis. These sensory cells are more numerous on the ventral surface of the earthworm. Photoreceptors cells are present in the basal part of the epidermis, and are most numerous on the prostomium and first and last segments. Other sensory cells, which can be stimulated by different chemical substance such as sucrose, glucose and quinine, are also present in the prostomium.

Two different muscle layers lie within the inner basal membrane of the epidermis: the circular muscle layer and the longitudinal muscle layer. The **circular muscle layer** is the outermost, and is constituted of muscle fibers extending around the circumference of the body, interrupted at the intersegmental positions. The **longitudinal muscle layer** is much thicker and continuous through the length of the body.

The **peritoneum** is a layer of epithelial cells, separating the inner surface of the longitudinal muscle from the coelom.

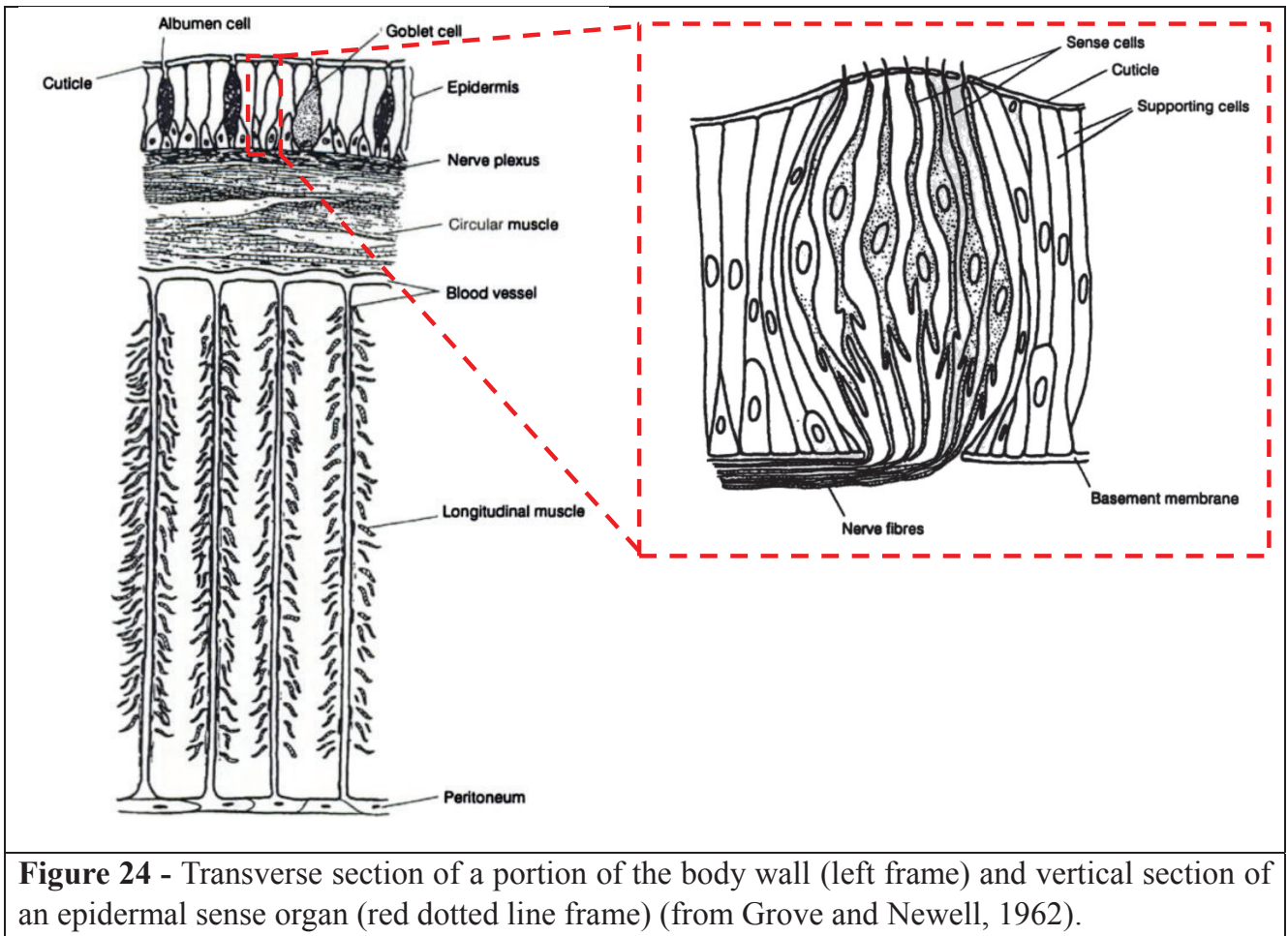


Figure 24 - Transverse section of a portion of the body wall (left frame) and vertical section of an epidermal sense organ (red dotted line frame) (from Grove and Newell, 1962).

I.C.1.iii. The coelom

The **coelom** is a large perivisceral cavity extending through the length of the body, filled with **coelomic fluid**. It is surrounded on its outer side by the peritoneum of the body wall and on its inner side by the peritoneum covering the alimentary canal (**Figure 23.B**). It is divided into segmental portions by transverse septa, which are constructed from muscle fibers, connecting tissue and blood vessels. These septa are perforated by pores allowing exchange of coelomic fluid between segmental portions of the coelom (Edwards and Bohlen, 1996).

I.C.1.i. The digestive track

The digestive track is central in the radial organization of the earthworm anatomy, just as ingestion and digestion are central in earthworm's vital functions, since the animal literally

‘eats its way through the ground’ (see section I.B.1 of this chapter). Along the longitudinal axis, the intestine constitutes the major part of the digestive track, but some specialized structures can be found in the anterior part of the animal.

The **mouth** is located in the first segment of the animal, and opens on the **buccal cavity** (segments 1-3) (Fox, 2006). It can be covered by a lip-like extension of the body wall: the **prostomium**. Prostomium can also serve as a wedge to force open cracks in the soil when the animal is burrowing. The **pharynx** is directly posterior to the buccal cavity (segments 3-5) and acts as a suction pump. In the pharynx, food is coated by lubricating mucous secretions, which facilitates its traveling through the esophagus. In the **esophagus** (segment 6-12), food acidity is balanced by the calcium carbonate secreted by the calciferous glands. Posterior to the esophagus is the **crop** (segments 12-16), a bulbous part of the gut serving as a temporary food storage. In the **gizzard** (segments 16-20), food is triturated into smaller fragments. Finally, posterior to the gizzard starts the **intestine**, where food is chemically digested by enzymes but also processed by bacteria which release unneeded nutrients. Wastes are evacuated through the nephridia and the **anus**, at the end of the intestine.

From an experimental point of view, choosing the anterior part of the animal as a target for US exposure would risk triggering parasite physiological responses from these digestive specialized structures, and would increase the inherent variability between US exposure. Indeed, it would not be possible to position the US beam relatively to the different digestive structures, in a repeatable manner, without visualizing these structures. Hence, it was decided that, with a few exceptions, all the US exposures involved in the experimental protocol presented in part III of this chapter would be performed in the region comprised between the posterior end of the clitellum and the posterior end of the animal, where the digestive track is spatially homogenous along the longitudinal axis.

I.C.2. Physiological characteristics of Lumbricus terrestris

I.C.2.i. Respiration

Earthworms do not present with an organ specifically dedicated to respiration, such as a lung, but breathe through their skin. Oxygen penetrates the skin by diffusion, which requires the body surface to be kept moist. This is achieved mainly by secretions from the mucous glands of the epidermis. The oxygen dissolved in the surface moisture film permeates through the cuticle and the epidermis to reach a network of small blood vessels buried within the body wall. It is worth noting that earthworms can survive for considerable lengths of time in water if the dissolved oxygen level is high enough (Edwards and Bohlen, 1996).

We took in consideration these physiological characteristic when designing the anesthesia protocol presented in Part III of this chapter, which ending up consisting in an immersion in a bath of non-degazed water mixed with alcohol for a score of minutes.

I.C.2.ii. Coelomic secretion

The coelom communicates with the exterior environment through the openings of the nephridia (an invertebrate organ performing a similar function to that of the vertebrate kidney), but also through dorsal pores. Additionally, the cavity has been found to communicate with the intermuscular spaces, letting the **coelomic fluid** permeates the somatic musculature of the earthworm (Keng, 1895).

Coelomic fluid is ejected through the dorsal pores in response to mechanical or chemical irritation, when the animal is subjected to extremes heat or cold, and in stressful situations. It is thought to have several functions: **preventing desiccation, promoting cutaneous respiration, providing protection from predators and parasites** (Vail, 1974; Keng, 1895; Edwards and Bohlen, 1996).

We took in consideration these physiological characteristic when defining the average duration of the trials presented in Part III of this chapter. Indeed, we noticed that the

function of coelomic secretion was somehow affected by anesthesia, which could in turn affect the cutaneous respiration of the animal. Since we could not manually moisturize the skin without risking creating shortcuts between electrodes, this consideration was another constraint in defining the duration of a trial where vital conditions were stable.

I.C.2.iii. Vascular organization

Earthworms have a closed vascular system, although it is not possible to distinguish “arteries” and “veins” as in vertebrates (Edwards and Bohlen, 1996). Instead, there is a system of vessels that distributes blood throughout the body. Two types of vessels can be distinguished in this system: longitudinal and commissural vessels. Longitudinal vessels run along the whole length of the animal and include, in the case of *Lumbricus terrestris*, one **dorsal blood vessel**, one **ventral blood vessel** and one **subneural blood vessel**. The dorsal vessel carries blood from the posterior part of the animal to the anterior, and the ventral vessel carries blood from the anterior to the posterior. Commissural vessels go by pair, are present in each segment, and form rings which connect the dorsal vessel with the ventral vessel. In *Lumbricus terrestris*, five of the anterior commissural vessels (segments 7-11) are enlarged, contractile and present valves, and referred to as **pseudo-hearts (Figure 25)**.

We took the earthworm vascular organization in consideration when defining the optimal placement of the electrodes used in the experimental protocol presenter in part III of this chapter. Our main concern was avoiding to damage one of the main longitudinal vessel. Indeed, not only a hemorrhage would risk to bias the electrophysiological recordings but it would also compromise the viability of the animal and thus the time window where the trial conditions are steady.

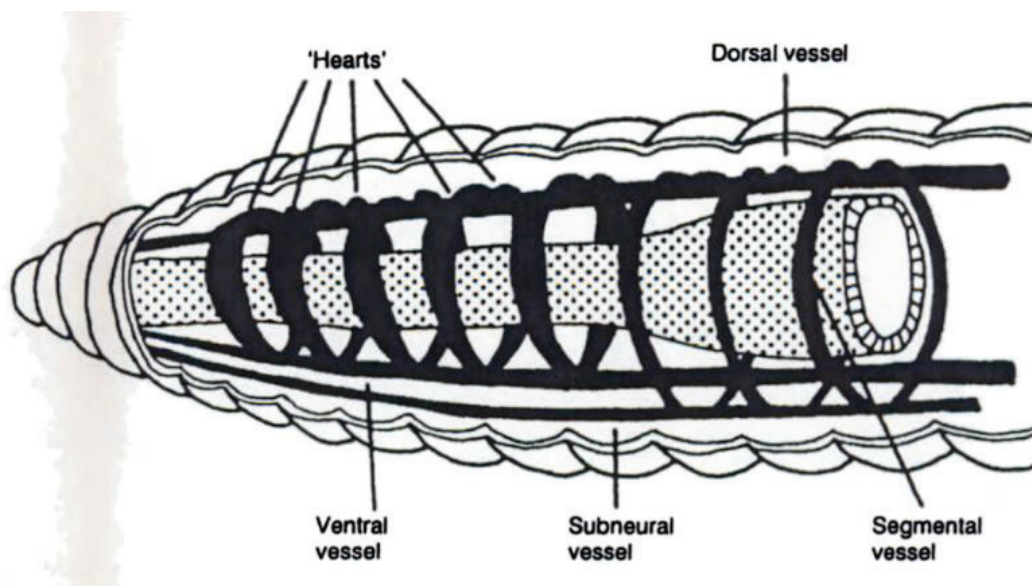


Figure 25 - The circulatory system of earthworms from the *Lumbricus* family (Edwards and Bohlen, 1996 from Wallwork, 1983).

I.C.2.i. Sexual differentiation

Being aware of the inherent animal variability, we tried as much as possible to homogenize the population of earthworms included in our study. Earthworms are **simultaneous hermaphrodites**, which means each individual present complete and simultaneously functional male and female systems (a detailed description of the earthworm reproductive system is provided in Annex N).

Hence, there were no criteria regarding the gender of the animal. However, it was possible to select only animals having reached sexual maturity, an external indicator of which is a clearly colored and swollen clitellum. Selecting only adult animals represented also a practical advantage for the placement of electrodes, as they present a larger and longer body.

I.D. Earthworm nervous architecture and its system of giant fibers

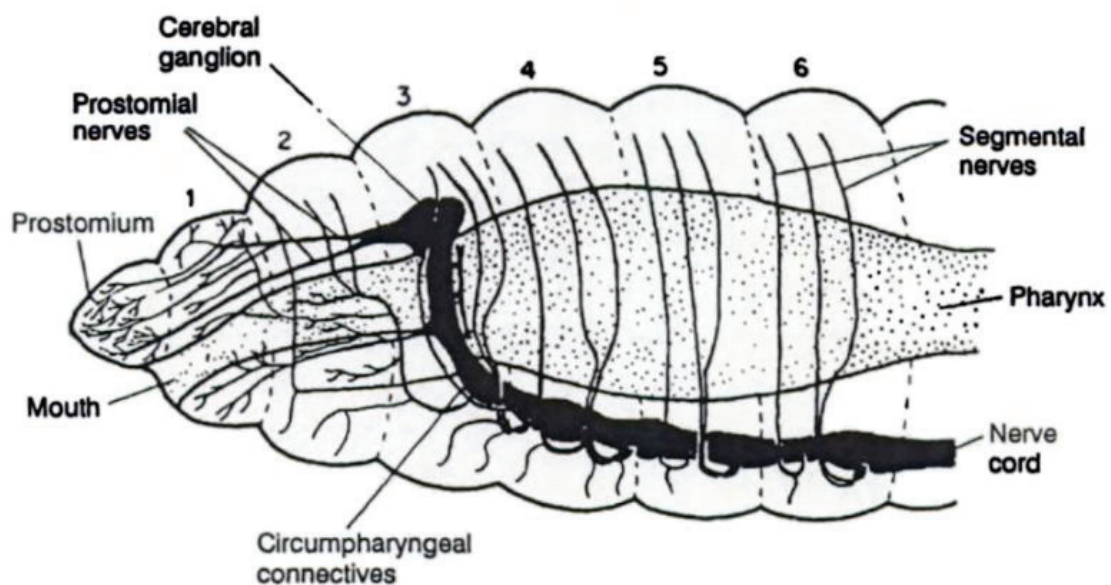
In this section we provide a description of the **global architecture** of the nervous system of *Lumbricus terrestris*. The **fine structure** of the ventral nerve cord, the systems of giant axons

and their associated afferent pathway will be discussed later in this chapter (II.C).

I.D.1. Ganglia and segmental nerves distribution

The earthworm's ventral nerve cord runs beneath the gut, longitudinally, from the last segment to segment 4. It passes into a **subesophageal ganglion**, then bifurcates into the **circumesophageal connectives** (sometimes called circumpharyngeal connectives), which pass up around either side of the esophagus and meet as the **cerebral ganglion** on the dorsal surface of the pharynx (**Figure 26**) (Edwards and Bohlen, 1996).

A



B

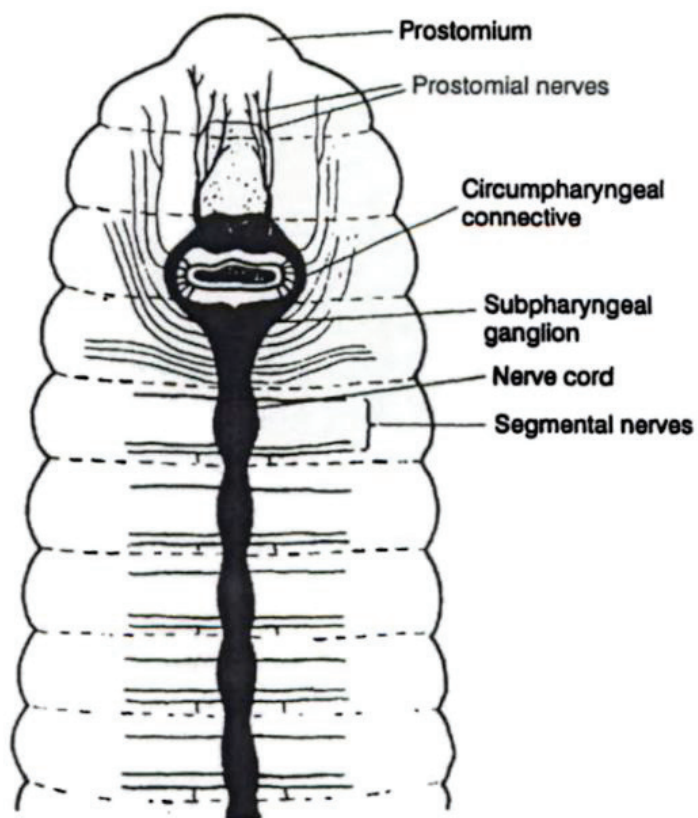


Figure 26 - Global structure of the nervous system of *Lumbricus terrestris*: (A) view from the side (Edwards and Bohlen, 1996 from Hess, 1925) and (B) from above (Edwards and Bohlen, 1996 from Grove and Newell, 1962).

The ventral nerve cord is swollen into **segmental ganglia** in each segment (**Figure 28**), working as “regional brain”. From segment 5 to the last segment, each of these ganglia present three pairs of **segmental nerves** branching from it: two of them are located posteriorly to the ganglion and the third one is located anteriorly to the ganglion (**Figure 26**). Segmental nerves extend around the body wall, first in the longitudinal muscle layer and then in the circular muscle layer, ending in the mid-dorsal line, thus forming an almost complete ring. Each nerve ring has branches connecting to the muscles and epidermis. In addition, a pair of **septal nerves** arises at the same level than the posterior segmental nerves, and supplies each septum (Edwards and Bohlen, 1996).

The distribution of the nerves in the anterior four segments of the body differs from that in the other segments, as illustrated in **Figure 26**. Segment 3 has the typical distribution of three pairs of segmental nerves, but they originate from segment 4, which also possesses three pairs, so that six pairs of segments nerves come from the ventral cord in segment 4. Segment 2 is supplied with pairs of nerve which originate from the junction of the circumesophageal connectives with the ventral nerve cord in segment 3, the larger posterior pair dividing, to give the normal three nerve rings in segment 2. The first segment is supplied by a pair of nerves originating in the lateral portion of the subpharyngeal connectives, which branch into two, shortly after they leave these nerves, and ramify through the first segment without forming nerve rings. A small nerve comes from the most ventral of these two branches to supply the ventral surface of the buccal cavity. The **prostomium** is innervated by the prostomial nerves, which originate from the front of the cerebral ganglion; these are the only nerves coming from this ganglion. A branch is given off from each prostomial nerve to supply the roof of the buccal cavity. The last caudal segment present six pairs of segmental nerves instead of three (Hess, 1925) arranged as if they were in two successive normal segments. The most posterior of these six pairs of nerves are lateral terminations of the nerve cord itself.

I.D.2. Nerve plexuses

A number of nerve plexuses supply the different muscles layers, membranes and other organs of *Lumbricus terrestris*. The **gut** is supplied by a nerve plexus lying between the

epithelium and the circular muscle layer of the alimentary canal throughout its length. In each segment, the **septum** is supplied by its own **septal nerve plexus** constituted of lateral nerves. Before bifurcating, branches of these nerves supply the **longitudinal muscles** of the body wall. An **intermuscular nerve plexus**, constituted of branches coming from the nerve rings, supply the **circular muscles** of the body wall. Finally, the **subepidermal nerve plexus**, situated between the basal membrane of the epidermis and the circular muscle layer, supply the layer of **epidermal** and **sensory cells** (Edwards and Bohlen, 1996). The peritoneum presents an extensive nerve net, derived from the nerves of the body wall.

*I.D.3. Anatomical organization of giant fibers in *Lumbricus terrestris**

As mentioned in the previous section, giant nerve fibers are found in nearly all earthworms from the *Oligochaeta* group. There have been a substantial number of correlated anatomical, physiological and behavioral studies related the rapid escape reflexes mediated by these giant fibers (Bullock, 1984; Drewes, 1984), the most extensively studied species being *Lumbricus terrestris*. In this section, we will review the anatomical specialization and physiological properties underlying rapid escape reflex in *Lumbricus terrestris*.

I.D.3.i. The ventral nerve cord

Lumbricus terrestris presents five giant fibers. Three of them are located in the dorsal portion of the ventral nerve cord: one medial giant fiber (MGF) and two lateral giant fibers (LGF). The other two are located in the ventral portion of the nerve cord, and will not be discussed here, for there is no proof that they are involved in the rapid escape reflex. MGF and LGF form a multisegmental through-conducting pathway.

In a cross section, MGF and LGF are easily identifiable by their large diameter and the presence of a thick myelinlike sheath surrounding them (**Figure 27**). In each segment, this sheath is interrupted by collateral projection arising from MGF and LGF on the ventral side (Günther and Walther, 1971), the number and position of these collaterals being constant from segment to segment. These collaterals represent the sites of synaptic inputs and outputs of the giant fibers.

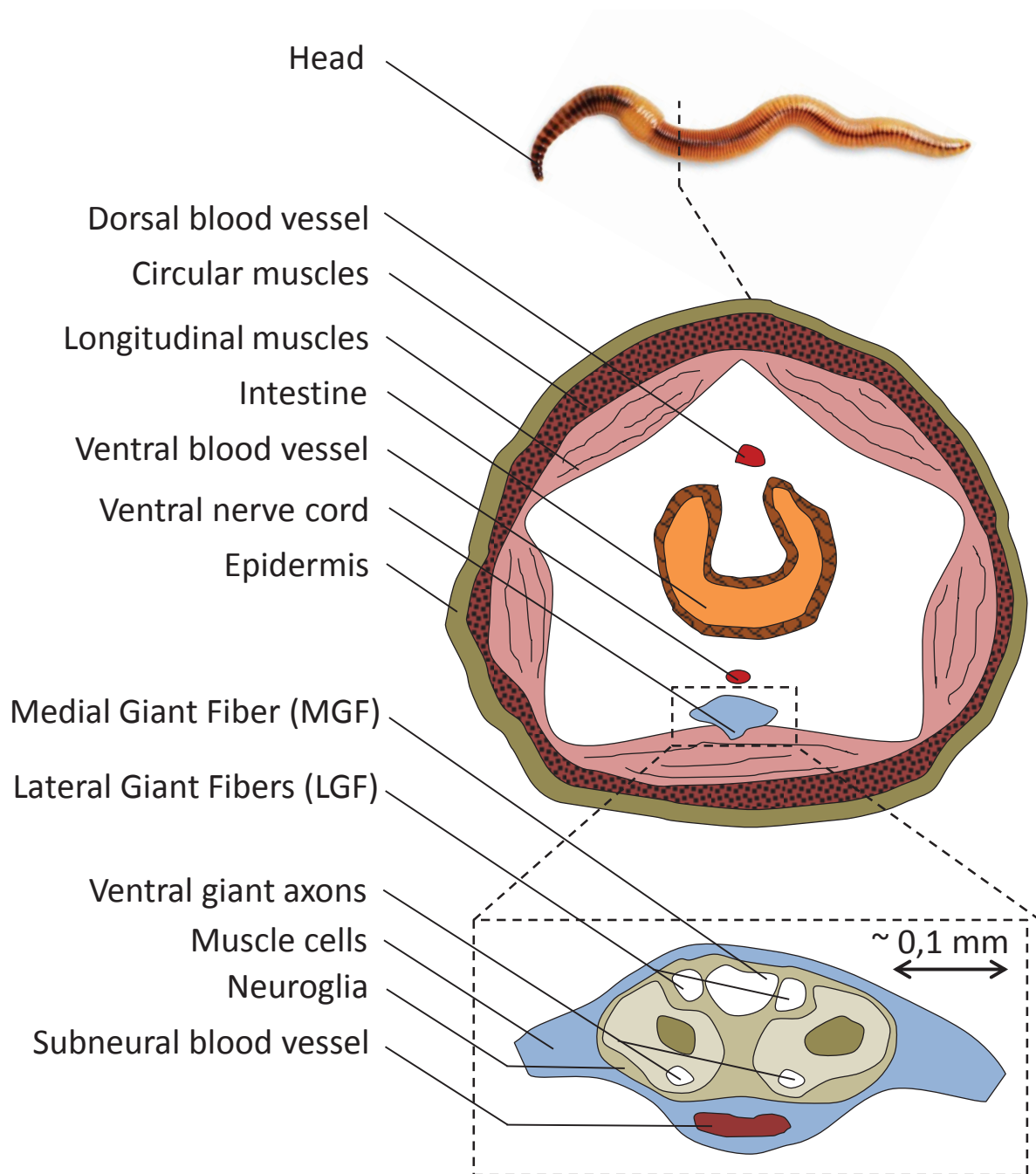


Figure 27 - Simplified illustration of a cross section of *Lumbricus terrestris* in segments posterior to the clitellum.

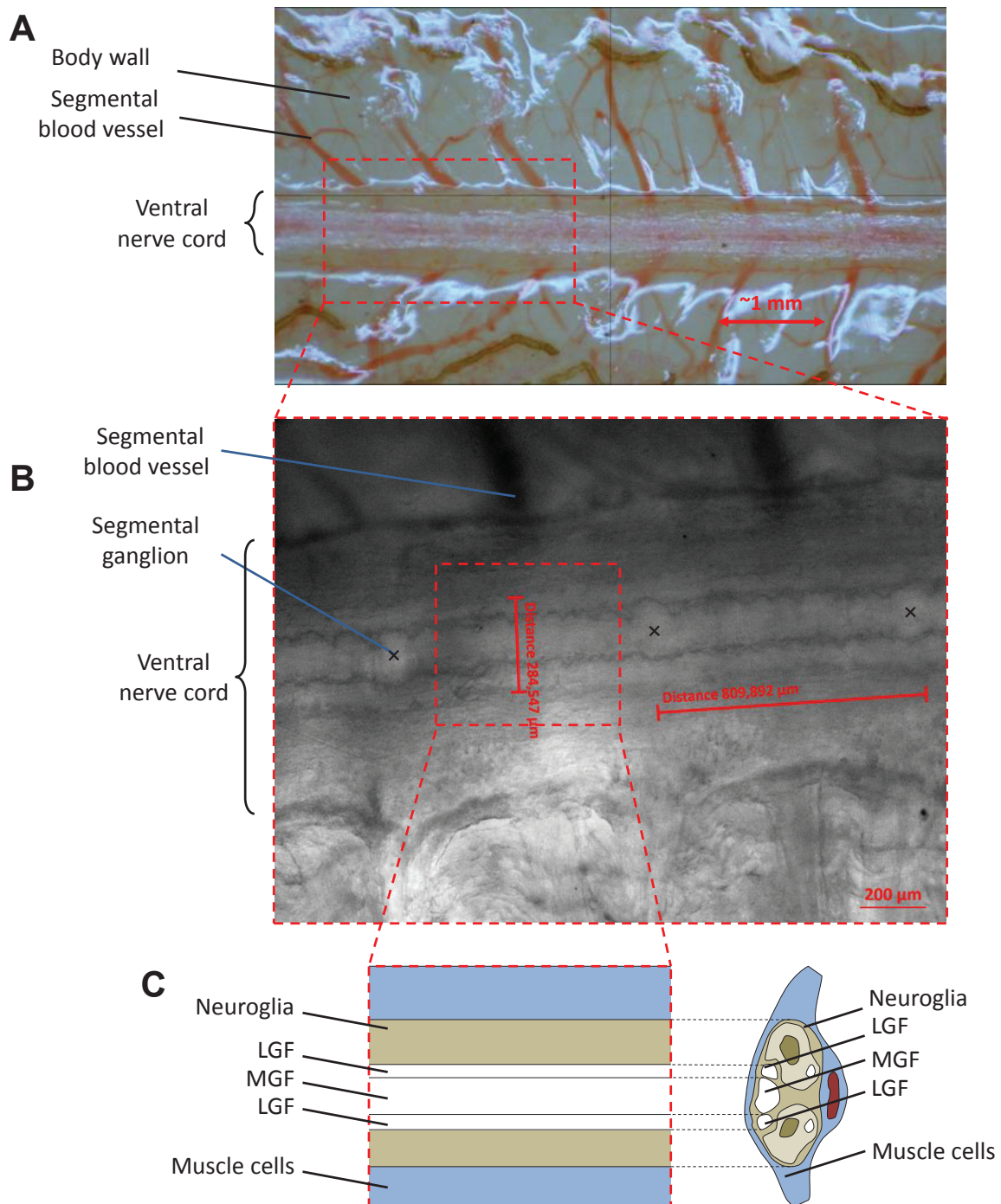


Figure 28 – Structure of the ventral nerve cord of *Lumbricus terrestris*. (A) Close view of an *ex vivo* preparation of the ventral part of the body wall of an earthworm, clearly displaying the segmental blood vessels. (B) Microscopic view of a similar preparation focusing on the exposed ventral nerve cord, allowing the identification of the segmental blood vessels, segmental ganglia and giant fibers. (C) Schematics of the inner structure of the ventral nerve cord.

I.D.3.ii. The medial giant fiber

Three ventral collaterals are associated with MGF in each segment (Figure 29). Two of them, relatively short, branch at the levels of the 1st and 3rd segmental nerves and terminate in the central neuropil of the nerve cord. The third and longest MGF collateral actually represents the neurite of the MGF cell body (Günther, 1971a; Mulloney, 1970; Günther and Walther, 1971; Günther, 1972). The main **outputs** of MGF are three pairs of giant motor neurons in each segment (**Figure 29**). The **inputs** of MGF are mediated by a giant interneuron in each segment, whose collaterals are associated with the ventral sensory neuropil and with the three MGF collaterals. The function of afferent processing associated with the giant interneurons has been justified by an interesting structural characteristic of them. Their diameter, as well as the caliber and length of their collaterals, are greatest in anterior segment and decrease in more posterior segments. **These morphological gradients correlate with physiological evidence for anterior localization of the MGF sensory field** (Günther and Walther, 1971).

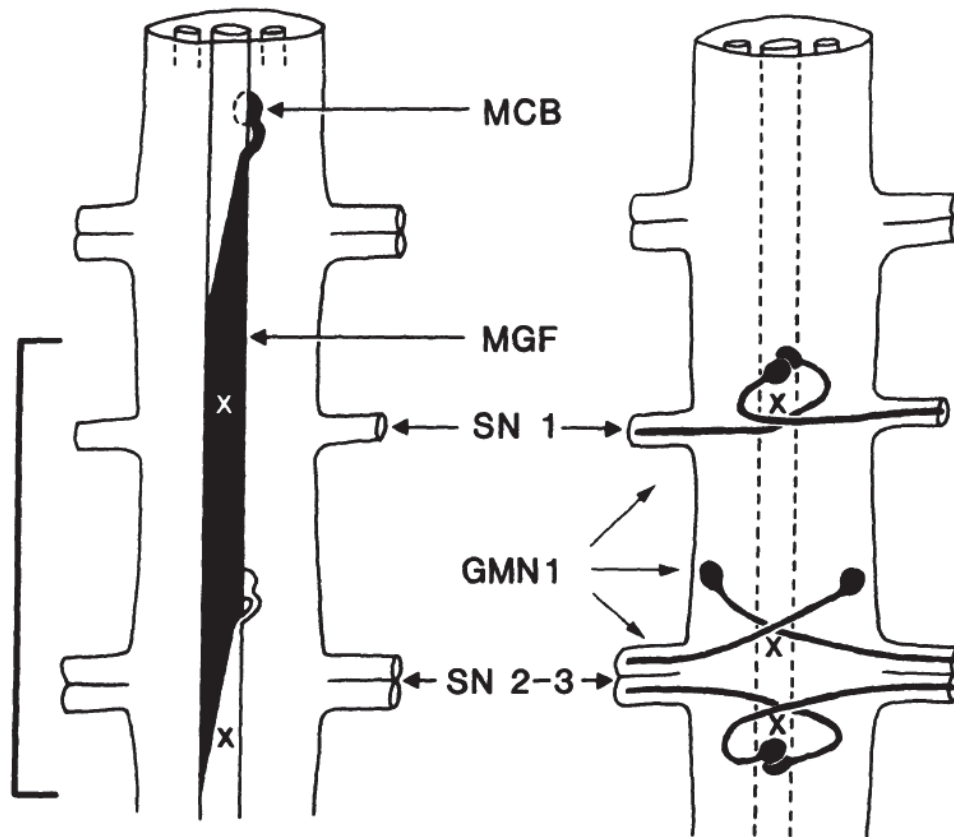


Figure 29 - Cellular organization of the MGF system. GMN = Giant motor neuron, SN = segmental nerve, MCB = MGF cell body (Drewes, 1984).

I.D.3.iii. The Lateral Giant Fibers

Four ventral collaterals are associated with LGF in each segment (Figure 30). One of them represents the neurite of the LGF cell body, which is located ventrolaterally on the opposite side of the nerve cord (Günther, 1971a; Günther and Walther, 1971; Günther and Schürmann, 1973). Neurites arising from the paired LGF cell bodies come into close association with one another at point of **decussation** ventral to the MGF (Drewes et al., 1978; Mulloney, 1970). Another collateral projects medially where one of its branches forms a **cross-bridge** with the corresponding branch of the contralateral LGF. Thus, there are two sites of close anatomical association between left and right LGF in each segment, involving two different collaterals in each LGF. These collateral connections lead to the **two LGF working as**

a **single functional unit**, characterized by an electronic coupling (Wilson, 1961) and a bilateral synchronization of LGF action potentials during propagation along the nerve cord (Rushton 1945a). The **outputs** of LGF include a pair of motor neurons in each segment, whose axons decussate and are closely associated with the LGF cross-bridge (**Figure 30**). The **inputs** of LGF are mediated, at least in posterior segments, by LGF collaterals projected into the ventral sensory neuropil.

The anatomical associations between giant fiber cell membranes from adjacent segments consist of obliquely arranged septa (Stough, 1926). Evidence of **electrical synapses** between the LGF of adjacent segments has been provided (Kensler et al., 1979). The non-rectifying properties of the septum account for the capability of **bidirectional impulse conduction** that was originally demonstrated in several classic studies of conduction in earthworm giant fibers (Bullock, 1945; Rushton, 1945).

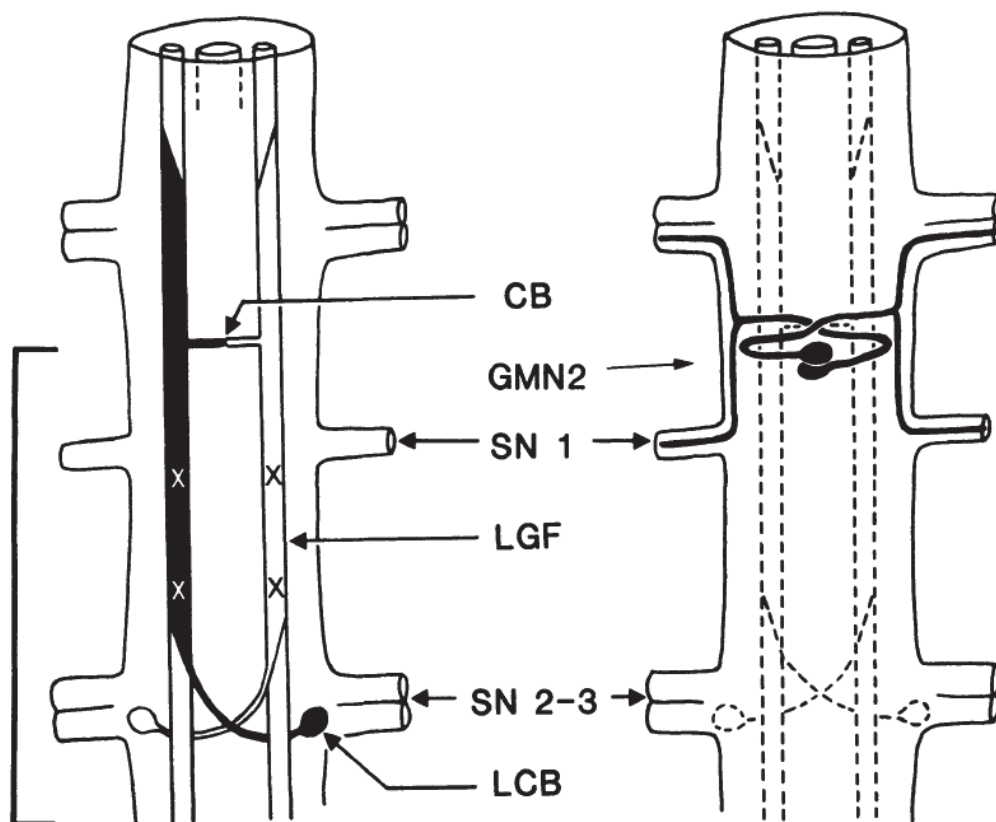


Figure 30 - Cellular organization of the MGF system. GMN = Giant motor neuron, SN = segmental nerve, LCB = LGF cell body, CB = Cross-bridge (Drewes, 1984).

*I.D.4. Conduction properties of giant fibers in *Lumbricus terrestris**

As previously mentioned, in animals with highly elongated body, there can be a substantial saving in escape reflex time by maximization of giant fiber conduction velocity along the animal. Large diameter axon is an important factor contributing to relatively high conduction velocity (CV) but is not the only one. In this section, we will review the different anatomic and physiologic factors responsible for the relatively high CV associated with the giant axons of *Lumbricus terrestris*.

I.D.4.i. Typical values of conduction velocities in MGF and LGF

Typical values of non-facilitated CV, measured in the intact non-anesthetized earthworm, are **30-38 m/s** for MGF and **11-15 m/s** in LGF (Drewes et al., 1978; Drewes, 1984). These values are considerably higher than those measured from isolated nerve cord (Kao and Grundfest, 1957), leading to think that isolation procedures somehow affect conduction properties in an adverse way. As we will see in the experimental results presented in part II, anesthetic procedures also seem to have an adverse impact on conduction properties.

I.D.4.ii. Large diameter

In earthworm giant fibers, the relationship between CV and **axonal diameter** is linear, with a slope of 0.5 (Adey, 1951; O’Gara et al., 1982). This value is substantially greater than for most other invertebrate giant fibers, which could be explained by the myelin sheath surrounding the giant fibers of *Lumbricus terrestris*. Hence, a 20 μm increase in diameter leads to a 10 m/s increase in CV. MGF’s diameter is typically 70 μm and LGF’s diameter typically 50 μm , but their difference in terms of CV is higher than 10 m/s because other factors than axonal diameter are at play.

I.D.4.iii. Insulating sheath

We already mentioned that the respective myelinlike sheaths of both MGF and LGF are interrupted in each segment where collaterals project from the main branch. In addition, MGF presents, in each segment, two openings in the dorsal surface of the sheath, 10-15 μm in diameter, called **dorsal nodes**. Dorsal nodes act as current sources and sinks during action potential propagation (Günther, 1973, 1976), hence representing focal point for electrogenesis.

I.D.4.iv. Formation of syncytia

Another factor contributing to the minimization of conduction time is the formation of multineuronal **syncytia** by elimination of septal boundaries (Günther, 1971a; Günther, 1975). Syncytia are cytoplasmic fusion of unicellular giant fiber metameres. In *Lumbricus terrestris*, it was found that about 60% of the septa were missing in MGF and 20% in LGF. CV across a septum is slower than CV in the same fiber in the absence of a septum (8 m/s against 25 m/s). Summed over the whole length of the animal, the presence of syncytia translates into a time saving of 3 ms for the propagation of an AP along MGF, which represent a substantial percentage of the total MGF conduction time, estimated at 5 ms (assuming an animal length of 150mm and an average MGF velocity of 30 m/s).

I.D.4.v. Facilitation of conduction velocity

A last factor affecting conduction velocity in giant fibers is **antecedent spiking activity in the fibers**. It has been shown, both in the isolated ventral nerve and in the intact animal that the giant fiber conduction velocity increases by as much as 20% for AP occurring shortly after a “conditioning AP”. Bullock showed that this phenomenon, which he refers to as “facilitation of conduction velocity”, was most pronounced about 6 ms after the conditioning spike but was still evident at interval greater than 100 ms. As a result of this phenomenon, the interspike interval between a given pair of AP tends to progressively diminish as the AP propagates along the giant fibers. An interesting physiological consequence of this reduced interspike interval is the enhanced probability for a pair of LGF spikes to trigger a giant motor neuron in anterior

segments, where the interspike interval will be shortest.

*I.D.5. Afferent pathway in *Lumbricus terrestris**

I.D.5.i. Sensory fields of MGF and LGF

In *Lumbricus terrestris*, giant **fibers** can be activated by various abruptly delivered mechanical stimuli including body wall touch, pressure and substrate vibration (Drewes, 1984). Functional differences between MGF and LGF afferent pathways can be highlighted by mapping their respective **sensory fields**. **Tactile stimulation of the most anterior segments systematically triggers APs in MGF, and tactile stimulation of the most posterior segment systematically trigger AP in LGF**. In addition to this sensory **polarity** exists a **longitudinal gradient of sensitivity**: the sensitivity of MGF and LGF sensory fields are the highest at the ends of the animal and diminish toward middle segments (Günther, 1973). An area of overlap between MGF and LGF respective sensory fields can be identified centered about one third of the way back along the animal (Moore, 1979). The amount of overlap is animal-dependent but also depends on the amount of previous stimulations.

I.D.5.ii. Characterization of mechanosensory neurons

Several sensory neurons involved in the excitation of giant fibers have been identified. They consist of serially homologous **mechanosensory neurons** with cell bodies in the ventral cord and with axons projecting into segmental nerves (Drewes, 1984). These neurons have been classified in two groups by Gunther, based on anatomical criteria (Günther, 1970; Günther, 1971b). The **PN2** group consists of 5-7 bilaterally arranged pairs of neurons per segments, with axons projecting longitudinally through the third segmental nerve (SN3) (**Figure 31**). The **PN3** group consists of two pairs of neurons, each of them giving rise to 2-3 axonal branches which exit ipsilaterally through the first (SN1) and third (SN3) segmental nerve of the same segment or adjacent segments.

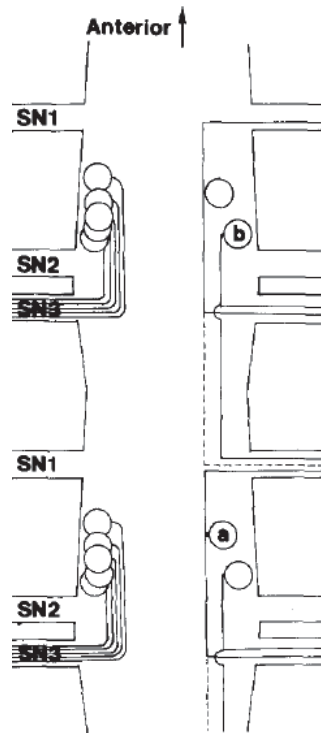


Figure 31 - Schematic representation of two consecutive segments of the nerve cord, with cell bodies and processes of the touch neurons (right side) and pressure neurons (left side) (Smith and Mittenthal, 1980).

Besides their anatomical organization, these two groups of neurons differ by their physiological function. **PN3** are classified as **touch-sensitive neurons**: they respond to light tactile stimulation of the body wall (with a thrust greater than 3 g), by evoking a **phasic** burst of spikes (Smith and Mittenthal, 1980). **PN2** are classified as **pressure-sensitive neurons**: they respond to relatively strong tactile stimulation (thrust from 10-20g) by a **tonic** spiking activity.

I.D.5.iii. Synaptic inputs to MGF and LGF

The synaptic inputs to MGF and LGF from PN2 and PN3 neurons have been studied by Smith and Mittenthal (Smith and Mittenthal, 1980).

In both type of giant fiber, each touch neuron spike (PN3 neuron) evokes a depolarizing

post-synaptic potential (PSP) that peaks after the touch neuron spike enters the ventral nerve cord, with a relatively small latency. In MGF, the amplitude of the PSP is greatest in anterior segments and absent in posterior segments. Symmetrically, in LGF, the amplitude of the PSP is greatest in posterior segment and absent in anterior segments.

In both MGF and LGF, each pressure neuron spike (PN2 group) evokes a depolarizing PSP initiated after a latency of about 3 ms. On the basis of the constancy of PSP amplitude and the absence of PSP failure during high-frequency bursts of pressure neuron spikes, the authors suggest the existence of an **electrical synapse** between afferent (at least pressure neurons) and giant fibers. For pressure neuron inputs, a longitudinal gradient in PSP amplitude could be exhibited, closely similar to that of touch neurons.

The **strength of the synaptic connection** between afferent fibers (both touch- and pressure- sensitive neurons) and giant fibers could provide a physiological explanation for the sensitivity gradients of MGF and LGF sensory fields.

I.D.6. Efferent pathway

The efferent pathway of the system of giant fibers will not be discussed at such a detailed level as the afferent pathway. Indeed, since the animals used in the studies presented later in this chapter are under anesthesia, our method of assessing if a stimulus was successful or not was not based on a motor response, but on the detection of actions potentials in the giant fibers (see II.A.3). Hence, the causal approach followed to interpret our results is solely focused on the afferent and giant pathway. However, some essential characteristics of the efferent pathway need to be known in order to understand the complex machinery underlying the whole escape reflex, whose different components are detailed in the next section.

MGF system is associated with three pair of serially homologous giant motor neurons, called **GMN1 (Figure 29)** (Günther and Walther, 1971; Günther, 1972). For each MGF spike in the ventral nerve cord, one GMN1 spike is triggered with a short latency (minimum = 0.6 ms), suggesting an electrical junction between MGF and GMN1. With repetitive stimulation, GMN1-mediated muscle potentials show facilitation in amplitude. Synaptic facilitation is a form of short-term plasticity that enhances synaptic transmission for less than a second (Jackman and Regehr, 2017). There is a pronounced longitudinal gradient in the amount of

facilitation along the animal, the greatest amount occurring in the most anterior 60 segments and gradually in more posterior segments.

LGF system is associated with a separate set of giant motor neurons, called **GMN2** (**Figure 30**) (Drewes, 1984). The transmission between LGF and GMN2 is less reliable than between MGF and GMN1, and results obtained in dissected preparation suggest some type of monosynaptic transmission (Günther and Walther, 1971). The efficiency of transmission is the highest in anterior segments, and diminishes in a monotonic anterior-posterior gradient along the animal, **except in extremely posterior segments where there is an increase in efficacy** (Drewes and McFall, 1980).

I.D.7. Rapid escape movement

In section I.C.1 have been presented the different layers of muscles interlacing the body wall and septa, and we just discussed in this section the afferent, giant and efferent nervous pathways and the transmission gradients existing between each of them. At last, we shall see how the different elements of this complex machinery work together to provide *Lumbricus terrestris* with an effective escape reflex. Moreover, studying the characteristic timings of this escape reflex will provide us useful insight to interpret the timings of the various nervous responses observed in the studies presented in part II of this chapter.

I.D.7.i. Anterior stimulation

The rapid response of an earthworm to abrupt tactile stimulation of anterior segments consists of several components: i) a rapid and vigorous **longitudinal shortening**, ii) a **dorso-ventral flattening** of the posterior part of the animal, and iii) a **forward pointing of setae** in tail segments. The last two components obviously play a role in anchoring the animal to facilitate the withdrawal away from the stimulus, elicited by the first component.

A prerequisite for the above mentioned **shortening** is a longitudinal muscle electrical potential of some critical amplitude. This potential amplitude, mediated by GMN1, requires at least two closely spaced MGF spikes (8-12 ms interspike interval) (Drewes and McFall, 1980). Because of the anterior-posterior gradient in muscle potential facilitation, this shortening tends

to be localized within anterior segments. Rapid shortening can occur in middle segments, but requires longer train of MGF spikes, is wicker and occurs 5-10 ms later than in anterior segments (Drewes, 1984). This focusing of MGF-mediated shortening into anterior segments makes sense in terms of survival strategy, since these segments are more vulnerable to be attacked as the animal's head is extended from its burrow.

The tail component of the response to anterior stimulation is also mediated by MGF, the effectors being in this case the septal muscles. It has been showed that the onset of tail-flattening responses to anterior tactile stimulation occurred 1-16 ms before the onset of anterior shortening, in spite of the fact that the antecedent MGF spikes were initiated in head segments (Pallas and Drewes, 1981). Hence, because of this time difference, tail flattening would help anchor the animal's tail in the burrow before longitudinal shortening of anterior segments occurs, which would increase the efficacy of the overall escape response.

The minimal time from the delivery of a mechanical stimulus to onset of an MGF spike in the most anterior segments is approximately **5 ms**. The total conduction along the animal is about **5 ms** (assuming an animal length of 150 mm and an average MGF velocity of 30 m/s). The minimal time from the occurrence of the first MGF spike in tail segments until onset of tail flattening is approximately **15 ms**. Hence, the minimal reflex time for tail flattening after anterior stimulation is estimated to be **25 ms**, with the longitudinal shortening occurring a few milliseconds later.

I.D.7.ii. Posterior stimulation

The rapid response of an earthworm to an abrupt tactile stimulation of posterior segments consists in a rapid and vigorous end-to-end shortening, particularly pronounced in posterior segments (Studnitz, 1937; Rushton, 1945; Drewes and McFall, 1980). The underlying neural basis seems to be a high-frequency train of LGF spikes, associated with a repetitive firing of GMN2 spikes and longitudinal muscles potentials along the entire animal. The focusing of withdrawal into posterior segments in response to posterior stimulation might have a neural basis similar to that involved in the response to anterior stimulation but has not been completely explained so far.

II. Characterization of the ultrasound transducer

II.A. Methods

II.A.1. Acoustic pressure field

The distribution of acoustic pressure generated by the US transducer, at $f_0 = 1.1$ MHz fundamental frequency, was measured in water using a certified and preliminary calibrated fiber-optic hydrophone (FOPH 2000, RP Acoustics, Germany). 2D mechanical raster-scanning were performed with a commercially available computer-driven 3-axis motorized hydrophone bench (UMS Test Tank, Precision Acoustics Ltd, Dorchester, UK) to reconstruct pressure maps in longitudinal (xOz and yOz) and transverse plans (xOy). A primary calibration of the US transducer was performed by measuring at the focus the evolution of the spatial peak pulse average acoustic pressure (pulse average performed on the steady part of a pulse with a 100% duty cycle), p_{sppa} , as a function of the amplified AC driving voltage, V_{AC} . The location and extent of the transducer focal spot was assessed by considering regions where normalized time peak acoustic intensities, I_{dB} , where greater or equal to -6dB, which corresponds on pressure maps to the regions with pulse average pressures, p_{pa} , greater or equal to $p_{sppa}/2$ (half maximum), according to equation (22) :

$$I_{dB} = 10 \cdot \log\left(\frac{I_{pa}}{I_{sppa}}\right) = 10 \cdot \log\left(\frac{p_{pa}^2}{p_{sppa}^2}\right) \geq -6dB \quad (22)$$

The size of the -6 dB focal spot in a given dimension (x, y or z) was given as the full width at half maximum pressure. Because of the cylindrical symmetry of the transducer, the focal spot widths along x and y will be referred as the radius of the -6 dB focal spot, r_{-6dB} , and the focal width along z will be referred as the length of the -6 dB focal spot, l_{-6dB} .

Complementarily, the acoustic field distribution was simulated using a simulation platform currently under development in a CEA-LIST/LabTAU partnership (CIVA Medical, V17, CEA-LIST/LabTAU, France) which provides a 3D CAD interface and allows reducing computation time with the use of optimized parallel computing (Chavrier et al., 2000). This modeling

method has been used to provide high spatial resolution 3D pressure maps of the US field generated at $f_0 = 1.1$ MHz fundamental frequency in water. The distribution of the US field generated at 3.3 MHz with the same transducer geometry was also simulated to model further experimental neurostimulation investigations using the 3rd harmonic frequency, f_3 , of the prototype.

II.A.2. Radiation force

The time average acoustic radiation force produced by a transducer, F_{ta} , on a target can be measured using a radiation force balance (RFB). For a plain (no centre hole) spherical transducer targeting a flat totally absorbing target, the RFB measurement allows accessing the time average acoustic power, P_{ta} , with the following expression:

$$P_{ta} = \frac{2}{1+\cos\alpha} \cdot F_{ta} \cdot c \quad \text{with} \quad F_{ta} = \Delta m \cdot g \quad (23)$$

Where:

- c is the speed of sound in water ($c = 1480$ m/s)
- Δm is the variation of mass measured by the RFB with and without ultrasound exposure
- α is the outer aperture ‘half-angle’ subtended by the transducer
- g is the standard acceleration due to gravity ($g = 9.8$ m/s²)

The factor $\frac{2}{1+\cos\alpha}$ translates the accounting for the particular geometry of the transducer, which is focused and thus induces a range of angles of incidence of the ultrasound beam on the target (Beissner, 1987). The outer aperture ‘half-angle’ is defined as follows:

$$\alpha = \arcsin\left(\frac{a}{R}\right) \quad (24)$$

Where:

- R is the radius of curvature of the focused transducer
- a is the radius of the active element.

As illustrated by **Figure 32**, the geometry of the focused transducer used in this study led to a α value of 30° .

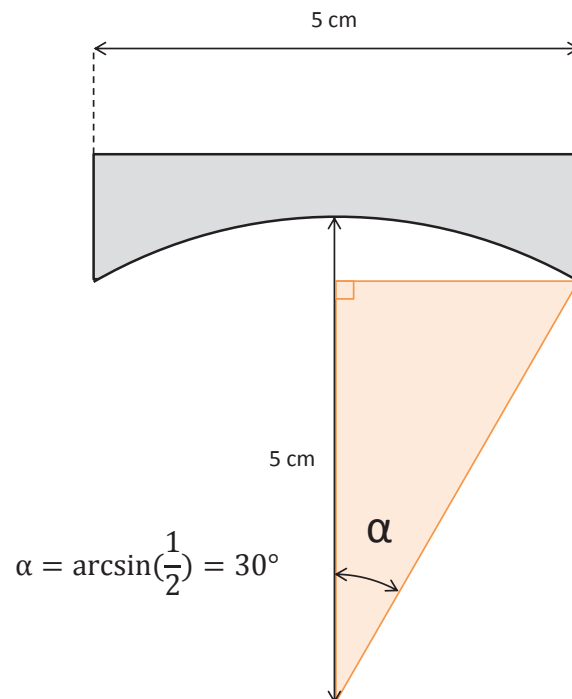


Figure 32 - Geometry of the focused ultrasound transducer used in chapters 2 and 3. A 5-cm radius of curvature and a 5-cm active element radius lead to an outer aperture ‘half-angle’ value of 30° .

A commercially available certified RFB device (RFB-2000, Onda Corporation, USA) was used which was composed of a cylindrical tank (22 cm high, 18 cm in diameter), on the bottom of which rests a force-sensitive platform. First, the tank was filled with degassed water. Secondly, as a precaution, a brush target (RFB-BTK) designed to measure radiation force at high power (Howard and Zanelli, 2007) was placed on the platform (**Figure 33**). Prior to submerging it in the degassed water, the brush target was placed in a vacuum chamber for 10 minutes, in order to remove any bubble potentially trapped in it. Then, the RFB set-up was

calibrated by measuring 5 times the static force generated by a 1-gram reference weigh placed on top of the brush target, and by removing and replacing the weigh between each measurement.

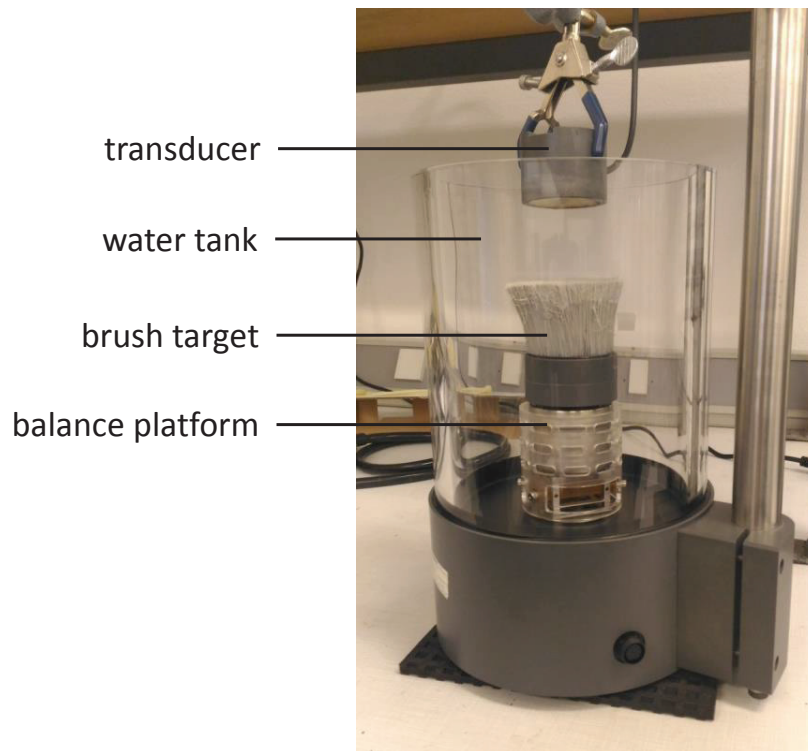


Figure 33 - Set-up for the measurement of the radiation force generated by the ultrasound transducer.

The transducer was hung 5 cm above the top of the brush, face down, its transverse plane parallel to the plane of the platform. The radiation force generated by the transducer was characterized at both its fundamental frequency ($f_0 = 1.1$ MHz) and third harmonic ($f_3 = 3.3$ MHz). For each frequency, the evolution of the ultrasound-induced radiation force was measured as a function of the driving voltage ranging from 20 to 260 Vpp with 30-Vpp increment. For each V_{AC} value, five consecutive radiation force measurements were performed and averaged. During the measurement, ultrasound was turned ON for 2 to 3 seconds, with a 6% duty cycle. This value of duty cycle was chosen arbitrarily to be closed to the typical values used in the US stimuli, and also to prevent any risk of damaging the brush target. The total

pulse average acoustic power generated by the transducer during the active part of the ultrasound pulse, P_{pa} , was thus given by the following expression:

$$P_{pa} = \frac{P_{ta}}{DT} \quad (25)$$

Where DT (%) is the duty cycle associated with an ultrasound pulse.

II.A.3. Definition and calculation of the “pulse intensity”

In the rest of the manuscript, we will use the term “pulse intensity” to refer to the ultrasound intensity generated at the focus by the US transducer on average spatially and temporally. The pulse intensity was calculated as the spatial average pulse average intensity, I_{sapa} , concentrated within the -6 dB focal spot in the transverse plan (hence ‘spatial average’), during the pulse duration (hence ‘pulse average’) while assuming a 100% duty cycle. I_{sapa} can be calculated from hydrophone measurements according to the following formula:

$$I_{sapa} = \iint_S I_{pa} = \frac{1}{2Z} \iint_S p_{pa}^2 \quad (26)$$

Where I_{pa} (and p_{pa}) are respectively the pulse average acoustic intensity (and pressure measurable by the hydrophone method) generated by the transducer for a pulse of a 100% duty cycle.

I_{sapa} can also be approximated from RFB measurements according to the following formula:

$$I_{sapa} = \frac{1}{S} \iint_S P_{pa}^2 \sim \frac{1}{S \cdot DT\%} \iint_{S_{RFB}} P_{ta}^2 \quad (27)$$

Where:

- P_{ta} is the time average acoustic power generated with a given duty cycle DT% by the transducer, and measurable by the RFB method
- P_{pa} is the pulse average acoustic power generated by the transducer for a pulse of a 100% duty cycle
- $S = \pi \cdot r_{-6dB}$ is the disc-shaped surface of the -6 dB focal spot of radius r_{-6dB} , in the transverse plan (see section II.A.1 for its definition and calculation)
- S_{RFB} is the total surface of measurement of the RFB brush target

II.B. Results

II.B.1. Acoustic pressure field

The acoustic pressure distribution generated by the transducer in water, at 1.1 MHz, was experimentally assessed. **Figure 34** presents the 2D map and 1D pressure profiles in the focal plan. From two values measured in orthogonal directions, the mean radius of the -6 dB focal spot was estimated at $r_{-6dB} = 0.96$ mm.

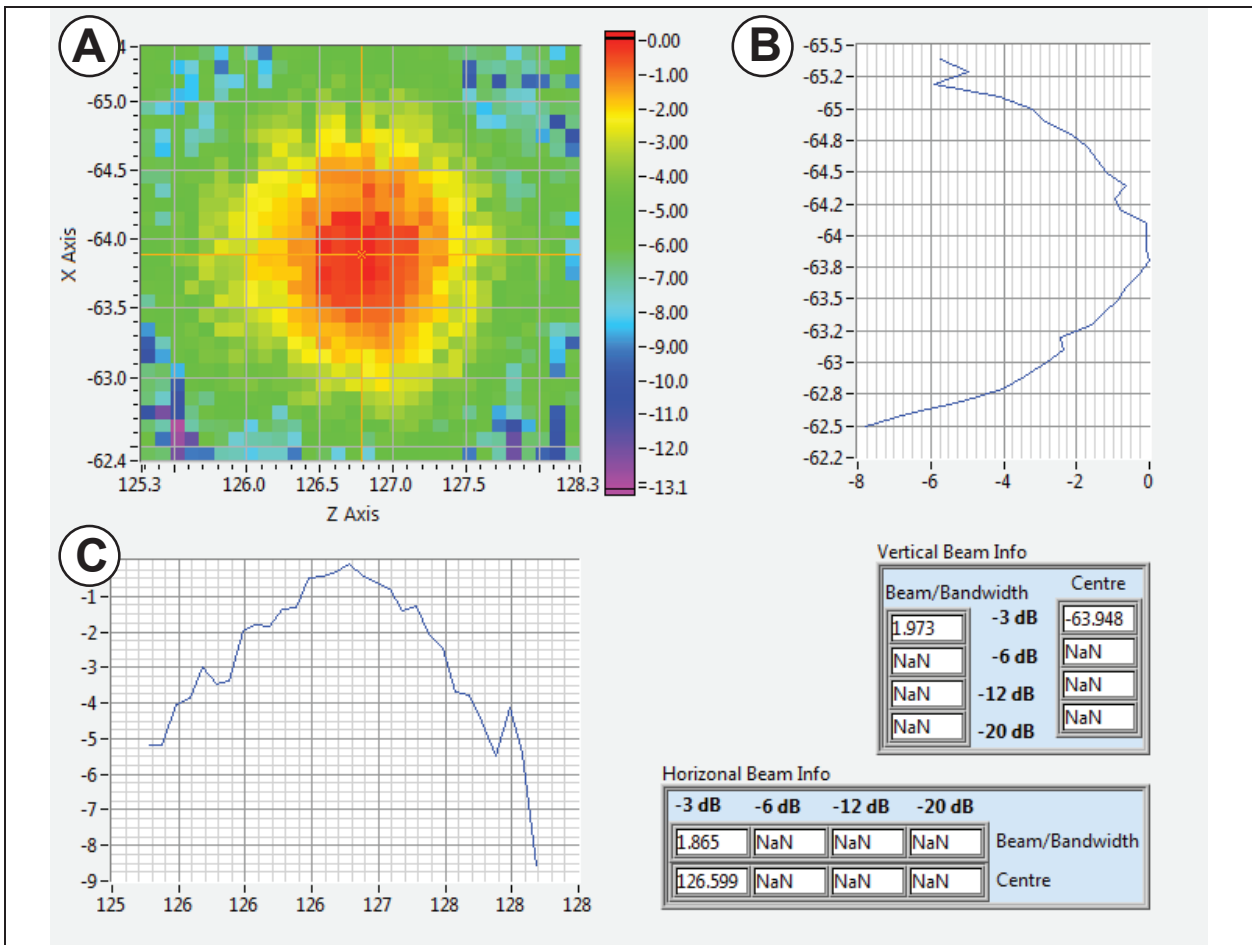


Figure 34 - Acoustic pressure field measured in the focal plan. The 2D map (A) displays the distribution of acoustic peak-to-peak pressure, in logarithmic scale. The 1D charts display the pressure profile passing by the pressure maximum, in the vertical (B) and horizontal (C) direction, respectively. A gain of -3 dB in terms of acoustic pressure corresponds to a gain of -6 dB in terms of net acoustic intensity. Hence, the -6 dB focal spot defined in section II.A.1 visually corresponds to the ‘-3 dB’ area on the pressure map.

Figure 35 presents the calibration curve built to evaluate the spatial-peak acoustic pressure in function of the transducer driving voltage amplitude, at 1.1 MHz.

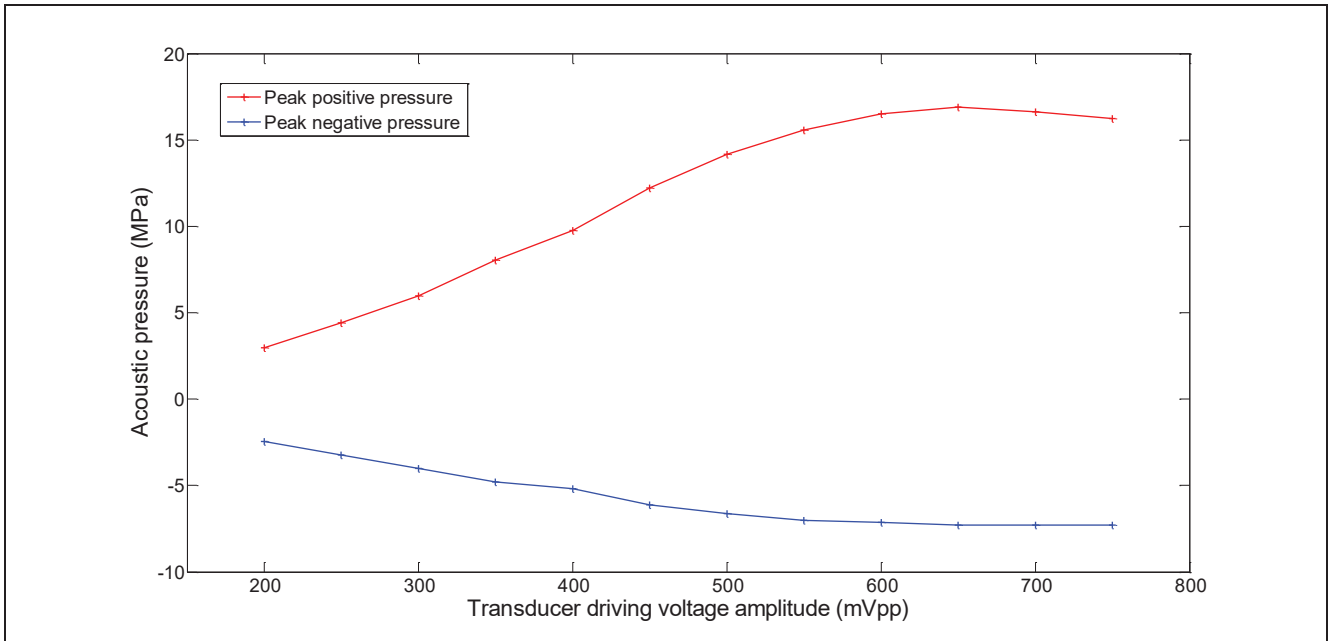


Figure 35 - Calibration curve of the spatial peak acoustic pressure generated by the transducer in function of its driving voltage amplitude. The red curve represents the value of the peak positive pressure, and blue curve the value of the peak negative pressure.

The results from the simulation of the acoustic pressure distribution are presented in **Figure 36** and **Figure 37**. At 1.1 MHz, the -6 dB focal spot was found to be 12 mm in depth and 1.86 mm in width. Hence the simulated radius of the -6 dB focal spot is 0.93 mm, which is relatively close to the experimental value ($r_{-6dB} = 0.96$ mm). At 3.3 MHz, the -6 dB focal spot was found to be 4 mm in depth and 0.64 mm in width. We can note that, at 3.3 MHz, the focal spot is about 3 times smaller than at 1.1 MHz, but that the spatial peak acoustic pressure is 3 times higher.

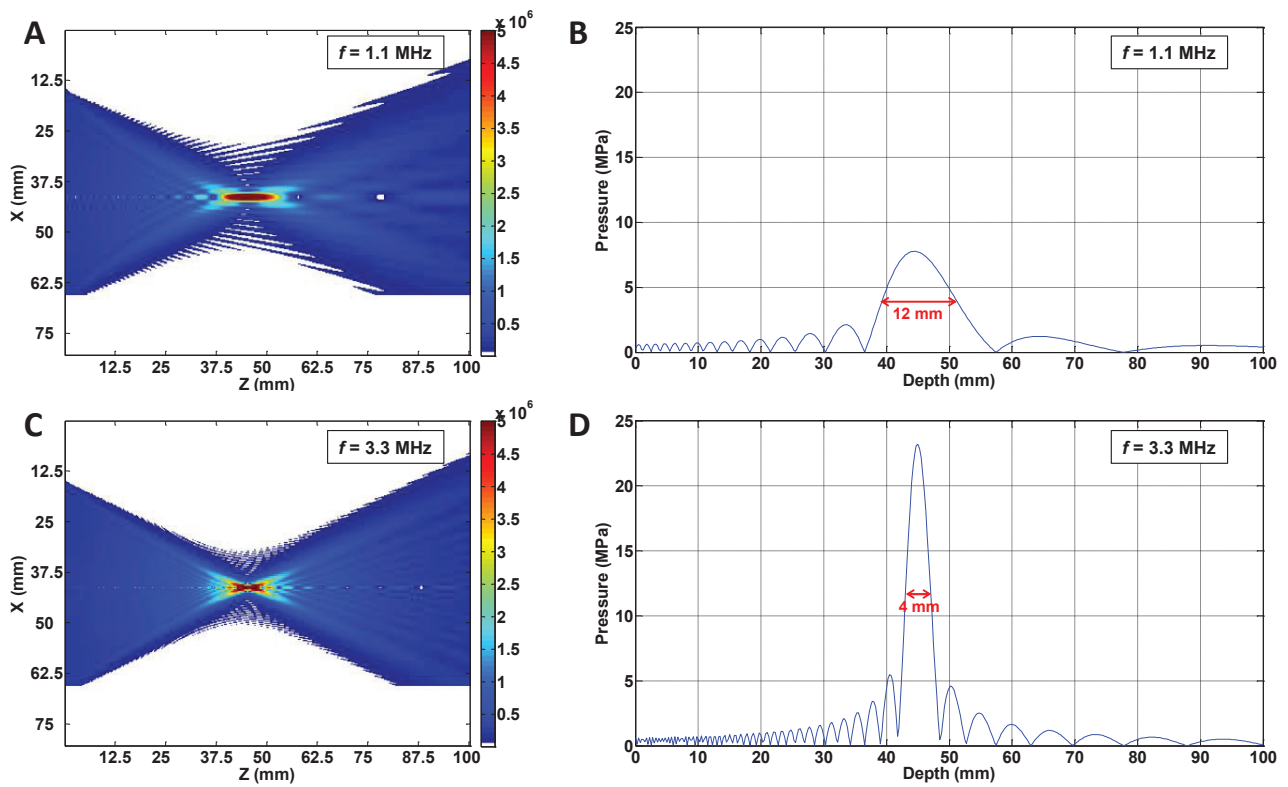


Figure 36 - Simulation of the acoustic pressure distribution generated by the transducer at 1.1 MHz (A, B) and 3.3 MHz (C, D). A and C show the pressure map in the longitudinal focal plan. B and D show the pressure profile along the longitudinal focal axis. Red arrows represent the length of the -6 dB focal spot.

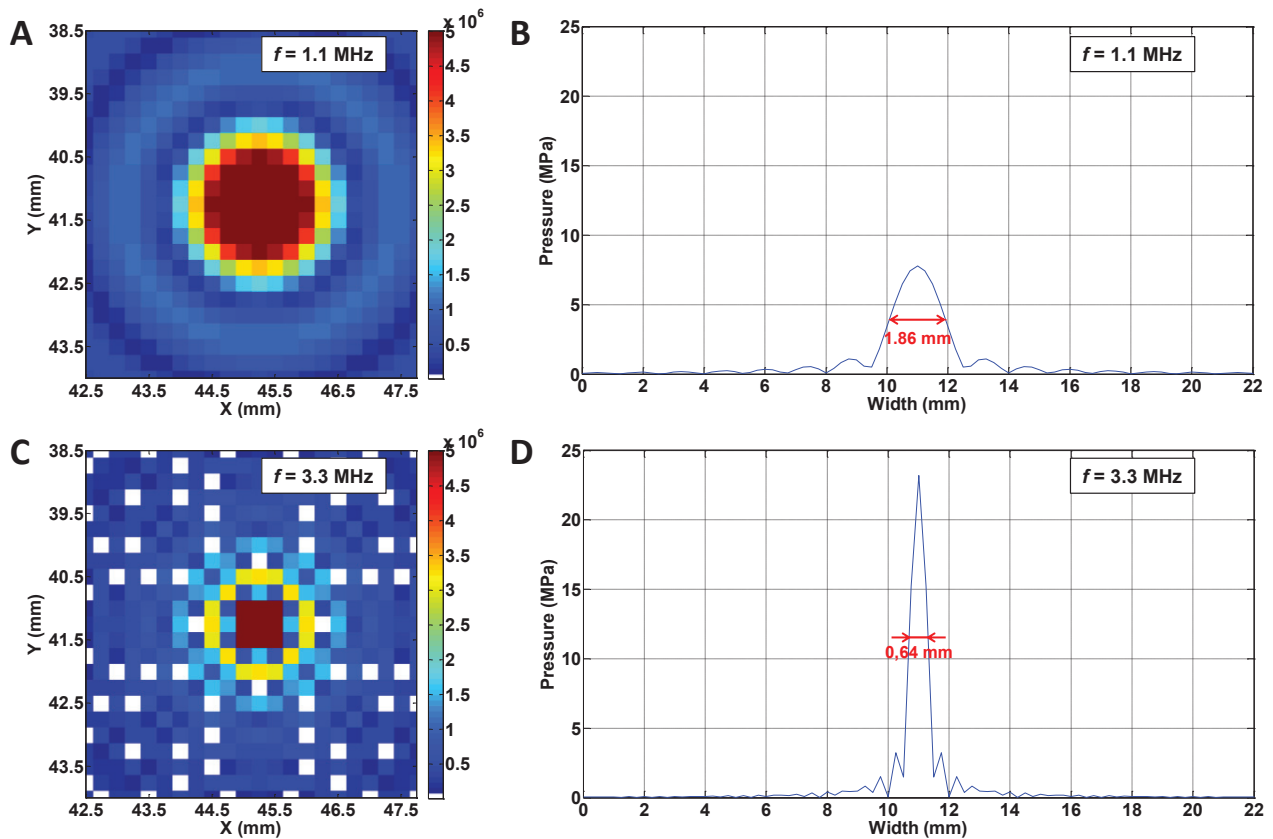


Figure 37 - Simulation of the acoustic pressure distribution generated by the transducer at 1.1 MHz (A, B) and 3.3 MHz (C, D). A and C show the pressure map in the transverse focal plan, close to the focal area. B and D show the pressure profile along a transverse axis crossing the spatial peak. Red arrows represent the width of the -6 dB focal spot.

II.B.2. Radiation force and pulse intensity

Table 1 presents the values of radiation force produced by the transducer for different values of driving voltage amplitudes, at 1.1 MHz and 3.3 MHz, for a duty cycle of 6%.

Table 1 – Radiation force values produced by the transducer for a duty cycle of 6%, in function of the driving voltage amplitude

V_{ds} (mVpp)	F (mN)	
	f = 1.1 MHz	f = 3.3 MHz
100	0,03	0,03
200	0,22	0,21
300	0,77	0,63
400	1,70	1,13
500	2,89	1,53
600	3,84	1,75
700	4,67	1,85
800	5,30	1,92
900	5,70	1,97

From these measurements of radiation force, the values of spatial average-pulse average acoustic intensity (I_{sapa}) corresponding to each driving voltage amplitude could be determined (**Table 2**).

Table 2 – I_{sapa} values produced by the transducer in function of the driving signal amplitude.

V_{ds} (mVpp)	I_{sapa} (kW/cm ²)	
	f = 1.1 MHz	f = 3.3 MHz
100	0,02	0,20
200	0,20	1,68
300	0,68	5,00
400	1,50	8,99
500	2,55	12,13
600	3,39	13,89
700	4,12	14,70
800	4,67	15,26
900	5,02	15,64

II.C. Discussion

After having detailed the organization of the earthworm's nervous system in part I, and that the ultrasound beam produced by the transducer has been characterized, it is possible to discuss the spatial selectivity of the stimulating modality we propose to employ in the study presented in part III.

The dimensions of the focal spot generated by the focused ultrasound transducer, in water, have been evaluated in section II.B.1 (measurement: $r_{-6dB} = 0.96$ mm; simulation: $r_{-6dB} = 0.93$ mm and $l_{-6dB} = 12$ mm). In the experimental set-up which will be presented in the next part of this chapter, the ventral part of the earthworm is placed in the focal region of the transducer, with water as a coupling medium. Compared to the shape of the focal spot in water, the shape of the focal spot at the interface between water and earthworm (whose radially organized layers have been presented in section I.C.1 will be distorted, but we will use the dimensions of the former represent as an approximation of the latter.

Hence, on one hand, we are equipped with a stimulating tool producing an ultrasound ‘paintbrush’ about 2 mm wide. On the other hand, the object of the stimulation is a longitudinally segmented nervous system, with segments about 1 mm wide (see I.C.1). These relative dimensions present a practical advantage for the experimentation. Indeed, because the US focal spot covers more than the width of a single segment, an accurate positioning of the US beam is not necessary to target all the segmental nervous structures with a relatively high degree of certainty. Conversely, it means that it is not possible to perform a fine study (spatial resolution < 1 mm) of the nervous structure responsive to US, within a given segment – even though such a study would not have been possible without an appropriate real-time beam tracking anyway).

III. Application of the proposed nervous model to a comparative study between different modalities of stimulation

III.A. Methods

III.A.1. General approach of the comparative study

In the present study, the respective nervous responses associated with three modalities of stimulation will be compared. On two of them, electrical stimulation (EStim) and mechanical stimulation (MStim), some fundamental knowledge is already available, regarding in particular the locus of interaction between the stimulus and the nervous system. These modalities of

stimulation will serve us as reference to get knowledge on the nervous response to US Stimulation (UStim). To go further, the sensitivity map (which giant fiber is activated, from which region of stimulation) and precise response dynamics (average delay of response, variability of this delay) associated with EStim and MStim, respectively, will be characterized. The same fine characterization will be performed on UStim and from there, a causal approach will be applied to make deductions or assumptions regarding the biophysical interaction between US and the present nervous model.

III.A.2. Animal preparation

Since January 1, 2013, the EU directive 2010/63/EU, on the protection of animals used for scientific purposes, is applicable in France. Points (8) and (9) of the directive specify that the scope of the directive includes vertebrates animals (including cyclostomes), cephalopods, embryonic and fetal forms of mammals. Hence, *Lumbricus terrestris* does not fall into the scope of application of this directive. However, although there is no particular regulation governing the use of this animal species, we followed the ethical principles of the 3Rs, by providing adequate anesthesia prior to any experimentation, and engaging as many relevant trials as possible within the same session, to optimize the use of each animal and reduce the total number of animals necessary to obtain statistically relevant data.

Earthworms were purchased in a local fishing shop and kept at 5°C in containers filled with enriched soil. They were utilized within the two following weeks, otherwise they were released back to the wild. Earthworms were anesthetized prior to each trial by being bathed in a 10% ethanol solution. Times of immersion ranged from 8 to 15 minutes, depending on the size of the animal (as already mentioned in part I of this chapter, earthworms can survive for considerable lengths of time in water if the dissolved oxygen level is high enough). The criterion chosen to end the immersion phase was the absence of response to mechanical stimuli at both ends of the animal. Earthworms were carefully rinsed and dried before being set on the neurostimulation platform. Throughout the trial, whenever the animals exhibited muscular artifacts biasing the measures or showing signs of awaking, they were put back in the anesthetic solution for 1 to 5 minutes, until the above-mentioned criterion of complete anesthesia was met. Nerve functionality was asserted through either mechanical or electrical stimulation. Whenever both

modalities of stimulation failed to trigger a nervous response, the animal was not included in the study.

III.A.3. Experimental set-up

The experimental set-up used throughout the different studies presented in this chapter was composed of the following elements (**Figure 38**):

- A **tank** filled with **degassed water**. Water was renewed on a daily basis. The level of water was adjusted in order for the focal region of the ultrasound transducer to intersect the water surface.
- A **custom-made plate-form** to lay down the earthworm. The plate-form was built with bulk Styrofoam to allow pinning needles into it, and insulated with tape to avoid water infiltration in the foam which would lead to short circuit between electrodes. The plate-form is compound of two separate pieces rigidly linked together, sufficiently spaced from each other to create a space allowing contact between the animal ventral side and the water surface.
- A **positioning system**, compound of three micrometric screws allowing precise displacement of the clip holding the plate-form in position.
- A **system of electrophysiological recording** described in detail in section III.A.4.
- A **system of electrical stimulation** electrical stimulation described in detail in section III.A.6.
- An **ultrasound transducer** place on the bottom of the tank, active face up, described in detail in section III.A.8.

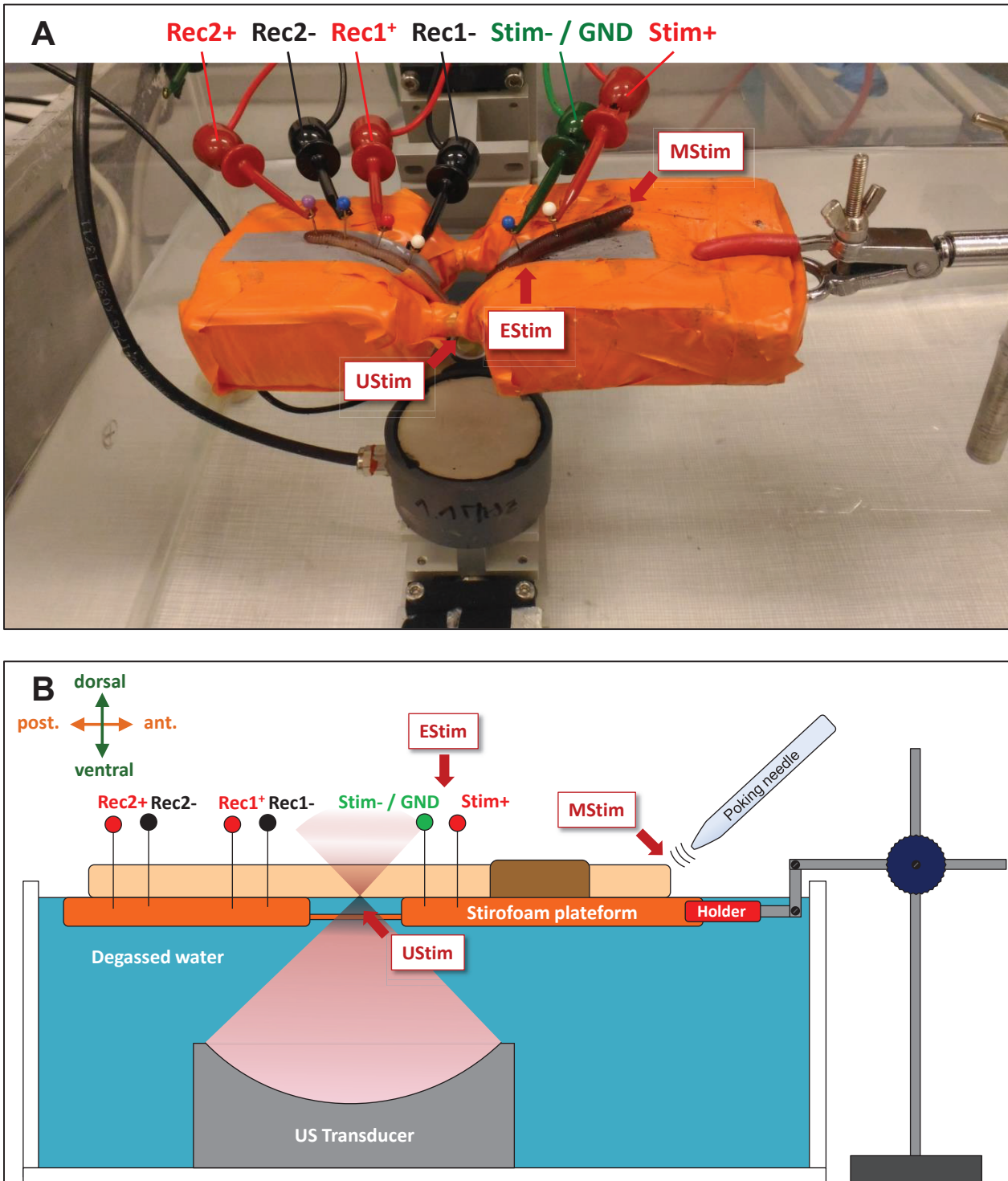


Figure 38 - Experimental set-up used throughout the different studies presented in this chapter: (A) photograph and (B) schematic representation of the set-up, from a lateral view. The configuration of the set-up allows switching from a modality of stimulation to another, with virtually no delay and without manipulating the animal. Recording of the associated nervous

responses is done in real-time, using two pairs of electrodes (Rec1-/Rec1+ and Rec2-/Rec2+). Mechanical stimulation is performed by a poking needle, at either end of the animal. Electrical stimulation is performed using a pair of electrodes (Stim-/Stim+). Ultrasound stimulation is performed by a focused transducer placed in the bottom of the water tank. The respective locations of stimulation of mechanical, electrical and ultrasound stimulation are indicated by the labels MStim, EStim and UStim, respectively.

III.A.4. Electrophysiological recording

Because of their exceptionally large diameter, MGF and LGF produce action potentials with high depolarization voltage amplitude. At this level, it is possible to detect the passing of an action potential by simply inserting macroscopic electrodes through the animal, with no necessity for them to be in the close vicinity of the ventral nerve cord. This method of detection, illustrated in detail in **Figure 39**, does not lead to the visualization of an AP waveform such as in the patch-clamp methods. At rest, the voltage recorded by a pair of longitudinally spaced electrodes is null in average. If an action potential is triggered at the region of stimulation, the voltage will display a short biphasic event a few milliseconds later. The positive and negative peaks respectively correspond to the passage of the AP at the level of the anode and cathode.

Two pairs of electrodes were inserted into the animal and connected to 2 of the 4 available input channels (DIN standard of connection) of the electrophysiological recording device (PowerLab 8/35, AD Instruments, New Zealand). The 4 electrodes were aligned in longitudinal direction and spaced 1 cm apart from each other. The 2 anodes were spaced 2 cm and placed closer to the region of stimulation than their associated cathode (**Figure 38**). The electrodes recorded APs propagating through both MGF and LGF and were easily distinguishable on the basis of their amplitude, shape and propagation speed. Using two sets of electrodes allowed the precise calculation of the conduction velocities characteristic of both types of giant axon (**Figure 40**).

The best compromise between the data acquisition quality and the procedure safety was found by inserting the electrodes at one quarter of the width of the animal in order to avoid any risk of hemorrhage, which could bias the stability of the nervous model during the trial. All electrophysiological signals presented in this work were filtered through a bandpass filter (120

– 1200 Hz). These cutoff frequencies were tuned to provide a steady baseline and to optimize the SNR.

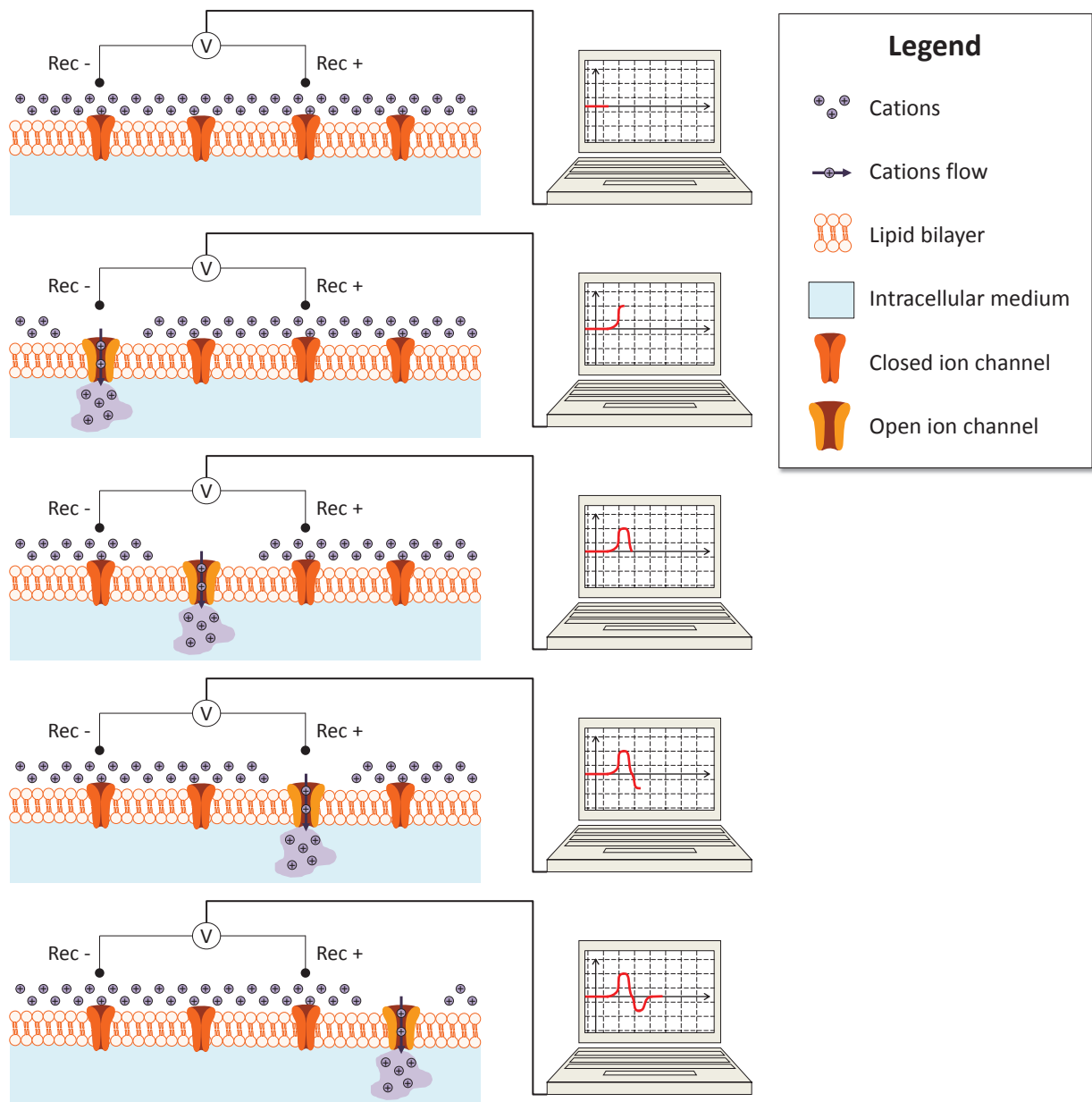


Figure 39 - Schematization of the principle of detection of the propagation of an AP. The different sections of the measured signal can be explained by the localization of the “cationic depletion wave” (DW) relatively to the couple of recording electrodes : a) in the resting state, the longitudinal difference of extracellular potential (DP) measured between the electrodes is null; b) as the DW get closer to the anode, DP rises and reaches a maximum when the DW arrives at the level of anode; c) when the DW crosses the exact middle between the electrodes, the sign of DP changes; d) when the depletion wave arrives at the level of the cathode, DP reaches a minimum; e) as the DW get further away from the couple of electrodes, DP goes back to its resting state’s value.

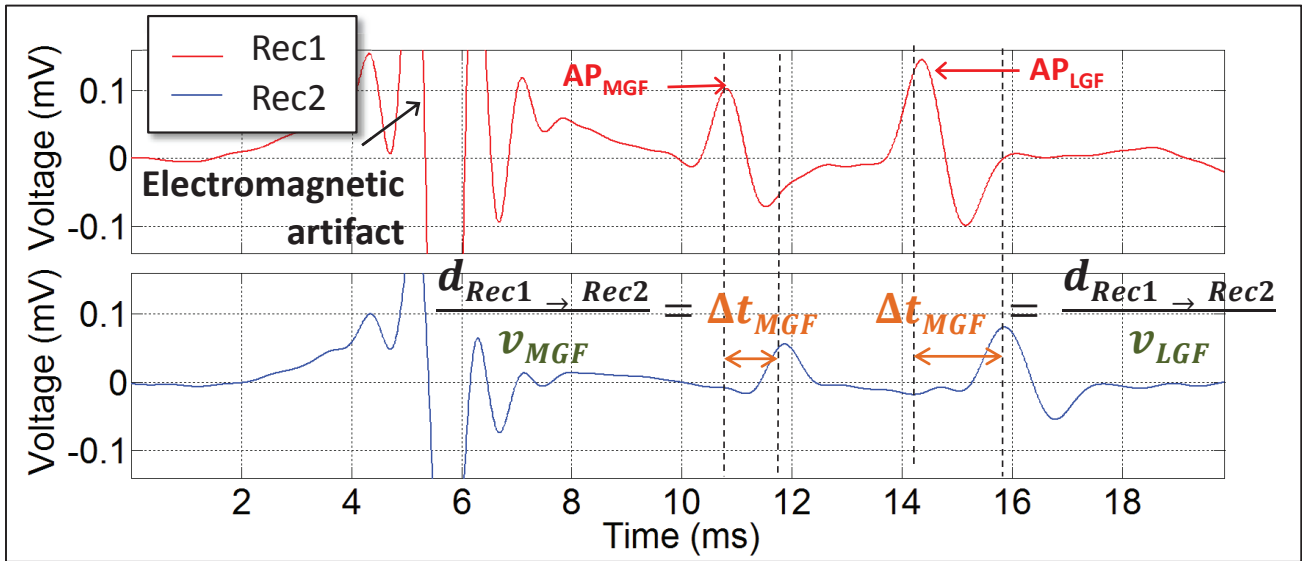


Figure 40 - Illustration of the calculation of the respective conduction velocities associated with both type of giant fibers, from an example of nervous response to electrical stimulation. Red curve on the upper charts represents to the signal recorded by the pair of electrodes closer to the site of stimulation, while blue curve on the lower charts represents to the signal recorded by the farthest pair of electrodes. The first waveform to appear, simultaneously on both signals, corresponds to the electromagnetic artifact generated by the stimulating electrical pulse. The following waveform corresponds to an AP mediated by MGF, and the last one to an AP mediated by LGF. Because MGF and LGF present different conduction velocities, their associated APs can be easily identified if recorded after several centimeters of propagation. Knowing the distance between the respective anodes of the two recordings channels (in this example, $d_{Rec1 \rightarrow Rec2} = 2$ cm), the values of the giant fibers conduction velocities (v_{MGF} and v_{LGF}) can be deduced from the relative delays of apparition of each AP at the two recording sites (Δt_{MGF} and Δt_{LGF}).

III.A.5. Mechanical stimulation (MStim)

Mechanical stimulation was performed by manually poking the animal with a needle at the surface of its skin. A 3rd input reading channel (DIN standard) of the recording device was dedicated to measure the voltage between the needle used for mechanical stimulation and a reference electrode coupled with the animal. An artifact was thus created on the recorded electrical signal when the needle was in contact with the animal's skin. The positive peak of this artifact was used as a time reference for the mechanical stimulus onset.

III.A.6. Electrical stimulation (EStim)

Electrical stimulation was performed by inserting 2 electrodes into the animal and sending a short electrical pulse (time slot, 50 μ s, 8 V). The characteristic of this electrical pulse were chosen in order to elicit a nervous response with the highest success rate possible without damaging the nerve, on the basis of a preliminary study whose results are detailed in section III.B.2. The electrical pulse naturally created an electromagnetic artifact on the signal measured by the recording electrodes, which was used as a time reference for the electrical stimulus onset.

III.A.7. Terminology relative to US stimuli

In this work, we consider that the unit element of an ultrasound stimulus is a monochromatic **ultrasound pulse**, which is defined by its fundamental harmonic frequency (f), its duration (PD) and acoustic intensity (I_{sapa}). An **ultrasound burst** is compound of several pulses, repeated at a fixed frequency, named pulse repetition frequency (PRF). In the present work, the burst is the level of stimulation we are interested in, hence we refer indifferently to an ultrasound stimulus and an ultrasound burst. When an ultrasound burst has effectively triggered a nervous response, compound of one or more APs, it is categorized as a **stimulating burst**. Otherwise, it is a **non-stimulating burst**. An **ultrasound sequence** is a repetition of bursts, not necessarily at a fixed frequency. A sequence typically lasts a few minutes, depending on the number of constitutive bursts (from a dozen to several scores), which are spaced of a few seconds. The bursts of a sequence are not necessarily identical, that is they are not necessarily produced using the same set of acoustic parameters. It is from the level of the sequence that can be drawn the notion of success rate.

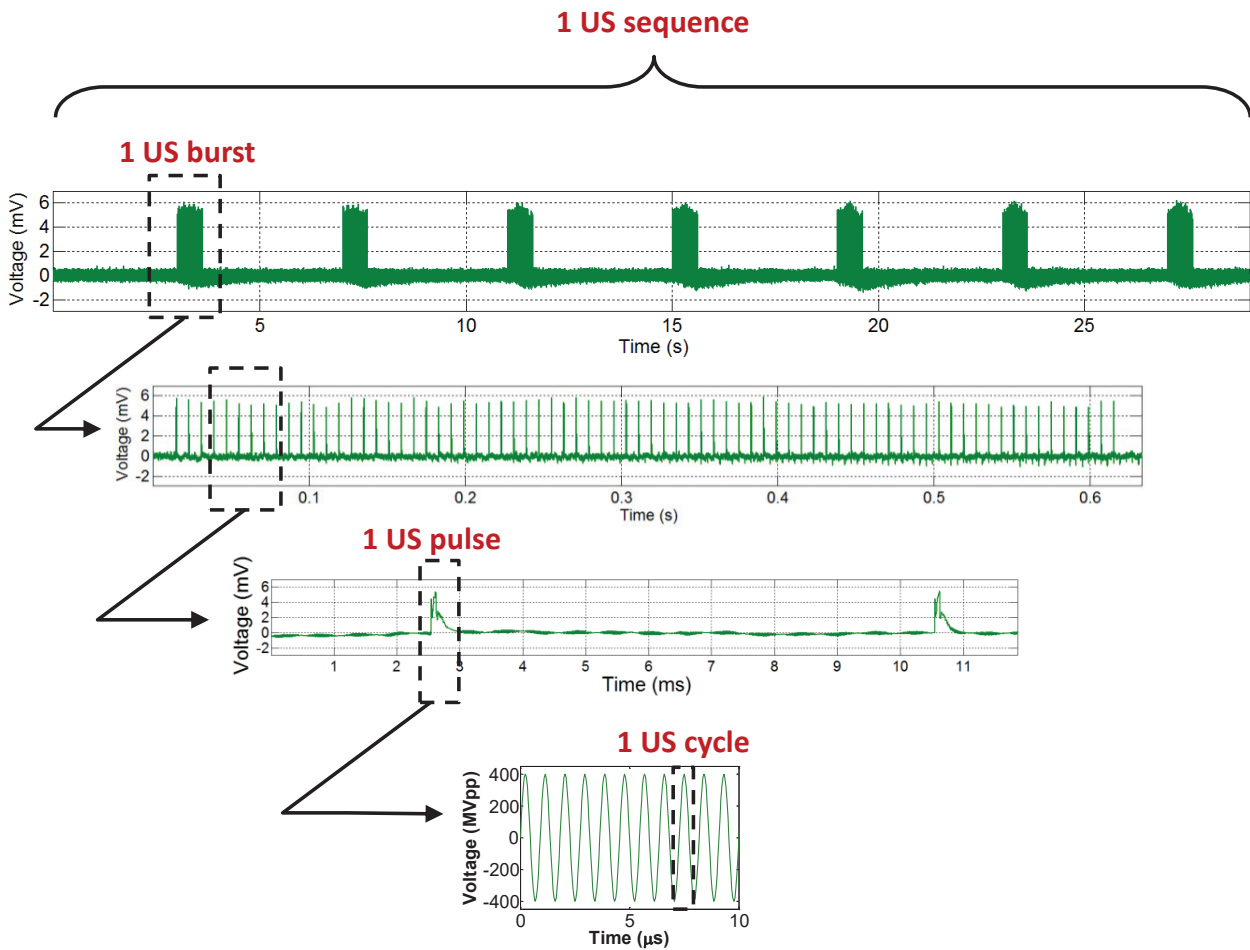


Figure 41 - Hierarchical relationships between US sequence, US burst and US pulse. From top to bottom, the time-scale enables to visualize a sequence of bursts, a single burst of pulses, two following pulses and finally the harmonic content of a single pulse.

III.A.8. Ultrasound stimulation (UStim)

A mono-element spherically focused piezoelectric transducer (PZ28, Ferroperm, Kvistgaard, Denmark) presenting a central frequency of 1.1 MHz and a radius of curvature of 50 mm was used. The driving signal was built from two function generators (AFG1062 and AFG 3102, Tektronix, France) and amplified by a 50 dB amplifier. The main ultrasound sequences used in this study consisted of a series of pulsed ultrasound bursts ($f = 1.1$ MHz, $N_{cycles} = 175$, $PRF = 125$ Hz, $N_{pulses} = 20$). The waveform of the electrical driving signal was controlled with an oscilloscope (Picoscope 3000 Series, Pico Technology Ltd., UK). Acoustic

pressure at the focal spot was calibrated with an optical hydrophone (FOPH 2000, RP Acoustics e.K., Germany). The levels of pressure amplitudes applied with US exposures ranged from 2.5 to 7.3 MPa. The ultrasound transducer was placed in the bottom of a tank filled with degassed water and was facing up in such a way that its focal point coincided with the surface plan of the water. The earthworm was laid out and pinned with the electrodes on a Styrofoam platform held above the water, on its ventral side, a medial portion of its body, or alternatively one of its ends being immersed 1 to 3 mm under the surface of the water.

III.A.9. Definition and calculation of particular times

The arrival delay Δt associated with an evoked AP was defined as the time difference between the stimulus onset and the peak of the AP. The time of propagation (TOP) associated with an AP was defined as the time necessary for the AP to propagate along the axonal distance between the point of stimulation and the recording anode. The TOP was calculated from the measurement of this distance and the mean value of the conduction velocity during the considered trial. Instantaneous values of conduction velocity were deduced from the time difference between the detection of the AP at two distinct recording sites. The time of generation (TOG) associated with an AP was defined as the difference between the arrival delay and the time of propagation:

$$TOG = \Delta t - TOP \quad (28)$$

III.A.10. Methodology followed in the comparative trials

To compare the MStim-associated TOGs with the UStim-associated TOGs, trials ($n = 4$) were performed where a given animal alternatively received mechanical and ultrasound stimuli, administered in the same location. For every response to a stimulus, the TOG was calculated and included in the group of data corresponding to its associated modality of stimulation.

Stimuli were triggered manually, about 2 s apart, following a random order numerically generated using the *randi* function from MATLAB (R2014a, The Mathworks, Inc., USA). Each generated list of administration was composed of 50 instances of stimulation in total, but the

trial was stopped in the cases where the animal started to show signs of awakening before the end of the list. Trials where a minimal number of each type of stimulus ($n=15$) had not been administered were not included in the results of the study.

III.A.11. Assessment of the results

To assess the TOG associated with each modality of stimulation, groups of APs generated within a relatively short period of stimulation (~ 2 min) were considered. The assumption of normality and standard deviation was inspected for the TOGs by performing a Jarque-Bera test and could not be justified in all of the groups. Hence, quantitative results were presented as Median Value [1st quartile – 3rd quartile]. Statistical significance for the comparison between MStim and UStim groups of TOG values was assessed using a Wilcoxon–Mann–Whitney test (H_0 : the distribution of the TOGs is the same for the MStim and UStim groups).

III.B. Results

III.B.1. Criteria of inclusion in the studies

Before formally starting the comparative study presented in this part of the manuscript, a considerable amount of time was dedicated to stabilize the experimental protocol, where hundreds of trials were performed to study the effect of anesthesia, test different ways to deliver an electrical or mechanical, observe the electrophysiological reaction to a variety of US stimuli. All the animals involved in these exploratory trials are not taken into account in the statistics presented in the results of the comparative study.

After stabilization of the protocol, out of the animals tested ($n = 84$), 92% presented a responsive nervous system to EStim and/or MStim after anesthesia, and could be integrated in the comparative study.

III.B.2. Preliminary evaluation of the electrical activation threshold

As mentioned in section III.A.6, prior to investigating the dynamic characteristics of the nervous response to electrical stimulation, we lead a preliminary study in order to choose the appropriate parameters to build the stimulating electrical pulse pattern. To do so, we built the strength-duration curves associated with MGF and LGF, respectively (**Figure 42**). Strength durations curves are characteristic curves used in electrophysiology, representing the minimal pulse amplitude necessary to trigger an action potential, as a function of pulse duration. In accordance with literature, we could note that for a given pulse duration, the value of the activation threshold associated with MGF was always lower than LGF's.

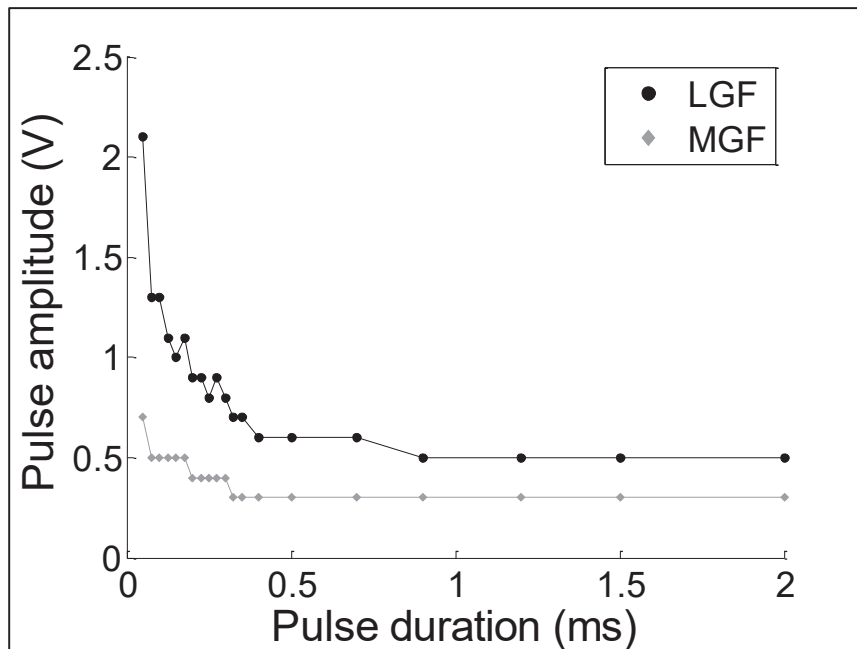


Figure 42 - Strength-duration curve built over an ESTIM trial. Each point corresponds to the amplitude threshold above which, for a given electric pulse duration, an electrically evoked AP can be triggered. For the same pulse duration, the LGF-associated threshold (black dots) is intrinsically higher than the MGF-associated threshold (grey diamonds). Above a certain pulse duration, the activation threshold reaches a plateau.

III.B.3. Nervous response to electrical stimulation (EStim)

The nervous response signal to EStim, regardless of the region of stimulation on the animal, systematically comprised a single MGF-associated AP and a single LGF-associated AP (**Figure 44.A**). In a minority of cases, a slight change (1 – 3 mm, longitudinally) to the position of either stimulating or recording electrodes was necessary before being able to observe both types of APs. The respective delays between the EStim onset and the times of arrival of MGF-associated and LGF-associated APs were stable from one response to another. In the example presented in Fig. 1A, the conduction velocities (CVs) of APs along both types of axons were measured as 16.6 m/s [16.5 – 16.8] and 9.0 m/s [9.0 – 9.1] in LGF and MGF, respectively. From these values, the estimated TOPs over an axonal distance of 8.4 cm were 5.1 ms [5.0 – 5.1] and 9.3 ms [9.2 – 9.4] for MGF and LGF, respectively, while the delays of arrival of the AP were 6.4 ms [6.3 – 6.4] and 11.7 ms [11.7 – 11.7], leading to TOGs of 1.3 ms [1.3 – 1.3 ms] and 2.4 ms [2.3 – 2.4 ms] for MGF and LGF, respectively.

III.B.4. Stability of the conduction velocity over time

Beside the fine characterization of the nervous response to EStim, the important piece of information to keep from these results presented in III.B.3 is the relative stability of the CVs associated with both giant fibers (RSE = 1.2 % for MGF, RSE = 0.9 % for LGF), which legitimizes the methodological approach for the calculation of TOPs, presented in III.A.9.

III.B.5. Nervous response to mechanical stimulation (MStim)

The nervous response signal to a manual MStim at the surface of the earthworm's skin was a variable number of either MGF-associated or LGF-associated APs, but never of both types of APs (**Figure 44.B**). A MStim administered in the anterior third of the animal would exclusively trigger the generation of MGF-associated APs, whereas a MStim administered in the posterior third of the animal would exclusively trigger the generation of LGF-associated APs. A MStim administered in the medial third of the animal occasionally triggered the generation of either type of AP, but did not lead to any nervous response in the majority of cases. In the example

presented in **Figure 44.B**, the mean conduction velocity of APs along LGF was measured at 8.2 m/s. From this value, the mean estimated TOP over an axonal distance of 7.5 cm was 9.2 ms, while the arrival delay of the AP was 42.2 ms [35.3 – 45.7], leading to a TOG of 33.0 ms [26.1 – 36.6].

III.B.6. Feasibility of response to US stimulation

Out of the animals included in the comparative study ($n = 77$), nervous responses to US exposures were successfully observed in 88% of cases. A typical pattern of response to a US sequence is provided in **Figure 43**. On the scale of a US sequence, it was observed that once the nerve had responded to a first US burst, the following bursts were likely to trigger nervous responses as well. On average, the number of APs per burst would decrease over time, until there was no more response, as illustrated by **Figure 43.A**. Waiting a substantial amount of time (1-20 min) without sending US bursts, or slightly displacing the focal area along the nerve (1-2 mm in longitudinal direction), would enable new responses to be triggered. Eventually, after a period of time ranging from 30 min to several hours, depending on the animal, the nerve would stop responding regardless of the localization of the focal spot or the period of rest.

On the time scale of a US burst, it was observed that on average the delay between two consecutive APs increased over time, as illustrated by **Figure 43.B**.

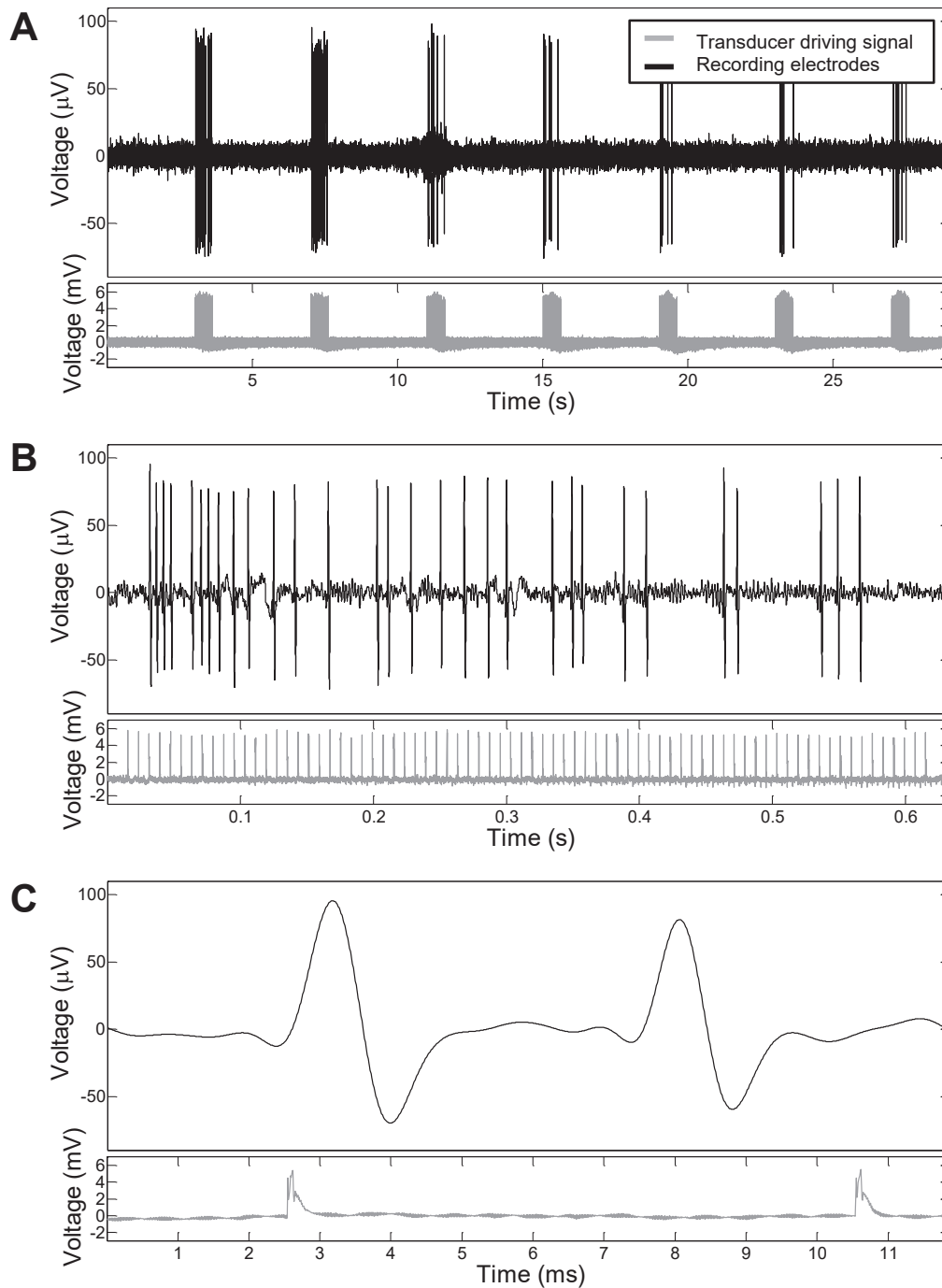


Figure 43 - Example of the structure of a US sequence and its associated nervous response. Different timescales are displayed, in a decreasing order: (A) the scale of a whole sequence of US bursts, (B) the scale of a burst of US pulses and (C) the scale of the period of repetition of US pulses.

III.B.7. Qualitative characterization of nervous response to ultrasound stimulation (UStim)

The nervous response signal to UStim was a variable number of either MGF-associated or LGF-associated APs, but never of both types of APs (**Figure 44.C**). A regional dependence could be highlighted, similar to that observed with MStim: an UStim administered in the anterior third of the animal would exclusively trigger the generation of MGF-associated APs, whereas an UStim administered in the posterior third of the animal would exclusively trigger the generation of LGF-associated APs. An UStim administered in the medial third would trigger no nervous response in the majority of cases. In the example presented in **Figure 44.C**, the conduction velocity of APs along LGF was measured at 8.1 m/s [8.0 – 8.3]. From this value, the estimated TOP over an axonal distance of 7.5 cm was 9.2 ms [9.1 – 9.3], while the arrival delay of the AP was 21.2 ms [20.3 – 22.5], leading to a TOG of 11.8 ms [11.2 – 13.1].

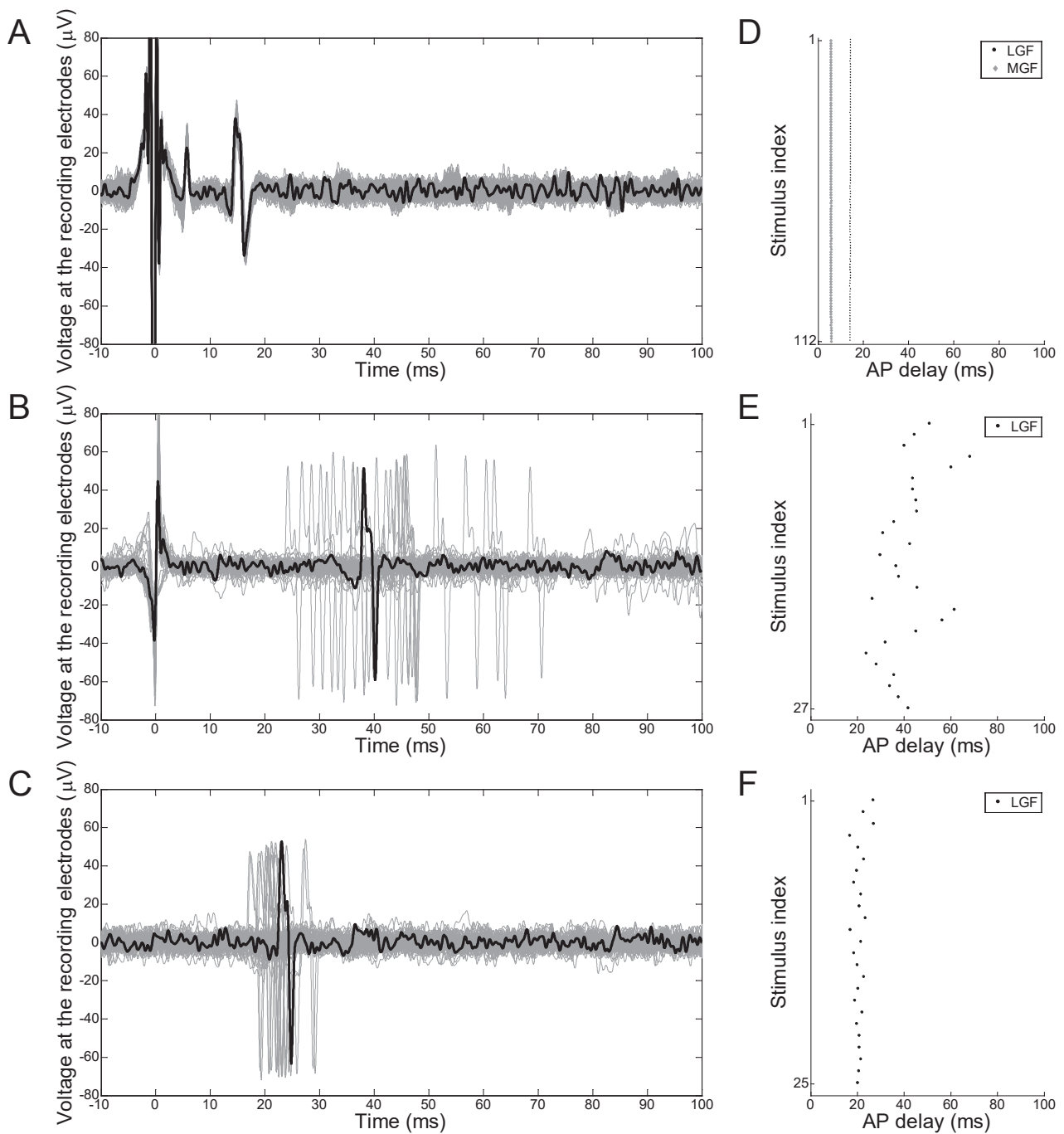


Figure 44 - Superposition of the response signals recorded in the ventral nerve cord following repeated instances of (A) EStim, (B) MStim and (C) UStim. Time reference is the stimulus onset. A random waveform is highlighted in black in order to identify the general shape of an AP. (D), (E) and (F) present the successive arrival delays corresponding to the APs displayed in (A), (B) and (C), respectively. Data for UStim and MStim were recorded during the same trial.

III.B.8. Quantitative comparison between respective nervous responses to mechanical and ultrasound stimulation

Further investigations directly compared the characteristics of these nervous responses by alternatively administering MStim and UStim in the same animal location. The respective distributions of TOGs associated with both modalities of stimulation, over every trial, are presented in **Figure 45**. These investigations revealed that, in every trial, the TOG of APs associated with UStim were significantly shorter and more stable than the TOG of APs associated with MStim ($***p < 0.001$).

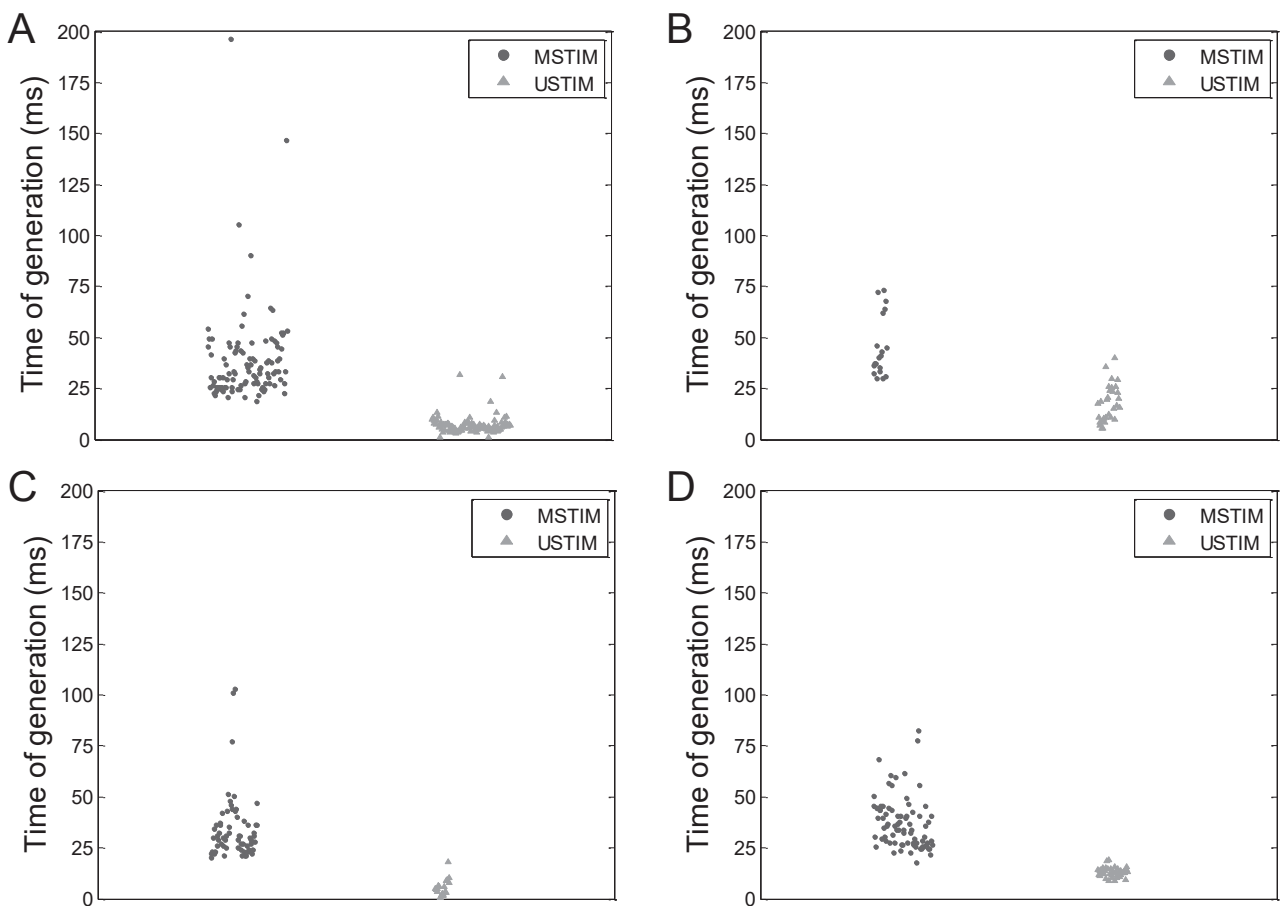


Figure 45 - Comparative trial between MStim and UStim. Distributions of TOG associated with MStim (black dots) and UStim (grey triangles), over 4 trials (A-D). In every trial, the animal received alternatively MStim and UStim, administered in the same location.

III.C. Discussion

III.C.1. Dynamics of the nervous response to electrical stimulation: an instantaneous depolarization of the membrane of the giant axons

It is established that an electrical stimulus can depolarize the membrane of an axon, leading to the generation of one to several APs. In previous works, the authors dedicated a large amount of time studying the responses of the earthworm nervous system to an electrical pulse administered through invasive electrodes. For a given pulse duration, there is a pulse amplitude threshold above which a nervous response of the giant axon will be triggered. According to the literature on the subject and experimental verification, the threshold associated with LGF is intrinsically higher than the threshold associated with MGF (**Figure 42**). Hence, the fact that EStim invariably triggered both MGF- and LGF-associated APs (**Figure 46**) can be explained by the use of a pulse amplitude (8 V) much higher to the experimentally assessed range of LGF-associated threshold (~ 2 V). In parallel, the very short pulse duration (50 μ s), relatively to the refractory period of the ion channels (several milliseconds), can explain the triggering of only one instance of each type of AP.

The depolarization of the membranes of the giant axons can be considered as instantaneous, with regard to the timescale of the AP propagation on distances such as used in the presented trials (centimeter scale). Besides, the stability of the conduction velocities of giant axons over time was experimentally assessed, and it was determined that they could be considered to be steady over the duration of a trial. This hypothesis was confirmed during the trials with EStim, since the delays between the stimulus onset and the times of arrival of the APs were steady (**Figure 44.D**).

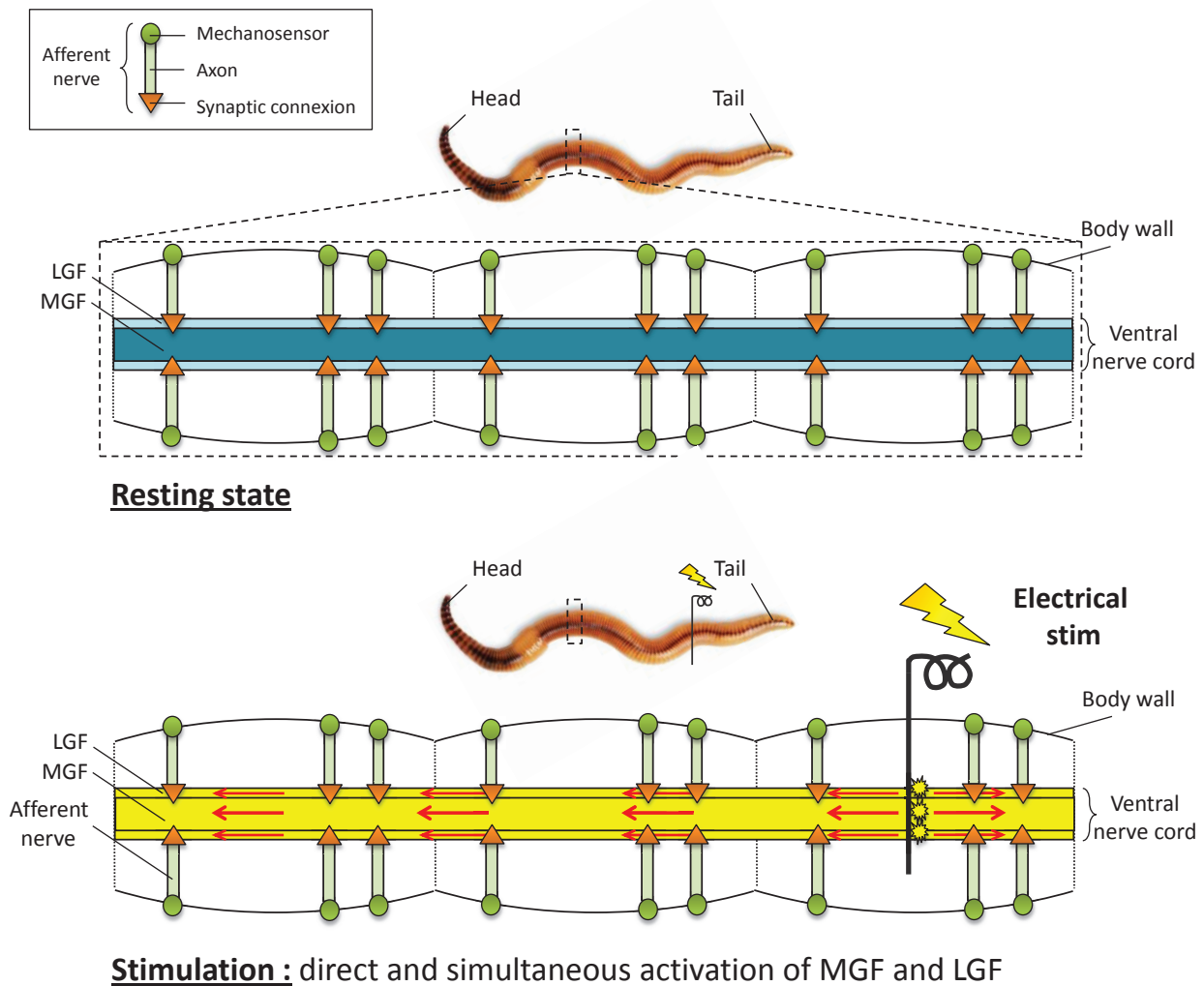


Figure 46 - Schematization of the EStim-associated response of the nervous model. The locus of interaction between EStim and the earthworm’s nervous system (which can be viewed as a ‘point of entry’ of the information) is the membranes of the giant fibers. The pulse amplitude of EStim was chosen to be substantially higher than the respective activation thresholds associated with MGF and LGF, which explains why EStim triggered both MGF- and LGF-associated APs.

III.C.2. Dynamics of the nervous response to mechanical stimulation: an excitation of giant axons mediated by the afferent pathway

The results related to the nervous response of *Lumbricus terrestris* to a mechanical stimulation are consistent with literature. The locus of interaction between a mechanical stimulus at the surface of the earthworm skin and its internal nervous system (which can be viewed as a ‘point of entry’ of the information) is the mechanosensitive end of the afferent

neurons (**Figure 47**). The activation of a mechanosensor leads to the generation of APs along the afferent nerve, or afferent spiking (Phase I) (Drewes, 1984). This afferent spiking propagates inward, to the synaptic connection with the giant axons (Phase II). The synaptic connection then translates this spiking into postsynaptic potential activity and eventually to the generation of an AP in the giant axon (Phase III). The incompressible durations of these different phases (Moore, 1979) explain why non-negligible TOGs have been observed by recording APs in the giant axons during MStim trials. Furthermore, these different phases of translation/propagation of the sensory information may all present a variability of their own, which is consistent with the TOGs measured during MStim being variable from one neural response to another.

The spatial polarity of the MStim-associated excitability map (MGF only activated by anterior mechanical stimulation and LGF only activated by posterior mechanical stimulation, see **Figure 47**) is consistent with the literature on the subject (Moore, 1979; Mulloney, 1970).

Over all trials performed, the TOG associated with a mechanical stimulation was never inferior to 5 ms (overall minimal value: 17.6 ms). This is also consistent with literature. Indeed, as was mentioned in section III.B.8, the time difference between the delivery of a mechanical stimulus and the onset of an AP in the giant fiber (what we call TOG in our study) was found to be 5 ms for a non-anesthetized earthworms (Drewes, 1984). Hence, it could be expected that the TOG obtained in our trials would not be lower than this value. The adverse effect of anesthesia on nerve conduction could explain why the range of value of the TOG associated with MStim is several fold greater than in non-anesthetized earthworms.

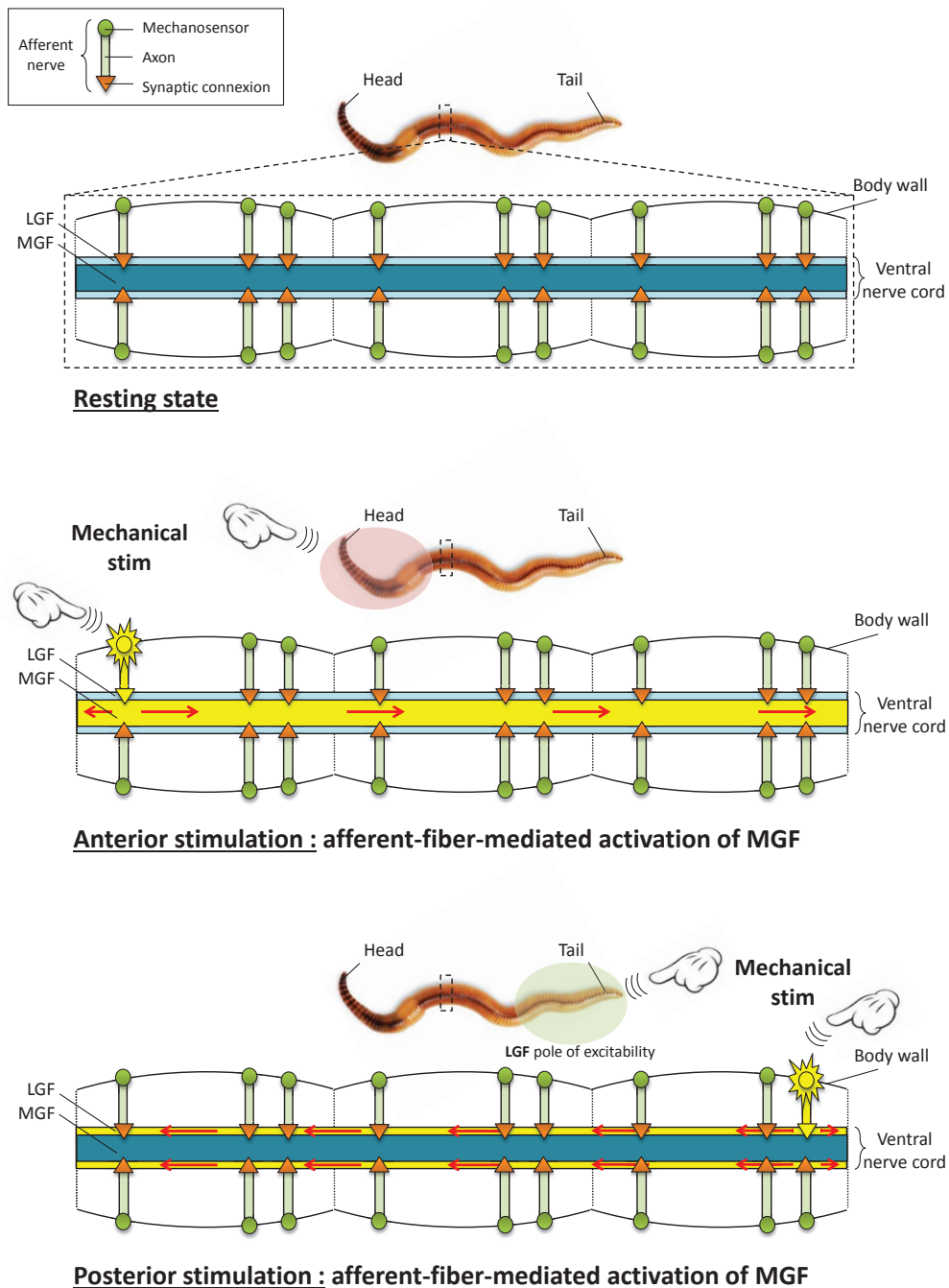


Figure 47 – Schematization of the MStim-associated response of the nervous model. The locus of interaction between MStim and the earthworm’s nervous system (which can be viewed as a ‘point of entry’ of the information) is the mechanosensitive end of the afferent neurons. The spatial polarity of the MStim-associated excitability map (MGF only activated by anterior mechanical stimulation and LGF only activated by posterior mechanical stimulation) is consistent with the literature on the subject (Moore, 1979; Mulloney, 1970).

III.C.3. Deductions on the interaction between ultrasound and the earthworm nervous system

Firstly, the fact that the excitability map associated with UStim presents the same polarity as that associated with MStim suggests that the locus of interaction between ultrasound and the earthworm nervous system is situated **on the afferent pathway upstream the synaptic connection between afferent neuron and giant axon**. Indeed, as it was explained in section I.D.5.iii, the monotonic longitudinal gradient in the strength of the synaptic connection between afferent fibers and giant fibers is considered to be the neural basis for the sensitivity gradients of MGF and LGF sensory fields. In other words, we deduced from this observation that focused US do not directly activate the giant axons. Otherwise, given the various parameters tested in the presented study, it is reasonable to believe that both types of APs (MGF- and LGF-related) would have been triggered similarly to responses induced by EStim.

Secondly, one important deduction can be made from the comparison between the distributions of TOGs associated with MStim and UStim. In every comparative trial, the TOGs were significantly shorter for UStim than for MStim. In other words, it takes a certain amount of time for a nervous signal triggered by a tactile stimulation to reach the giant fibers, and it takes less time for a nervous signal triggered by an ultrasound stimulus to reach the giant fibers. One way to explain it would be that ultrasound-induced nervous signal is initiated somewhere *closer* to the giant fiber, downstream the mechanosensor but still on the afferent pathway (as established in the previous paragraph). Another hypothesis would be that ultrasound does interact with mechanosensor to trigger a nervous response, but in a different and more efficient way than a tactile stimulus. We lack information regarding the timing of the mechanotransduction step to validate or reject this hypothesis with certainty. However, we do know that, over all trials performed, the TOG associated with an ultrasound stimulation was occasionally inferior to 5 ms (down to 1.1 ms, in the trial presented in **Figure 45.A**), which means that an ultrasound-induced nervous signal can reach the giant fibers even faster in an anesthetized animal than a tactile-induced nervous signal would do in a non-anesthetized worm. This suggests strongly that our first hypothesis is the most likely, and that the locus of interaction between ultrasound and the nervous system is somewhere **on the afferent pathway downstream the mechanosensors (Figure 48)**.

To sum up, our results suggest the ultrasound stimuli used in our experimentation interact with the nervous system of the earthworm through the afferent pathway, but not necessarily by activating the mechanosensors of the body wall. If they do activate the mechanosensors, it is through a different mechanism than this of a tactile stimulation, which would induce a shorter transduction delay.

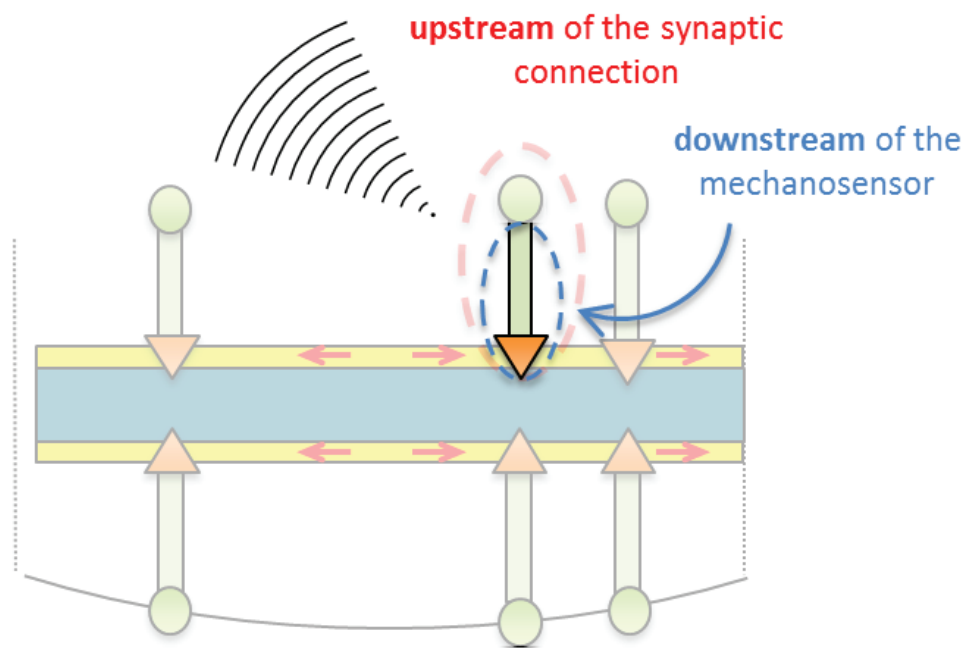


Figure 48 – Summarization of the deductions made from the comparative study. The fact that the excitability map associated with UStim presents the same polarity as that associated with MStim suggests that the locus of interaction between ultrasound and the earthworm nervous system is situated on the afferent pathway **upstream the synaptic connection** between afferent neuron and giant axon (area circled by a red dotted line). Additionally, the comparison between the distributions of TOGs associated with MStim and UStim suggests strongly that the locus of interaction between ultrasound and the nervous system is somewhere **on the afferent pathway downstream the mechanosensors** (area circled by a blue dotted line).

Conclusion

In this chapter, we presented the anatomy and some aspects of the physiology of *Lumbricus terrestris*, with a particular focus on the structure of its nervous system. The system of giant fibers and its associated afferent pathway was described in detail, as they provided the basis for the causal approach used to interpret some of our experimental results.

The feasibility of using pulsed focused ultrasound to induce nervous response from the anesthetized earthworm was demonstrated. Ultrasound stimuli were delivered at both animal extremities, or ventrally in the median third of its length. The form of nervous response evoked was serials of action potentials in the giant fibers.

The response of our study model to alternative modalities of stimulation was studied. We applied a causal approach to interpret on one hand the respective sensory fields associated with these different modalities, and on the other hand the delays between stimulus onset and detection of an action potential in the giant fibers. Two strong interpretations could be built from these observations. Firstly, the burst of focused ultrasound used in our study do not interact directly with the giant fibers but rather activate the afferent pathway at a level high enough to eventually trigger a spiking in the giant fibers. Secondly, the burst of focused ultrasound in our study do not interact with the mechanosensitive end of the segmental nerves such a tactile stimulus would do, but rather interact somewhere downstream on the afferent pathway. In conclusion, our hypothesis is that during the phenomenon of ultrasound neurostimulation highlighted in our studies, the structures functionally responding to the ultrasound stimulus are the segmental afferent nerves. This study and its conclusions illustrated the relevance of the present nervous model to study the phenomenon of ultrasound neurostimulation.

Chapter 3: Investigation of the acoustic bio-effects involved during *in-vivo* ultrasound neurostimulation in a simple invertebrate system of giant fibers

Introduction

In the previous chapter, we demonstrated the feasibility of using focused ultrasound to stimulate the ventral nerve cord of *lumbricus terrestris*. The high potential of this nervous model for the study of ultrasound neurostimulation was illustrated by investigating the dynamics of AP triggering for three different natures of stimulus. By developing a causal approach, it was possible to conclude that, in the presented nervous model, focused ultrasound is functionally interacting with segment afferent nerves rather than giant axons themselves, and some results suggested that this interaction was not a simple activation of the mechanosensors of the skin through radiation force. This piece of knowledge is helping but not sufficient to make conclusions regarding the biomechanisms involved in the observed phenomenon. In this chapter, we will set the basis for a mechanistic study of the phenomenon of ultrasound neurostimulation applied to our *in vivo* invertebrate nervous model. It is largely based on a set of parametric studies, where the causal relationship between the variation of a given acoustic parameter and the electrophysiological outcome is investigated. Complementarily, we will explore the hypothesis of cavitation as a leading mechanism by proposing a monitoring approach of cavitation events, and different modalities to study their correlation with US-induced nervous responses. Since the main discussion of this chapter will be centered around the acoustic parameters of the stimulus, the first part will be dedicated to the characterization of the ultrasound beam produced by the transducer.

I. Parametric study of the influence of acoustic parameters on the success rate of neurostimulation

I.A. Methods

I.A.1. General approach of the parametric studies

The general method to evaluate the influence of an acoustic parameter on the success rate of ultrasound stimulation consisted in administrating ultrasound sequences (section I.A.1.i, reminder from chapter 2) compound of **randomly mixed** types of bursts (section I.A.1.ii), **each type of burst varying from one another only by the value of the investigated parameter** (section I.A.1.iii). The **success rate** (section I.A.1.iv) associated with each type of subgroup of stimuli of the sequence was then calculated.

I.A.1.i. Terminology relative to US stimuli

In this work, we consider that the unit element of an ultrasound stimulus is a monochromatic **ultrasound pulse**, which is defined by its fundamental harmonic frequency (f), its duration (PD) and acoustic intensity (I_{sapa}). An **ultrasound burst** is compound of several pulses, repeated at a fixed frequency, named pulse repetition frequency (PRF). In the present work, the burst is the level of stimulation we are interested in, hence we refer indifferently to an ultrasound stimulus and an ultrasound burst. When an ultrasound burst has effectively triggered a nervous response, compound of one or more APs, it is categorized as a **stimulating burst**. Otherwise, it is a **non-stimulating burst**. An **ultrasound sequence** is a repetition of bursts, not necessarily at a fixed frequency. A sequence typically lasts a few minutes, depending on the number of constitutive bursts (from a dozen to several scores), which are spaced of a few seconds. The bursts of a sequence are not necessarily identical, that is they are not necessarily produced using the same set of acoustic parameters. It is from the level of the sequence that can be drawn the notion of success rate.

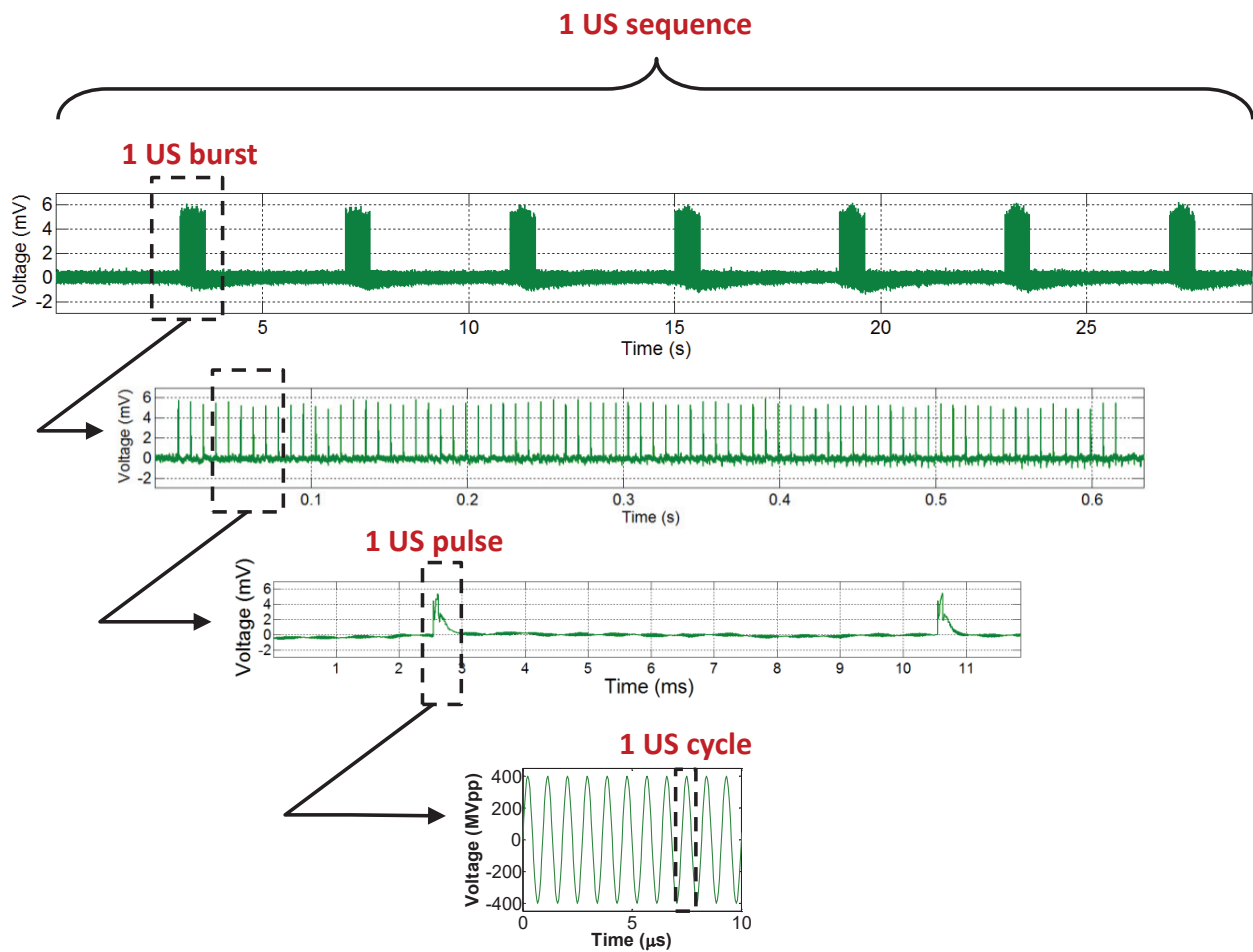


Figure 49 – Hierarchical relationships between US sequence, US burst and US pulse. From top to bottom, the time-scale enables to visualize a sequence of bursts, a single burst of pulses, two following pulses and finally the harmonic content of a single pulse.

I.A.1.ii. Motivations for the randomization

Within a sequence, bursts were **randomly alternated** in order to limit several possible analysis biases:

1) The nerve inherent fatigue: Even if the mechanisms underlying it are still unknown to us, we empirically observed a trend from the nerve to fatigue after a certain number of effective stimulations. An ultrasound sequence compound of long blocs of the same type of stimulus (*e.g.* 20 A-type, 20 B-type, 20 A-type, 20 B-type) would risk to bring a bias of interpretation of the success rates associated with all the groups ulterior

to the first one.

2) The temporal evolution of the anesthesia level: Though we designed relatively short sequences (<10 min.) in order to reasonably consider the anesthesia level as steady for the sequence duration, randomly alternating the burst types is an additional precaution to prevent a decrease of anesthesia level to bias the success rate of the latter bursts of the sequence (either because the nervous system becomes more responsive to stimulation or because the earthworm starts moving).

3) The dependence on the stimulation history: Again, as the mechanisms involved in the studied stimulation phenomenon are not known, we assumed that the subsequent nervous response to a given stimulus could be dependent on the stimulation history. This dependence could be the result of a simple cumulative effect (repeating the same stimulus either reduce or increase the probability for a nervous response) or could reflect a more complex pattern (e.g. 10 A-type followed by one B-type more likely leads to a nervous response).

I.A.1.iii. Burst of reference

To give uniformity to the various types of burst tested in the parametric studies, a burst of reference was defined. The constitutive bursts of a sequence were then built from this burst of reference by changing only the value of the acoustic parameter investigated, all other acoustic parameters being identical to the burst of reference. For this reference, we chose a burst which has proved to induce a high success rate in our exploratory studies, and which is characterized by the following set of acoustic parameters: $f = 1.1$ MHz, $PD = 160$ μ s, $I_{sapa} = 2.5$ kW/cm², $PRF = 125$ Hz, $N_{pulses} = 20$.

I.A.1.iv. Definition of the Neurostimulation Success Rate (NSR)

The **Neurostimulation Success Rate (NSR)** is defined as the number of stimulating bursts of a given type divided by the total number of bursts of this same type, fired within a sequence. Hence, the NSR is a notion associated with a subgroup of stimuli of an ultrasound sequence.

I.A.2. Influence of US pulse intensity and duration on the NSR

The respective influences of pulse duration (PD) and pulse intensity (I_{sapa}) on the NSR were studied over the course of the same trials. During each trial ($n = 4$), the animal was exposed to sequences of randomly mixed instances of different types of ultrasound burst. The different types of burst were built from different combinations of pulse intensity and pulse duration, all other acoustic parameters being identical ($f = 1.1$ MHz, $PRF = 125$ Hz, $N_{pulses} = 20$). Eight pulse duration values ($PD = 20, 40, 80, 160, 320, 480, 640$ and 800 μ s, corresponding to duty cycles ranging from 0.25% to 10%) and 8 pulse intensity values ($I_{sapa} = 0.2, 0.7, 1.5, 2.5, 3.4, 4.1, 4.7$ and 5.0 kW/cm²) were employed, but all 64 combinations were not investigated. Indeed, building on the observations from preliminary trials, the experimental protocol was refined in order to optimize the ratio between the quantity of significant data recorded and duration of the trial. For the same reasons, the pseudo-randomization of the bursts was not numerically generated but manually controlled, largely based on empirical knowledge acquired by the operator on the nervous model behavior. Further explanations on the refinement of the experimental protocol are provided in section I.B.3.

I.A.3. Influence of US PRF on the NSR

To study the effect of the PRF on the success rate, trials ($n = 6$) were performed wherein a given animal was exposed to 2 types of US sequences randomly. The 2 types of US sequences were respectively built with PRFs of 125 and 25 Hz, all other acoustic parameters being identical ($f = 1.1$ MHz, $PD = 160$ μ s, $I_{sapa} = 1.5$ kW/cm², $N_{pulses} = 20$). The randomization was numerically generated using the *randi* function from MATLAB (R2014a, The Mathworks, Inc., USA). The value of the highest PRF was chosen such that the pulse repetition period of 8 ms is twice as high as the mean value of the refractory period of the giant axons. In this way, the membrane ion channels had enough time to go back to their resting state between two US pulses. Our intent was to avoid any bias in the analysis of the number of APs triggered by an US burst, by making sure each US pulse was in theory applied to an excitable neural structure.

I.A.4. Influence of the number of US pulses per burst on the NSR

To study the impact of the number of US pulses per burst (N_{pulses}) on the NSR, trials were performed where the animal was exposed to different US sequences randomly. Six configurations of number of pulses per burst were investigated ($N_{pulses} = 1, 2, 3, 5, 20$ and 200). Each US sequence was designed to compare a given pair of values, the nature of which was adapted along the trial in order to minimize the necessary number of values to test in order to highlight a trend.

I.A.5. Investigation of the influence of higher US frequency on the NSR

The influence on the NSR of using a burst with a higher US frequency (f) could not be investigated as for the other acoustic parameters. Indeed, the harmonic frequency of the US burst is conditioned by the resonance frequency of the US transducer used to produce it. The ideal method would have been to use 2 different transducers with 2 different resonance frequencies but generating the same focusing (same shape and orientation of the focal region, same peak intensity). But the uncertainty regarding the mechanical alignment between the US beam and the giant nerve is a challenge and would require a complex mechanical set-up to replace one transducer with the other. Another possibility would have been to use a pair of confocal transducers, and build sequences randomly alternating bursts produced by each of them. Although mechanical alignment is less challenging (the transducers are fixed once and for all), the main limitation of this configuration is that a potential effect of the US propagation direction on the NSR is not taken into account. The strategy chosen in the presented study was to generate US sequences with different frequencies using a single transducer, driven either at its fundamental frequency (f_0) or its third harmonic frequency ($f_3 = 3f_0$). Despite some limitations (the distribution of pressure, and the shape of the focal region are not similar), this very simple configuration allowed generating a focal region with an equal orientation and a controlled peak intensity, while switching between frequencies could be done instantaneously with no need for additional mechanical alignment.

Nonetheless, we took advantage of the third harmonic of the transducer, $f = 3.3$ MHz, which generated sufficiently high acoustic power, in order to investigate the feasibility of performing ultrasound neurostimulation using a higher frequency than that used for the exploratory studies (Cf chapter II). Some of the trends highlighted in the other parametric studies performed at 1.1 MHz were also verified at 3.3 MHz.

I.A.6. Assessment of the results

Statistical significance for the comparison, within a given trial, between the NSR value and number of APs triggered by high-PRF stimuli and low-PRF stimuli was assessed using a Wilcoxon–Mann–Whitney test for paired samples. The statistical analyses were performed using MATLAB (R2014a, The Mathworks, Inc., USA) and the BiostaTGV platform (<https://biostatgv.sentiweb.fr/>, UMR S 1136, INSERM, UPMC, France).

I.B. Results

I.B.1. Influence of pulse intensity on the NSR

Over all trials performed (more than 1000 bursts tested over 4 animals), the NSR was found to be systematically increasing with increasing values of pulse intensity (I_{sapa}). **Figure 50** presents 6 representative examples of the results of such trials, performed at different pulse durations (PD = 80, 160 and 320 μ s), and the same effect of I_{sapa} over the NSR can be observed in each of them.

In particular, we noticed that in some cases (**Figure 50.D**) an increase in pulse intensity of 1 kW/cm² could result in a jump in the NSR from less than 20% to 100%. The pulse intensity necessary to achieve a 100% NSR varied with the value of pulse duration, but its order of magnitude was consistent from one trial to another when the same pulse duration was used.

It is also worth noting that, in each trial, it was possible to identify some sets of parameters evoking nervous responses with a success rate strictly intermediate between 0 and 100. The existence of these ‘intermediate’ success rates underlines one of the differences between the respective phenomena of ultrasound and electrical stimulations.

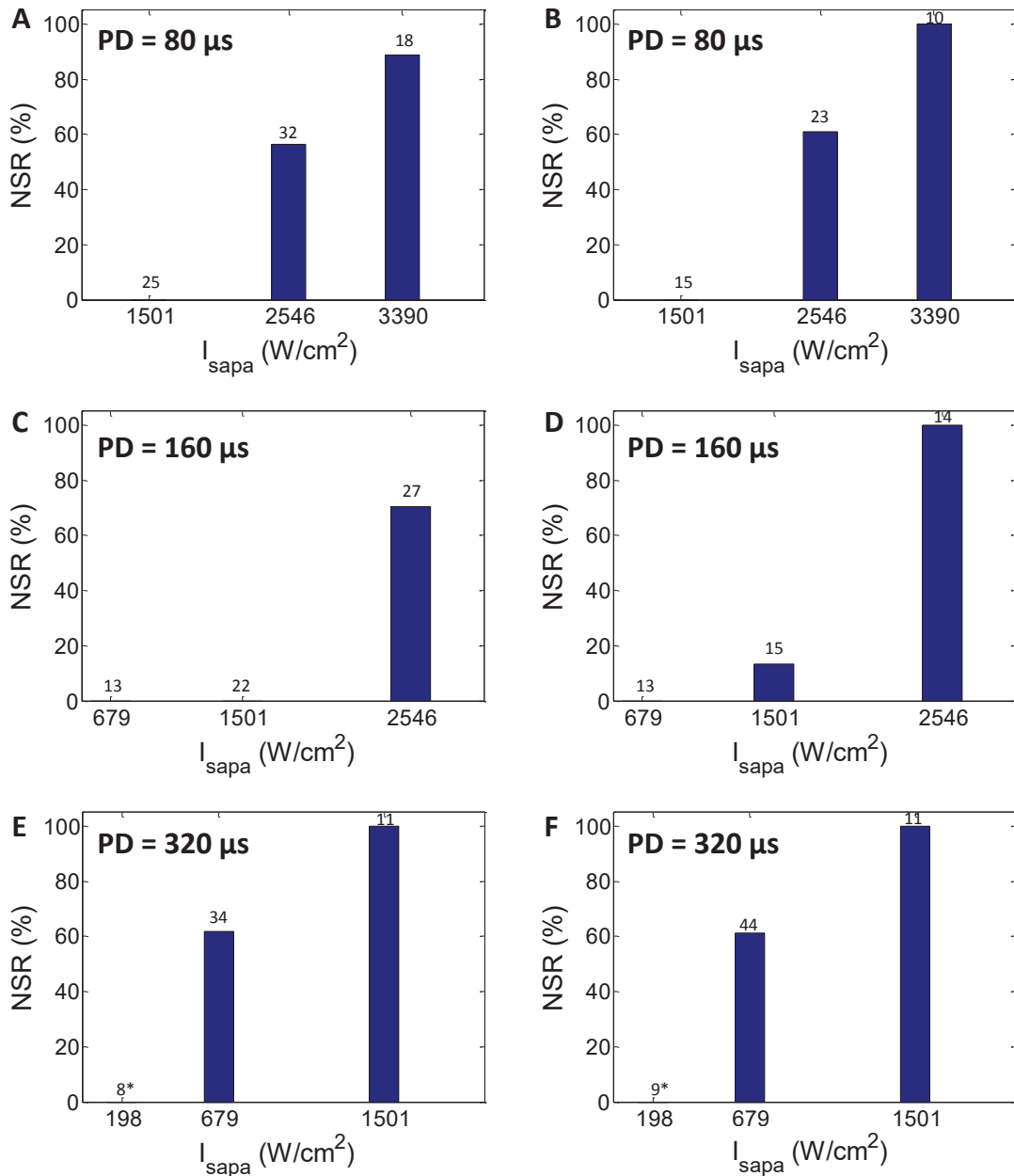


Figure 50 - Illustration of the influence of I_{sapa} on the Neurostimulation Success Rate (NSR). Each chart corresponds to a separate trial and displays the NSR associated with 3 different values of pulse intensity tested within the trial. These investigations were repeated for different values of pulse duration: $PD = 80 \mu s$ (A-B), $160 \mu s$ (C-D) and $320 \mu s$ (E-F). All other acoustic parameters were identical in each trial ($f = 1.1 \text{ MHz}$, $PRF = 125 \text{ Hz}$, $N_{pulses} = 20$). In each chart, the number of stimuli tested for a given value of I_{sapa} is indicated above the associated bar. When these numbers are inferior to the arbitrary fixed criterion of 10 stimuli, they are marked by an asterisk (*) to indicate they are potentially less relevant to interpret.

I.B.2. Influence of pulse duration on the NSR

Over all trials performed (more than 1000 bursts tested over 4 animals), the NSR was systematically increasing with increasing values of pulse duration. **Figure 51** presents 6 representative examples of the results of such trials, performed at different pulse intensities ($I_{sapa} = 0.7, 1.5$ and 2.5 kW/cm^2), and the same effect of the pulse duration on the NSR could be observed in each of them.

In particular, in some cases (**Figure 51.C** and **Figure 51.F**), an increase in pulse duration of $80 \mu\text{s}$ could result in a jump in the the NSR from less than 10% to more than 80%. For a given animal, the pulse duration necessary to achieve a 100% NSR varied with the value of pulse intensity. For a given value of pulse intensity, the pulse duration necessary to achieve a 100% NSR varied from one animal to another, highlighting a substantial inter-animal variability in this area.

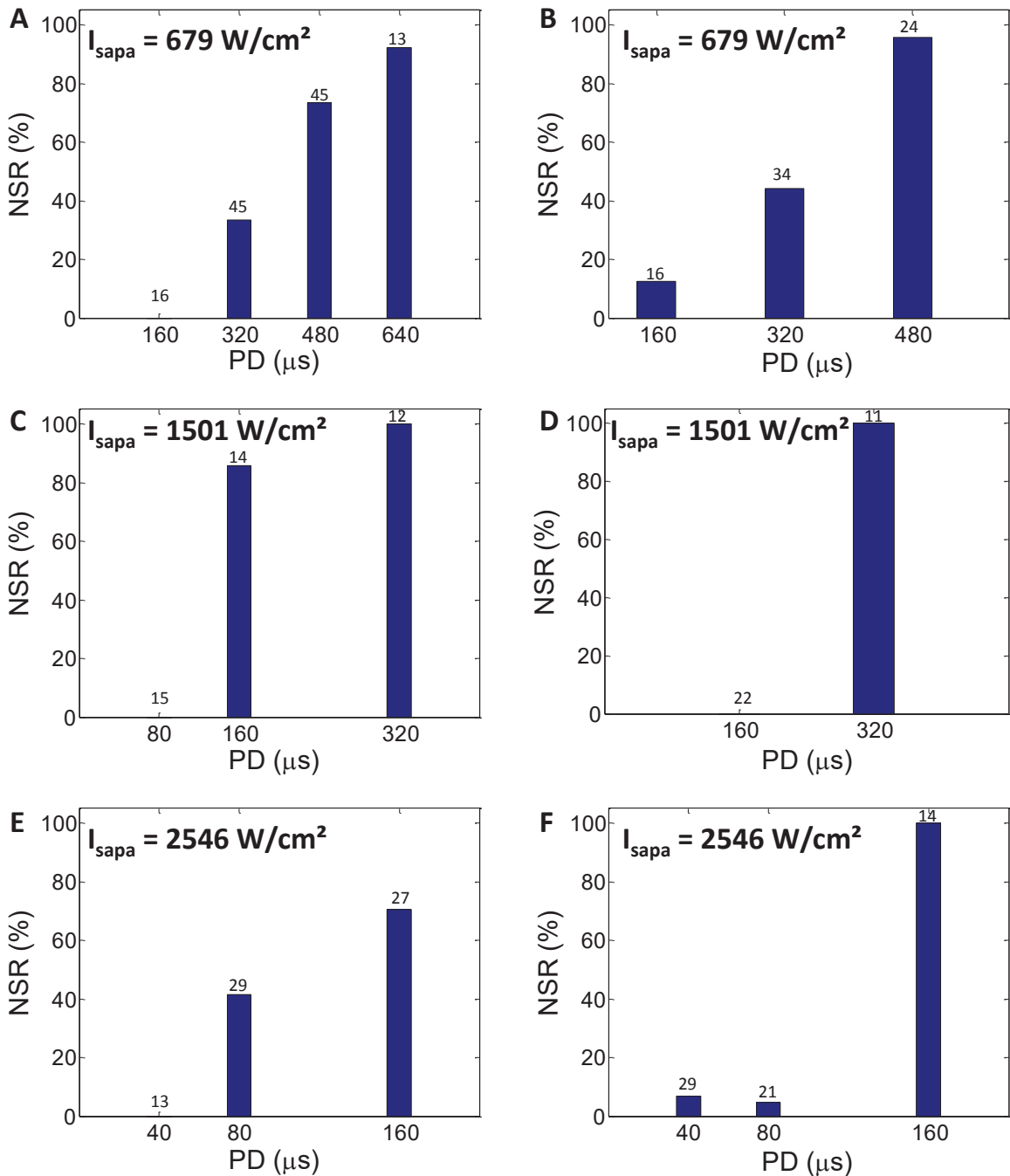


Figure 51 - Illustration of the influence of pulse duration (PD), on the Neurostimulation Success Rate (NSR). Each chart corresponds to a separate trial and displays the NSR associated with 2 to 4 different values of pulse duration tested within the trial. These investigations were repeated for different values of acoustic intensity: $I_{sapa} = 679 \text{ W/cm}^2$ (A-B), 1501 W/cm^2 (C-D) and 2546 W/cm^2 (E-F). All other acoustic parameters were identical in each trial ($f = 1.1 \text{ MHz}$, $PRF = 125 \text{ Hz}$, $N_{pulses} = 20$). In each chart, the number of stimuli tested for a given value of pulse duration is indicated above the associated bar.

I.B.3. Combined influence of I_{sapa} and PD on the NSR

While studying the respective influences of pulse intensity and pulse duration on the NSR , it was noticed that the effects of these two parameters were linked. To further investigate this relationship, trials were performed where the animals were exposed to long US sequences presenting different combinations of I_{sapa} and PD values (more than 1000 bursts tested over 4 animals). **Figure 53** presents the results of these trials, and **Figure 52** illustrates how the representation of data in **Figure 53** can be linked with those of **Figure 50** and **Figure 51**. Each trial required a large number of stimuli, hence we tried to optimize the available time window. To do so, we took advantage of how we already assumed the NSR was evolving in function of both parameters. When enough measurements had been done to evaluate a SNR of 90% or more for a given combination of pulses, we did not try to further increase one of the two parameters. Indeed, after reaching a repeated NSR value of 90%, we could already predict that the NSR would reach 100% for every combination of higher pulse intensity or higher pulse duration. In addition, by optimizing the amount of relevant data to record, we lessened the risk to damage nerve structure and bias the rest of the trial.

The charts presented in Figure 10 allow highlighting two experimental findings. Firstly, it was possible to identify an ‘overall’ I_{sapa} threshold, under which no nervous response could be triggered for any value of PD . Secondly, for a low PD , a compensation by a higher I_{sapa} was necessary to trigger nervous response, and the $NSRs$ associated with these combinations of parameters tend to be much lower than those obtained from combinations involving higher PDs . Dedicated trials should be performed to assess if, for low PDs , the NSR is limited to an upper threshold strictly inferior to 100%. The inner limitation of the amplifier used in the experimental set-up did not allow to investigate higher I_{sapa} , hence did not allow to investigate lower PDs either, since these parameters are linked in terms of NSR .

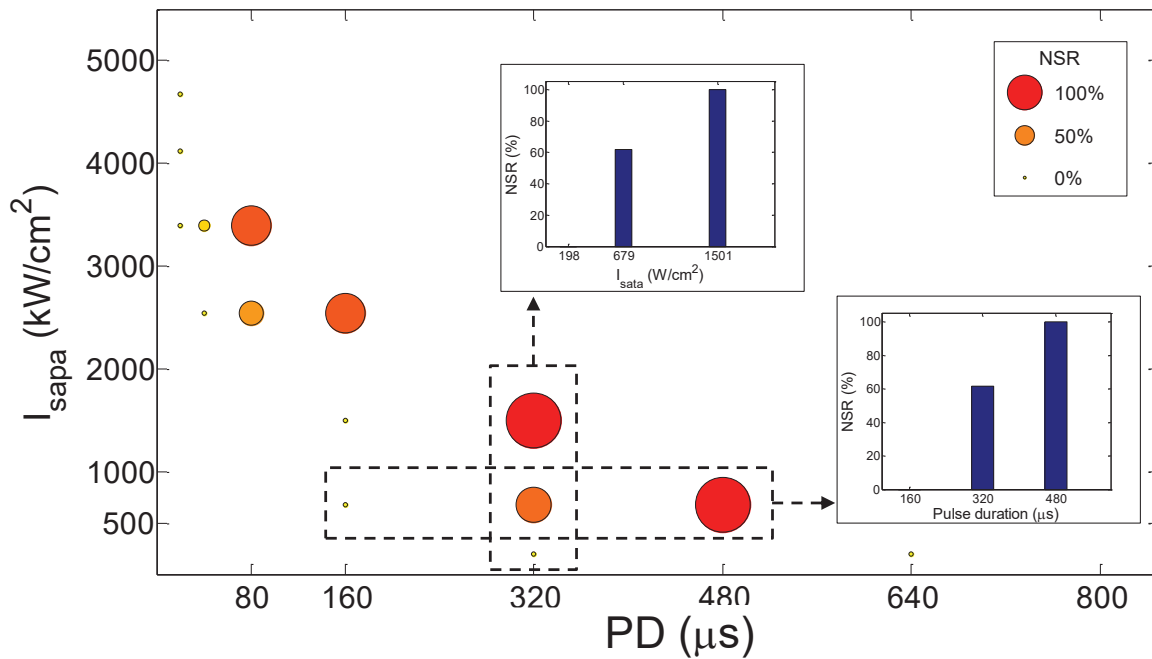


Figure 52 - The bubble chart of Figure 10 synthesizes the entirety of results obtained from the trials investigating the influence of PD and I_{sapa} on NSR. From a single column or row of bubbles, respectively, can be built the bar charts presented in Figure 8 or 9, respectively.

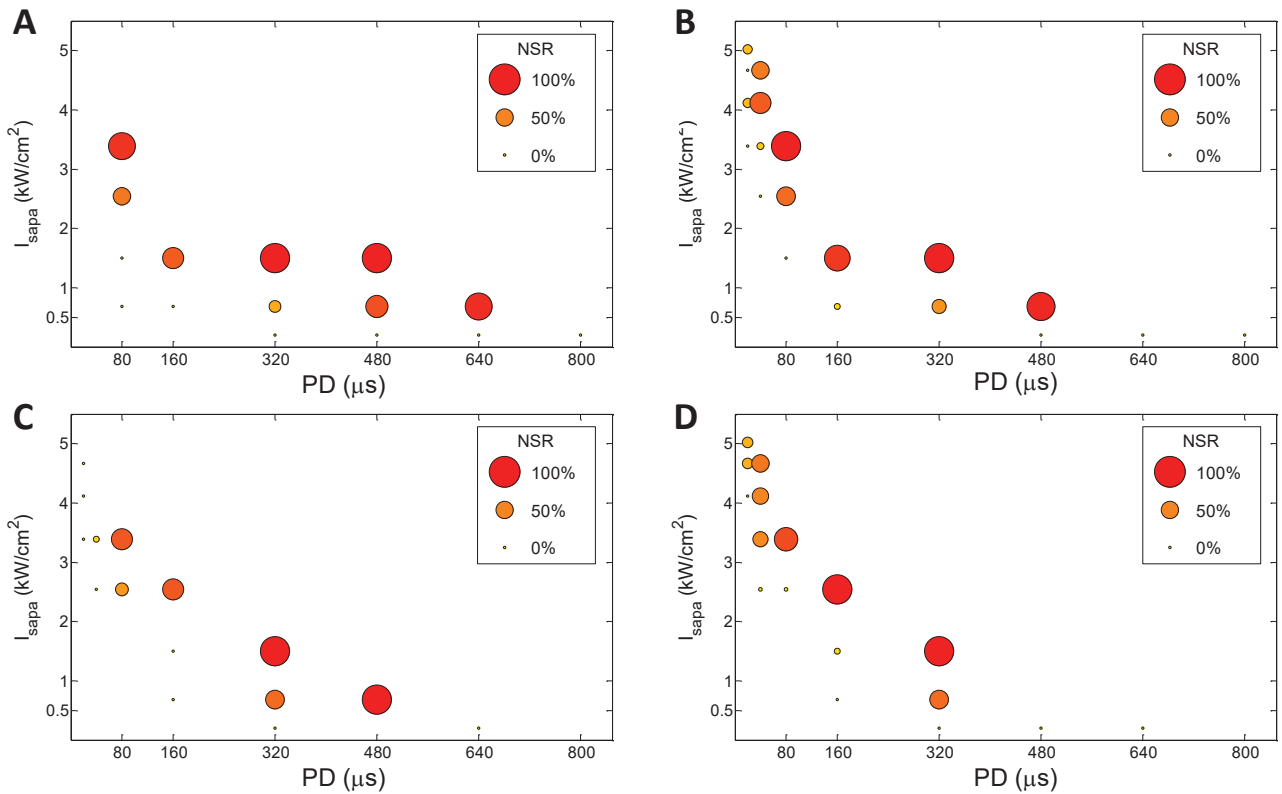


Figure 53 - Illustration of the combined influence of pulse intensity (I_{sapa}) and pulse duration over the neurostimulation success rate (NSR). Each chart (A-B) presents the results associated with a single trial, performed on a single animal. Each colored disc represents a NSR value associated with a combination of pulse intensity and pulse duration. More than 250 stimuli were administered in each trial to obtain a set of NSR values associated with a large variety of parametric combinations. Through all trials, the values of I_{sapa} tested ranged from 198 to 5025 W/cm², and the values of pulse duration tested ranged from 20 to 800 μ s. All other acoustic parameters were identical in every trial ($f = 1.1$ MHz, $PRF = 125$ Hz, $N_{pulses} = 20$).

I.B.4. Influence of pulse repetition frequency on the NSR

Over every trial ($n = 6$), it was observed that the success rate associated with the high PRF was significantly higher than the success rate associated with the low PRF ($*p < 0.05$) (**Figure 54**). Furthermore, in every trial except one (trial n°4, $p > 0.1$), the number of APs triggered per response tended to be significantly higher for the high PRF stimuli ($***p < 0.001$).

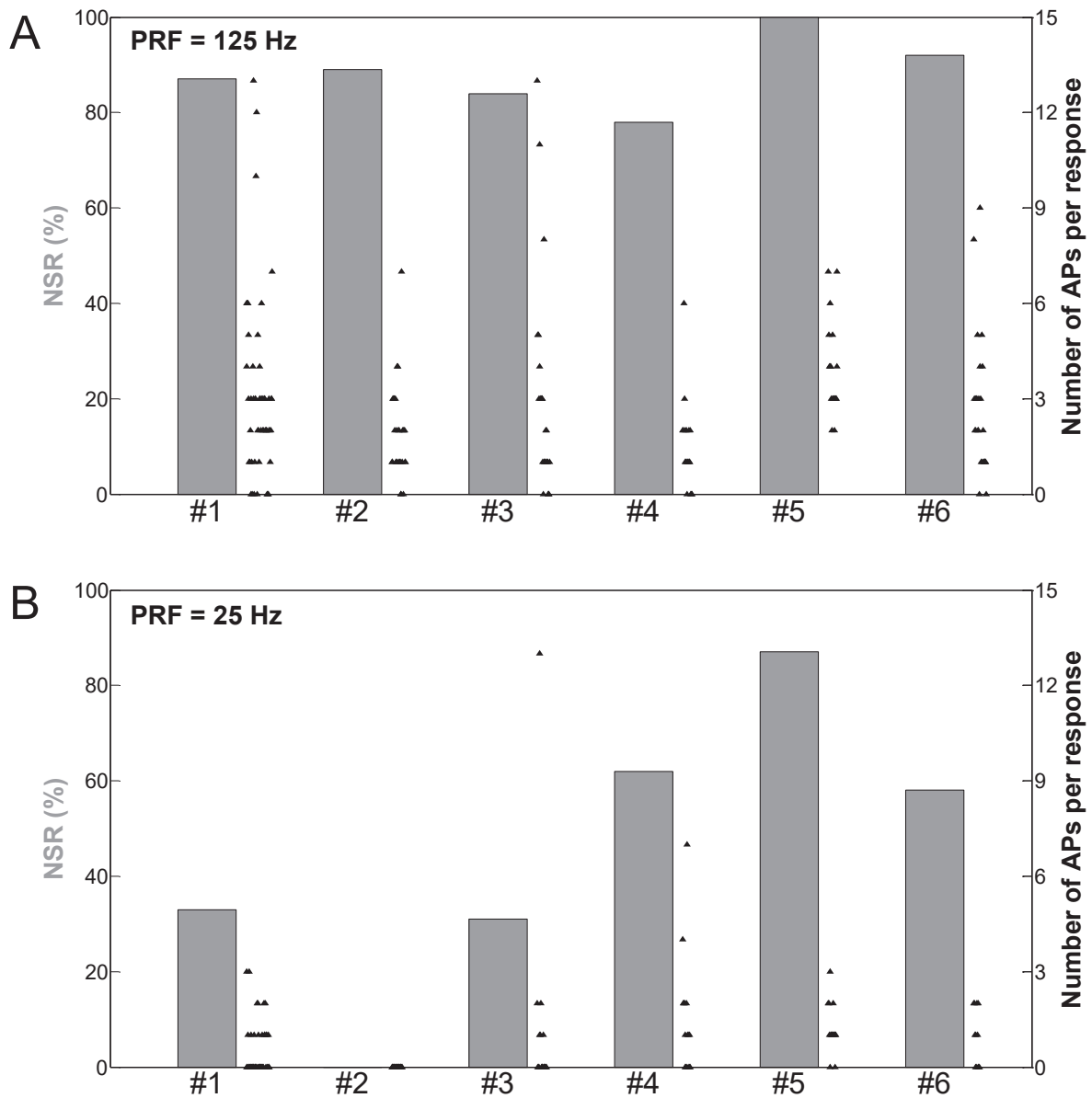


Figure 54 – Illustration of the influence of PRF over the NSR. Success rates (grey bars) and number of APs triggered per response (each black triangle represents a stimulus, including those which did not trigger any nervous response), associated with two types of pulsed ultrasound sequences, with respective PRF of (A) 125 Hz and (B) 25 Hz. All other acoustic parameters were identical in each trial ($f = 1.1$ MHz, $PD = 160$ μ s, $I_{sapa} = 2.5$ kW/cm², $N_{pulses} = 20$).

I.B.5. Influence of the number of pulses per burst on the NSR

Figure 55 presents a synthesis of the results obtained from the trials investigating the influence of the number of US pulses per burst (N_{pulses}) over the NSR. Complementarily, **Figure 56** presents the mean number of APs triggered per response in function of N_{pulses} . The different values of N_{pulses} investigated were compared by pair, in 5 sequences, as detailed in **Table 3**. In each trial, all other acoustic parameters were fixed ($f = 1.1$ MHz, $PRF = 125$ Hz, $PD = 480$ μ s, $I_{sapa} = 0.7$ kW/cm²).

Table 3 – Number of instances associated with the pairs of N_{pulses} values tested in each trial

US Sequence	N_{pulses}		Number of instances	
	US Burst # 1	US Burst # 2	Stimulus # 1	Stimulus # 2
1	20	200	7	5
2	5	20	16	13
3	1	5	30	19
4	1	3	15	39
5	1	2	11	6

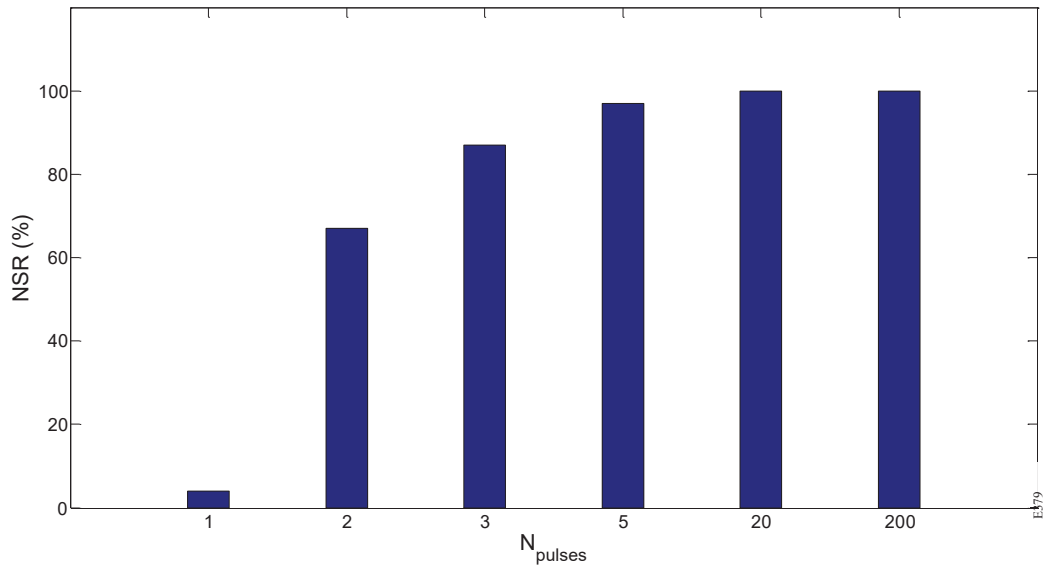


Figure 55 - Evolution of the NSR as a function of the number of US pulses per burst (N_{pulses}). Two different values of N_{pulses} were investigated randomly within a given US sequence. Five US sequences were performed to populate the dataset and build 6 groups of comparisons ($N_{pulses} : 1, 2, 3, 5, 20, 200$). In each trial, all other acoustic parameters were fixed ($f = 1.1$ MHz, $PRF = 125$ Hz, $PD = 480$ μ s, $I_{sapa} = 0.7$ kW/cm²).

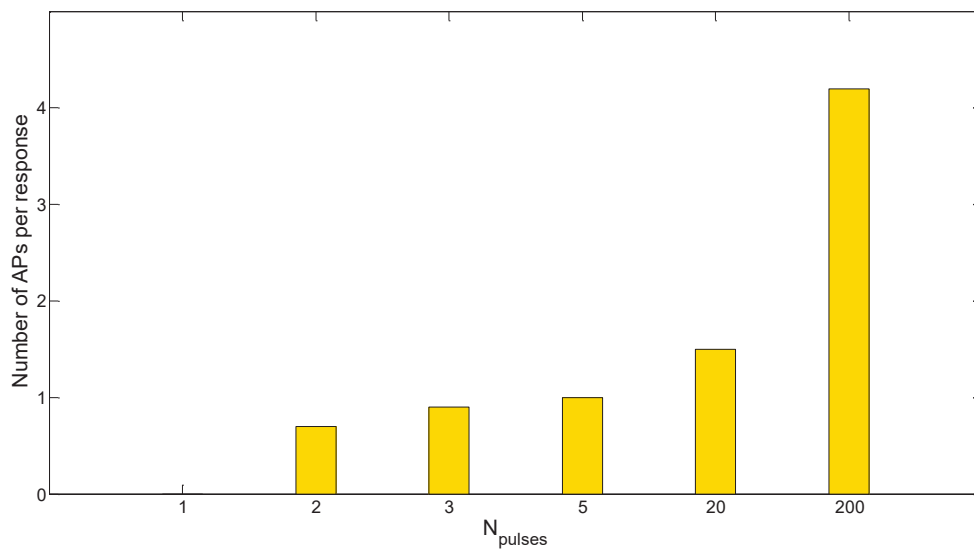


Figure 56 - Evolution of the number of APs triggered per response as a function of the number of US pulses per burst (N_{pulses}). In each trial, all other acoustic parameters were fixed ($f = 1.1$ MHz, $PRF = 125$ Hz, $PD = 480$ μ s, $I_{sapa} = 0.7$ kW/cm²).

Several observations can be made out of these results. Firstly, a very small amount of pulses (about 5 pulses) is sufficient to trigger nervous response with a satisfying repeatability (NSR>95%).

Secondly, a single pulse is highly unlikely to trigger a nervous response (NSR<5%), but the NSR is substantially higher as soon as the burst presents 2 or more pulses. In other words, the difference in the electrophysiological neural response induced by a single US pulse or two successive pulses is comparable to an all-or-nothing response.

Thirdly, the number of APs triggered per nervous response does not increase proportionally with the number of US pulses per burst. Above a certain threshold, increasing the number of US pulses within a single burst will not lead to more APs in the nervous response. From our experience through many trials ($n > 300$), this ‘saturation’ in the number of APs is dependent on other acoustic parameters such as the US pulse intensity and duration. In the example presented in **Figure 57**, the number of APs per nervous response saturated around 5. It is worth noting that for long US bursts of 200 pulses, the APs tend to appear only during the first 400 ms of the burst (the burst lasting 1.6 s in total, **Figure 57**), suggesting a real effect of ‘nerve saturation’. This assumption is reinforced by another observation, illustrated in **Figure 58**. A very long US burst of 4 s will trigger APs during the early phase of the burst but not ever after. However, two shorter US bursts of 1.6 s, spaced of 0.8 s (that is also a total duration of 4 s) will both trigger APs during their early phase. To put it differently, after ‘nerve saturation’, the nerve cannot go back to a ‘ready for stimulation’ state, as long as the ultrasound exposure is on. These observations are highly empirical and qualitative, and have not been the subject of a dedicated quantitative study.

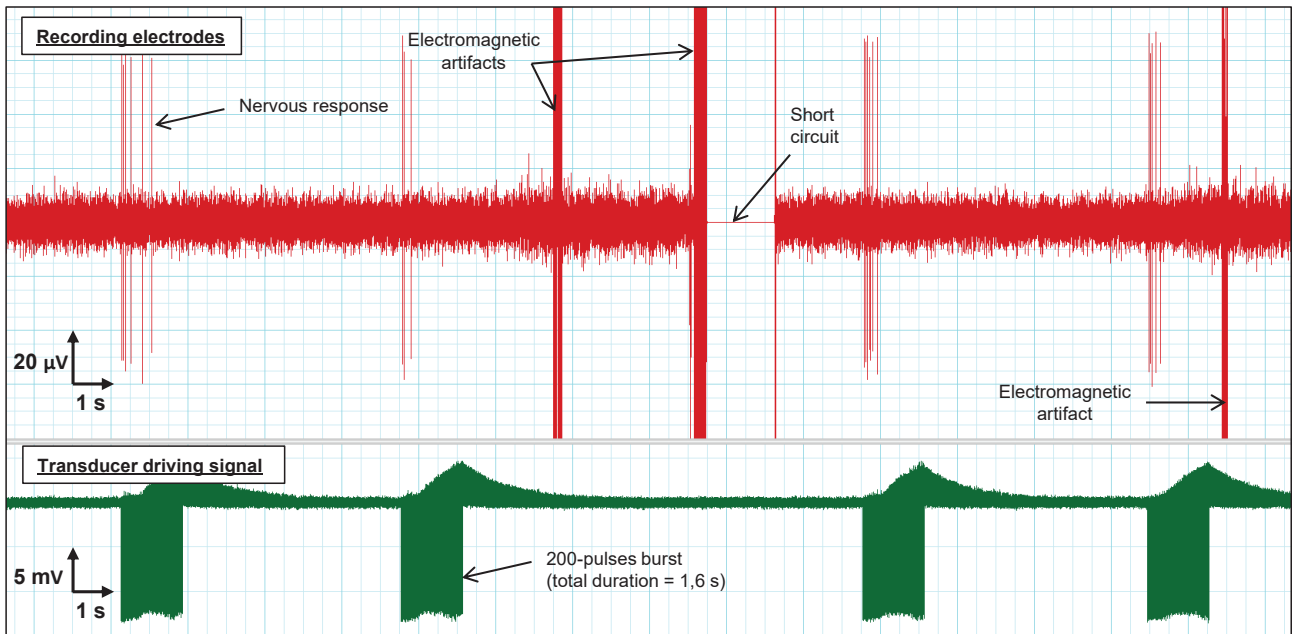


Figure 57 - Examples of nervous responses to relatively long US bursts of 200 pulses. The train of APs constituting the nervous response tends to be triggered during the early stage of the US burst, suggesting an effect of ‘nerve saturation’. The chart is a direct screenshot from the electrophysiological recording software (LabChart Pro v8, AD Instruments, New Zealand). The red channel corresponds to the signal recorded by the electrodes, and the green channel corresponds to the ultrasound transducer driving signal. The three rapidly saturated signals, correspond to electromagnetic artifacts. The rupture of signal at about the middle of the recording corresponds to a short circuit, most probably due to water infiltrating the platform which the electrodes are pinned in.

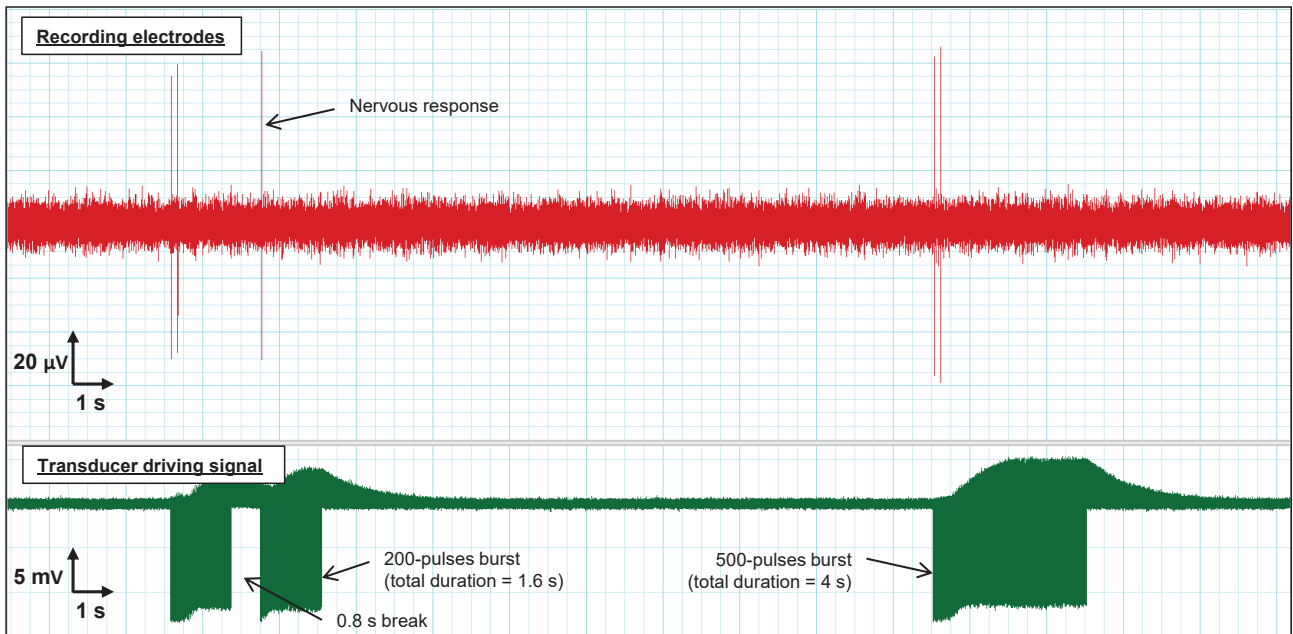


Figure 58 - Illustration of the difference between the respective nervous responses to a pair of two US bursts of 1.6 s, spaced of 0.8 s, and a burst of 4 s. The two types of US stimulus share the same total duration. The long US burst of 4s triggers APs during its early phase but not ever after. The pair of two shorter US bursts triggers APs during the early phase of both bursts. This example empirically highlights the fact that the pause time (ultrasound OFF) between the two shorter US bursts is critical for the re-induction of a nervous response. This could be interpreted as a phenomenon of US-induced ‘nerve saturation’, where the stimulated nervous structure cannot go back to a ‘ready for stimulation’ state as long as ultrasound is ON. The chart is a direct screenshot from the electrophysiological recording software (LabChart Pro v8, AD Instruments, New Zealand). The red channel corresponds to the signal recorded by the electrodes, and the green channel corresponds to the ultrasound transducer driving signal.

I.B.6. Influence of a higher US frequency on the NSR

Every trials of ultrasound neurostimulation reported so far involved a harmonic frequency of 1.1 MHz. But we also demonstrated the feasibility of using a harmonic frequency three times greater ($f_3 = 3.3$ MHz) to induce nervous responses. To go further, we investigated different combinations of US pulse intensity and duration, at 3.3 MHz. The results of this trial are presented in **Figure 59**, according to the same modality of data representation used in section I.B.3.

A first important observation is that nervous responses could be triggered at 3.3 MHz with success rates of the same order of magnitude as reported at 1.1 MHz.

The data presented in **Figure 59** are not sufficient to highlight a clear monotonous relationship between NSR and pulse intensity or pulse duration. However, it is possible identify a threshold under which no nervous response could be triggered for any pulse duration, similarly to what was observed at 1.1 MHz.

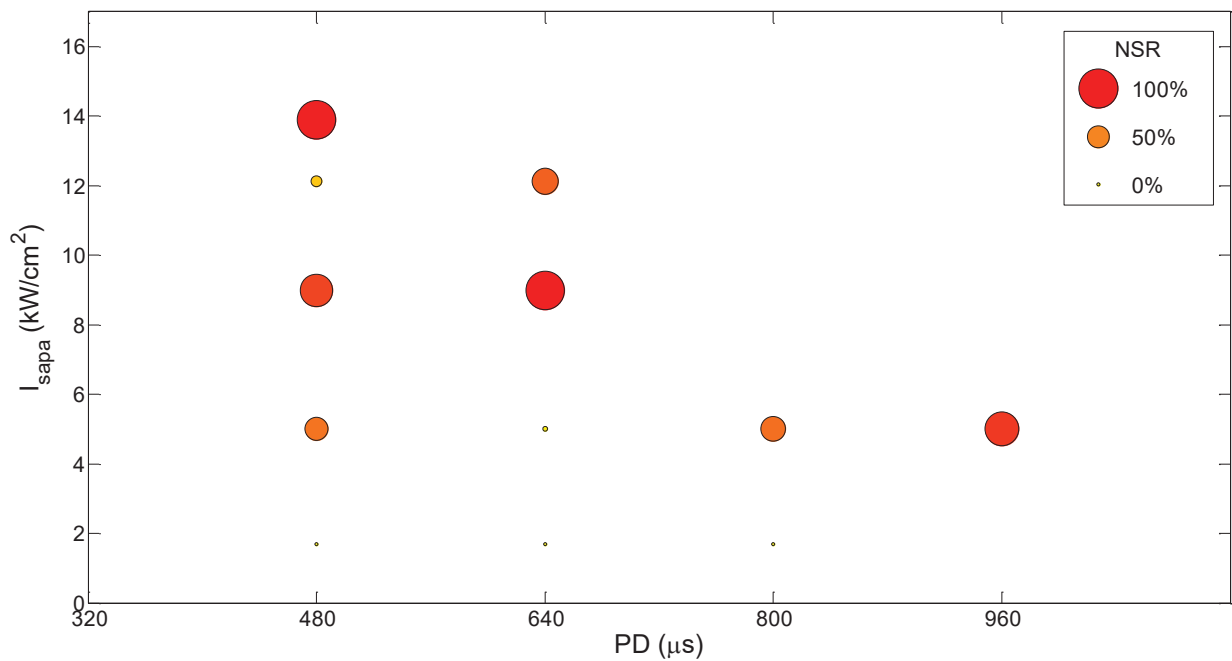


Figure 59 - Neurostimulation success rates induced by 3.3-MHz US stimuli, for different combinations of US pulse intensity (I_{sapa}) and duration (PD), all other parameters being identical ($PRF = 125$ Hz, $N_{pulses} = 20$).

I.C. Discussion

I.C.1. Cross-analysis of the influence of three US parameters on the NSR: I_{sapa} , PD and PRF

The parametric studies presented in this chapter investigated separately the individual influence of each US burst key parameter on the neurostimulation success rate (NSR). The goal

was to highlight a shared pattern leading to a particular ultrasound bio-effect, and which could be correlated with the evolution of the NSR.

Amongst several clearly identified trends, increases in the NSR with increasing values of US pulse intensity (I_{sapa}), duration (PD) and repetition frequency (PRF) have been reported. An US parameter dependent on each of these three former parameters is the spatial-average time-average acoustic intensity, I_{sata} , which can be calculated as follows:

$$I_{sata} = I_{sapa} \cdot PD \cdot PRF$$

According to our studies highlighting the respective influences of I_{sapa} , PD and PRF on the NSR, and the mutual dependence of I_{sapa} and PD in terms of nervous response threshold, it seems reasonable to investigate the role of I_{sata} in the triggering and facilitation of an US-induced nervous response.

In the hypothesis of I_{sata} as the key parameter to control US neurostimulation, the associated US interaction with nervous tissues should be a time averaged. One possibility would be the notion of ‘mean radiation force perceived’ by the nerve, which is proportional to I_{sata} (see section II.A.3 of chapter 2). Similarly to the mean radiation force measured (‘perceived’) by the RFB, this mean radiation force would be averaged over time because of the temporal resolution of the target. In our case, the target is the earthworm, and the inertia of the response of its biological tissue to a mechanical push could be responsible for this temporal averaging effect. It is thus likely that, because of their viscoelastic properties, the biological structures responding to ultrasound are sensitive to the mean radiation force carried by the US beam, whatever combinations of I_{sapa} , PD and PRF that lead to it, and as soon as the minimal threshold for each of these parameters are reached. It could then explain why it has been observed that high level of NSR could be achieved with various combinations of I_{sapa} , PD and PRF , having in common that a certain threshold in term of I_{sata} had been reached, as illustrated in **Figure 60**.

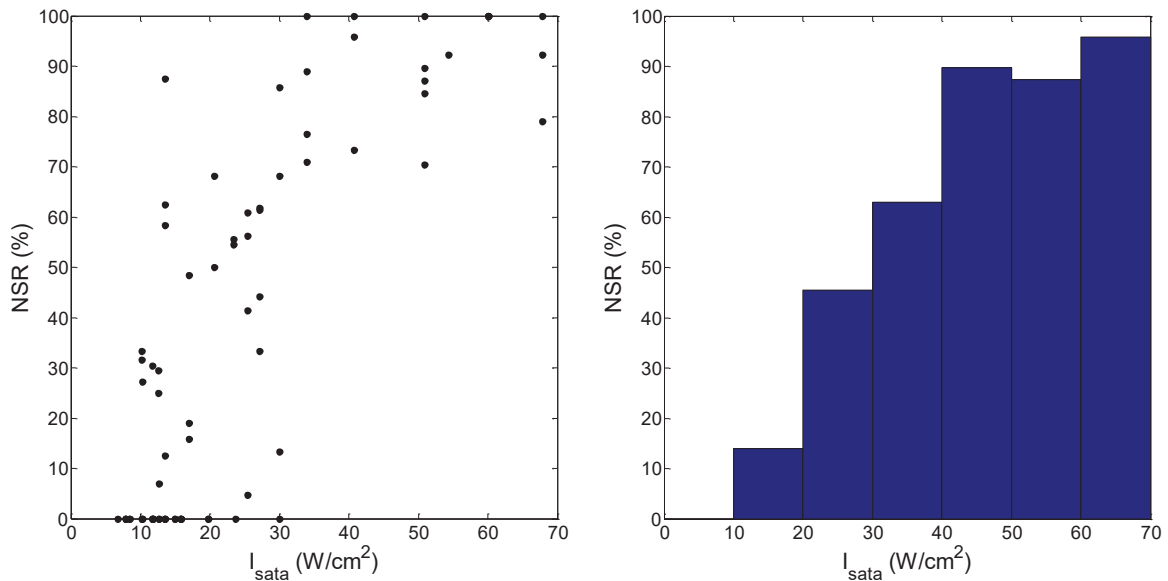


Figure 60 - Synthesis of the results obtained with the trials investigating I_{sapa} , PD and PRF separately, by presenting here the NSR as a function of $I_{sata} = I_{sapa} \cdot PD \cdot PRF$ (which depends on these 3 parameters). Left and right charts represent the same data, in the form of a point cloud and a bar plot, respectively. The values of I_{sata} result from a large variety of combinations of I_{sapa} , PD and PRF . When $I_{sata} > 30$ W/cm², the NSR > 50%.

I.C.2. Influence of the number of US pulses per burst

Two important mechanistic clues should be retained from the study investigating the influence on the nervous response of the number of US pulses per burst. Firstly, a phenomenon of US-induced nerve saturation had been highlighted. After responding to US stimulation, the involved nervous structure needs a resting time without US exposure in order to be ready again and respond to US stimulation. Secondly, we observed that there was a qualitative difference between the response to a single pulse and to two following pulses, in terms of NSR. This would suggest that some biophysical effects occurring only when at least 2 pulses are successively sent is at play.

I.C.3. Feasibility of using a higher US frequency

From the investigation on the influence of the US frequency, the main conclusion is that the neurostimulating effect of ultrasound on our nervous model is not specific to the 1.1 MHz frequency, since it can be achieved at least at 3.3 MHz. However, we cannot gain as much knowledge in terms of biophysical effects as from the studies discussed in the previous section, for two reasons. Firstly, the 3.3 MHz stimuli were tested on only one animal, since our primary goal was to provide a proof of feasibility. Secondly, the notion of space average-pulse average intensity is, by definition, dependent on the size of the -6 dB focal spot. As presented in section I.B.1, the distribution of acoustic pressure substantially varies between the ultrasound beams simulated at 1.1 and 3.3 MHz, respectively, leading to -6 dB focal spot area ten-fold smaller at 3.3 MHz. This has a direct consequence on the order of magnitude of I_{sapa} at 3.3 MHz, hence the bubble plot from section I.B.6 should not be directly compared to those presented in section I.B.3. We shall stress, again, that our primary goal was to demonstrate the feasibility of US neurostimulation at 3.3 Mhz, and the form in which we presented our results was chosen in an attempt to unify the modality of representation of NSR in function of different combined values of two parameters.

The only set of results available at 3.3 MHz shows levels of NSR globally inferior to levels of NSR at 1.1 MHz. We would need to repeat trials at 3.3 MHz, for a larger range of PD- I_{sapa} combinations, in order to prove or disprove this trend. If it was proven that NSR tends to globally decrease with harmonic frequency, then we could formulate hypotheses regarding the role played by bubble oscillation in the phenomenon of ultrasound neurostimulation. Hence, even though it represents a considerable amount of trials, there would be much to win in terms of mechanistic knowledge if the whole campaign of parametric studies performed at 1.1 MHz was reproduced for higher and lower harmonic frequencies.

II. Study of the cavitation as a possible mechanism underlying US neurostimulation

II.A. Methods

II.A.1. Imaging of the cavitation cloud

An ultrafast ultrasound imaging system (Vantage 256, Verasonics, USA) was used to detect the presence and monitor the activity of the cavitation cloud generated by the US pulses. Acquisitions of 2D US images were performed with a 1D-linear array at a frame rate of 8000 images per second, which provided several dozens of images between two consecutive pulses. Complementary to the observation of the ultrasound scan, correlation images were built, according to a method previously described in literature (Prieur et al., 2015). The correlation between two consecutive US images for speckle tracking. If a decorrelation of the signal is detected in the image, it is interpreted as the direct consequence of the creation, fast oscillation and dissolution of a cavitation cloud. Hence, by observing this area of decorrelation, it is possible to spatially and temporally characterize the cavitation cloud.

II.A.2. Monitoring of the cavitation indexes

In order to investigate the possible role played by acoustic cavitation in the phenomenon of ultrasound neurostimulation, trials were performed where the acoustic signature associated with each ultrasound burst was monitored. Different indexes have been proposed in literature to control acoustic cavitation (Sabraoui et al., 2011; Desjouy et al., 2015; Cornu et al., 2018), aiming to develop or improve applications to sonodynamic therapy (El Maalouf et al., 2009) and gene transfection (Reslan et al., 2010; Lo et al., 2014). The methodology described in this section is inspired from these works, and particularly from a technic of ultrafast monitoring of a bubble cloud during pulsed sonification, developed in our lab (Cornu et al., 2018).

Acoustic signatures associated with individual pulses were recorded using a custom-made hydrophone (sampling frequency of 62.5 kHz), oriented towards the transducer focal area, at 5 cm from it. The signal duration considered to analyze the whole acoustic signature of the US stimulation was fixed at 1.5 ms, on the basis of preliminary trials. The frequency spectrum,

associated with the acoustic signature of each US pulse, was calculated using the Fast Fourier Transfer function. For each US burst, a spectrum averaged over every US pulse was calculated. From this averaged signal, two indexes were extracted, named IC and ESC, characterizing the occurrence of stable and inertial cavitation, respectively (Cornu et al., 2018).

IC is the difference between the mean amplitude value of the spectrum and a reference value. The reference value was arbitrarily chosen equal to -60 dB, but roughly corresponds to the mean amplitude value of the frequency spectrum associated with the signal recorded by the hydrophone in the absence of an acoustic wave. **IC reflects the increase of the broadband noise, which is characteristic of the occurrence of inertial cavitation.**

ESC is the difference between the mean amplitude value around the first subharmonic and the emergence noise. **ESC reflects the presence of oscillations at half the fundamental frequency, which is characteristic of the occurrence of stable cavitation.**

Figure 61 sums up the global process leading to the calculation of these two indexes. In the past, similar indexes have been used to control acoustic cavitation

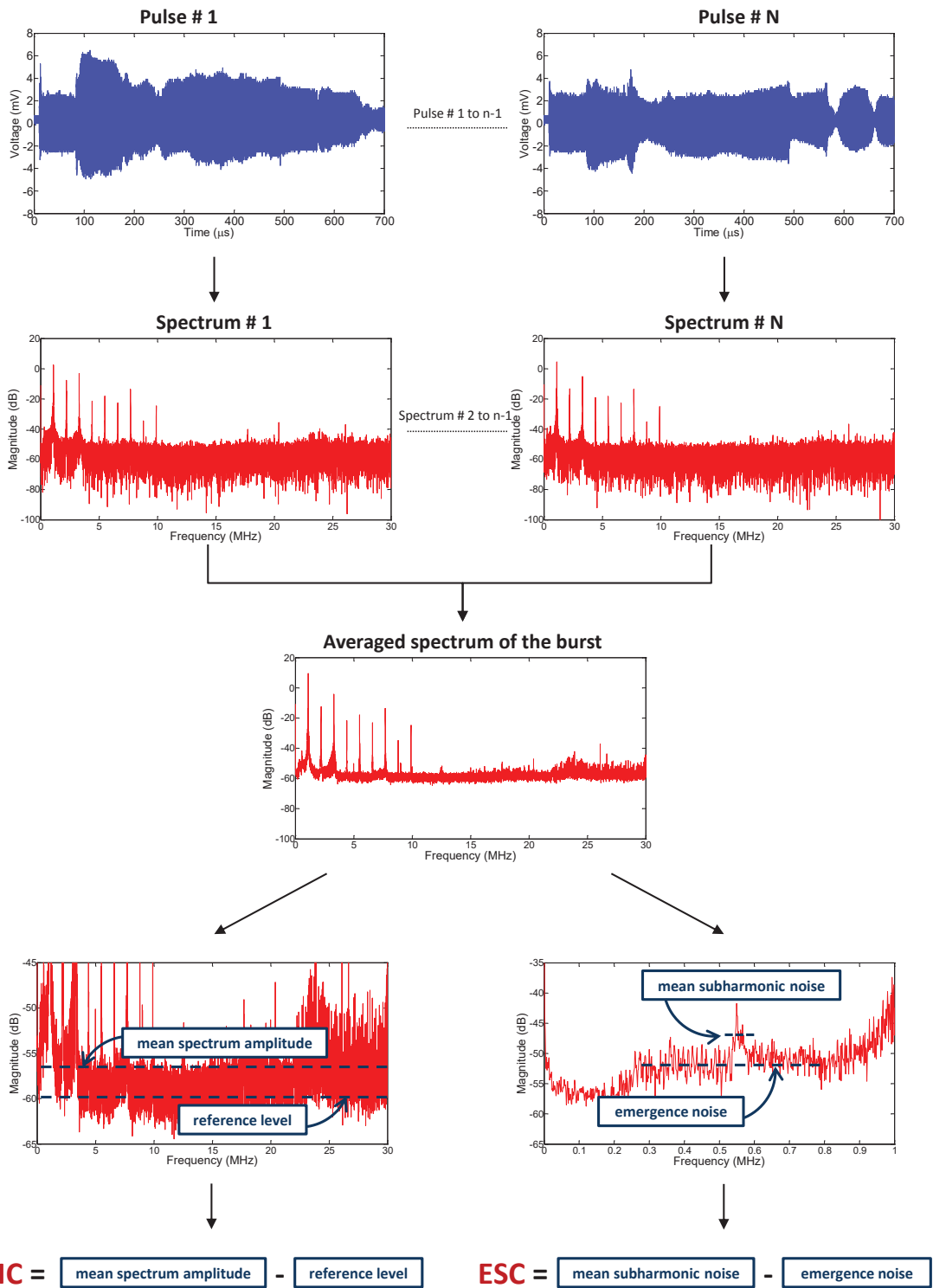


Figure 61 - Schematic representation of the calculation process of the two cavitation indexes: IC, characterizing the level of inertial cavitation, and ESC, characterizing the level of stable cavitation.

II.B. Results

II.B.1. Characteristics of the cavitation cloud

The presence of a cloud of bubbles can be clearly identified on the correlation images (**Figure 62.B**), but not as clearly on the ultrasound images (**Figure 62.A**) unless they are observed in real-time. The imaging plan in **Figure 62** is transverse to the animal, at the level of the ultrasound beam focus. **Figure 63** shows the temporal evolution of the correlation images. An important loss of signal correlation can be locally observed, immediately after the artifact corresponding to the US pulse duration. This is characteristic of the occurrence of cavitation in the medium. The bubble cloud disappears from the correlation images about 3 ms after the end of the US pulse.

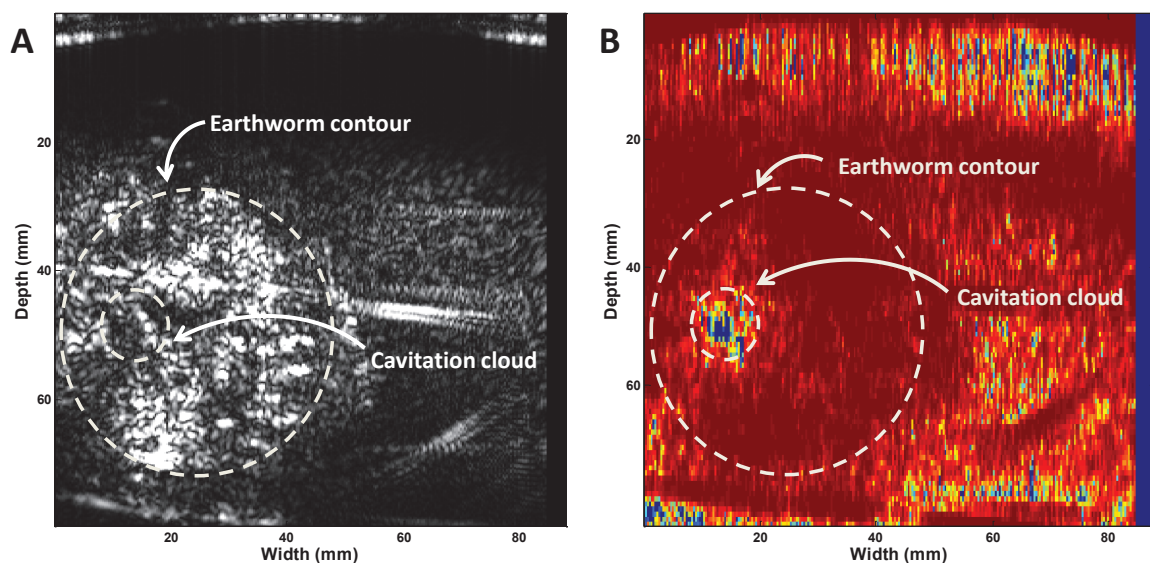


Figure 62 - Localization of the cavitation cloud on an transverse ultrasound image (left chart) and a correlation image (right chart).

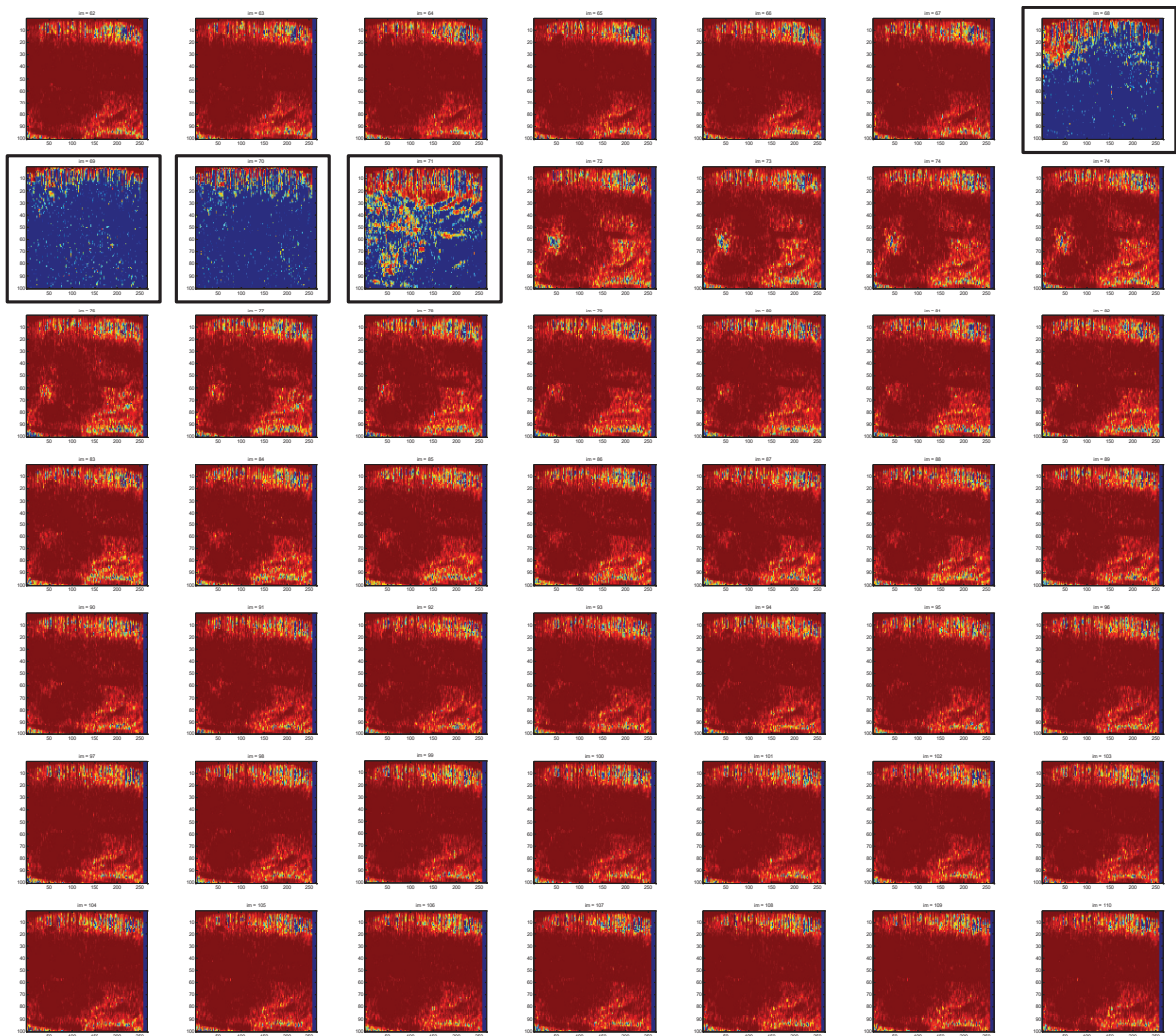


Figure 63 - Temporal evolution of the correlation images. The frame rate is 8 kHz, so the 49 images represent 6 ms of acquisition. The 4 images presenting a widespread loss of correlation signal (black-framed) mark the arrival and duration of the US pulse. On the image directly following the end of the ultrasound pulse, an important loss of signal correlation can be locally observed, which corresponds to the apparition of an US-induced cloud of cavitation bubbles. The cavitation cloud disappears from the correlation images about 3 ms (~25 frames) after the end of the US **pulse**.

II.B.2. Correlation between cavitation events and stimulating events

The parametric studies presented in part II allowed to design US sequences likely to trigger a nervous response with a 100% NSR (stimulating bursts), but also US sequences which

triggered a nervous response more or less occasionally (edge bursts), that is with a NSR roughly comprised between 20 and 70%. We took advantage of these two types of sequences to create a large variety of events presenting different combinations of cavitation indexes (IC and ESC), leading to nervous responses or not, in order to investigate the potential role played by cavitation in the phenomenon of ultrasound neurostimulation.

Different ways of representing data were explored in order to analyze our results.

II.B.2.i. MOD-1: distribution of each cavitation index over a single trial

A first and simple way to represent data, referred to as MOD-1, consists in plotting the values of either IC or ESC associated with the stimuli of a given US sequence, and mark the stimulating event by a color code, as illustrated in **Figure 64**. The 2 examples presented in **Figure 64** are representative of the majority of the US sequences performed ($n = 27$). MOD-1 did not bring to light an obvious correlation between US-induced nervous responses and either one of the two cavitation indexes. Particularly, no neurostimulation threshold value of IC or ESC could be identified.

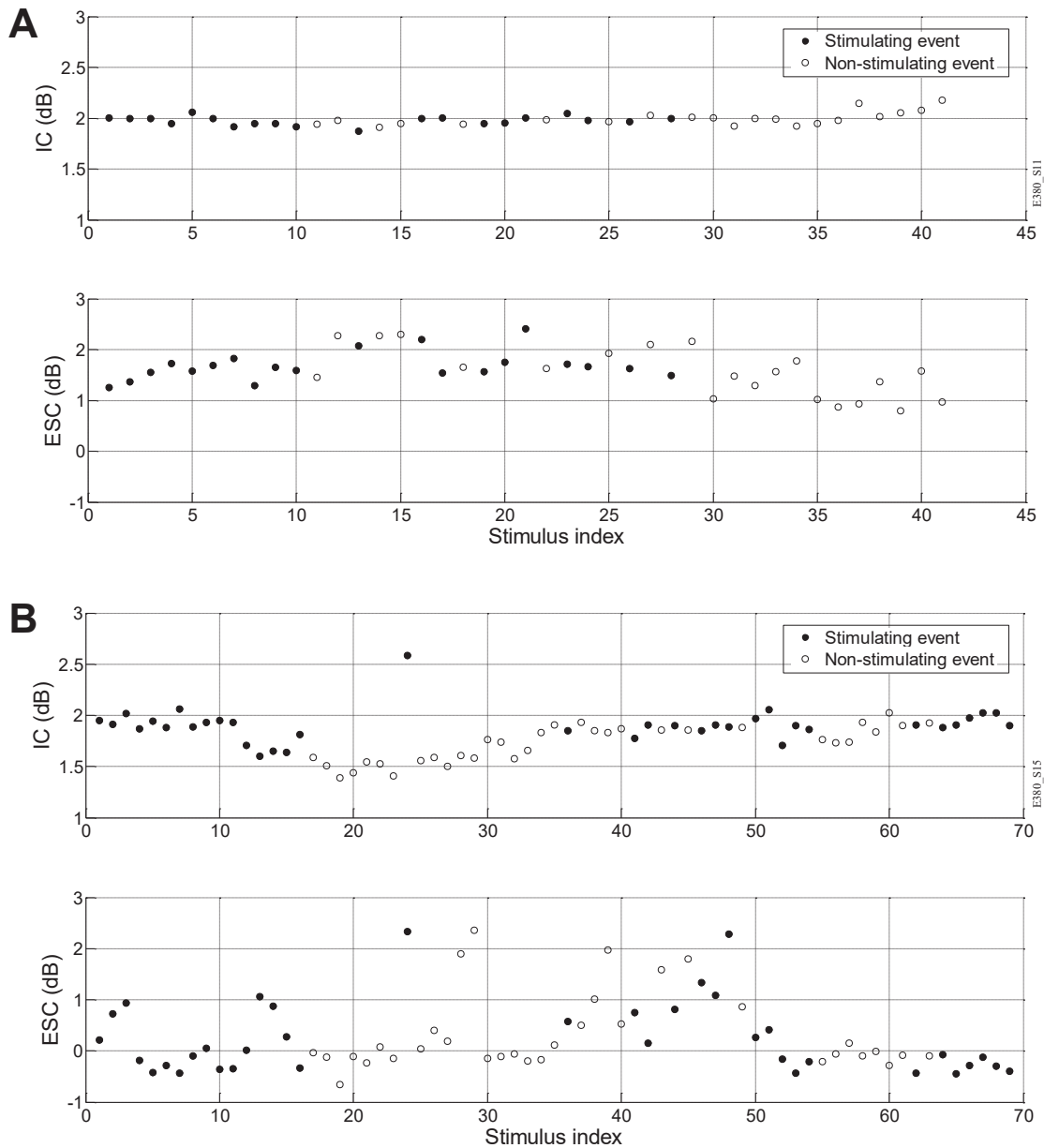


Figure 64 - Examples of the MOD-1 modality of representing the results from the trials of cavitation monitoring. A and B display data corresponding to two different trial / sequences, performed on two different animals. Each section is itself divided in one chart representing the different values taken by IC over the ultrasound trial, and a similar chart for ESC. Black-filled dots represent stimulating events and empty dots represent non-stimulating events.

Nonetheless, this first intuitive modality of data representation was useful to easily identify some individual events bearing in themselves more concrete clues. Similarly to those appearing

in **Figure 64.B**, we observed many examples where a stimulating burst was associated with a null or negative ESC. A null or negative ESC reflects the absence of subharmonic peak in the mean spectrum associated with the considered US burst, as exemplified by **Figure 65**, which corresponds to the burst (stimulus) #4 of the US sequence displayed in **Figure 64.B**. The existence of these particular situations suggests that, in our study, stable cavitation is not a necessary condition to US-induced nervous response.

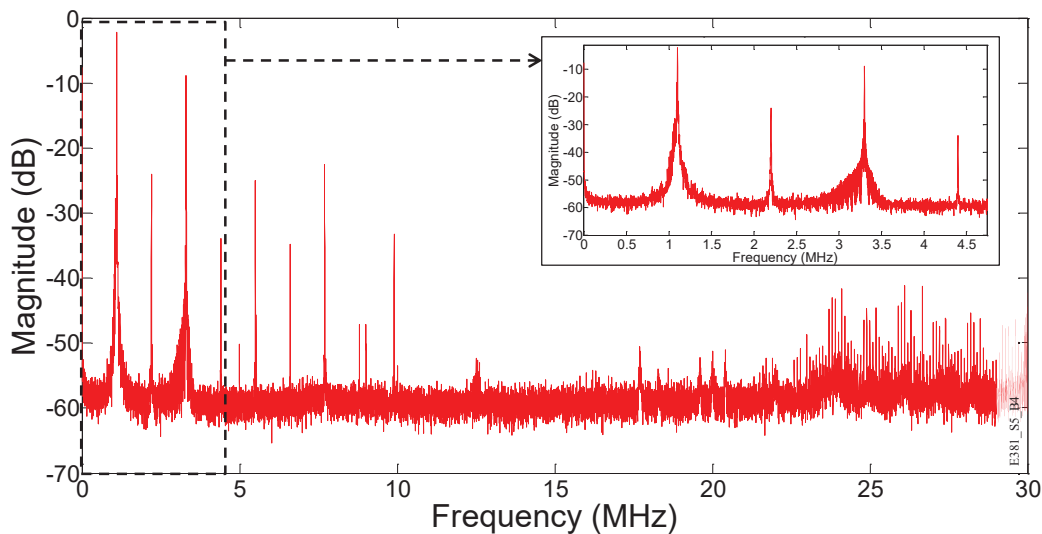


Figure 65 - Example of stimulating burst whose mean frequency spectrum shows no sign of subharmonic peak (ESC < 0).

II.B.2.ii. MOD-2 : distribution of combination of cavitation index over the whole set of trials

In a second attempt to represent the data from our trials of cavitation monitoring (MOD-2), the results recorded over all trials were plotted, which represented 1074 US bursts, in an IC-ESC space, using the same color code as in MOD-1 to mark the stimulating US bursts (**Figure 66**). This modality of representation has been successfully employed in the past to identify ranges of cavitation index eliciting optimal level of US-induced sonoporation in cell preparation (Cornu et al., 2018).

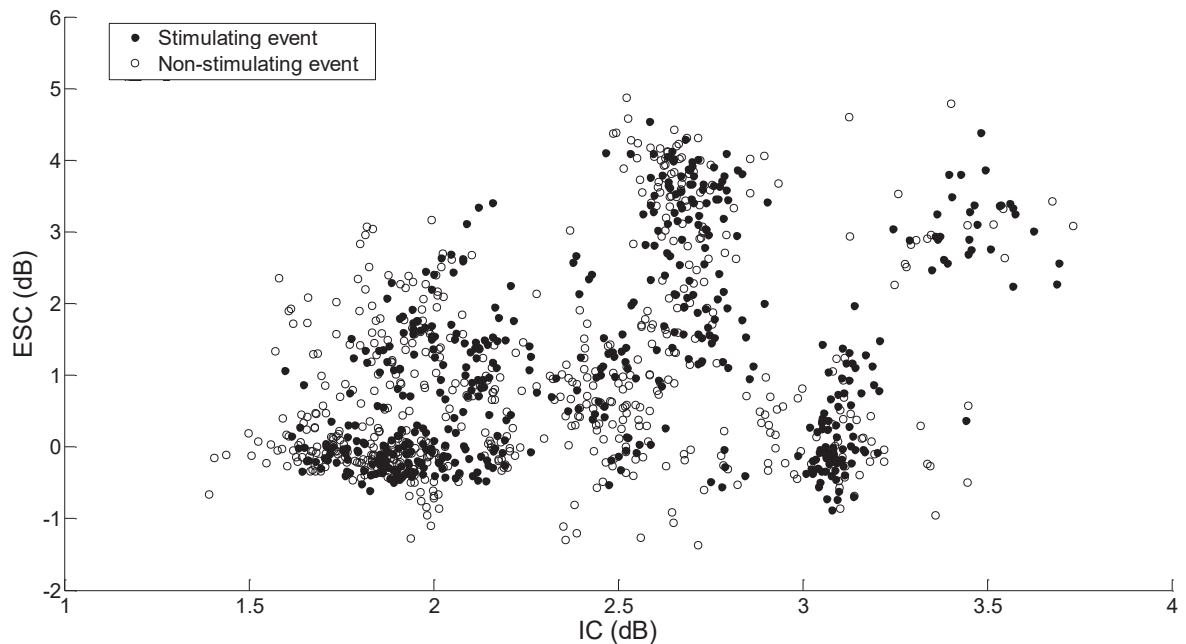


Figure 66 - MOD-2 modality of representing the results from the trials of cavitation monitoring. Black-filled dots represent stimulating events and empty dots represent non-stimulating events.

We can visually observe in **Figure 66** that the stimulating and non-stimulating events are largely distributed in both IC and ESC ranges. A large number of a stimulating events associated with negative ESC can be identified, confirming the observations from MOD-1 and strengthening the idea that stable cavitation is not a necessary condition for the occurrence of US-induced nervous response. Some stimulating events are associated with IC as low as 1.6 dB. This value is relatively close to the minimal IC value recorded amongst all US bursts of these trials, which is about 1.4 dB.

From a more global perspective, the MOD-2 representation used in **Figure 66** could suggest that some regions of the IC-ESC space are more concentrated in stimulating events than other. This first impression is biased by the fact that: 1) some combinations of cavitation indexes occurred more frequently than other during our trials and 2) the black-filled dots may hide empty dots. In order to clear up any doubt, we came with a third modality of data representation, referred to as MOD-3.

II.B.2.iii. MOD-3 : display of the regional NSR in the IC-ESC space

In MOD-3, the IC-ESC space is discretized into regions of equal dimensions (0.5 dB in the IC dimension, 1 dB in the ESC dimension). Each region is attributed a neurostimulation success rate (NSR), on the basis of the number of stimulating events and total number of stimulating events within its borders, which is translated into a grey level. **Figure 67** presents the same results as previously, with the MOD-3 representation of data.

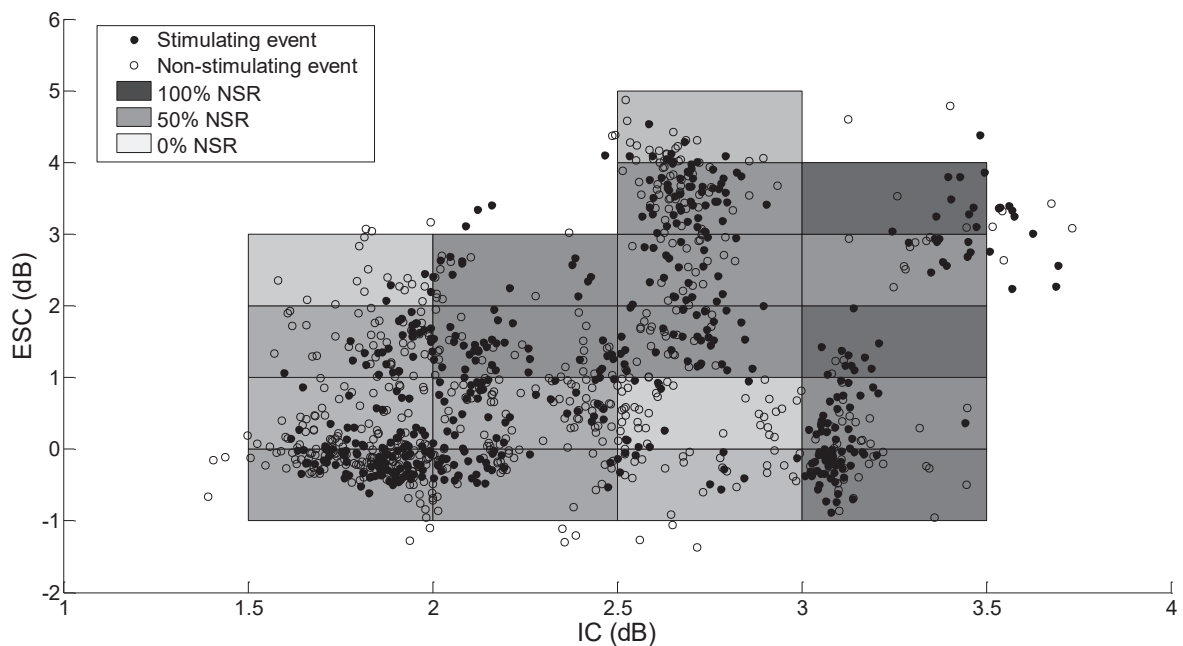


Figure 67 - MOD-3 modality of representing the results from the trials of cavitation monitoring. Black-filled dots represent stimulating events and empty dots represent non-stimulating events. The grey-scale indicates the level of NSR associated with each region. The minimal number of events per regions to calculate a relevant regional NSR was fixed at 10.

Figure 67 shows that the NSR is relatively homogenous in the tested IC-ESC sub-space, with a slight elevation in in the regions of high IC (>3 dB).

II.C. Discussion

Firstly, ultrafast ultrasound imaging provided some proofs that the typical US stimuli used in our studies could induce cavitation in the earthworm, generating bubbles clouds lasting at

least 3 ms in the medium.

Secondly, the US focus was casted on the early phase of the cloud existence, when the bubbles were still oscillating. The acoustic signature associated with each US burst of a sequence was recorded and translated into two indexes, ESC and IC, characteristic of the occurrence of stable and inertial cavitation, respectively. These trials provided numerous examples of stimulating US burst which were associated with ESC levels translating the absence of stable cavitation. From this observation, we can conclude that stable cavitation is not a necessary condition to the occurrence of US-induced nervous response. This conclusion is contextual to our particular nervous model, hence we do not discard the potential role played by stable cavitation in some experimental results of neurostimulation, but simply claim that such mechanistic postulations as the Neuronal Intramembrane Bilayer Model (Krasovitski et al., 2011; Plaksin et al., 2014) do not apply in this invertebrate model.

Regarding the second cavitation index, IC, it was not possible to apply the same approach as for ESC, where finding counter-examples was enough to draw a logical conclusion. Indeed, the calculation of IC involves a reference value, which is the subject of many discussions in the field of cavitation characterization. As explained in section II.A.2, a reference value of -60 dB was arbitrary chosen, roughly corresponding to the mean amplitude of the frequency spectrum recorded by the hydrophone in the absence of ultrasound vibration in the tank. Hence, looking for stimulation events where IC is close to zero would not necessarily make sense, as they can simply not exist at all. A better approach is to consider the lowest IC value associated with a stimulating event. In our trials, some stimulating events are associated with IC value as low as 1.6 dB. This value is relatively close to the minimal IC value recorded amongst all US bursts of these trials, which is about 1.4 dB. Hence, from the presented results, the most cautious conclusion is that high levels of inertial cavitation are not necessary to trigger US-induced nervous response. Complementarily, we can stress that we did not find any evidence of a particular correlation between inertial cavitation occurrence and US-induced nervous responses.

Conclusion

In this chapter, we studied first the respective influence on the Neurostimulation Success Rate of several acoustic parameter defining an US stimulus. From the trends highlighted, we hypothesized that the nervous structure responding to the stimulus is sensitive to the ‘mean radiation force’ carried by this stimulus, whatever combination of parameters that lead to it (although a minimal activation threshold was identified in terms of pulse intensity).

Second, cavitation indexes were monitored in order to investigate a possible correlation between cavitation events and stimulating events. Numerous counter-examples lead us to conclude that the occurrence of stable cavitation was not a necessary condition to the occurrence of a US-induced nervous response. Complementarily, high levels of inertial cavitation were not necessary to trigger US-induced nervous response.

These experimental findings are to be contextualized in the nervous model they came from. Ultrasound neurostimulation, as a general phenomenon, is likely to involve multiple mechanisms working in concert, and whose contribution differs from one nervous model to another. However, the methodology employed for the mechanistic study presented in this chapter is universal, and the next chapter will present our first attempts to apply it to a different and more complex nervous model.

Chapter 4: Feasibility of using a vertebrate ex vivo nervous model to study ultrasound stimulation

Introduction

In Chapter II was presented the long-term methodology work that have been followed to study the biomechanisms responsible for the phenomenon of ultrasound (US) neurostimulation. It consisted in identifying US sequences triggering nervous responses in a simple nervous model of giant neuron, by investigating different sets of acoustic parameters to optimize their success rate and gain mechanistic knowledge, before switching to a nervous model of higher complexity and repeat the same process. It is a time-consuming strategy, but a robust one, where each experimental cycle benefits from the protocol refinement and mechanistic clues resulting from the previous steps. Chapter II and III presented the first iteration of this long-term strategy, applied to a relatively simple in vivo invertebrate nervous model. In this chapter will be presented the preliminary steps of the second iteration, involving an ex vivo neural model of vertebrate central nervous system. As in the earthworm model, these steps consisted in demonstrating the feasibility of generating and recording US-induced nervous responses from the neural model, and trying to increase the success rate associated with these responses, to allow the realization of ulterior parametric studies.

This new study, which is still going on, was initiated one year ago with the collaboration of a team of neurophysiologists (INSERM U1129, Center for Interdisciplinary Research in Biology, Collège de France) who brought to the project their expertise on both the animal model (mouse cortical slice) and the associated technic of electrophysiological recording (multielectrode array, or MEA).

I. Feasibility of generating and recording US-induced nervous responses from a mouse cortical slice, using an MEA device

I.A. Methods

I.A.1. Ethical statement

All animal experiments were carried out in strict accordance with the legal conditions of the French National Ethics Committee for Reflection on Animal Experimentation (CNREEA). To reduce the number of animals involved in an experimental protocol, the presented exploratory investigations were performed at the end of an ongoing in vivo study carried out at the Center for Interdisciplinary Research in Biology, including the eventually the animal's sacrifice.

I.A.2. Slice preparation

The mice received deep sedation and a laparotomy was then performed as to perfuse the animal with artificial cerebrospinal fluid (aCSF). The mice were then sacrificed and their brains extracted for subsequent slicing in the transverse plane using a vibratome (Leica VT1200, Leica Microsystems). The transverse slices (thickness: 300-400 μm) were halved with a scalpel and placed inside an aCSF-perfused bath for 1 hour prior to be transferred inside the aCSF-perfused MEA chip (**Figure 68**). The slice was positioned so that the electrodes covered the hippocampal region (**Figure 68.D**), for the nervous connections leading to this brain area are well known by the team of neurophysiologist we were working with. A weighted grid was placed on top of the brain slice in order to prevent the sample from floating, ensure a good electrical contact between the sample and the MEA electrodes, while reducing potential motion due to the aCSF circulation or US emissions (**Figure 68.C**).

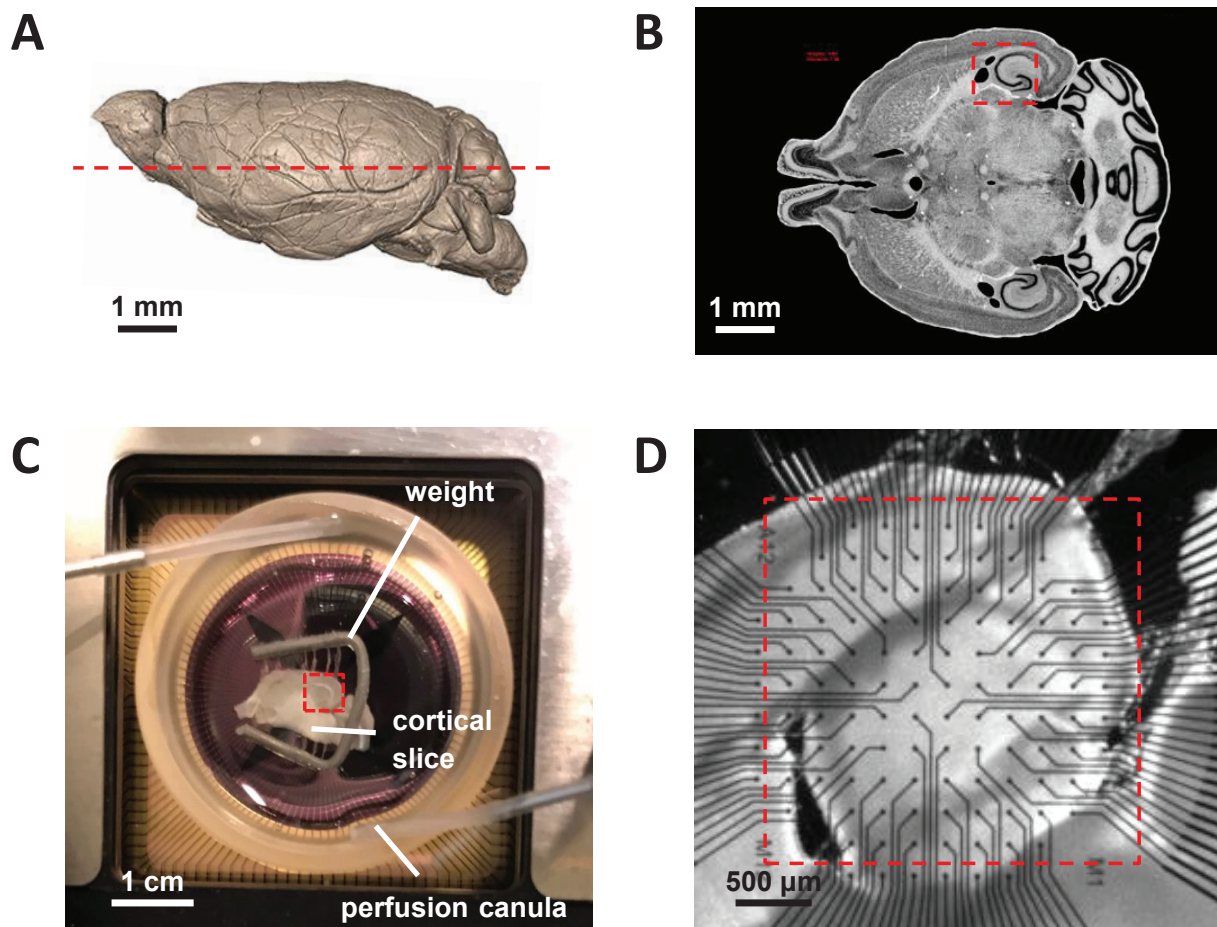


Figure 68 - Localization of the mouse cortical area used for stimulation and recording. (A) Profile view of a mouse brain. The dotted red line corresponds to the plan of visualization in (B). (B) Transverse section of the mouse cortex. (C) Half transverse cortical slice placed in the aCSF-perfused MEA chip (petri dish). (D) Microscopic view from under the MEA chip. In (B), (C) and (D), the white dotted frame indicates the area in contact with the MEA grid of electrodes.

I.A.3. Experimental set-up

Generally, the experimental set-up used throughout the different studies presented in this chapter was composed of the following elements (**Figure 69**):

- An **electrophysiological recording device**, compound of the MEA platform and the MEA chip, described in detail in section I.A.3.
- A **microscopic camera**, placed under the MEA chip, enabling the precise positioning of

the cortical slice relatively to the electrodes.

- An **ultrasound stimulation system**, placed above the MEA chip so that its focal region intersects the cortical slice, described in detail in section I.A.5.
- A **positioning system**, compound of a micromanipulator with 3 degrees of freedom, enabling the precise positioning of the transducing system.
- A **perfusion system** maintaining a constant level of oxygenated aCSF in the MEA chip.

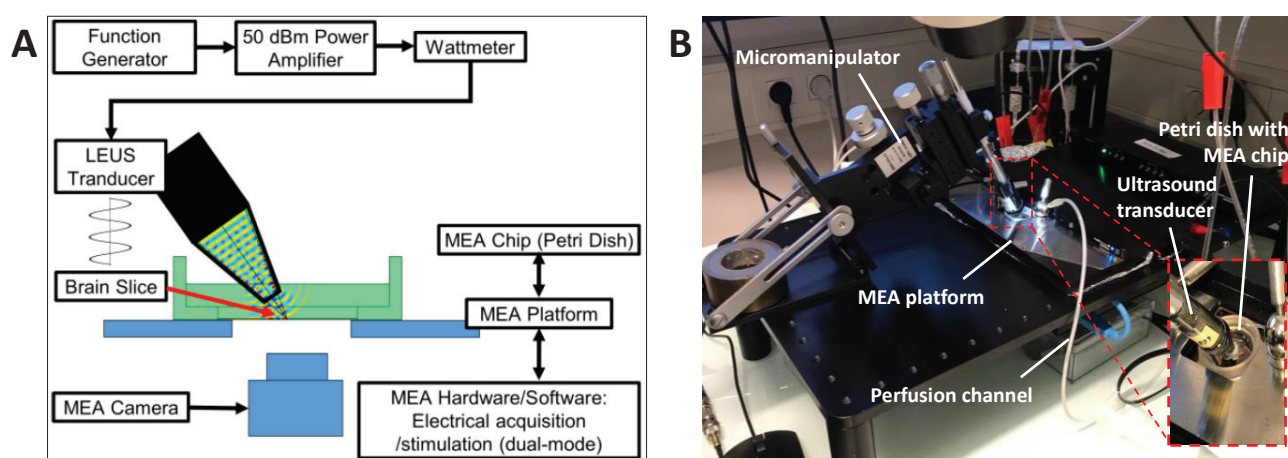


Figure 69 - Experimental set-up designed for the MEA-recording of US-induced nervous responses from cortical slices. The US transducer is placed above the MEA chip so that its focal region intersects the cortical slice, slightly immersed in the aCSF bath in order to insure acoustic coupling. A microscopic camera, placed under the MEA platform and hence not visible in the picture, enables the precise positioning of the cortical slice relatively to the electrodes. (A) Schematic of the combined MEA/US platform. (B) Picture of the experimental set-up.

I.A.4. Electrophysiological recording

The MEA system (MEA2100, MultiChannel Systems, Reutlingen, Germany) allows for the study of electrical activity with high spatial and temporal resolution.

The MEA chip (120MEA200/30iR-Ti) contained a grid of 120 extracellular electrodes spreading every 200 μm (**Figure 68.C**), thus allowing the recording of single action potentials (APs), actions potentials from multiple neurons (Multi Unit Activity) as well as synchronized synaptic potentials (Local Field Potentials).

The electrical activity detected by the electrodes in the MEA chip was recorded at a sampling rate of 10 kHz (software: MC_Rack V4.6.2, MultiChannel Systems). The recorded data were then converted into ASCII files (software: MC_DataTool V2.6.15, MultiChannel Systems) for further import and analysis using MATLAB.

I.A.5. Electrical stimulation

Prior to every trial, the nervous response of the brain slice to electrical stimulation was tested, in order to check the functionality of the preparation but also to identify the general aspect of the waveform, for ulterior comparison with our US-induced signals. The electrical stimulations were performed using one of the 120 electrodes of the MEA as a stimulating electrodes. The stimulating electrode was chosen on the basis of its location in order to maximize the chances to trigger the response of a nervous fiber.

I.A.6. Ultrasound stimulation

The US stimulation system consisted of a custom-made focused transducer with resonant frequency of 1.78 MHz, as determined by impedance measurements with an impedance meter. Ultrasound waveforms were generated using a Tektronix TDS3014 function generator (GEN-45, Tektronix Inc., Beaverton, Oregon, USA) and were amplified (50 dB gain) using a Kalmus 150 RF amplifier (Amplifier Research Modular RF, Bothell, WA, USA). A 3D-printed, acrylonitrile butadiene styrene (ABS) cone filled with 0.2% agarose gel was used to couple and guide the generated ultrasound wave from the transducer to the extracellular medium contained in the MEA chip. The combination US-transducer + waveguide was carefully positioned inside the MEA chip in direct contact with the solution bathing the brain slice using a micromanipulator.

The ultrasound stimulus consisted of single US pulses, presenting a number of cycles per pulse (N_{cycles}) varying from 800 to 6200 (corresponding to a duty cycle (DT) ranging from 1 to 2%). Pulses were sent continuously for several seconds at a relatively low PRF of 4 Hz, which limits the possibilities of cumulative effect between pulses. Hence the US pulses were

considered as independent stimuli, rather than constitutive elements of a pulsed sequence.

I.A.7. Control experiments

After some trials of US exposures, brain slices were perfused with a sodium channel blocker Tetrodotoxin (TTX) to inhibit brain response, and submitted to US exposures again. These experiments served as negative controls, highlighting any signal unrelated to neural activity (electromagnetic or mechanical motion artifacts).

I.B. Results

I.B.1. Comparison of the neural model's response to electrical and ultrasound stimulation

Figure 70 presents examples of signals recorded from a mouse cortical preparation consequently to electrical stimulation or US exposure. It was possible to observe US-induced signals ($f = 1.78$ MHz, $N_{cycles} = 284$, $p = 0.75$ MPa) (**Figure 70.B**) sharing similar waveform characteristics (amplitude and duration of the depolarization) as the neural response to electrical stimulation (bipolar, ± 5 V, 4 stimulating electrodes) (**Figure 70.A**), which suggests to interpret these signals as US-induced neural responses rather than artifacts associated with the US exposure. This interpretation is reinforced by the fact that these US-induced signals were not consistent in time and space. Indeed, in some cases, no particular form of response to US exposures was observed on a given electrode, except for a relatively short artifact (**Figure 70.C**). In some other cases, consecutive US exposures will induce repeatedly signals recorded on a given electrodes, with variable but still similar waveforms characteristics (**Figure 70.D**).

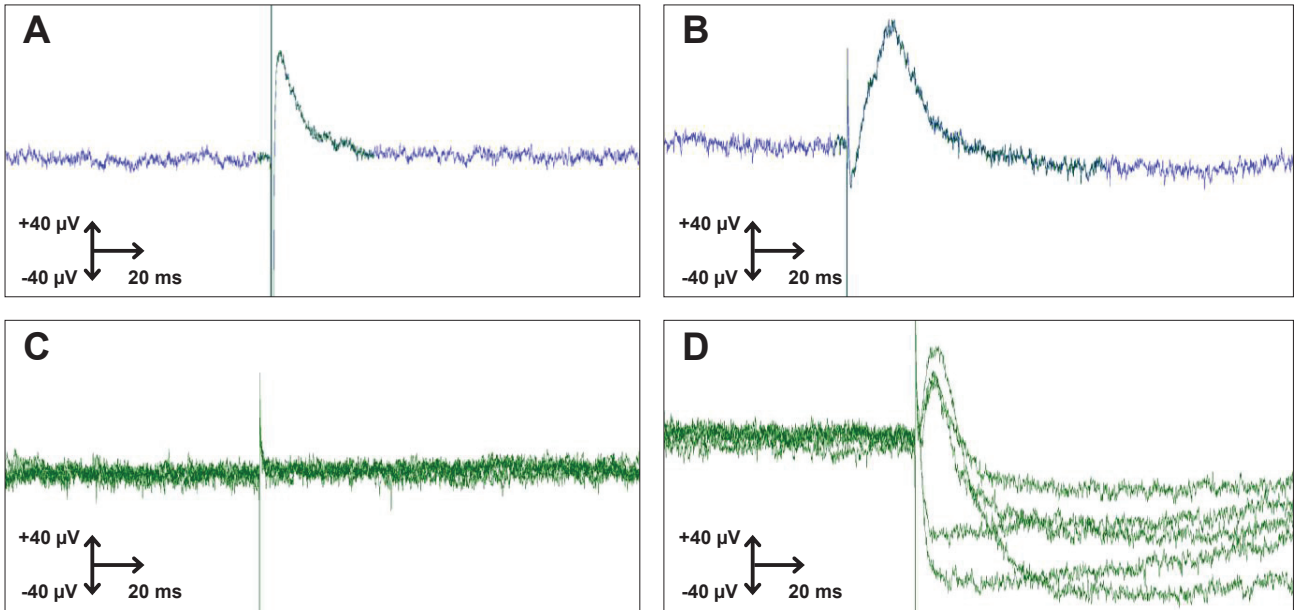


Figure 70 - Example of MEA-recorded neural response to electrical stimulation, from a mouse cortical preparation. (A) Neural response to electrical stimulation (bipolar, ± 5 V, 4 stimulating electrodes). (B) Neural response to US stimulation ($f = 1.78$ MHz, $N_{cycles} = 284$, $PRF = 1$ Hz, $N_{pulses} = 100$, $p = 0.75$ MPa). (C) Superposition of 5 consecutive signals showing no response to US exposure. (D) Superposition of 5 consecutive neural responses to 5 consecutive US exposures.

I.B.2. Spatial distribution of the US-induced neural responses

Figure 71 presents the distribution of raw signals recorded by the entire MEA chip, following an US exposure ($f = 1.78$ MHz, $N_{cycles} = 8900$, $p = 0.75$ MPa) of a mouse cortical preparation. Every electrode of the grid has recorded simultaneously a sharp negative slot, lasting for 5 ms. The duration of this signal component is equal to the duration of the US pulse used as a stimulus in this trial, suggesting to interpret it as an US-associated artifact. However, only some electrodes of the grid, gathered in localized and continuous groups, have recorded a relatively slow positive depolarization similar to the US-induced waveform mentioned in the previous section. Moreover, these signal components present a certain variability in their waveform characteristics, in particular with amplitude ranging from some μ V to more than 150 μ V. These observations (spatial regrouping and variability of the waveform characteristic) are additional arguments in favor of interpreting the above mentioned US-induced signals as US-

induced neuronal responses, rather than US-associated artifacts.

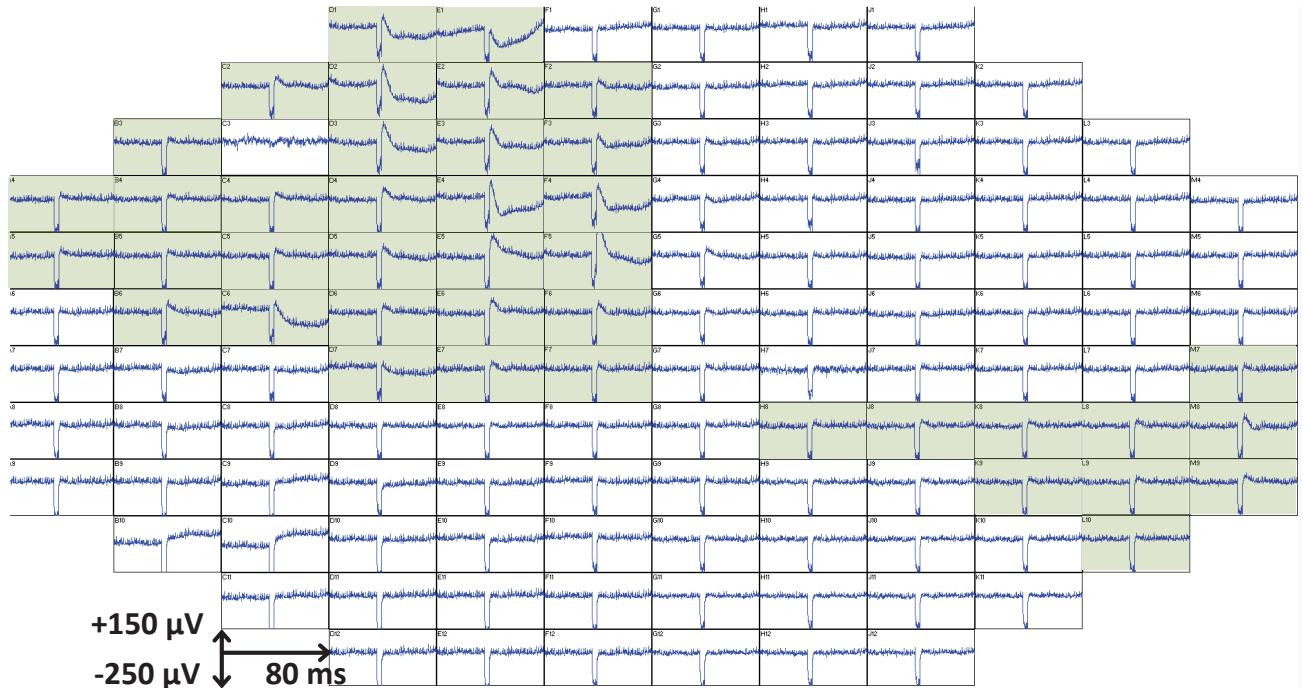


Figure 71 - Example of the matrix of signals recorded by the entire MEA chip following US exposure of a mouse cortical preparation ($f = 1.78$ MHz, $N_{cycles} = 8900$, $p = 0.75$ MPa).

I.B.3. US-induced MEA-recorded signal evolution as a function of pulse duration

Figure 72 presents the signal recorded by a given electrode consequently to US exposure, for different pulse durations (PD) ($N_{cycles} = 800 - 6200$ ie $PD = 0.45 - 3.48$ ms). The vertical purple line represents the start and duration of the US pulse administered to the slice. In order to reduce the SNR, individual US-pulse-induced MEA-recorded signals were averaged by group of 25.

In all cases, a sharp depolarization of the signal was observed which lasted approximately the duration of the US pulse. Following this depolarization, a sharp repolarization took place with evidently increasing amplitudes, as N_{cycles} was increased. The signal then appeared to gradually depolarize, reaching negative values before eventually

returning to baseline.

The measured amplitudes of the positive peak (repolarization) immediately following the end of the US pulse (after the vertical purple line) are summarized in **Table 4**, along with the duration of the response, which was defined as the time between the positive peak and the return to baseline following signal depolarization to negative potentials.

Table 4 – Average amplitude and signal duration of US-induced signals for different pulse durations, recorded from a mouse cortical slice ($f = 1.78$ MHz, $P_{ac} = 1.1$ MPa)

N_{cycles}	PD (ms)	Average amplitude (μV)	Signal duration (ms)
800	0.45	19	16
1600	0.90	34	33
3200	1.80	100	50
4200	2.36	109	50
5200	2.92	130	50
6200	3.48	125	55

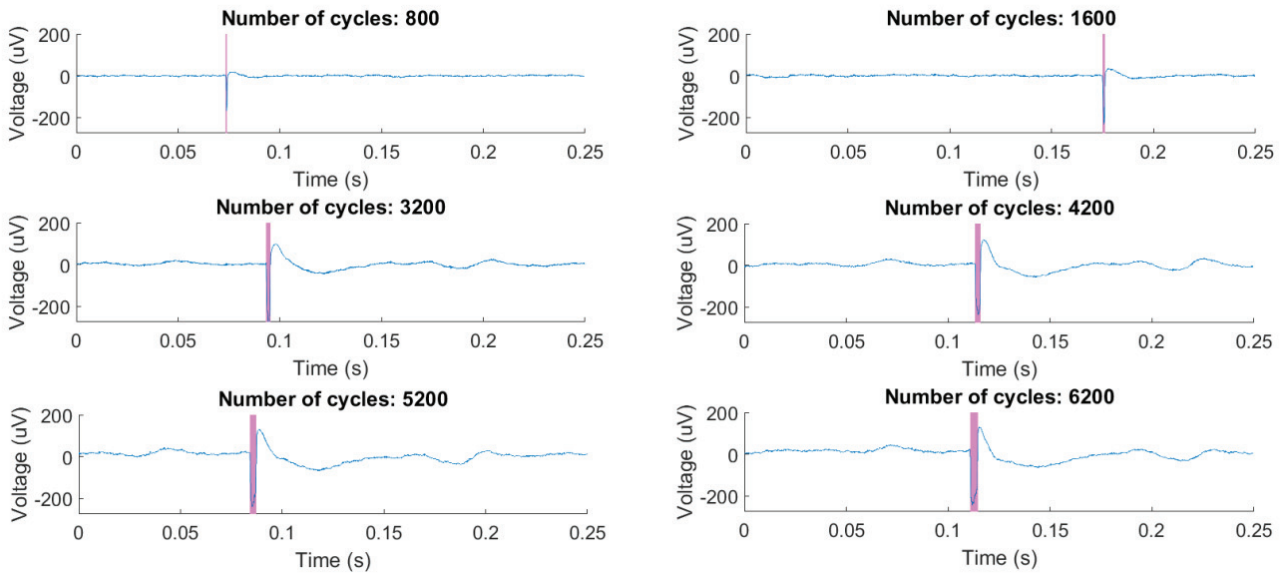


Figure 72 - Averaged US-induced signals with 1.78 MHz focused transducer for varying number of cycles per pulse ($N_{cycles} = 800 - 6200$ ie $PD = 0.45 - 3.48$ ms). The vertical purple line marks the US onset period.

I.B.4. Influence of the introduction of a channel-blocker in the medium on the waveform characteristic of the signal

As previously described in a functional brain slice (before TTX), the recorded MEA signal included a strong repolarization immediately after the end of the US pulse, followed by a gradual depolarization to negative values and a subsequent return to baseline.

Ten minutes after changing the brain perfusion solution from aCSF to TTX, the repolarization (peak positive signal) was still visible during US exposures but had decreased by 80% in magnitude (**Figure 73**). In addition, the originally observed gradual depolarization to negative values had disappeared.

Approximately 12 minutes after the introduction of TTX in the brain environment, the repolarization itself had almost disappeared during US exposures (85% decrease). Comparative measurements of signal durations were not possible after addition of TTX due to the rapid elimination of the depolarization signals. The effect of the TTX on the measured amplitudes of the repolarization signals, and on the duration of the response was summarized in **Table 5**.

Table 5 – Average amplitude and signal duration of US-induced signals recorded from a mouse cortical slice, recorded before and 10 and 12 minutes after starting perfusing the slice with TTX
 ($f = 1.78$ MHz, $N_{cycles} = 6200$ ie $PD = 3.48$ ms, $P_{ac} = 1.1$ MPa)

Phase	Average amplitude (μV)	Signal duration (ms)
Before TTX introduction	125	55
10 mn into TTX perfusion	24	N/A
12 min into TTX perfusion	19	N/A

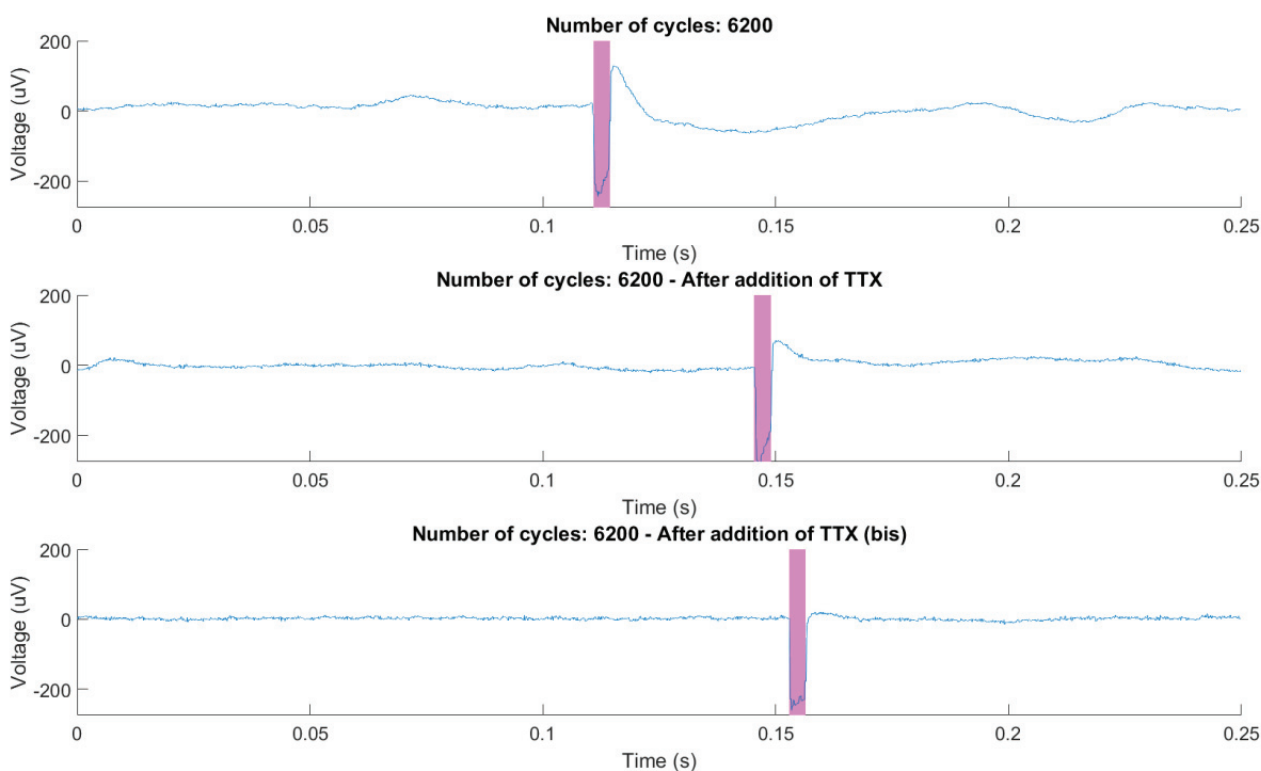


Figure 73 - Influence of TTX perfusion with time on the averaged signal induced by a single US pulse ($f = 1.78$ MHz, $P_{ac} = 1.1$ MPa, $N_{cycles} = 6200$): before starting TTX perfusion (top frame), after 10 mn of TTX perfusion (middle frame) and after 12 mn of TTX perfusion (bottom frame). The vertical purple line marks the US onset period.

I.C. Discussion

The exposition of mouse cortical preparation to various forms of US pulses ($f = 1.78$ MHz) has led to the triggering of MEA-recorded signals assimilable to neural responses. This interpretation is based on the comparison of the waveform characteristics of these US-induced signals with those of electrically induced nervous responses from the same neural preparation. The waveform characteristics are also consistent with those reported by previous groups (Muratore et al., 2012; Moore et al., 2015). The spatial localization of the recorded signals on the MEA grid and the variability of their waveform characteristics (in both time and space) are additional arguments in favor of interpreting these US-induced signals as US-induced neuronal responses, rather than mere US-associated artifacts.

Complementary, two studies were led to investigate the nature of these observed US-induced neural signals. In the first one, the magnitude of the repolarization of the signal was shown to first increase when increasing the pulse duration from 800 to 3200 cycles, but then stayed constant when further increasing US pulse duration from 3200 to 6400 cycles. In the second one, the use, as a negative control, of a sodium channel blocker (TTX) to inhibit the generation of electrical activity in the brain slice during US exposures, allowed confirming that the first observed negative peak was an artifact purely generated by the US exposure (timing and duration matched exactly the ultrasound pulse). In parallel, the magnitude of the repolarization progressively decreased with time, suggesting that the observed signal corresponded to actual neural responses.

II. Refinement of the experimental protocol and further investigations

II.A. Methods

On the basis of the outcomes and practical experience acquired from the first experimental campaign, described in the previous section, several refinements were brought to the experimental protocol. The goal for these modifications was either to improve the quality of

the MEA-recorded signal, or to increase the probability of generating US-induced nervous responses.

II.A.1. Improvement of the quality of the MEA-recorded signal

- A 3D MEA chip was used (60-3DMEA200/12/50iR-Ti, MultiChannel Systems, Reutlingen, Germany), designed to record signals from inner cell layers (60 electrodes, 200 μm spaced, 50 μm high).
- In order to reduce the movement artifact caused by the acoustic radiation force, another model of weighed grid was used, with a finer mesh (**Figure 74**).
- Instead of averaging the signal, a 2nd order high-pass Bessel filter (cutoff frequency: 100 Hz) was applied to suppress the movement artifact (Chen et al., 2017).
- In order reduce the electromagnetic artifacts, the different metallic elements of the set-up (micromanipulator, MEA platform, transducer) were connected using a system of chassis ground.

II.A.2. Acoustic parameters

In this second experimental campaign, the same US transducing system as before was used ($f = 1.78$ MHz). Relatively long single US pulses ($N_{cycles} = 8900$ cycles *ie* $PD = 5$ ms) were tested, as well as bursts of US pulses closer to those which successfully trigger nervous responses in the invertebrate model presented in the previous chapters. These US bursts ($N_{pulses} = 20$) were characterized by shorter pulses ($N_{cycles} = 284$ *ie* $PD = 160$ μs), with a pulse repetition frequency ($PRF = 62.5$ Hz) leading to the a relatively low duty cycle ($DT = 1\%$).

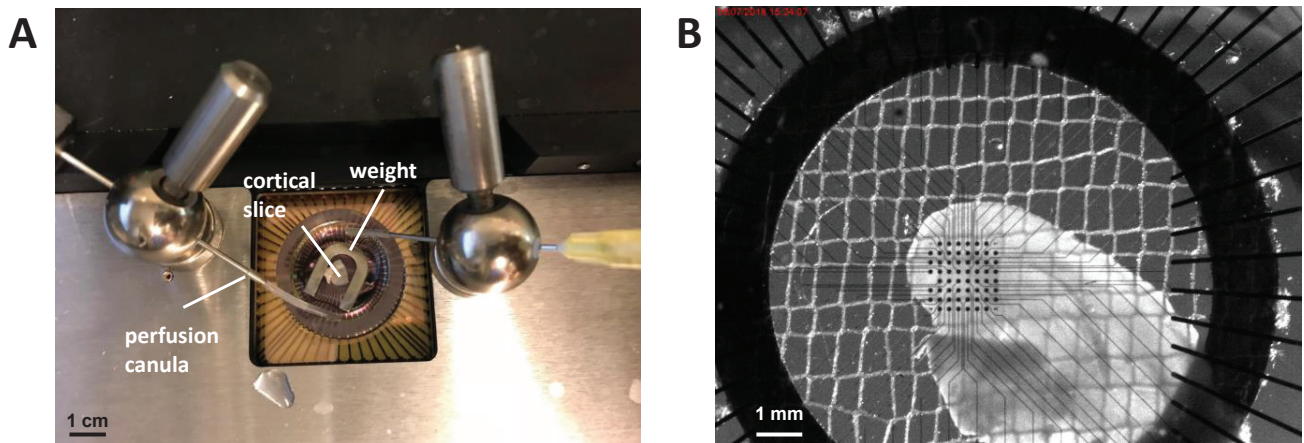


Figure 74 - Mouse cortical slice placed in the aCSF-perfused petri dish, in the refined experimental set-up: (A) microscopic view from under the MEA chip and (B) macroscopic view from above the MEA chip. The refined experimental set-up includes a 3D-mea chip and a more effective weighted grid.

II.B. Results

II.B.1. Waveforms characteristics of the US-pulse-induced signal with the refined recording protocol

An example of signal recorded by one of the MEA electrode in response to a relatively long single US pulse ($f = 1.78$ MHz, $N_{cycles} = 8900$ ie $PD = 5$ ms) is shown in **Figure 75**, without and with filtering. The reduction of the movement artefact allows for the identification of two components of the response in the filtered signal. A relatively fast component starts a few hundreds of microseconds after the stimulus onset, lasts for about 3 ms and is compound of sharp depolarization follow by a sharp repolarization, leading to a total amplitude of about 120 μ V. A relatively slow depolarizing response occurs about 4 ms after the stimulus onset, lasts for about 8 ms and presents an amplitude of about 120 μ V. The amplitude of this slow component is comparable to the amplitude of the responses to the longest US pulses tested during the first experimental campaign (cf. **Table 4**).

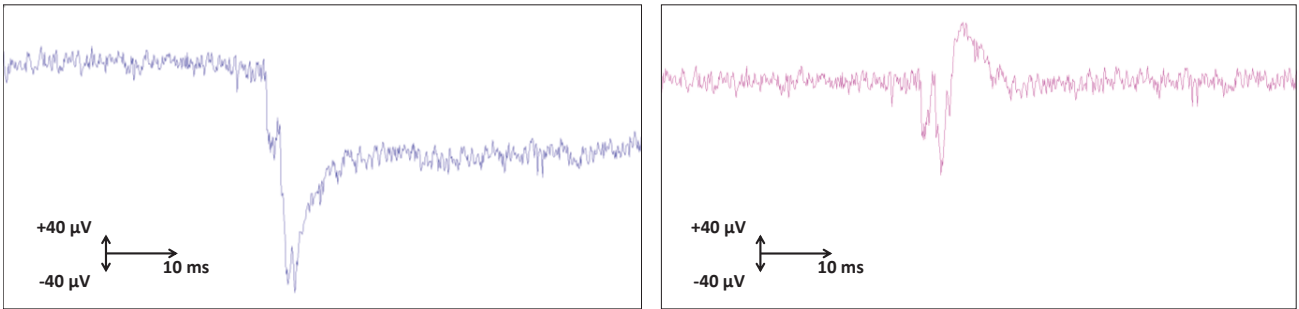


Figure 75 - Example of signal recorded by one of the MEA electrode in response to a relatively long single US pulse ($f = 1.78$ MHz, $N_{cycles} = 8900$ ie $PD = 5$ ms), without artifact filtering (left frame) and after applying a 2nd order high-pass Bessel filter.

II.B.2. Nervous response to a train of US pulses

An example of the matrix of signals recorded by the entire MEA chip following the exposure of a brain slice to a burst of US pulses ($f = 1.78$ MHz, $N_{pulses} = 20$, $N_{cycles} = 284$ ie $PD = 160$ μ s) is shown in **Figure 76** (signals are filtered as previously described). Electrode 62 and 63 were switched off for a previous electrical neurostimulation, and were kept that way through the trial, hence the large level of noised observed in the signals recorded by these particular electrodes. Most electrodes of the MEA did not record any substantial variation of the local electrical potential. Three electrodes in particular (E41, E51 and E54) recorded a train of periodic signals. The number and period of these signal are those of the burst of US pulses (PRF = 62.5 Hz), suggesting us to associate each individual signal to a given US pulse stimulus. As can be seen in **Figure 77**, which presents a closer view of the train of signals recorded by the electrodes of interest, each individual signal is compound of a fast component immediately followed by a slow component, whose amplitudes varies from one signal to another. It can be noticed that, in E41 and E51, the slow component presents the same duration (8 ms) and an amplitude of the same order of magnitude as the slow components of the signals previously recorded in response to a relatively long US pulse (cf. II.B.1). The fast components of the signals last for about 2 ms, and their amplitude is greatly varying from one signal to another.

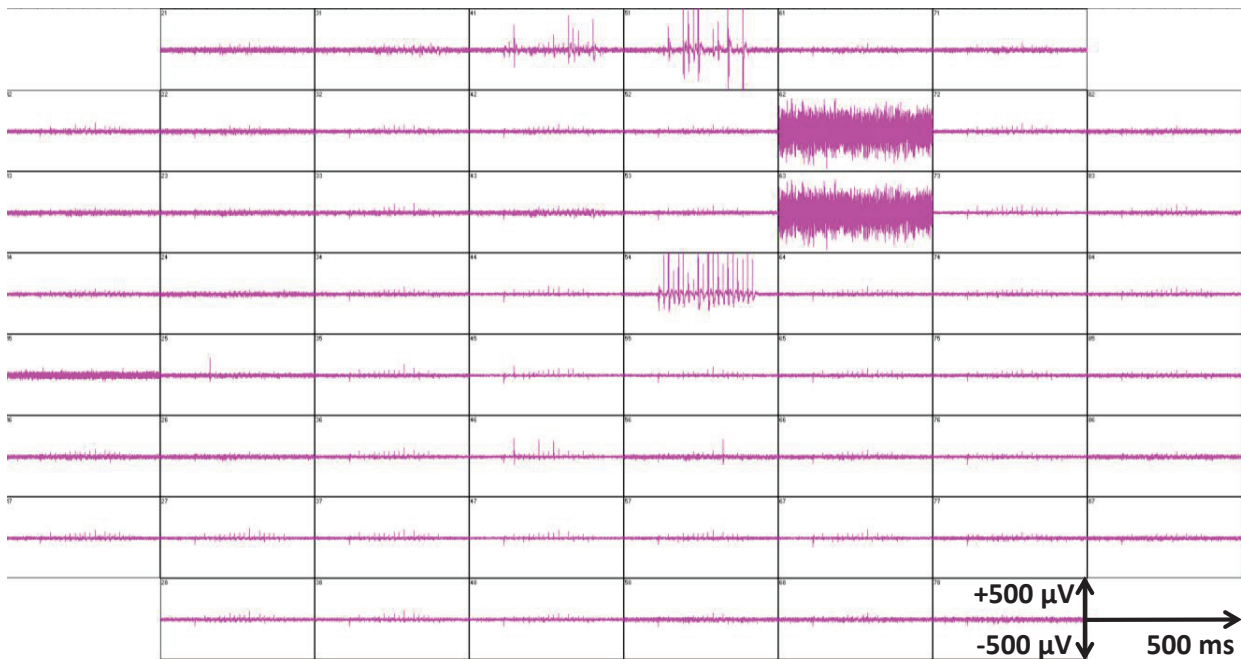


Figure 76 - Example of the matrix of signals recorded by the entire MEA chip following the exposure of a brain slice to a burst of US pulses ($f = 1.78$ MHz, $N_{pulses} = 20$, $N_{cycles} = 284$ ie $PD = 160$ μ s). The large level of noised observed in the signals recorded by E62 and E63 are du to these electrodes having been switched off for a previous electrical neurostimulation and kept that way through the trial. It can be noticed that three electrodes in particular (E41, E51 and E54) recorded a train of periodic signals.

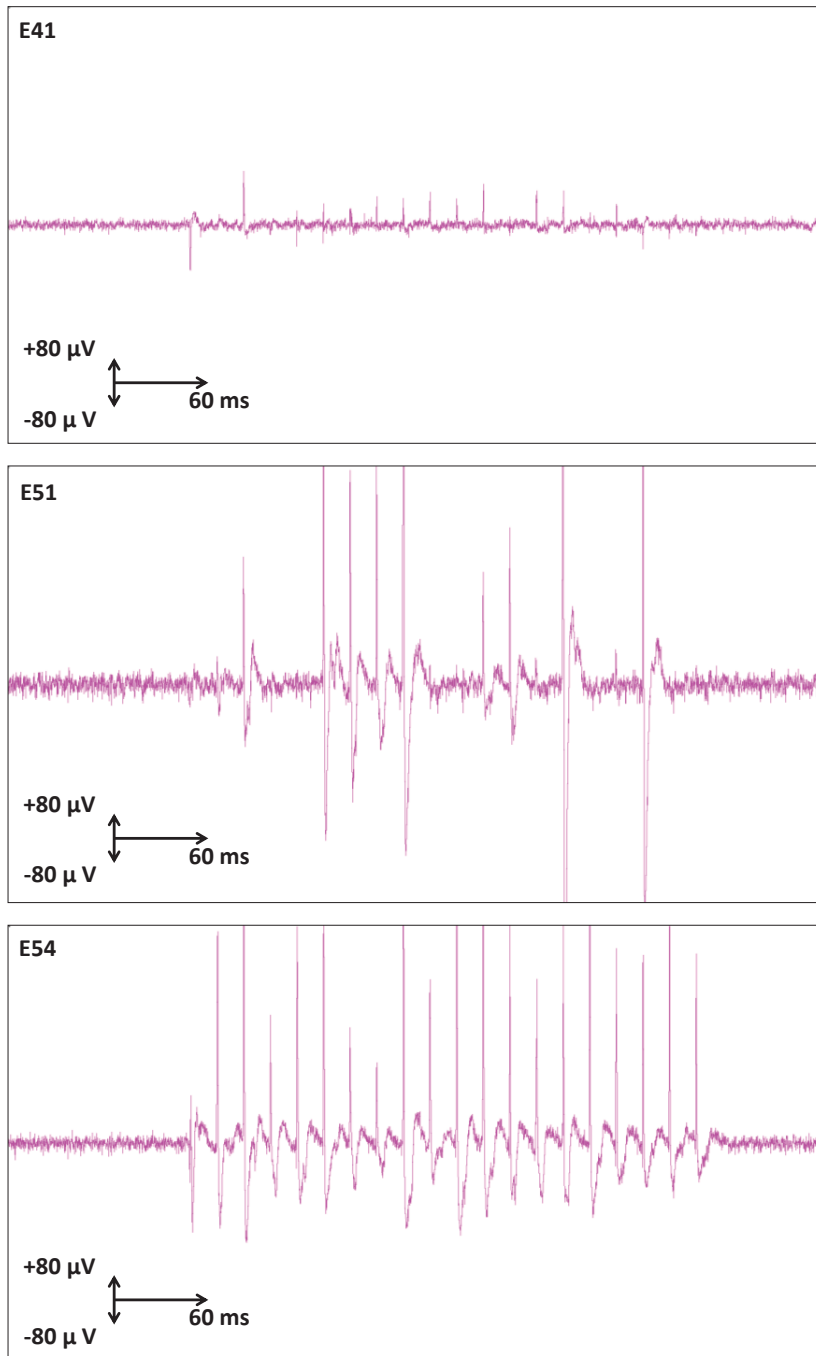


Figure 77 - Focus on the signals recorded by 3 electrodes of interest from **Figure 76** (E41, E51 and E54), following the exposure to a burst of US pulses ($f = 1.78$ MHz, $PD = 160$ μ s, $PRF = 62.5$ Hz, $P_{ac} = 1.1$ MPa). The number and period of these signals are those of the burst of US pulses ($PRF = 62.5$ Hz), suggesting us to associate each individual signal to a given US pulse stimulus. Furthermore, it can be noticed that each individual signal is compound of a fast component and a slow component, whose amplitude varies from one individual signal to another.

II.C. Discussion

The refinements brought to the experimental protocol have enabled the visualization of a fast component in the US-induced MEA-recorded signal, in addition to the relatively slow component already identified with the previous experimental protocol. Several elements suggest us to interpret these fast and slow components as part of one and the same US-induced Action Potential (AP).

Firstly, the fact that the waveforms recorded by the MEA have the same characteristics, whether they are consequent to a single long US pulse or a burst of shorter US pulses, discourages us to interpret them as mere US-associated artifacts.

Secondly, the fact that these waveforms appeared on isolated electrodes, and not systematically after every stimulus, is another argument in favor of their considering as neuronal responses. Indeed, considering the size of the focal spot, if these waveforms were signal artifacts generated by acoustic radiation force, they would be observable on group of contiguous electrodes and not only on one isolated electrode.

Finally, the comparison of the waveforms observed in this study with those presented in the literature as neural responses is a further argument supporting our interpretation. **Figure 78** shows single-unit recordings from mouse sciatic nerve filament, displaying electrically evoked APs presenting similar temporal characteristics with those of our recordings in mouse brain (Chen et al., 2017). **Figure 79** shows MEA recordings from rat neuron cultures, displaying spontaneously fired signals whose waveform are interpreted by the author as action potentials (Tateno and Nishikawa, 2014). These waveforms share similar amplitude and durations with those measured in our own MEA recordings.

Hence, on the basis of all the elements presented, we can conclude that the signals triggered by both long individual US pulses and bursts of shorter US pulses correspond to nervous responses. These nervous responses are compounded of fast and slow components, which seem to the characteristic phases of depolarization, repolarization and hyperpolarization of APs. The varying amplitude of the APs, from one response to another, within a given US-

burst-induced burst of responses, could translate the varying level of fiber recruitment associated with each US pulse of the stimulus.

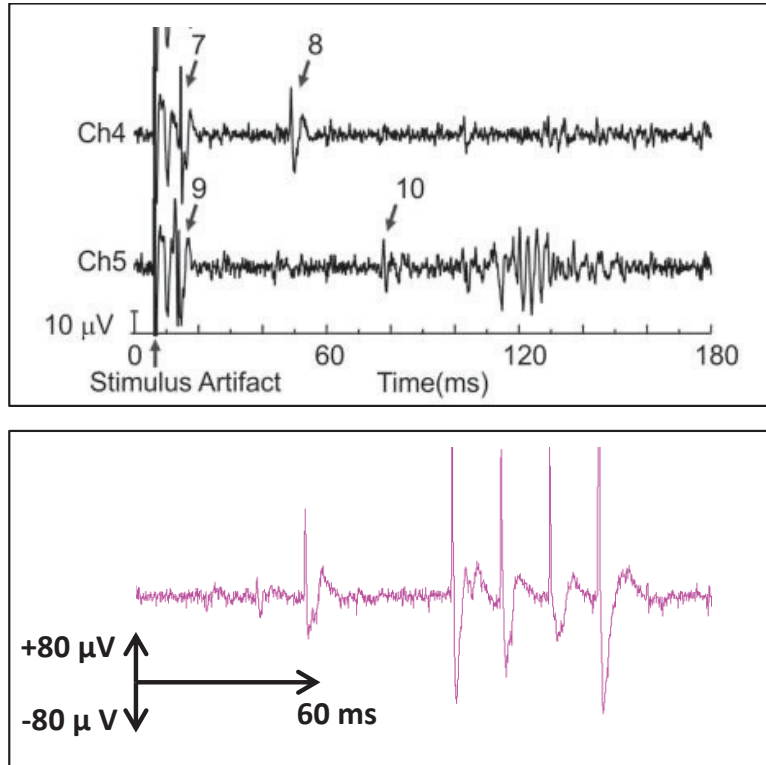


Figure 78 - Single-unit recordings from mouse sciatic nerve filament (top frame, courtesy of Chen et al. 2017), displaying electrically evoked APs presenting similar temporal characteristics to the recordings from mouse cortical slices following US exposure (bottom frame).

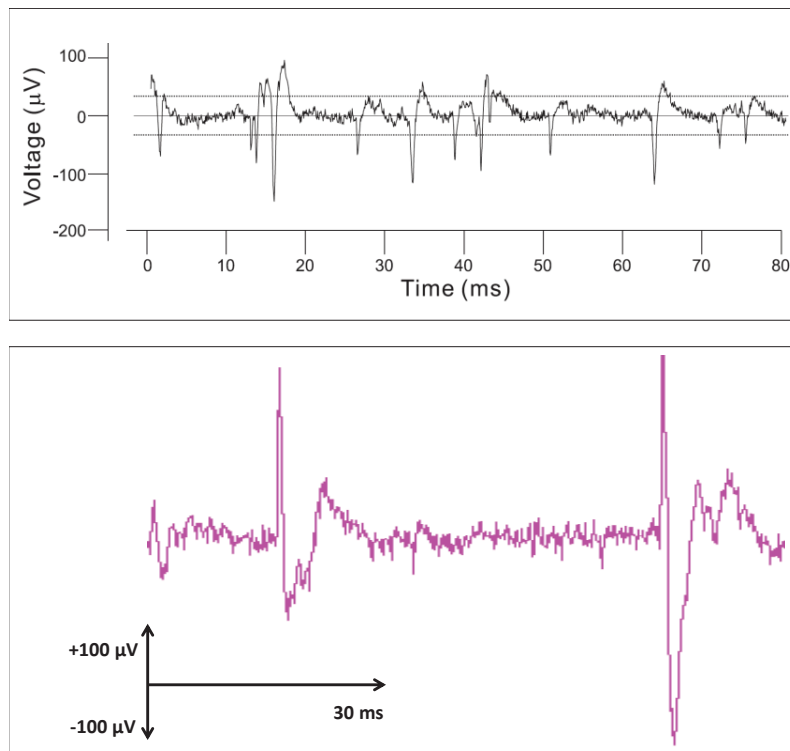


Figure 79 - MEA recordings from rat neuron cultures, displaying spontaneously fired signals whose waveform (top frame, courtesy of Tateno 2014), interpreted by the author action potentials, sharing similar amplitude and durations with those of the recordings from mouse cortical slices following US exposure (bottom frame).

Conclusion

A new experimental protocol was designed in order to study the phenomenon of ultrasound neurostimulation on an *ex vivo* vertebrate nervous model. Electrophysiological recordings from mouse cortical slices were performed using a MicroElectrode Array (MEA) system. Ultrasound exposure, delivered by custom-made piezoelectric transducers with a central frequency of 1.78 MHz, consisted in either relatively long pulses or bursts of shorter pulses, similar to those used in our previous study on the earthworm nervous model. After preliminary trials, several refinements were brought to the experimental protocol, namely to eliminate the artifact component from the waveform due to the movement of the slice induced by acoustic radiation force. In these conditions, it was possible to observe, on the recordings of isolated electrodes in the dendrite gyrus area, the generation of waveforms consequently to

both types of US exposures. The waveforms were compound of a rapid component and a slower one that were interpreted as the different phases associated with an AP, by comparing them with literature on similar electrophysiological studies. Hence, it was concluded that the proposed experimental protocol can allow for the successful generation and recording of nervous responses from an *ex vivo* mouse cortical model.

Further validations will be sought to confirm these first proofs of feasibility, particularly by producing various control experiments. The next steps will consist in identifying ‘activation thresholds’ of the response, optimizing the neurostimulation success rate, and finally starting to perform the same parametric studies as those described in the previous chapter for the invertebrate nervous model. If those first results were confirmed, this methodology will allow for directly comparing different stimulation techniques on neuronal model whose circuit architecture is well known in the field of electrophysiology.

General conclusion

Neurostimulation technics such as Deep Brain Stimulation or Transcranial Magnetic Stimulation have been successfully applied to the treatment of various neurological diseases, including motor disorders, sensory disabilities, chronic pain and epilepsy. Nevertheless, these technics are not optimal, as each of them presents its own limitations, either in terms of invasiveness, spatial resolution or access to deep tissues. Hence, there is great interest in investigating alternative procedure for therapeutic neurostimulation. Focused ultrasound is considered to be a promising tool to modulate or stimulate the nervous system, in a noninvasive and spatiotemporally precise manner, as proven by numerous proofs of feasibility provided at the preclinical level. To translate these findings into effective clinical applications, it is necessary to understand clearly the biomechanisms underlying the phenomenon of ultrasound (US) neurostimulation, and to clearly control the causality between parameters of the stimulation and characteristics of the nervous response, which is not the case yet.

In the present work, the ventral nerve cord of the common earthworm (*Lumbricus terrestris*) was proposed as an *in vivo* nervous model of study for ultrasound neurostimulation. The feasibility of inducing nervous response with a relatively high success rate (>90%) using ultrasound bursts was demonstrated. The US-induced nervous responses were characterized by the generation of action potentials in the giant fibers – Medial Giant Fiber (MGF) and Lateral Giant Fibers (LGF) – of the ventral nerve cord consequently to US exposure. Thanks to a particular property of the synaptic connection between the afferent nerves and the giants fibers – two symmetrical synaptic strength gradients exist along MGF and LGF – it was deduced that the locus of interaction between the US beam and the nervous system was located on the afferent pathway, upstream the synaptic connection. Hence, relying on an indirect electrophysiological measurement, the proposed nervous model allows for studying the response of a nervous structure which would be difficult to record in *in vivo* conditions otherwise. This is made possible by the specificity of the giant axons, which are involved in the rapid escape reflex but not in conscious movements of the animal, which implies that they receive their input solely from the afferent pathway.

Throughout this work, we tried to apply critical thinking to each of our results. Hence,

just as we did not directly jump to conclude on the direct activation of giant fibers by the US bean, we also questioned whether we were effectively in presence of a true phenomenon of ultrasound neurostimulation of the afferent nerves. Indeed, from the start we were aware of the possibility of US to trigger nervous response of the animal through acoustic-force-radiation-mediated tactile stimulation. To disambiguate the actual cause of stimulation, we compared the temporal characteristics of the US-induced nervous responses with the nervous responses to mechanical stimulation and concluded that the mechanosensors were not the locus of initiation of the nervous response, or at least were not activated in the same way they are by a “natural” tactile stimulus.

At the end of this first experimental campaign, we had identified, by trial and error, a typical structure of US sequence leading to relatively high Neurostimulation Success Rates (NSR). Relying on this basis of highly efficient US sequences, we investigated the respective influence of a variety of acoustic parameters on the NSR. Several trends were highlighted, in particular the increase of the NSR with increasing values of pulse-averaged acoustic intensity (I_{sapa}), pulse duration (PD) and pulse repetition frequency (PRF). From those trends, we hypothesized that the nervous structure responding to the stimulus is sensitive to the ‘mean radiation force’ carried by this stimulus, whatever combination of parameters that lead to it. Additionally, we investigated a possible correlation between cavitation events and stimulating events, using different methodological approaches. Numerous counter-examples led us to conclude that the neither the occurrence of stable cavitation nor that of particularly high level of inertial cavitation was a necessary condition to the triggering of an US-induced nervous response.

Finally, we laid the ground for the next iteration of mechanistic investigation, by developing a new experimental protocol involving *in vivo* recording of mouse cortical slices using a MicroElectrode Array (MEA) system. US sequences sharing the same temporal structure as those successfully applied to the invertebrate model, but with substantially lower acoustic pressure levels, were tested on this more complex nervous model and their ability to trigger nervous activity in the gyrus dendrite was proven. Now that the feasibility of using this model to study ultrasound neurostimulation has been demonstrated, the same methodology as that employed for the invertebrate nervous model will be applied, relying mainly on studies of the impact of each individual acoustic parameter on the NSR. The third iteration of this long-

term mechanistic study of US neurostimulation, and will involve *in vivo* experimentation on bigger mammals, which nervous activity will be monitored by MRI-imaging.

If the field of US neurostimulation continues to develop, it will provide a new therapeutic modality to tackle the numerous affections which are the targets of current neurostimulation technics, such as chronic pain. In some cases, the properties of US will bring significant improvements to the pain alleviation approach, for the benefit of the patient quality of life, which has been reported to be as a major cause of concern especially in patients suffering from cancer-related pain. Furthermore, US neurostimulation could be a promising tool for the treatment and management of other health issues with a neurological basis, such as Alzheimer's disease and sensory disabilities.

Références

- Adey, W.R., 1951. The nervous system of the earthworm *Megascolex*. *Journal of Comparative Neurology* 94, 57–103.
- Agarwal, S.M., Shivakumar, V., Bose, A., Subramaniam, A., Nawani, H., Chhabra, H., Kalmady, S.V., Narayanaswamy, J.C., Venkatasubramanian, G., 2013. Transcranial Direct Current Stimulation in Schizophrenia. *Clin Psychopharmacol Neurosci* 11, 118–125. <https://doi.org/10.9758/cpn.2013.11.3.118>
- Alberts, W.W., Feinstein, B., Levin, G., Wright, E.W., 1966. Electrical stimulation of therapeutic targets in waking dyskinetic patients. *Electroencephalography and Clinical Neurophysiology* 20, 559–566. [https://doi.org/10.1016/0013-4694\(66\)90020-4](https://doi.org/10.1016/0013-4694(66)90020-4)
- Alonso, P., Cuadras, D., Gabriëls, L., Denys, D., Goodman, W., Greenberg, B.D., Jimenez-Ponce, F., Kuhn, J., Lenartz, D., Mallet, L., Nuttin, B., Real, E., Segalas, C., Schuurman, R., Tezenas du Montcel, S., Menchon, J.M., 2015. Deep Brain Stimulation for Obsessive-Compulsive Disorder: A Meta-Analysis of Treatment Outcome and Predictors of Response. *PLoS One* 10. <https://doi.org/10.1371/journal.pone.0133591>
- Arul-Anandam, A.P., Loo, C., Sachdev, P., 2009. Transcranial direct current stimulation-what is the evidence for its efficacy and safety? *F1000 medicine reports* 1.
- Association, A.P., 2013. Diagnostic and statistical manual of mental disorders (DSM-5®). American Psychiatric Pub.
- Bagot, C.N., Arya, R., 2008. Virchow and his triad: a question of attribution. *British journal of haematology* 143, 180–190.
- Bailey, M.R., 1997. Control of acoustic cavitation with application to lithotripsy. *The Journal of the Acoustical Society of America* 102, 1250–1250.
- Bailey, M.R., Blackstock, D.T., Cleveland, R.O., Crum, L.A., 1999. Comparison of electrohydraulic lithotripters with rigid and pressure-release ellipsoidal reflectors. II. Cavitation fields. *The Journal of the Acoustical Society of America* 106, 1149–1160.
- Ballantine, H.T., Bouckoms, A.J., Thomas, E.K., Giriunas, I.E., 1987. Treatment of psychiatric illness by stereotactic cingulotomy. *Biological Psychiatry* 22, 807–819.
- Bartholow, R., 1874. ART. I.—Experimental Investigations into the Functions of the Human Brain. *The American Journal of the Medical Sciences (1827-1924)* 305.
- Bechtereva, N.P., Bondartchuk, A.N., Smirnov, V.M., Meliutcheva, L.A., Shandurina, A.N., 1975. Method of Electrostimulation of the Deep Brain Structures in Treatment of Some Chronic Diseases. *SFN* 37, 136–140. <https://doi.org/10.1159/000102727>
- Beissner, K., 1987. Radiation force calculations. *Acta Acustica united with Acustica* 62, 255–263.
- Bejjani, B.-P., Damier, P., Arnulf, I., Thivard, L., Bonnet, A.-M., Dormont, D., Cornu, P., Pidoux, B., Samson, Y., Agid, Y., 1999. Transient Acute Depression Induced by High-Frequency Deep-Brain Stimulation. *New England Journal of Medicine* 340, 1476–1480. <https://doi.org/10.1056/NEJM199905133401905>
- Benabid, A.L., Pollak, P., Hoffmann, D., Gervason, C., Hommel, M., Perret, J.E., de Rougemont, J., Gao, D.M., 1991. Long-term suppression of tremor by chronic stimulation of the ventral intermediate thalamic nucleus. *The Lancet*, Originally published as Volume 1, Issue 8738 337, 403–406. [https://doi.org/10.1016/0140-6736\(91\)91175-T](https://doi.org/10.1016/0140-6736(91)91175-T)
- Benwell, C.S.Y., Learmonth, G., Miniussi, C., Harvey, M., Thut, G., 2015. Non-linear effects of

- transcranial direct current stimulation as a function of individual baseline performance: Evidence from biparietal tDCS influence on lateralized attention bias. *Cortex* 69, 152–165. <https://doi.org/10.1016/j.cortex.2015.05.007>
- Berk, L., 1995. Prospective trials for the radiotherapeutic treatment of bone metastases. *American Journal of Hospice and Palliative Medicine*® 12, 24–28.
- Berman, B.D., Starr, P.A., Marks Jr, W.J., Ostrem, J.L., 2009. Induction of bradykinesia with pallidal deep brain stimulation in patients with cranial-cervical dystonia. *Stereotactic and functional neurosurgery* 87, 37–44.
- Biri, H., Küpeli, B., İsenm.d., K., Sinik, Z., Karaoğlan, Ü., Bozkirli, I., 1999. Treatment of Lower Ureteral Stones: Extracorporeal Shockwave Lithotripsy or Intracorporeal Lithotripsy? *Journal of Endourology* 13, 77–81. <https://doi.org/10.1089/end.1999.13.77>
- Bittar, R.G., Otero, S., Carter, H., Aziz, T.Z., 2005. Deep brain stimulation for phantom limb pain. *Journal of Clinical Neuroscience* 12, 399–404.
- Blahak, C., Capelle, H.-H., Baezner, H., Kinfe, T.M., Hennerici, M.G., Krauss, J.K., 2011. Battery lifetime in pallidal deep brain stimulation for dystonia. *European Journal of Neurology* 18, 872–875. <https://doi.org/10.1111/j.1468-1331.2010.03290.x>
- Borrelli, M.J., Bailey, K.I., Dunn, F., 1981. Early ultrasonic effects upon mammalian CNS structures (chemical synapses). *The Journal of the Acoustical Society of America* 69, 1514–1516.
- Bruera, E.D., Portenoy, R.K., 2009. *Cancer pain: assessment and management*. Cambridge University Press.
- Bullock, T., 1948. Physiological mapping of giant nerve fiber systems in polychaete annelids. *Physiologia Comparata et Oecologia* 1, 1.
- Bullock, T., Horridge, G.A., 1965. Structure and function in the nervous systems of invertebrates.
- Bullock, T.H., 1984. Comparative Neuroethology of Startle, Rapid Escape, and Giant Fiber-Mediated Responses, in: Eaton, R.C. (Ed.), *Neural Mechanisms of Startle Behavior*. Springer US, Boston, MA, pp. 1–13. https://doi.org/10.1007/978-1-4899-2286-1_1
- Bullock, Theodore H., 1953. A contribution from the study of cords of lower forms, in: *Ciba Foundation Symposium-The Spinal Cord*. Wiley Online Library, pp. 3–13.
- Bullock, Theodore Holmes, 1953. Properties of some natural and quasi-artificial synapses in polychaetes. *Journal of Comparative Neurology* 98, 37–68.
- Bullock, T.H., 1945. Functional organization of the giant fiber system of *Lumbricus*. *Journal of Neurophysiology* 8, 55–71.
- Byrne, T.N., 1992. Spinal Cord Compression from Epidural Metastases. *New England Journal of Medicine* 327, 614–619. <https://doi.org/10.1056/NEJM199208273270907>
- Caraceni, A., Portenoy, R.K., 1999. An international survey of cancer pain characteristics and syndromes. *PAIN* 82, 263–274. [https://doi.org/10.1016/S0304-3959\(99\)00073-1](https://doi.org/10.1016/S0304-3959(99)00073-1)
- Carr, D.B., Goudas, L.C., 1999. Acute pain. *The Lancet* 353, 2051–2058.
- Cathignol, D., Mestas, J.L., Gomez, F., Lenz, P., 1991. Influence of water conductivity on the efficiency and the reproducibility of electrohydraulic shock wave generation. *Ultrasound in Medicine & Biology* 17, 819–828. [https://doi.org/10.1016/0301-5629\(91\)90165-S](https://doi.org/10.1016/0301-5629(91)90165-S)
- Cathignol, E., Tavakkoli, J., Birer, A., Arefiev, A., 1998. Comparison between the effects of cavitation induced by two different pressure-time shock waveform pulses. *IEEE transactions on ultrasonics, ferroelectrics, and frequency control* 45, 788–799.
- Chaussy, C., Schmiedt, E., 1984. Extracorporeal shock wave lithotripsy (ESWL) for kidney stones. An alternative to surgery? *Urol Radiol* 6, 80–87. <https://doi.org/10.1007/BF02923707>
- Chaussy, C.H., Brendel, W., Schmiedt, E., 1980. Extracorporeally induced destruction of kidney stones by shock waves. *The Lancet* 316, 1265–1268.

- Chavrier, F., Chapelon, J.Y., Gelet, A., Cathignol, D., 2000. Modeling of high-intensity focused ultrasound-induced lesions in the presence of cavitation bubbles. *The Journal of the Acoustical Society of America* 108, 432–440.
- Chen, L., Ilham, S.J., Guo, T., Emadi, S., Feng, B., 2017. In vitro multichannel single-unit recordings of action potentials from the mouse sciatic nerve. *Biomed. Phys. Eng. Express* 3, 045020. <https://doi.org/10.1088/2057-1976/aa7efa>
- Chiang, A., Zeng, L., Zhang, L., Lochray, F., Korol, R., Loblaw, A., Chow, E., Sahgal, A., 2013. Pain flare is a common adverse event in steroid-naive patients after spine stereotactic body radiation therapy: a prospective clinical trial. *International Journal of Radiation Oncology* Biology* Physics* 86, 638–642.
- Chua, K.S., Reddy, S.K., Lee, M.-C., Patt, R.B., 1999. Pain and loss of function in head and neck cancer survivors. *Journal of pain and symptom management* 18, 193–202.
- Church, C.C., 1989. A theoretical study of cavitation generated by an extracorporeal shock wave lithotripter. *The Journal of the Acoustical Society of America* 86, 215–227.
- Cif, L., El Fertit, H., Vayssiere, N., Hemm, S., 2003. Treatment of dystonic syndromes by chronic electrical stimulation of the internal globus pallidus. *Journal of neurosurgical sciences* 47, 52.
- Clarke, R.H., 1908. THE STRUCTURE AND FUNCTIONS OF THE CEREBELLUM EXAMINED BY A NEW METHOD. By SIR VICTOR HORSLEY, FRS, FRCS, AND. *Brain: A Journal of Neurology* 45.
- Cleveland, R.O., Sapozhnikov, O.A., Bailey, M.R., Crum, L.A., 2000. A dual passive cavitation detector for localized detection of lithotripsy-induced cavitation in vitro. *The Journal of the Acoustical Society of America* 107, 1745–1758.
- Cobbold, R.S., 2006. *Foundations of biomedical ultrasound*. Oxford University Press.
- Coleman, A.J., Saunders, J.E., Crum, L.A., Dyson, M., 1987. Acoustic cavitation generated by an extracorporeal shockwave lithotripter. *Ultrasound in medicine and biology* 13, 69–76.
- Cook, A.W., 1976. Electrical stimulation in multiple sclerosis. *Hospital practice* 11, 51–58.
- Cook, I.J., Kahrilas, P.J., 1999. AGA technical review on management of oropharyngeal dysphagia. *Gastroenterology* 116, 455–478.
- Coonfield, B.R., 1932. The peripheral nervous system of earthworms. *Journal of Comparative Neurology* 55, 7–17. <https://doi.org/10.1002/cne.900550103>
- Cooper, Irving S., Amin, I., Riklan, M., Waltz, J.M., Poon, T.P., 1976. Chronic cerebellar stimulation in epilepsy: clinical and anatomical studies. *Archives of neurology* 33, 559–570.
- Cooper, I. S., Riklan, M., Amin, I., Waltz, J.M., Cullinan, T., 1976. Chronic cerebellar stimulation in cerebral palsy. *Neurology* 26, 744–744.
- Cornu, C., Guédra, M., Béra, J.-C., Liu, H.-L., Chen, W.-S., Inserra, C., 2018. Ultrafast monitoring and control of subharmonic emissions of an unseeded bubble cloud during pulsed sonication. *Ultrasonics sonochemistry* 42, 697–703.
- Coubes, P., Cif, L., El Fertit, H., Hemm, S., Vayssiere, N., Serrat, S., Picot, M.C., Tuffery, S., Claustres, M., Echenne, B., 2004. Electrical stimulation of the globus pallidus internus in patients with primary generalized dystonia: long-term results. *Journal of neurosurgery* 101, 189–194.
- Crum, L.A., 1988. Cavitation microjets as a contributory mechanism for renal calculi disintegration in ESWL. *The Journal of urology* 140, 1587–1590.
- Curie, J., Curie, P., 1881. Contractions et dilatations produites par des tensions électriques dans les cristaux hémihédres à faces inclinées. *Compt. Rend* 93, 1137–1140.
- Curie, J., Curie, P., 1880. Développement par compression de l'électricité polaire dans les cristaux hémihédres à faces inclinées. *Bulletin de minéralogie* 3, 90–93.
- Damianou, C., Hynynen, K., 1993. Focal spacing and near-field heating during pulsed high temperature

- ultrasound therapy. *Ultrasound in medicine & biology* 19, 777–787.
- Darwin, C., 1892. *The formation of vegetable mould through the action of worms: with observations on their habits.* Appleton.
- DaSilva, A.F., Truong, D.Q., DosSantos, M.F., Toback, R.L., Datta, A., Bikson, M., 2015. State-of-art neuroanatomical target analysis of high-definition and conventional tDCS montages used for migraine and pain control. *Frontiers in neuroanatomy* 9, 89.
- Deffieux, T., Younan, Y., Wattiez, N., Tanter, M., Pouget, P., Aubry, J.-F., 2013. Low-Intensity Focused Ultrasound Modulates Monkey Visuomotor Behavior. *Current Biology* 23, 2430–2433. <https://doi.org/10.1016/j.cub.2013.10.029>
- Degertekin, F.L., Guldiken, R.O., Karaman, M., 2006. Annular-ring CMUT arrays for forward-looking IVUS: Transducer characterization and imaging. *IEEE transactions on ultrasonics, ferroelectrics, and frequency control* 53, 474–482.
- Delalande, A., Kotopoulis, S., Rovers, T., Pichon, C., Postema, M., 2011. Sonoporation at a low mechanical index. *Bubble Science, Engineering & Technology* 3, 3–12.
- Delanian, S., Lefaix, J.-L., Pradat, P.-F., 2012. Radiation-induced neuropathy in cancer survivors. *Radiotherapy and Oncology* 105, 273–282.
- Denstedt, J.D., Clayman, R.V., 1990. Electrohydraulic Lithotripsy of Renal and Ureteral Calculi. *The Journal of Urology* 143, 13–17. [https://doi.org/10.1016/S0022-5347\(17\)39850-6](https://doi.org/10.1016/S0022-5347(17)39850-6)
- Denstedt, J.D., Eberwein, P.M., Singh, R.R., 1992. The Swiss Lithoclast: A New Device for Intracorporeal Lithotripsy. *The Journal of Urology* 148, 1088–1090. [https://doi.org/10.1016/S0022-5347\(17\)36827-1](https://doi.org/10.1016/S0022-5347(17)36827-1)
- Denys, D., 2006. Pharmacotherapy of obsessive-compulsive disorder and obsessive-compulsive spectrum disorders. *The Psychiatric clinics of North America* 29, 553–84.
- Desjoux, C., Fouqueray, M., Lo, C.W., Muleki Seya, P., Lee, J.L., Bera, J.C., Chen, W.S., Inserra, C., 2015. Counterbalancing the use of ultrasound contrast agents by a cavitation-regulated system. *Ultrasonics Sonochemistry* 26, 163–168. <https://doi.org/10.1016/j.ultsonch.2014.12.017>
- Deuschl, G., Raethjen, J., Hellriegel, H., Elble, R., 2011. Treatment of patients with essential tremor. *The Lancet Neurology* 10, 148–161. [https://doi.org/10.1016/S1474-4422\(10\)70322-7](https://doi.org/10.1016/S1474-4422(10)70322-7)
- Dogu, O., Sevim, S., Camdeviren, H., Sasmaz, T., Bugdayci, R., Aral, M., Kaleagasi, H., Un, S., Louis, E.D., 2003. Prevalence of essential tremor door-to-door neurologic exams in Mersin Province, Turkey. *Neurology* 61, 1804–1806.
- Dooley, D.M., Kasprak, M., Stibitz, M., 1976. Electrical stimulation of the spinal cord in patients with demyelinating and degenerative diseases of the central nervous system. *The Journal of the Florida Medical Association* 63, 906–909.
- Drewes, C.D., 1984. Escape reflexes in earthworms and other annelids, in: *Neural Mechanisms of Startle Behavior.* Springer, pp. 43–91.
- Drewes, C.D., Landa, K.B., McFall, J.L., 1978. Giant nerve fibre activity in intact, freely moving earthworms. *Journal of Experimental Biology* 72, 217–227.
- Drewes, C.D., McFall, J.L., 1980. Longitudinal variations in the efficacy of lateral giant fiber to giant motor neuron transmission in intact earthworms. *Comparative Biochemistry and Physiology Part A: Physiology* 66, 315–321.
- Eaton, R.C., 1984. *Neural Mechanisms of Startle Behavior.* Springer Science & Business Media.
- Edwards, C.A., Bohlen, P.J., 1996. *Biology and ecology of earthworms.* Springer Science & Business Media.
- Eisenmenger, W., 2001. The mechanisms of stone fragmentation in ESWL. *Ultrasound in medicine & biology* 27, 683–693.
- Eisenmenger, W., Du, X.X., Tang, C., Zhao, S., Wang, Y., Rong, F., Dai, D., Guan, M., Qi, A., 2002.

- The first clinical results of “wide-focus and low-pressure” ESWL. *Ultrasound in medicine & biology* 28, 769–774.
- El Maalouf, J., Béra, J.-C., Alberti, L., Cathignol, D., Mestas, J.-L., 2009. In vitro sonodynamic cytotoxicity in regulated cavitation conditions. *Ultrasonics* 49, 238–243.
- Elbaz, A., Carcaillon, L., Kab, S., Moisan, F., 2016. Epidemiology of Parkinson’s disease. *Revue Neurologique, Neuroepidemiology* 172, 14–26. <https://doi.org/10.1016/j.neurol.2015.09.012>
- Evan, A.P., Willis, L.R., McAteer, J.A., Bailey, M.R., Connors, B.A., Shao, Y., Lingeman, J.E., Williams Jr, J.C., Fineberg, N.S., Crum, L.A., 2002. Kidney damage and renal functional changes are minimized by waveform control that suppresses cavitation in shock wave lithotripsy. *The Journal of urology* 168, 1556–1562.
- Faber, D.S., Korn, H., 1978. *Neurobiology of the mauthner cell*. Raven Press.
- Fava, M., 2003. Diagnosis and definition of treatment-resistant depression. *Biological psychiatry* 53, 649–659.
- Favilla, C.G., Ullman, D., Wagle Shukla, A., Foote, K.D., Jacobson IV, C.E., Okun, M.S., 2012. Worsening essential tremor following deep brain stimulation: disease progression versus tolerance. *Brain* 135, 1455–1462.
- Fjield, T., Fan, X., Hynynen, K., 1996. A parametric study of the concentric-ring transducer design for MRI guided ultrasound surgery. *The Journal of the Acoustical Society of America* 100, 1220–1230.
- Flor, H., 2002. Phantom-limb pain: characteristics, causes, and treatment. *The Lancet Neurology* 1, 182–189. [https://doi.org/10.1016/S1474-4422\(02\)00074-1](https://doi.org/10.1016/S1474-4422(02)00074-1)
- Flourens, P., 1842. *Recherches expérimentales sur les propriétés et les fonctions du système nerveux dans les animaux vertébrés*. Ballière.
- Flynn, H.G., 1982. Generation of transient cavities in liquids by microsecond pulses of ultrasound. *The Journal of the Acoustical Society of America* 72, 1926–1932. <https://doi.org/10.1121/1.388622>
- Flynn, H.G., 1964. Physics of acoustic cavitation in liquids. *Physical acoustics* 1, 57–172.
- Follett, K.A., Weaver, F.M., Stern, M., Hur, K., Harris, C.L., Luo, P., Marks, W.J., Rothlind, J., Sagher, O., Moy, C., Pahwa, R., Burchiel, K., Hogarth, P., Lai, E.C., Duda, J.E., Holloway, K., Samii, A., Horn, S., Bronstein, J.M., Stoner, G., Starr, P.A., Simpson, R., Baltuch, G., De Salles, A., Huang, G.D., Reda, D.J., 2010. Pallidal versus Subthalamic Deep-Brain Stimulation for Parkinson’s Disease. *New England Journal of Medicine* 362, 2077–2091. <https://doi.org/10.1056/NEJMoa0907083>
- Fox, R., n.d. *Invertebrate Anatomy OnLine Lumbricus terrestris*\copyright.
- Franzini, A., Ferroli, P., Leone, M., Broggi, G., 2003. Stimulation of the Posterior Hypothalamus for Treatment of Chronic Intractable Cluster Headaches: First Reported Series. *Neurosurgery* 52, 1095–1101. <https://doi.org/10.1093/neurosurgery/52.5.1095>
- Fregni, F., Boggio, P.S., Nitsche, M.A., Marcolin, M.A., Rigonatti, S.P., Pascual-Leone, A., 2006. Treatment of major depression with transcranial direct current stimulation. *Bipolar disorders* 8, 203–204.
- Friedlander, B., 1894. Central nervous coordination of earthworm movement. *Pflugers Arch. ges. Physiol* 58, 168–207.
- Fritsch, G., 1870. Über die elektrische Erregbarkeit des Grosshirns. *Arch, anat. Physiol. Wiss. Med.* 37, 300–332.
- Fry, F.J., Ades, H.W., Fry, W.J., 1958. Production of Reversible Changes in the Central Nervous System by Ultrasound. *Science* 127, 83–84. <https://doi.org/10.1126/science.127.3289.83>
- Fry, W.J., Dunn, F., 1962. *Ultrasound: Analysis and experimental methods in biological research, in: Special Methods*. Elsevier, pp. 261–394.

- Fry, W.J., Wulff, V.J., Tucker, D., Fry, F.J., 1950. Physical factors involved in ultrasonically induced changes in living systems: I. Identification of non-temperature effects. *The Journal of the Acoustical Society of America* 22, 867–876.
- Galvani, L., Aldini, G., 1792. *De viribus electricitatis in motu musculari comentarius cum joannis aldini dissertatione et notis; accesserunt epistolae ad animalis electricitatis theoriam pertinentes.* Apud Societatem Typographicam.
- Gardner, A., Gardner, E., Morley, T., 2011. Cauda equina syndrome: a review of the current clinical and medico-legal position. *Eur Spine J* 20, 690–697. <https://doi.org/10.1007/s00586-010-1668-3>
- Gavrilov, L., V. Gersuni, G., B. Ilyinski, O., Tsirulnikov, E., Shchekanov, E., 1977. A study of reception with the use of focused ultrasound. I. Effects on the skin and deep receptor structures in man. *Brain research* 135, 265–77. [https://doi.org/10.1016/0006-8993\(77\)91030-7](https://doi.org/10.1016/0006-8993(77)91030-7)
- Gavrilov, L.R., 1984. Use of focused ultrasound for stimulation of nerve structures. *Ultrasonics* 22, 132–138. [https://doi.org/10.1016/0041-624X\(84\)90008-8](https://doi.org/10.1016/0041-624X(84)90008-8)
- Gavrilov, L.R., Tsirulnikov, E.M., 2012. Focused ultrasound as a tool to input sensory information to humans (Review). *Acoust. Phys.* 58, 1–21. <https://doi.org/10.1134/S1063771012010083>
- Gavrilov, L.R., Tsirulnikov, E.M., 1980. *Focused ultrasound in physiology and medicine.* Nauka, Leningrad.
- Gildenberg, P.L., 2005. Evolution of neuromodulation. *Stereotactic and functional neurosurgery* 83, 71–79.
- Gillespie, P.G., Walker, R.G., 2001. Molecular basis of mechanosensory transduction. *Nature* 413, 194.
- Gould, S.J., 1994. *Hen's Teeth and Horse's Toe: Further Reflections in Natural History.* Norton, New York.
- Gracewski, S.M., Dahake, G., Ding, Z., Burns, S.J., Everbach, E.C., 1993. Internal stress wave measurements in solids subjected to lithotripter pulses. *The Journal of the Acoustical Society of America* 94, 652–661.
- Greenberg, B.D., Price, L.H., Rauch, S.L., Friehs, G., Noren, G., Malone, D., Carpenter, L.L., Rezai, A.R., Rasmussen, S.A., 2003. Neurosurgery for intractable obsessive-compulsive disorder and depression: critical issues. *Neurosurgery Clinics of North America* 14, 199–212.
- Groppa, S., Oliviero, A., Eisen, A., Quartarone, A., Cohen, L.G., Mall, V., Kaelin-Lang, A., Mima, T., Rossi, S., Thickbroom, G.W., Rossini, P.M., Ziemann, U., Valls-Solé, J., Siebner, H.R., 2012. A practical guide to diagnostic transcranial magnetic stimulation: Report of an IFCN committee. *Clinical Neurophysiology* 123, 858–882. <https://doi.org/10.1016/j.clinph.2012.01.010>
- Grove, A.J., Newell, G.E., 1962. *Animal Biology, revised.* University Tutorial Press, London.
- Günther, J., 1976. Impulse conduction in the myelinated giant fibers of the earthworm. Structure and function of the dorsal nodes in the median giant fiber. *J. Comp. Neurol.* 168, 505–531. <https://doi.org/10.1002/cne.901680405>
- Günther, J., 1975. Neuronal syncytia in the giant fibres of earthworms. *Journal of neurocytology* 4, 55–62.
- Günther, J., 1973. A new type of 'node' in the myelin sheath of an invertebrate nerve fibre. *Experientia* 29, 1263–1265.
- Günther, J., 1972. Giant motor neurons in the earthworm. *Comparative Biochemistry and Physiology Part A: Physiology* 42, 967–973.
- Günther, J., 1971. Der cytologische Aufbau der dorsalen Riesenzellen von *Lumbricus terrestris* L. *Z Wiss Zool* 183, 51–70.
- Günther, J., 1971. Mikroanatomie des Bauchmarks von *Lumbricus terrestris* L. (Annelida, Oligochaeta). *Zeitschrift für Morphologie der Tiere* 70, 141–182.
- Günther, J., 1970. Zur Organisation der exteroceptiven Afferenzen in den Körpersegmenten des

Regenwurms. Verh Deut Zool Ges.

- Günther, J., Schürmann, F.W., 1973. Ultrastructure of the dorsal giant fibre system in the ventral nerve cord of the earthworm. II. Synaptic connections of the proximal collaterals of the giant fibres. *Zeitschrift für Zellforschung und mikroskopische Anatomie* (Vienna, Austria: 1948) 139, 369.
- Günther, J., Walther, J.B., 1971. Funktionelle anatomie der dorsalen riesenfaser-systeme von *Lumbricus terrestris*. *Zeitschrift für Morphologie der Tiere* 70, 253–280.
- Haller, M.I., Khuri-Yakub, B.T., 1996. A surface micromachined electrostatic ultrasonic air transducer. *IEEE transactions on ultrasonics, ferroelectrics, and frequency control* 43, 1–6.
- Hamani, C., Schwalb, J.M., Rezai, A.R., Dostrovsky, J.O., Davis, K.D., Lozano, A.M., 2006. Deep brain stimulation for chronic neuropathic pain: Long-term outcome and the incidence of insertional effect. *Pain* 125, 188–196. <https://doi.org/10.1016/j.pain.2006.05.019>
- Hariz, M.I., 2002. Complications of deep brain stimulation surgery. *Movement disorders: official journal of the Movement Disorder Society* 17, S162–S166.
- Hartline, D.K., Colman, D.R., 2007. Rapid Conduction and the Evolution of Giant Axons and Myelinated Fibers. *Current Biology* 17, R29–R35. <https://doi.org/10.1016/j.cub.2006.11.042>
- Hassler, R., Riechert, T., Munding, F., Umbach, W., Ganglberger, J.A., 1960. Physiological observations in stereotaxic operations in extrapyramidal motor disturbances. *Brain* 83, 337–350.
- Heath, R.G., 1996. Exploring the Mind Brain Relationship. Moran Printing, Inc.
- Heimburg, T., Jackson, A., 2005. On soliton propagation in biomembranes and nerves. *Proceedings of the National Academy of Sciences of the United States of America* 102, 9790–5. <https://doi.org/10.1073/pnas.0503823102>
- Hess, W.N., 1925. Nervous system of the earthworm, *lumbricus terrestris* L. *Journal of Morphology* 40, 235–259. <https://doi.org/10.1002/jmor.1050400203>
- Higdon, M.L., Higdon, J.A., 2006. Treatment of oncologic emergencies. *American family physician* 74.
- Hird, A., Wong, R., Flynn, C., Hadi, S., de Sa, E., Zhang, L., DeAngelis, C., Chow, E., 2009. Impact of pain flare on patients treated with palliative radiotherapy for symptomatic bone metastases. *J Pain Manag* 2, 401–406.
- Hodgkin, A.L., 1964. Conduction of the nervous impulse.
- Holden, A.V., Winlow, W., 1984. *The Neurobiology of Pain: Symposium of the Northern Neurobiology Group, held at Leeds on 18 April 1983, First Edition*. ed. Manchester Univ Pr, Manchester.
- Hong, Y.K., Park, D.S., 2009. Ureteroscopic Lithotripsy Using Swiss Lithoclast for Treatment of Ureteral Calculi: 12-Years Experience. *J Korean Med Sci* 24, 690–694. <https://doi.org/10.3346/jkms.2009.24.4.690>
- Hosobuchi, Y., Adams, J.E., Rutkin, B., 1973. Chronic thalamic stimulation for the control of facial anesthesia dolorosa. *Archives of Neurology* 29, 158–161.
- Howard, S.M., Zanelli, C.I., 2007. P1B-4 Characterization of a HIFU Field at High Intensity, in: *2007 IEEE Ultrasonics Symposium Proceedings*. Presented at the 2007 IEEE Ultrasonics Symposium Proceedings, pp. 1301–1304. <https://doi.org/10.1109/ULTSYM.2007.327>
- Hynynen, K., 1991. The threshold for thermally significant cavitation in dog's thigh muscle in vivo. *Ultrasound in Medicine and Biology* 17, 157–169.
- Isaacson, W., 2003. *Benjamin Franklin: An American Life*. Simon and Schuster.
- Iwasa, K., Tasaki, I., Gibbons, R.C., 1980. Swelling of nerve fibers associated with action potentials. *Science* 210, 338–339.
- Jackman, S.L., Regehr, W.G., 2017. The mechanisms and functions of synaptic facilitation. *Neuron* 94, 447–464.
- Jankovic, J., 2013. Medical treatment of dystonia. *Movement Disorders* 28, 1001–1012.

- Jin, X., Ladabaum, I., Degertekin, F.L., Calmes, S., Khuri-Yakub, B.T., 1999. Fabrication and characterization of surface micromachined capacitive ultrasonic immersion transducers. *Journal of Microelectromechanical systems* 8, 100–114.
- Kao, C.Y., Grundfest, H., 1957. Postsynaptic electrogenesis in septate giant axons. I. Earthworm median giant axon. *Journal of neurophysiology* 20, 553–573.
- Kehlet, H., Jensen, T.S., Woolf, C.J., 2006. Persistent postsurgical pain: risk factors and prevention. *The Lancet* 367, 1618–1625.
- Keng, L.B., 1895. On the Coelomic Fluid of *Lumbricus terrestris* in Reference to a Protective Mechanism. *Philosophical Transactions of the Royal Society of London. B* 186, 383–399.
- Kensler, R.W., Brink, P.R., Dewey, M.M., 1979. The septum of the lateral axon of the earthworm: a thin section and freeze-fracture study. *Journal of neurocytology* 8, 565–590.
- Kessler, R.C., Berglund, P., Demler, O., Jin, R., Koretz, D., Merikangas, K.R., Rush, A.J., Walters, E.E., Wang, P.S., 2003. The epidemiology of major depressive disorder: results from the National Comorbidity Survey Replication (NCS-R). *Jama* 289, 3095–3105.
- Khan, K.J., Stride, P.C., Cooper, G.M., 1993. Does a bloody tap prevent postdural puncture headache? *Anaesthesia* 48, 628–629. <https://doi.org/10.1111/j.1365-2044.1993.tb07132.x>
- Khuri-Yakub, B.T., Oralkan, Ö., 2011. Capacitive micromachined ultrasonic transducers for medical imaging and therapy. *Journal of micromechanics and microengineering* 21, 054004.
- King, R.L., Brown, J.R., Newsome, W.T., Pauly, K.B., 2013. Effective Parameters for Ultrasound-Induced In Vivo Neurostimulation. *Ultrasound in Medicine & Biology* 39, 312–331. <https://doi.org/10.1016/j.ultrasmedbio.2012.09.009>
- Kleiner-Fisman, G., Liang, G.S.L., Moberg, P.J., Ruocco, A.C., Hurtig, H.I., Baltuch, G.H., Jaggi, J.L., Stern, M.B., 2007. Subthalamic nucleus deep brain stimulation for severe idiopathic dystonia: impact on severity, neuropsychological status, and quality of life.
- Krasovitski, B., Frenkel, V., Shoham, S., Kimmel, E., 2011. Intramembrane cavitation as a unifying mechanism for ultrasound-induced bioeffects. *Proc Natl Acad Sci U S A* 108, 3258–3263. <https://doi.org/10.1073/pnas.1015771108>
- Krey, J.F., Gillespie, P.G., 2012. Chapter 53 - Molecular Biology of Hearing and Balance, in: Brady, S.T., Siegel, G.J., Albers, R.W., Price, D.L. (Eds.), *Basic Neurochemistry (Eighth Edition)*. Academic Press, New York, pp. 916–927. <https://doi.org/10.1016/B978-0-12-374947-5.00053-5>
- Kringelbach, M.L., Jenkinson, N., Owen, S.L.F., Aziz, T.Z., 2007. Translational principles of deep brain stimulation. *Nature Reviews Neuroscience* 8, 623–635. <https://doi.org/10.1038/nrn2196>
- Kulisevsky, J., Berthier, M.L., Gironell, A., Pascual-Sedano, B., Molet, J., Pares, P., 2002. Mania following deep brain stimulation for Parkinson's disease. *Neurology* 59, 1421–1424. <https://doi.org/10.1212/WNL.59.9.1421>
- Kung, C., 2005. A possible unifying principle for mechanosensation. *Nature* 436, 647.
- Kupsch, A., Benecke, R., Müller, J., Trottenberg, T., Schneider, G.-H., Poewe, W., Eisner, W., Wolters, A., Müller, J.-U., Deuschl, G., 2006. Pallidal deep-brain stimulation in primary generalized or segmental dystonia. *New England Journal of Medicine* 355, 1978–1990.
- Kurahashi, T., Miyake, H., Oka, N., Shinozaki, M., Takenaka, A., Hara, I., Fujisawa, M., 2007. Clinical outcome of ureteroscopic lithotripsy for 2,129 patients with ureteral stones. *Urol Res* 35, 149–153. <https://doi.org/10.1007/s00240-007-0095-3>
- Lafon, C., Chavrier, F., Prat, F., Chapelon, J.Y., Cathignol, D., 1999. Theoretical comparison of two interstitial ultrasound applicators designed to induce cylindrical zones of tissue ablation. *Medical & biological engineering & computing* 37, 298–303.
- Lakhan, S.E., Callaway, E., 2010. Deep brain stimulation for obsessive-compulsive disorder and treatment-resistant depression: systematic review. *BMC Res Notes* 3, 60.

<https://doi.org/10.1186/1756-0500-3-60>

- Larson, P.S., 2014. Deep brain stimulation for movement disorders. *Neurotherapeutics* 11, 465–474.
- Lefaucheur, J.-P., André-Obadia, N., Antal, A., Ayache, S.S., Baeken, C., Benninger, D.H., Cantello, R.M., Cincotta, M., de Carvalho, M., De Ridder, D., Devanne, H., Di Lazzaro, V., Filipović, S.R., Hummel, F.C., Jääskeläinen, S.K., Kimiskidis, V.K., Koch, G., Langguth, B., Nyffeler, T., Oliviero, A., Padberg, F., Poulet, E., Rossi, S., Rossini, P.M., Rothwell, J.C., Schönfeldt-Lecuona, C., Siebner, H.R., Slotema, C.W., Stagg, C.J., Valls-Sole, J., Ziemann, U., Paulus, W., Garcia-Larrea, L., 2014. Evidence-based guidelines on the therapeutic use of repetitive transcranial magnetic stimulation (rTMS). *Clinical Neurophysiology* 125, 2150–2206. <https://doi.org/10.1016/j.clinph.2014.05.021>
- Lind, C.D., 2003. Dysphagia: evaluation and treatment. *Gastroenterology Clinics of North America* 32, 553–575.
- Lippmann, M.G., 1881. On the principle of the conservation of electricity. *The London, Edinburgh, and Dublin Philosophical Magazine and Journal of Science* 12, 151–154.
- Litwin, M.S., Saigal, C.S., Yano, E.M., Avila, C., Geschwind, S.A., Hanley, J.M., Joyce, G.F., Madison, R., Pace, J., Polich, S.M., Wang, M., 2005. UROLOGIC DISEASES IN AMERICA PROJECT: ANALYTICAL METHODS AND PRINCIPAL FINDINGS. *The Journal of Urology* 173, 933–937. <https://doi.org/10.1097/01.ju.0000152365.43125.3b>
- Lo, C.-W., Desjouis, C., Chen, S.-R., Lee, J.-L., Inserra, C., Béra, J.-C., Chen, W.-S., 2014. Stabilizing in vitro ultrasound-mediated gene transfection by regulating cavitation. *Ultrasonics Sonochemistry* 21, 833–839. <https://doi.org/10.1016/j.ultsonch.2013.10.017>
- Loske, A.M., Prieto, F.E., Fernández, F., van Cauwelaert, J., 2002. Tandem shock wave cavitation enhancement for extracorporeal lithotripsy. *Physics in Medicine & Biology* 47, 3945.
- Louis, E.D., Ottman, R., Allen Hauser, W., 1998. How common is the most common adult movement disorder? Estimates of the prevalence of essential tremor throughout the world. *Movement disorders: official journal of the Movement Disorder Society* 13, 5–10.
- Lynn, J.G., Zwemer, R.L., Chick, A.J., Miller, A.E., 1942. A NEW METHOD FOR THE GENERATION AND USE OF FOCUSED ULTRASOUND IN EXPERIMENTAL BIOLOGY. *J Gen Physiol* 26, 179–193.
- Macdonald, L., Bruce, J., Scott, N.W., Smith, W.C.S., Chambers, W.A., 2005. Long-term follow-up of breast cancer survivors with post-mastectomy pain syndrome. *British journal of cancer* 92, 225.
- Makin, I.R.S., Mast, T.D., Faidi, W., Runk, M.M., Barthe, P.G., Slayton, M.H., 2005. Miniaturized ultrasound arrays for interstitial ablation and imaging. *Ultrasound in medicine & biology* 31, 1539–1550.
- Malhis, M., 2002. Contrôle actif modal flou des rotors flexibles par plan d'action piézoélectrique (PhD Thesis). Lyon, INSA.
- Martinelli, I., Bucciarelli, P., Mannucci, P.M., 2010. Thrombotic risk factors: basic pathophysiology. *Critical care medicine* 38, S3–S9.
- McDonald, R., Chow, E., Rowbottom, L., DeAngelis, C., Soliman, H., 2014. Incidence of pain flare in radiation treatment of bone metastases: A literature review. *Journal of bone oncology* 3, 84–89.
- Melodelima, D., Prat, F., Fritsch, J., Theillere, Y., Cathignol, D., 2008. Treatment of esophageal tumors using high intensity intraluminal ultrasound: first clinical results. *Journal of translational medicine* 6, 28.
- Melzack, R., Wall, P.D., 1965. Pain mechanisms: a new theory. *Science* 150, 971–979.
- Menz, M.D., Oralkan, O., Khuri-Yakub, P.T., Baccus, S.A., 2013. Precise neural stimulation in the retina using focused ultrasound. *J. Neurosci.* 33, 4550–4560. <https://doi.org/10.1523/JNEUROSCI.3521-12.2013>

- Mindell, E.R., 2001. Enzinger and Weiss's Soft Tissue Tumors. *JBJS* 83, 1778.
- Mindus, P., Rasmussen, S.A., Lindquist, C., 1994. Neurosurgical treatment for refractory obsessive-compulsive disorder: implications for understanding frontal lobe function. *The Journal of neuropsychiatry and clinical neurosciences*.
- Moore, M.E., Loft, J.M., Clegern, W.C., Wisor, J.P., 2015. Manipulating neuronal activity in the mouse brain with ultrasound: A comparison with optogenetic activation of the cerebral cortex. *Neuroscience letters* 604, 183–187.
- Moore, M.J., 1979. The Rapid Escape Response of the Earthworm *Lumbricus Terrestris* L.: Overlapping Sensory Fields of the Median And Lateral Giant Fibres. *Journal of Experimental Biology* 83, 231–238.
- Morgan, J.P., 1982. The First Reported Case of Electrical Stimulation of the Human Brain. *J Hist Med Allied Sci XXXVII*, 51–64. <https://doi.org/10.1093/jhmas/XXXVII.1.51>
- Morishita, T., Fayad, S.M., Higuchi, M., Nestor, K.A., Foote, K.D., 2014. Deep Brain Stimulation for Treatment-resistant Depression: Systematic Review of Clinical Outcomes. *Neurotherapeutics* 11, 475–484. <https://doi.org/10.1007/s13311-014-0282-1>
- Morris, C.E., Juranka, P.F., 2007. Lipid Stress at Play: Mechanosensitivity of Voltage-Gated Channels. *Current Topics in Membranes, Mechanosensitive Ion Channels, Part B* 59, 297–338. [https://doi.org/10.1016/S1063-5823\(06\)59011-8](https://doi.org/10.1016/S1063-5823(06)59011-8)
- Mulloney, B., 1970. Structure of the Giant Fibers of Earthworms. *Science* 168, 994–996. <https://doi.org/10.1126/science.168.3934.994>
- Muratore, R., LaManna, J.K., Lamprecht, M.R., Morrison III, B., 2012. Hippocampal culture stimulus with 4-megahertz ultrasound, in: *AIP Conference Proceedings*. AIP, pp. 254–258.
- Murray, C.J., Lopez, A.D., 1997. Global mortality, disability, and the contribution of risk factors: Global Burden of Disease Study. *The lancet* 349, 1436–1442.
- N'Djin, W.A., Burtnyk, M., Kobelevskiy, I., Hadjis, S., Bronskill, M., Chopra, R., 2012. Coagulation of human prostate volumes with MRI-controlled transurethral ultrasound therapy: Results in gel phantoms. *Medical physics* 39, 4524–4536.
- N'Djin, W.A., Gerold, B., Vion-Bailly, J., Canney, M.S., Nguyen-Dinh, A., Carpentier, A., Chapelon, J.-Y., 2017. Capacitive Micromachined Ultrasound Transducers for Interstitial High-Intensity Ultrasound Therapies. *IEEE transactions on ultrasonics, ferroelectrics, and frequency control* 64, 1245–1260.
- Nitsche, M.A., Boggio, P.S., Fregni, F., Pascual-Leone, A., 2009. Treatment of depression with transcranial direct current stimulation (tDCS): a review. *Experimental neurology* 219, 14–19.
- Nitsche, M.A., Paulus, W., 2000. Excitability changes induced in the human motor cortex by weak transcranial direct current stimulation. *The Journal of Physiology* 527, 633–639. <https://doi.org/10.1111/j.1469-7793.2000.t01-1-00633.x>
- O'Gara, B., Vining, E.P., Drewes, C.D., 1982. Electrophysiological correlates of rapid escape reflexes in intact earthworms, *Eisenia foetida*. I. Functional development of giant nerve fibers during embryonic and postembryonic periods. *Journal of Neurobiology* 13, 337–353.
- Olds, J., Milner, P., 1954. Positive reinforcement produced by electrical stimulation of septal area and other regions of rat brain. *Journal of comparative and physiological psychology* 47, 419.
- O'Neil, H., 1949. Theory of focusing radiators. *The Journal of the Acoustical Society of America* 21, 516–526.
- Oralkan, O., Ergun, A.S., Johnson, J.A., Karaman, M., Demirci, U., Kaviani, K., Lee, T.H., Khuri-Yakub, B.T., 2002. Capacitive micromachined ultrasonic transducers: Next-generation arrays for acoustic imaging? *IEEE transactions on ultrasonics, ferroelectrics, and frequency control* 49, 1596–1610.

- Ostrem, J.L., Racine, C.A., Glass, G.A., Grace, J.K., Volz, M.M., Heath, S.L., Starr, P.A., 2011. Subthalamic nucleus deep brain stimulation in primary cervical dystonia. *Neurology* 76, 870–878.
- Owen, S.L.F., Green, A.L., Nandi, D.D., Bittar, R.G., Wang, S., Aziz, T.Z., 2007. Deep brain stimulation for neuropathic pain, in: Sakas, D.E., Simpson, B.A. (Eds.), *Operative Neuromodulation: Volume 2: Neural Networks Surgery*, Acta Neurochirurgica Supplements. Springer Vienna, Vienna, pp. 111–116. https://doi.org/10.1007/978-3-211-33081-4_13
- Pahapill, P.A., O'connell, B., 2010. Long-term follow-up study of chronic deep brain stimulation of the subthalamic nucleus for cervical dystonia. *Neuromodulation: Technology at the Neural Interface* 13, 26–30.
- Pallas, S.L., Drewes, C.D., 1981. The rapid tail flattening component of MGF-mediated escape behavior in the earthworm, *Lumbricus terrestris*. *Comparative Biochemistry and Physiology Part A: Physiology* 70, 57–64.
- Petrov, A., 1975. Flexoelectric Model for Active Transport. *Physical and Chemical Bases of Biological Information Transfer* 111–125. https://doi.org/10.1007/978-1-4684-2181-1_9
- Pishchalnikov, Y.A., Sapozhnikov, O.A., Bailey, M.R., Williams Jr, J.C., Cleveland, R.O., Colonius, T., Crum, L.A., Evan, A.P., McAteer, J.A., 2003. Cavitation bubble cluster activity in the breakage of kidney stones by lithotripter shockwaves. *Journal of endourology* 17, 435–446.
- Plaksin, M., Shoham, S., Kimmel, E., 2014. Intramembrane Cavitation as a Predictive Bio-Piezoelectric Mechanism for Ultrasonic Brain Stimulation.
- Pool, J.L., 1956. Psychosurgery in elderly people. *J Am Geriatr Soc* 2, 456–465.
- Potter, P., Perry, A., 2004. *Fundamentals of Nursing*. {C.V. Mosby}.
- Prasad, D., Schiff, D., 2005. Malignant spinal-cord compression. *The Lancet Oncology* 6, 15–24. [https://doi.org/10.1016/S1470-2045\(04\)01709-7](https://doi.org/10.1016/S1470-2045(04)01709-7)
- Prat, F., Chapelon, J.-Y., Arefiev, A., Cathignol, D., Souchon, R., Theillière, Y., 1997. High-intensity focused ultrasound transducers suitable for endoscopy: feasibility study in rabbits. *Gastrointestinal endoscopy* 46, 348–351.
- Prosser, C.L., 1935. Impulses in the segmental nerves of the earthworm. *Journal of Experimental Biology* 12, 95–104.
- Radiation Induced Dysphagia [WWW Document], 2017. . Department of Otolaryngology Head and Neck Surgery. URL <http://entcolumbia.org/health-library/radiation-induced-dysphagia> (accessed 10.16.18).
- Rajer, M., Kovač, V., 2008. Malignant spinal cord compression. *Radiology and Oncology* 42, 23–31.
- Rautakorpi, I., Takala, J., Marttila, R.J., Sievers, K., Rinne, U.K., 1982. Essential tremor in a Finnish population. *Acta Neurologica Scandinavica* 66, 58–67.
- Reale, C., Turkiewicz, A.M., Reale, C.A., 2001. Antalgic treatment of pain associated with bone metastases. *Critical Reviews in Oncology/Hematology* 37, 1–11. [https://doi.org/10.1016/S1040-8428\(99\)00066-9](https://doi.org/10.1016/S1040-8428(99)00066-9)
- Recordare, A., Bonariol, L., Caratozzolo, E., Callegari, F., Bruno, G., Di, F.P., Bassi, N., 2002. Management of spontaneous bleeding due to hepatocellular carcinoma. *Minerva Chir* 57, 347–356.
- Reslan, L., Mestas, J.-L., Herveau, S., Béra, J.-C., Dumontet, C., 2010. Transfection of cells in suspension by ultrasound cavitation. *Journal of Controlled Release* 142, 251–258.
- Riesz, P., Kondo, T., 1992. Free radical formation induced by ultrasound and its biological implications. *Free Radical Biology and Medicine* 13, 247–270.
- Rosa, M.A., Lisanby, S.H., 2012. Somatic treatments for mood disorders. *Neuropsychopharmacology* 37, 102.

- Rossi, S., Hallett, M., Rossini, P.M., Pascual-Leone, A., 2009. Safety, ethical considerations, and application guidelines for the use of transcranial magnetic stimulation in clinical practice and research. *Clinical Neurophysiology* 120, 2008–2039.
<https://doi.org/10.1016/j.clinph.2009.08.016>
- Ruscio, A.M., Stein, D.J., Chiu, W.T., Kessler, R.C., 2010. The epidemiology of obsessive-compulsive disorder in the National Comorbidity Survey Replication. *Molecular Psychiatry* 15, 53–63.
<https://doi.org/10.1038/mp.2008.94>
- Rush, A.J., Trivedi, M.H., Wisniewski, S.R., Nierenberg, A.A., Stewart, J.W., Warden, D., Niederhe, G., Thase, M.E., Lavori, P.W., Lebowitz, B.D., 2006. Acute and longer-term outcomes in depressed outpatients requiring one or several treatment steps: a STAR* D report. *American Journal of Psychiatry* 163, 1905–1917.
- Rushton, W.A., Barlow, H.B., 1943. Single-fibre response from an intact animal. *Nature* 152, 597.
- Rushton, W.A.H., 1946. Reflex conduction in the giant fibres of the earthworm. *Proc. R. Soc. Lond. B* 133, 109–120.
- Rushton, W.A.H., 1945. Action potentials from the isolated nerve cord of the earthworm. *Proc. R. Soc. Lond. B* 132, 423–437.
- Sabraoui, A., Inserra, C., Gilles, B., Béra, J.-C., Mestas, J.-L., 2011. Feedback loop process to control acoustic cavitation. *Ultrasonics sonochemistry* 18, 589–594.
- Sako, A., Ishida, K., Fukada, M., Asafusa, K., Sano, S., Izumi, M., 2009. Development of ultrasonic transducer “Mappie” with cMUT technology. *Medix* 51, 31–34.
- Sapozhnikov, O.A., Khokhlova, V.A., Bailey, M.R., Williams Jr, J.C., McAteer, J.A., Cleveland, R.O., Crum, L.A., 2002. Effect of overpressure and pulse repetition frequency on cavitation in shock wave lithotripsy. *The Journal of the Acoustical Society of America* 112, 1183–1195.
- Sassaroli, E., Vykhodtseva, N., 2016. Acoustic neuromodulation from a basic science perspective. *Journal of Therapeutic Ultrasound* 4, 17. <https://doi.org/10.1186/s40349-016-0061-z>
- Schneider, H.D., Hopp, J.P., 2011. The use of the Bilingual Aphasia Test for assessment and transcranial direct current stimulation to modulate language acquisition in minimally verbal children with autism. *Clinical linguistics & phonetics* 25, 640–654.
- Shakir, S.H., Dindal, D.L., 1997. Density and biomass of earthworms in forest and herbaceous microecosystems in central New York, North America. *Soil Biology and Biochemistry* 29, 275–285. [https://doi.org/10.1016/S0038-0717\(96\)00051-X](https://doi.org/10.1016/S0038-0717(96)00051-X)
- Shealy, C.N., Mortimer, J.T., Reswick, J.B., 1967. Electrical inhibition of pain by stimulation of the dorsal columns. *Anesth Analg* 46, 489–491.
- Shimazaki, H., Nakano, I., 2008. Radiation myelopathy and plexopathy. *Brain and nerve= Shinkei kenkyu no shinpo* 60, 115–121.
- Siegfried, J., 1977. 2 different aspects of neurosurgical treatment of spasticity. Cerebral intervention and stimulation of the posterior spinal cord. *Neuro-Chirurgie* 23, 344.
- Smith, A.D., 2007. *Smith’s textbook of endourology*. PMPH-USA.
- Smith, P.H., Mittenenthal, J.E., 1980. Intersegmental variation of afferent pathways to giant interneurons of the earthworm, *Lumbricus terrestris* L. *J. Comp. Physiol.* 140, 351–363.
<https://doi.org/10.1007/BF00606275>
- Smith, W.C.S., Bourne, D., Squair, J., Phillips, D.O., Chambers, W.A., 1999. A retrospective cohort study of post mastectomy pain syndrome. *Pain* 83, 91–95.
- Sokolov, D.L., Bailey, M.R., Crum, L.A., 2001. Use of a dual-pulse lithotripter to generate a localized and intensified cavitation field. *The Journal of the Acoustical Society of America* 110, 1685–1695.
- Spiegel, E.A., Wycis, H.T., Marks, M., Lee, A.J., 1947. Stereotaxic apparatus for operations on the

- human brain. *Science* 106, 349–350.
- Spinazzé, S., Caraceni, A., Schrijvers, D., 2005. Epidural spinal cord compression. *Critical reviews in oncology/hematology* 56, 397–406.
- Stephenson, J., 1930. *The Oligochaeta*. Clarendon Press.
- Stillings, D., 1975. A survey of the history of electrical stimulation for pain to 1900 Xk. *Med. Instrum* 9, 255–259.
- Stough, H.B., 1926. Giant nerve fibers of the earthworm. *Journal of comparative neurology* 40, 409–463.
- Studnitz, G. von, 1937. Der Zuckreflex der Regenwürmer. *Zool. Jahrb. Abt. Allg. Zool. Physiol. Tiere* 38, 127–158.
- Sukharev, S., Corey, D.P., 2004. Mechanosensitive Channels: Multiplicity of Families and Gating Paradigms. *Sci. STKE* 2004, re4–re4. <https://doi.org/10.1126/stke.2192004re4>
- Tasaki, I., 1988. A macromolecular approach to excitation phenomena: mechanical and thermal changes in nerve during excitation. *Physiological chemistry and physics and medical NMR* 20, 251–268.
- Tasaki, I., Kusano, K., Byrne, P., 1989. Rapid mechanical and thermal changes in the garfish olfactory nerve associated with a propagated impulse. *Biophysical journal* 55, 1033–1040.
- Tateishi, A., Higaki, S., Abe, S., Nakano, H., 1997. [Treatment of pathological fractures caused by metastatic bone cancer]. *Gan To Kagaku Ryoho* 24, 285–291.
- Tateno, T., Nishikawa, J., 2014. A CMOS IC-based multisite measuring system for stimulation and recording in neural preparations in vitro. *Frontiers in neuroengineering* 7, 39.
- Teichman, J.M., Kamerer, A.D., 2000. Use of the holmium: YAG laser for the impacted stone basket. *The Journal of urology* 164, 1602–1603.
- ter Haar, G., 1999. Therapeutic ultrasound. *European Journal of Ultrasound* 9, 3–9. [https://doi.org/10.1016/S0929-8266\(99\)00013-0](https://doi.org/10.1016/S0929-8266(99)00013-0)
- Thair, H., Holloway, A.L., Newport, R., Smith, A.D., 2017. Transcranial Direct Current Stimulation (tDCS): A Beginner’s Guide for Design and Implementation. *Front Neurosci* 11. <https://doi.org/10.3389/fnins.2017.00641>
- Tufail, Y., Matyushov, A., Baldwin, N., Tauchmann, M.L., Georges, J., Yoshihiro, A., Tillery, S.I.H., Tyler, W.J., 2010. Transcranial pulsed ultrasound stimulates intact brain circuits. *Neuron* 66, 681–694. <https://doi.org/10.1016/j.neuron.2010.05.008>
- Turk, D.C., Okifuji, A., 2001. Pain terms and taxonomies of pain. Loeser JD. *Bonica’s management of pain*. Philadelphia: Lippincott Williams & Wilkins.
- Turnbull, D.K., Shepherd, D.B., 2003. Post-dural puncture headache: pathogenesis, prevention and treatment. *Br J Anaesth* 91, 718–729.
- Tyler, W.J., 2011. Noninvasive neuromodulation with ultrasound? A continuum mechanics hypothesis. *Neuroscientist* 17, 25–36. <https://doi.org/10.1177/1073858409348066>
- Tyler, W.J., Tufail, Y., Finsterwald, M., Tauchmann, M.L., Olson, E.J., Majestic, C., 2008. Remote Excitation of Neuronal Circuits Using Low-Intensity, Low-Frequency Ultrasound. *PLOS ONE* 3, e3511. <https://doi.org/10.1371/journal.pone.0003511>
- Tysnes, O.-B., Storstein, A., 2017. Epidemiology of Parkinson’s disease. *J Neural Transm (Vienna)* 124, 901–905. <https://doi.org/10.1007/s00702-017-1686-y>
- Urch, C.E., Suzuki, R., Higginson, I.J., Hearn, J., Murtagh, F., Twycross, R., Bennett, M., El Osta, B., Bruera, E., Monroe, B., 2008. Pathophysiology of somatic, visceral, and neuropathic cancer pain. *Clinical Pain Management Second Edition: Cancer Pain* 3, 13.
- Vail, V.A., 1974. Contributions on North American earthworms (Annelida II): Observations on the hatchlings of *Eisenia foetida* and *Bimastos tumidus* (Oligochaeta: Lumbricidae). *Bull Tall*

- Timbers Res Sta 16, 1–8.
- Valdeoriola, F., Regidor, I., Mínguez-Castellanos, A., Lezcano, E., García-Ruiz, P., Rojo, A., Salvador, A., Castro, A., Grandas, F., Kulisevsky, J., 2010. Efficacy and safety of pallidal stimulation in primary dystonia: results of the Spanish multicentric study. *Journal of Neurology, Neurosurgery & Psychiatry* 81, 65–69.
- Vercueil, L., Pollak, P., Fraix, V., Caputo, E., Moro, E., Benazzouz, A., Xie, J., Koudsie, A., Benabid, A.-L., 2001. Deep brain stimulation in the treatment of severe dystonia. *Journal of neurology* 248, 695–700.
- Vidailhet, M., Vercueil, L., Houeto, J.-L., Krystkowiak, P., Benabid, A.-L., Cornu, P., Lagrange, C., Tézenas du Montcel, S., Dormont, D., Grand, S., Blond, S., Detante, O., Pillon, B., Ardouin, C., Agid, Y., Destée, A., Pollak, P., 2005. Bilateral Deep-Brain Stimulation of the Globus Pallidus in Primary Generalized Dystonia. *New England Journal of Medicine* 352, 459–467. <https://doi.org/10.1056/NEJMoa042187>
- Vilensky, J.A., Gilman, S., 2002. Horsley was the first to use electrical stimulation of the human cerebral cortex intraoperatively. *Surgical neurology* 58, 425–426.
- Villamar, M.F., Volz, M.S., Bikson, M., Datta, A., DaSilva, A.F., Fregni, F., 2013. Technique and considerations in the use of 4x1 ring high-definition transcranial direct current stimulation (HD-tDCS). *Journal of visualized experiments: JoVE*.
- Volkman, J., Wolters, A., Kupsch, A., Müller, J., Kühn, A.A., Schneider, G.-H., Poewe, W., Hering, S., Eisner, W., Müller, J.-U., 2012. Pallidal deep brain stimulation in patients with primary generalised or segmental dystonia: 5-year follow-up of a randomised trial. *The Lancet Neurology* 11, 1029–1038.
- Wallwork, J.A., 1983. *Earthworm biology*. E. Arnold (Publishers) Ltd.
- Walton, A.J., Reynolds, G.T., 1984. Sonoluminescence. *Advances in Physics* 33, 595–660.
- Wan, H., VanBaren, P., Ebbini, E.S., Cain, C.A., 1996. Ultrasound surgery: Comparison of strategies using phased array systems. *IEEE transactions on ultrasonics, ferroelectrics, and frequency control* 43, 1085–1098.
- Wells, P.N.T., 1977. *Biomedical ultrasonics*. Academic Pr.
- White, R.H., 2003. The epidemiology of venous thromboembolism. *Circulation* 107, I–4.
- Williams Jr, J.C., Woodward, J.F., Stonehill, M.A., Evan, A.P., McAteer, J.A., 1999. Cell damage by lithotripter shock waves at high pressure to preclude cavitation. *Ultrasound in medicine & biology* 25, 1445–1449.
- Willscher, M.K., Conway, J.F., Babayan, R.K., Morrisseau, P., Sant, G.R., Bertagnoll, A., 1988. Safety and Efficacy of Electrohydraulic Lithotripsy By Ureteroscopy. *The Journal of Urology* 140, 957–958. [https://doi.org/10.1016/S0022-5347\(17\)41897-0](https://doi.org/10.1016/S0022-5347(17)41897-0)
- Wilson, D.M., 1961. The connections between the lateral giant fibers of earthworms. *Comparative biochemistry and physiology* 3, 274–284.
- Wong, S.H., Kupnik, M., Watkins, R.D., Butts-Pauly, K., Khuri-Yakub, B.T., 2010. Capacitive micromachined ultrasonic transducers for therapeutic ultrasound applications. *IEEE transactions on Biomedical Engineering* 57, 114–123.
- Wong, S.H., Watkins, R.D., Kupnik, M., Pauly, K.B., Khuri-Yakub, B.T., 2008. Feasibility of MR-temperature mapping of ultrasonic heating from a CMUT. *IEEE transactions on ultrasonics, ferroelectrics, and frequency control* 55, 811–818.
- Wrenn, S.P., Dicker, S.M., Small, E.F., Dan, N.R., Mleczo, M., Schmitz, G., Lewin, P.A., 2012. Bursting Bubbles and Bilayers. *Theranostics* 2, 1140–1159. <https://doi.org/10.7150/thno.4305>
- Xi, X., Zhong, P., 2000. Improvement of stone fragmentation during shock-wave lithotripsy using a combined EH/PEAA shock-wave generator—in vitro experiments. *Ultrasound in medicine &*

- biology 26, 457–467.
- Yi, P., Pryzbylkowski, P., 2015. Opioid Induced Hyperalgesia. *Pain Med* 16, S32–S36. <https://doi.org/10.1111/pme.12914>
- Yoo, S.-S., Bystritsky, A., Lee, J.-H., Zhang, Y., Fischer, K., Min, B.-K., McDannold, N.J., Pascual-Leone, A., Jolesz, F.A., 2011. Focused ultrasound modulates region-specific brain activity. *Neuroimage* 56, 1267–1275. <https://doi.org/10.1016/j.neuroimage.2011.02.058>
- Younan, Y., Deffieux, T., Larrat, B., Fink, M., Tanter, M., Aubry, J.-F., 2013. Influence of the pressure field distribution in transcranial ultrasonic neurostimulation. *Medical Physics* 40, 082902. <https://doi.org/10.1118/1.4812423>
- Young, J.Z., 1936. Structure of nerve fibres and synapses in some invertebrates, in: *Cold Spring Harbor Symposia on Quantitative Biology*. Cold Spring Harbor Laboratory Press, pp. 1–6.
- Zalc, B., 2006. The acquisition of myelin: a success story, in: *Novartis Foundation Symposium*. Chichester; New York; John Wiley; 1999, p. 15.
- Zauber, S.E., Watson, N., Comella, C.L., Bakay, R.A., Metman, L.V., 2009. Stimulation-induced parkinsonism after posteroventral deep brain stimulation of the globus pallidus internus for craniocervical dystonia: Case report. *Journal of neurosurgery* 110, 229–233.
- Zhao, D., Zhuang, S., Daigle, R., 2015. A commercialized high frequency CMUT probe for medical ultrasound imaging, in: *Ultrasonics Symposium (IUS), 2015 IEEE International*. IEEE, pp. 1–4.
- Zhong, P., Cioanta, I., Cocks, F.H., Preminger, G.M., 1997. Inertial cavitation and associated acoustic emission produced during electrohydraulic shock wave lithotripsy. *The Journal of the Acoustical Society of America* 101, 2940–2950.
- Zhu, S., Cocks, F.H., Preminger, G.M., Zhong, P., 2002. The role of stress waves and cavitation in stone comminution in shock wave lithotripsy. *Ultrasound in medicine & biology* 28, 661–671.

Annexes

Annexe I – Reproductive system of *Lumbricus terrestris*

Earthworms are **simultaneous hermaphrodites**, which means each individual present complete and simultaneously functional male and female systems. In the species *Lumbricus terrestris*, internal mechanisms prohibit self-fertilization, unlike in other species such as *Eisenia andrei*. This method of biparental reproduction is known as cross-fertilization, and leads eventually to the formation of two separate cocoons sheltering two sets of embryos.

The **male system** is essentially composed of testes, sperm reservoirs, sperm vesicles, gonoducts and male gonopores. Testes are relatively small and nested in the sperm reservoirs (segments 10-11) which are specialized coelomic spaces where autosperm (*i.e.* sperm produced by *this* worm) is matured. Sperm vesicles present as lateral outpockets of the reservoirs. Gonoducts convey the sperm from the sperm vesicles to the gonopores, situated in segment 15 (Fox, 2006).

The **female system** is essentially composed of seminal receptacles, ovaries, oviducts and female gonopores. Seminal receptacles, also called spermathecae and located in segment 9 and 10, are similar to seminal vesicles of the male system. While seminal vesicles are the site of storage of autosperm, seminal receptacles are the site of storage of allosperm (*i.e.* sperm produced by copulatory partner). Short ducts penetrate the body wall and connect the seminal receptacles with external pores (**Figure 80.A**). Ovaries produce unfertilized eggs, and connect via the oviduct to the female gonopores located on segment 14.

In *Lumbricus terrestris*, copulation and reproduction are two separate stages. Copulation occurs at the surface, and can last several hours. Mating partners align in opposite direction, their ventral sides in contact with each other (**Figure 80.B**) in such a way that female seminal receptacles are in juxtaposition with male gonopores. Once seminal receptacles have received allosperm and stored it, mating partners part from each other. Each earthworm then produces an annular mucous cocoon from its clitellum, and executes backward movements in order to translate the cocoon upstream. During its translation the cocoon will successively pass the female gonopores in segment 14, where it will obtain unfertilized eggs, and the seminal

receptacles in segments 9-10, where allosperm will fertilized the eggs. Finally, the earthworm get out of the annular cocoon which seals itself as a lemon-shaped incubator (**Figure 80.C**).

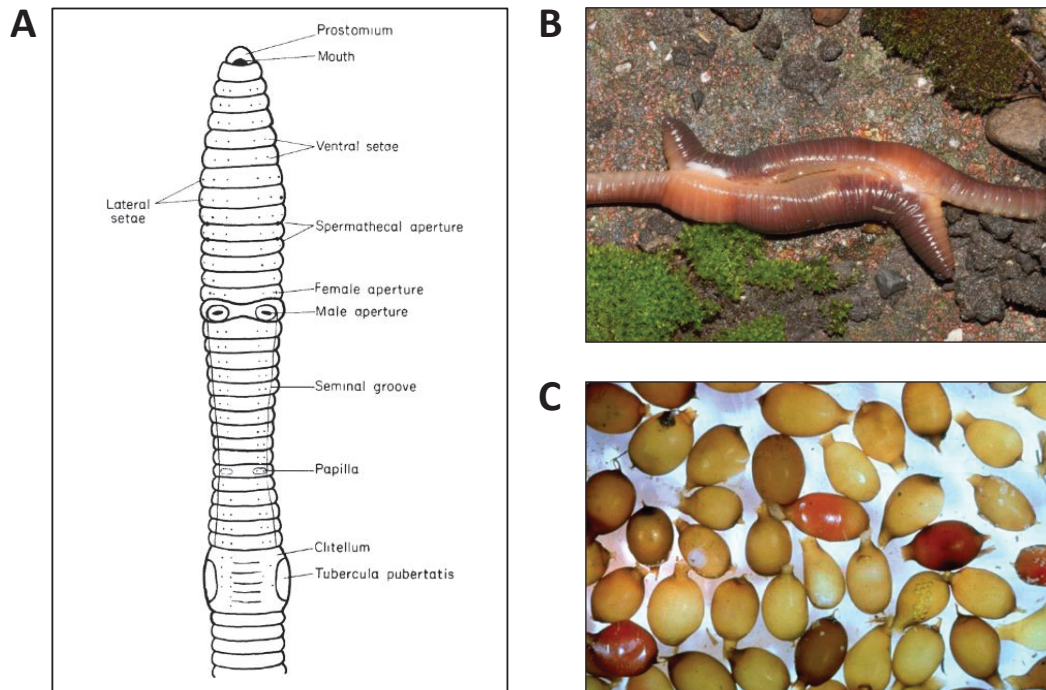


Figure 80 - Characteristics of the reproductive system of *Lumbricus terrestris*. (A) Ventral view of the anterior part of the animal. (B) Photograph of a mating pair of earthworms. (C) Photograph of cocoons.